Title
Function and Signaling Specificity of the Hog1 Mitogen-Activated Protein Kinase in the Yeast Saccharomyces cerevisiae

Author
Patterson, Jesse Christopher

Publication Date
2011

Peer reviewed|Thesis/dissertation

Function and Signaling Specificity of the Hog1 Mitogen-Activated Protein Kinase in the Yeast *Saccharomyces cerevisiae*

by

Jesse Christopher Patterson

A dissertation submitted in partial satisfaction of the

requirements for the degree of

Doctor of Philosophy

in

Molecular and Cell Biology

in the

Graduate Division

of the

University of California, Berkeley

Committee in charge:

Professor Jeremy W. Thorner, Chair
Professor David G. Drubin
Professor Thomas C. Alber
Professor Sheng Luan

Spring 2011

Function and Signaling Specificity of the Hog1 Mitogen-Activated Protein Kinase in the Yeast *Saccharomyces cerevisiae*

by

Jesse Christopher Patterson

Abstract

Function and Signaling Specificity of the Hog1 Mitogen-Activated Protein Kinase in the Yeast *Saccharomyces cerevisiae*

by

Jesse Christopher Patterson

Doctor of Philosophy in Molecular and Cell Biology

University of California, Berkeley

Professor Jeremy W. Thorner, Chair

Multiple mitogen-activated protein kinases (MAPKs) enable eukaryotic cells to evoke an appropriate response when presented with a particular stimulus. In the yeast *Saccharomyces cerevisiae*, MAPK Hog1 is activated by osmosensors in the high-osmolarity glycerol (HOG) pathway during hyperosmotic stress, MAPK Fus3 is activated by pheromone-binding receptors in the mating pathway, and MAPK Kss1 is activated by mucins in the filamentous growth (FG) pathway during nutrient limitation. These pathways provide an excellent model for studying mechanisms and principles of signal transduction in a genetically and biochemically tractable organism because these conserved pathways have served countless species in their struggle to adapt to change throughout evolution.

Upon hyperosmotic shock, yeast cells accumulate intracellular glycerol to balance the osmotic gradient. It had been accepted that Hog1 elevates glycerol production by inducing the transcription of enzymes necessary for glycerol synthesis. Using global microarray analysis, I found that Hog1-dependent transcription is not necessary for hyperosmotic shock survival. Instead, Hog1 increases glycerol production by directly regulating metabolism and work presented in this thesis describes progress made towards understanding how this control is exerted.

The HOG, mating and FG pathways share common upstream activators, including Ste50 (adapter protein), Ste20 [p21-activated protein kinase (PAK)], Ste11 [MAPK kinase kinase (MAPKKK)] and Cdc42 [guanosine tri-phosphatase (GTPase)]. Activation of Ste11 within the HOG pathway does not result in Ste11-mediated activation of the mating or FG pathways. Tellingly, if Hog1 function is absent, hyperosmotic stress does result in Ste11-mediated activation of these other MAPK pathways, a situation called crosstalk. Therefore, a mechanism of Hog1-enforced crosstalk prevention exists. Using single-cell analysis of both HOG and mating pathway activation, I found that crosstalk is prevented by insulation of the HOG pathway from other MAPK pathways, over-turning a previously established erroneous model of cross-inhibition. Through a genetic selection, I found that Rga1 [a Cdc42 GTPase-activating protein (GAP)] is required for HOG pathway insulation, that Rga1 is a substrate of Hog1, that it contributes to negative feedback regulation of the HOG pathway, and that Rga1 presumably helps prevent crosstalk by limiting the extent and duration of Cdc42 activation.

To Doug, Dorothy and Emily

Acknowledgements

My graduate education and this dissertation are the products of countless individuals. First and foremost, the successes I have been able to muster during this time are in large part due to the patience, open-mindedness and sage guidance of my advisor Jeremy Thorner. Jeremy is a wonderful teacher, a top-notch scientist and great person. I am extremely fortunate to have had the opportunity to work with him. I would also like to thank the members of my thesis committee, Drs. David Drubin, Sheng Luan and Tom Alber, for their invaluable discussions throughout the years.

I have also had the privilege of working with a long list of intelligent and friendly members of the Thorner lab, who have always given me advice, challenged my ideas, taught me new skills, and served as a support group. I would like to thank Dr. Françoise Roelants for her encouragement, friendship and doing such a good job at keeping the lab running smoothly. Dr. Patrick Westfall played a very important role during my first year in the Thorner lab, by training me and introducing me to the HOG MAPK pathway. The post-doctorates of the Thorner lab, Drs. Micheal McMurray, Allison O'Donnell and Zhu Li, also deserve a very large thanks, and possibly an apology, for my incessant questions.

My fellow graduate students also each contributed to my maturation as a scientist. Dr. Lindsay Garrenton was an immense resource of know-how while she was here and a great example of how to take a set of ideas and turn it into a finished story. Dr. Raymond Chen was constantly challenging my critical thinking skills. Jane Klimenko, who was my "bay-mate", started in the Thorner lab the same day as me and is finishing at the same time, has been a valuable comrade, and I think we can both appreciate having a person around a the same stage of grad school to watch each others back. I would also like to acknowledge the younger crowd of graduate students, Alex Muir and Chris Alvaro, for keeping things interesting. Louise Goupil, a very bright Chemical Biology Honors undergraduate student has been extremely helpful. The work described in Chapter 5 was done together with her, and I think we made an exceedingly good team. Moreover, I would also like to thank the advisors from my undergraduate studies at the Georgia Institute of Technology including Dr. Yury Chernoff and Dr. Susanne Müller, who introduced me to scientific research.

Jessica Piel has kept me sane during this whole process through her love and support. I cannot thank her enough for being by my side. Having her and our cat Emma at home for the past few years has enriched my life beyond belief.

My family is the reason I have gotten to where I am today. They have supported me in all my endeavors, and I cannot thank them enough.

Table of Contents

Acknowledgements ..... **ii**

List of Tables ..... **vi**

List of Figures ..... **vii**

List of Abbreviations ..... **x**

Chapter 1 Introduction **1**

Stress resistance and osmoregulation 1

Structure and function of the HOG MAPK pathway 2

The mating MAPK pathway in yeast 5

The filamentous growth pathway in yeast 8

Crosstalk between MAPK pathways 11

Overview of this thesis 11

Chapter 2 Materials and Methods **14**

Yeast strains and growth conditions 14

Plasmids and recombinant DNA methods 20

Microarray analysis of yeast cultures during hyperosmotic stress 24

Purification of ZZ-3C-HA-6XHIS tagged proteins from yeast 25

Purification of GST tagged proteins from *E. coli* 26

In vitro protein kinase assays 27

Measurement and calculation of FRET *in vivo* 27

Imaging of fluorescent proteins in yeast cells 27

Automated cell identification and subsequent quantitation of fluorescent protein expression in single cells 28

Preparation of protein extracts and Immuno-bloting 29

Immunoprecipitation and Calf intestinal phosphatase treatment of HA-Rga1 30

Chapter 3 Hog1-dependent Hyperosmotic Stress Resistance Is Mediated by an Increase in Glycerol Production Via the Glycerol-phosphate Shunt **31**

Introduction 31

Results 34

Microarray analysis shows HOG pathway dependent transcription is dispensable for hyperosmotic stress resistance 34

Glyceraldehyde-3-phosphate dehydrogenases as possible Hog1 substrates..... 37

Is GAPDH activity reduced *in vivo* in a Hog1-dependent manner under hyperosmotic stress..... 43

FRET analysis of GAPDHs during hyperosmotic shock..... 48

The NADH redox balance and glycerol production..... 59

Discussion..... 62

Chapter 3 Insulation, Not Cross-inhibition, Maintains Signaling Specificity between the HOG and Mating Pheromone Response Pathway..... 65

Introduction..... 65

Results..... 67

Construction of HOG and mating pathway reporters..... 67

Co-stimulation leads to co-activation of the HOG and mating MAPK pathways..... 70

Discrepancies between my data and previously published results..... 92

Crosstalk occurs from the HOG pathway to Fus3 in a Ste5 dependent manner..... 97

Toxicity associated with hyperosmotic shock and pheromone treatment..... 100

Using the dual fluorescent reporters and MAPK analog-sensitive alleles to investigate pathway specificity at the single-cell level..... 100

Discussion..... 111

Chapter 5 The Cdc42-GAP Rga1 is Required for HOG MAPK Pathway Insulation..... 113

Introduction..... 113

Results..... 116

Hog1-dependent phosphorylation of Ste50 is dispensable for crosstalk prevention..... 116

A genetic selection to identify potential substrates of Hog1 that prevent crosstalk to the mating pathway..... 116

Truncated alleles of *RGA1* result in *SHO1* dependent activation of the mating pathway..... 125

Rga1 is a negative regulator of Cdc42 in the context of the HOG pathway..... 140

Rga1 is a substrate of the Hog1 MAPK *in vitro*..... 143

The phosphorylation state of Rga1 changes during hyperosmotic shock *in vivo* 149
Hog1-mediated phosphorylation of the middle region of Rga1 is not sufficient for preventing crosstalk 150
Discussion 158
Chapter 6 Conclusions and Perspectives 161
HOG pathway dependent hyperosmotic stress resistance 161
Insulation of the HOG pathway 162
The Cdc42-GAP Rga1 contributes to HOG pathway insulation 162
Literature Cited 164

List of Tables

Table 2.1 Yeast Strains used in this study..... 15

Table 2.2 Plasmids used in this study..... 21

Table 5-1 The location and nature of *RGA1* mutants isolated..... 128

List of Figures

Figure 1-1 The HOG pathway and its response to hyperosmotic stress in *S. cerevisiae*..... 3

Figure 1-3 The mating MAPK pathway in S. cerevisiae..... 6

Figure 1-3 The filamentous/invasive growth MAPK pathway in *S. cerevisiae*..... 9

Figure 3-1 Microarray analysis of transcription in cells expressing plasma membrane tethered Hog1..... 35

Figure 3-2 The glycerol-3-phosphate shuttle and NAD+/NADH redox balance..... 38

Figure 3-3 Crystal structure of human liver GAPDH and the location of potential phosphophorylation sites..... 41

Figure 3-4 *In vitro* Hog1 kinase assay..... 44

Figure 3-5 Deletion of yeast GAPDHs increases hyperosmotic stress resistance, but is not sufficient to rescue the lack of *HOG1*..... 46

Figure 3-6 Serine 302 is important for yeast GAPDH function and reduced GAPDH function does not compromise hyperosmotic stress resistance..... 49

Figure 3-7 FRET analysis of GAPDH homotetramers during hyperosmotic shock..... 52

Figure 3-8 Changes in the Tdh3 FRET ratio during hyperosmotic shock are not entirely due to molecular crowding..... 55

Figure 3-9 Changes in the Tdh3 FRET ratio during hyperosmotic shock are not due direct phosphorylation by Hog1 but are correlated with glycerol production..... 57

Figure 3-10 Potential Hog1 consensus phosphorylation sites within the Por1 protein are not required for hyperosmotic stress resistance..... 60

Figure 4-1 Single-cell fluorescent reporters for the HOG and mating MAPK pathways..... 68

Figure 4-2 Dual stimulation results in dual activation of the transcriptional fluorescent reporters..... 71

Figure 4-3 Co-stimulation for 1 h results in co-activation of the HOG and mating pathway in single cells..... 73

Figure 4-4 Co-stimulation for 2 h results in co-activation of the HOG and mating pathway in single cells..... 75

Figure 4-5 Localization-specific reporters indicate insulation between MAPK pathways on the minute timescale..... 77

Figure 4-6 Flow cytometry confirms co-activation of MAPK pathways during co-

stimulation..... 80
Figure 4-7 The mating pathway does not inhibit the Sho1 branch of the HOG pathway during co-stimulation..... 82
Figure 4-8 The mating pathway does not inhibit the Sln1 branch of the HOG pathway during co-stimulation..... 84
Figure 4-9 The HOG pathway does not inhibit the Fus3 MAPK of the mating pathway during co-stimulation..... 86
Figure 4-10 The HOG pathway does not inhibit the Kss1 MAPK of the mating pathway during co-stimulation..... 88
Figure 4-11 Pre-activation of one MAPK pathway does not alter the response of subsequent stimulation of the other MAPK..... 90
Figure 4-12 Differences between my results and previously published observations are not due to any differences in genetic background or reporter construction..... 93
Figure 4-13 The combination of sonication and hyperosmotic shock results in cell death accompanied by an increase in auto-fluorescence..... 95
Figure 4-14 Cross-activation of the mating pathway during hyperosmotic stress in strains lacking *HOG1*..... 98
Figure 4-15 *FUS1* dependent toxicity associated with pheromone treatment in high osmolarity..... 101
Figure 4-16 Titration of 1-NM-PP1 during hyperosmotic stress in a *HOG1-AS* strain..... 104
Figure 4-17 Sustained Hog1 activity is required to prevent crosstalk to the mating pathway..... 106
Figure 4-18 Cross activation from the mating pathway to the HOG pathway does not occur in mating pathway mutants treated with pheromone..... 108
Figure 5-1 Hog1-dependent feedback phosphorylation of Pbs2 and Ste50 does not contribute to crosstalk prevention..... 117
Figure 5-2 Genetic selection to identify the substrate of Hog1 that prevents crosstalk..... 120
Figure 5-3 Characterization of mutants isolated by this genetic selection..... 123
Figure 5-4 FACS enrichment of complemented transformants..... 126
Figure 5-5 Domains and general structure of the confirmed Cdc42-GAPs..... 129
Figure 5-6 Rga1 truncations mutants result in crosstalk to the mating pathway..... 132
Figure 5-7 Rga1 and Rga2 work together to prevent mating pathway activation..... 136
Figure 5-8 Fus3 and Kss1 activation during hyperosmotic shock in *rga1*

mutants..... 138
Figure 5-9 Rga1 negatively regulates the Sho1 branch of the HOG pathway..... 141
Figure 5-10 Rga1 is required to complete the attenuation of Hog1 activation after hyperosmotic stress adaptation..... 144
Figure 5-11 Hog1 phosphorylates Rga1 *in vitro*..... 146
Figure 5-12 Phosphorylation state of HA-Rga1 changes *in vivo* during hyperosmotic shock in a Hog1-dependent manner..... 151
Figure 5-13 Resting state of HA-Rga1 phosphoprotein is due to phosphorylation of Thr541 by Cdc28..... 153
Figure 5-14 Hog1-mediated phosphorylation of the middle domain of Rga1 is not required for prevention of crosstalk..... 155

List of Abbreviations

aRNA	amino-allyl-UTP-containing anti-sense RNA
AS	Analog sensitive
CIP	Calf-intestinal phosphatase
DHAP	Dihydroxyacetone-phosphate
FG	Filamentous growth
FRET	Fluorescence-resonance energy transfer
GAP	GTPase activating protein
GAPDH	glyceraldehyde-3-phosphate dehydrogenases
GEF	Guanine nucleotide exchange factor
GPCR	G-protein-coupled receptor
GTPase	Guanosine tri-phosphatase
HOG	High-osmolarity glycerol
IP	Immunoprecipitation
MAPK	Mitogen-activated protein kinase
MAPKAPK	Mitogen-activated protein kinase-activated protein kinase
MAPKK	Mitogen-activated protein kinase kinase
MAPKKK	Mitogen-Activated Protein Kinase Kinase Kinase
PAGE	Polyacrylamide-gel electrophoresis
PAK	p21-Activated Kinase
SAM	Significance analysis of microarrays
SDS	sodium-dodecyl sulfate
SGD	*Saccharomyces cerevisiae* Genome Database
YPD	Yeast extract peptone dextrose

All other undefined abbreviations are accepted nomenclature of *The Journal of Biological Chemistry*.

Chapter 1
Introduction

Stress resistance and osmoregulation

Heraclitus, a Greek philosopher (circa 500 BC), based his entire ethos on the observation that the only constant in life is change. This insightful statement holds true at every scale — in our own lives, in the cosmos and in the hidden world of microorganisms. In their microscopic habitat, unicellular organisms are subjected to continual changes in temperature, nutrient sources, the types of predators and prey surrounding them, the amount of water present, the availability of potential mating partners, the presence of various toxins and the concentration of extracellular solutes. The ability to adapt to these changes is often a life or death situation. Therefore, organisms have evolved mechanisms, including complex signaling pathways, that allow them to sense change and respond appropriately to ensure their survival.

The presence of a high concentrations of an extracellular solute that cannot be readily equilibrated across the plasma membrane of a cell (external hyperosmolarity) presents a challenge to the viability of the cell by decreasing the internal specific water activity. Specific water activity is a measure of the ability of H_2O to interact with itself and cellular constituents in a solution (Gervais et al., 1992). When a solute is added to water, it occupies space that otherwise would be occupied by the water; this increases the disorder of the water, increasing the entropy of the system, and thus decreases the overall free energy. When a solution of high solute concentration has the chance to equilibrate with one at a lower concentration across a semi-permeable membrane, like the plasma membrane of a cell, a chemical potential is created. That is, if the concentration of solute outside the cell is greater than that within, entropy demands that what water is present in the cell be used to solvate and be dispersed among the extracellular solute molecules (Sweeney and Beuchat, 1993). This situation creates osmotic pressure that exerts force on the outside of the cell, squeezing the water out until the energy exerted as osmotic pressure is equal to the remaining difference in free energy between the solutions inside and outside the cell. Hyperosmolarity thus causes cells to shrink (plasmolysis) and, if not dealt with adequately, will lead to death. Moreover, organisms must continually create their own outward osmotic pressure, specifically called turgor pressure, which helps maintain the shape of the cell and allows for increases in volume during growth.

To respond to increases in external osmolarity, cells generally employ the strategy of increasing the concentration of an internal compatible solute. The accumulation of a solute within the cell balances the internal osmolyte concentration against that outside the cell. These solutes can be synthesized *de novo* or transported from the external medium and are described as compatible solutes because they can be accumulated at high concentrations without interfering with other cellular processes. Various compatible solutes utilized by different organisms include: amino acids (primarily proline or glutamate), quaternary amines (glycine betaine, carnatine), sugars (sucrose, trehalose) or polyols (glycerol, sorbitol) (Poolman and Glaasker, 1998). For instance, in the human renal medulla, cells accumulate sorbitol to balance their osmolarity and maintain their volume in the face of concentrated salts and urea in the external milieu (Burg and Kador, 1988).

The budding yeast *Saccharomyces cerevisiae* has evolved particularly sophisticated mechanisms for surviving extreme changes in solute concentration. In one of its natural environments, the surface of grapes, glucose concentrations can vary between 2% and 20% and change rapidly during development of the fruit of the grape and depend on temperature, relative

humidity and weather conditions (Coombe, 1987). During times of hyperosmotic stress, yeast cells accumulate glycerol by closing the aquaglyceroporin Fps1 and by synthesizing more glycerol from the glycolytic intermediate dihydroxyacetone-phosphate (DHAP). DHAP is reduced to glycerol-3-phosphate by two dehydrogenases (Gpd1 and Gpd2) and then phosphate is removed by two phosphatases (Gpp1 and Gpp2) (Nevoigt and Stahl, 2006). This increase in intracellular glycerol concentration is accomplished through the activation of the High Osmolarity Glycerol (HOG) Mitogen-Activated Protein Kinase (MAPK) pathway. Acute hyperosmotic stress also results in significant changes in transcript levels for ~2,000 genes, and ~500 of these genes are under the transcriptional control of the HOG pathway (O'Rourke and Herskowitz, 2004). These transcriptional changes are evoked not only by the hyperosmotic stress that elicits the HOG response, but also by a large number of disparate stresses and, hence, has been termed the Environmental Stress response (Gasch et al., 2000). All eukaryotes examined thus far have an orthologous pathway to the HOG pathway that can be activated by hyperosmotic and other (e.g. oxidative) stress. In yeast, activation of the HOG pathway is essential for survival and sustained growth in response to an increase in external osmolarity of 0.25 osmols or greater (Brewster et al., 1993; Pearson et al., 2001).

Structure and function of the HOG MAPK pathway

The HOG pathway responds to hyperosmotic stress and represents a well studied model for MAPK signal transduction (Figure 1-1). Like all MAPK pathways, it has at its core a three kinase cascade of the MAPK Kinase Kinase (MAPKKK), the MAPK Kinase (MAPKK) and MAPK. However, the HOG pathway is composed of two branches, each with its own MAPKKK(s) that converge on the MAPKK Pbs2, that in turn activates the MAPK Hog1 (Maeda et al., 1995). The Sho1 branch of the HOG pathway contains the putative osmosensor Sho1. The other branch of the HOG pathway, the Sln1 branch, has at its apex the putative osmosensor Sln1, which contains both a histidine kinase and receiver domain, similar to signal transducers found in prokaryotes. Under iso-osmotic conditions, Sln1 is an active kinase and auto-phosphorylates an Asp in its receiver domain. That phosphate is transferred to a His within the intermediate protein, Ypd1. Ypd1, in turn, transfers the phosphate to an Asp in the receiver domain of the regulatory protein, Ssk1. This overall phospho-relay system resembles the two-component signaling systems observed in bacteria. In its phosphorylated state, Ssk1 cannot productively interact with and activate two semi-redundant MAPKKKs, Ssk2 and Ssk22. However, in its unphosphorylated state, Ssk1 binds to and blocks the effect of N-terminal auto-inhibitory domains in Ssk2 and Ssk22, thus activating these MAPKKKs (Saito and Tatebayashi, 2004). Hyperosmotic conditions somehow inactivate the Sln1 kinase, increasing the amount of unphosphorylated Ssk1, thus activating Ssk2 and Ssk22, which then phosphorylate and activate Pbs2 and, in turn, Hog1 (Posas et al., 1996).

The Sho1 branch of the HOG pathway contains a handful of transmembrane proteins that coalesce around the four-pass transmembrane protein Sho1. Two single-pass transmembrane proteins, Msb2 and Hkr1, that resemble mammalian mucins associate with Sho1 during hyperosmotic stress and purportedly bind the GTPase Cdc42 in its GTP-bound state (O'Rourke and Herskowitz, 2002; Tatebayashi et al., 2007). Another single-pass transmembrane protein Opy2 binds the Ste50 adapter protein (Wu et al., 2006). Ste50 is tightly bound to and essentially a non-catalytic subunit of the MAPKKK Ste11, and when brought to the membrane via interactions with Sho1 and Opy2 then interacts with Cdc42 as well (Tatebayashi et al., 2006; Truckses et al., 2006). Ste20, a p21-activated kinase (PAK), is stimulated by Cdc42-GTP (the p21 in this instance) and phosphorylates Ste11 (Raitt et al., 2000). Ste11 then phosphorylates

Figure 1-1. The HOG pathway and its response to hyperosmotic stress in *S. cerevisiae*

Components of the HOG pathway are either blue or red. Proteins colored red are shared between the HOG, mating and FG pathways. Transcription factors and chromatin-remodeling proteins are in green and yellow proteins are substrates of Hog1 or proteins related to the adaptation process. Hyperosmotic shock is initiated by high concentrations of osmolytes outside the cell; sorbitol is used as an example in this schematic. Upon hyperosmotic shock, the HOG pathway is activated resulting in dually phosphorylated Hog1 (red "lollipops"). Red "X"'s indicate protein activities that are inhibited during hyperosmotic stress. Hog1 is then transported into the nucleus through the nuclear pore complex, which is accomplished by an interaction with the karyopherin Nmd5. Genes that contain stress response elements (STRE) in their promoters are transcriptionally induced. The accumulation of glycerol in the cytoplasm is one of the important outcomes of HOG pathway activation.

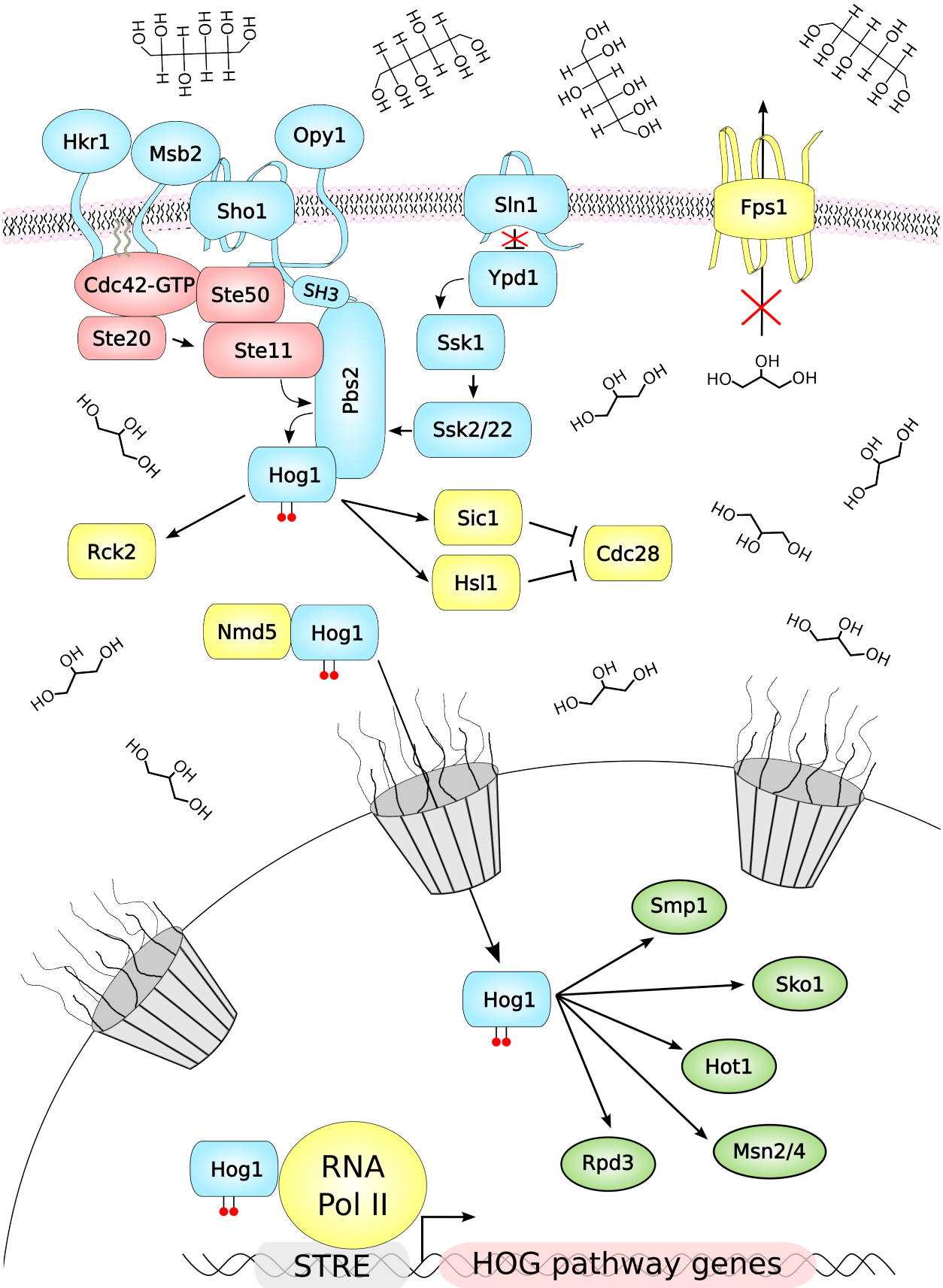
Hkr1
Msb2
Opy1
Sho1
Sln1
Fps1
Cdc42-GTP
Ste50
SH3
Ypd1
Ste20
Ste11
Pbs2
Ssk1
Ssk2/22
Hog1
Rck2
Sic1
Hsl1
Cdc28
Nmd5
Hog1
Smp1
Hog1
Sko1
Hot1
Msn2/4
Rpd3
Hog1
RNA
Pol II
STRE
HOG pathway genes

and activates the MAPKK Pbs2 (Posas and Saito, 1997). Sho1 and Pbs2 act as co-scaffolds in this pathway. The C-terminal SH3 domain of Sho1 binds a proline-rich sequence in the N-terminus of Pbs2. The MAPKKK Ste11 and the MAPK Hog1also bind Pbs2 (Posas and Saito, 1997). Both Sln1 and Sho1 have been called "putative osmosensors," mainly due to their upstream position in their respective branches. However, there is yet no biophysical evidence to support the notion that either proteins, or any other protein currently known to be involved in the HOG pathway, directly detects changes in extracellular osmolarity.

Hog1 is active only after it has been phosphorylated on Thr174 and Tyr176 within its activation loop by Pbs2 (Jacoby et al., 1997). Once activated, Hog1 rapidly translocates into the nucleus via the karyopherin Nmd5 (Ferrigno et al., 1998). In the nucleus, Hog1 phosphorylates the transcription factors Msn1, Msn2/Msn4, Sko1 and Smp1, as well as the histone deacetylase Rpd3 (Westfall et al., 2004; De Nadal et al., 2004). Hog1 also directly interacts with RNA polymerase II at some promoters and reportedly occupies the coding regions of certain genes (Pokholok et al., 2006; Pascual-Ahuir et al., 2006). Other demonstrated targets of Hog1 include: a mitogen-activated protein kinase activated protein kinase (MAPKAPK), Rck2; solute transporters, Fps1, Nha1 and Tok1; metabolic enzymes, Tdh3, Shm2 and Krs1; a chaperone, Hsp26; components of the HOG pathway itself, namely Ste50 and Sho1; and cell cycle checkpoint proteins, Sic1 and Hsl1 (Thorsen et al., 2006; Kim and Shah, 2007; Hao et al., 2007, 2008; Clotet et al., 2006). Sic1 is a cyclin-dependent kinase (CDK) inhibitor, which specifically inhibits the Cdc28 CDK in the G1 phase of the cell cycle. Hog1 phosphorylation of Sic1 prevents its proteosome-mediated degradation and induces cell cycle arrest (Escote et al., 2004). Hog1-mediated phosphorylation of Hsl1 blocks its role in down regulating Swe1, causing accumulation of Swe1, which is a kinase that inhibits Clb-bound Cdc28, thereby arresting cell cycle progression in G2 phase (Clotet et al., 2006; Escote et al., 2004).

The levels of dually phosphorylated Hog1 peak at 5 min after hyperosmotic shock then gradually decrease for a period of 45 min. However, even after adaptation to increased levels of extracellular osmolarity (post 60 min and beyond), the amount of dually phosphorylated Hog1 remains elevated at ~10% of its peak level relative to the pre-shock basal activation. Inactivation of Hog1 in the nucleus is accomplished by two protein-tyrosine phosphatase Ptp2 and Ptp3 and in the cytosol and at the plasma membrane by Type 2C Ser/Thr phosphatases Ptc1, Ptc2 and Ptc3 (Jacoby et al., 1997; Mapes and Ota, 2004; Wurgler-Murphy et al., 1997).

The mating MAPK pathway in yeast

During its life cycle, *Saccharomyces cerevisiae* cells can exist in both haploid and diploid state. There are two haploid mating types called *MAT***a** and *MAT*α. When any two yeast cells of opposite mating type come in contact with each other they differentiate into a pear shaped cell type known as a shmoo (based on the resemblance of its shape to a cartoon character). The *MAT***a** and *MAT*α shmoos undergo cellular conjugation and nuclear fusion creating a diploid zygote, which then can produce more diploid cells. Under conditions of nitrogen deprivation, diploids will undergo meiosis and sporulate, ultimately forming four haploid spores (Chen and Thorner, 2007).

Haploid cells communicate with each other during the mating process using small peptide pheromones that bind to G-protein-coupled receptors (GPCRs) at the head of the mating MAPK pathway (Figure 1-2). *MAT***a** cells secrete **a**-factor which binds to the GPCR Ste3 on α cells. *MAT*α cells secrete α-factor which binds to the GPCR Ste2 on **a** cells. Aside from the pheromones and the receptors, the other components of this signaling pathway are the same in *MAT***a** and *MAT*α cells (Chen and Thorner, 2007).

Figure 1-2. The mating MAPK pathway in *S. cerevisiae*

Components of the mating pathway are either blue or red. Proteins colored red are shared between the HOG, mating and FG pathways. Transcription factors are in green and yellow proteins are other substrates of Fus3 or Kss1, or are proteins related to the output of the mating pathway. The mating pathway is stimulated by peptide pheromenes binding to their cognate GPCR. The situation for *MAT***a** cells is depicted in this figure, where α-factor pheromone, produced by a *MAT*α cells, would bind to the Ste2 GPCR expressed by a *MAT***a** cell. In *MAT*α cells, **a**-factor binds to the Ste3 GPCR. Tec1 is a transcription factor used in the filamentous growth pathway, in that pathway it interacts with Ste12 and binds to a distinct set of promoters than those activated during mating. To prevent Kss1-dependent filamentous growth, Fus3 initiates the ubiquitinylation and subsequent proteasome-mediated degradation of the Tec1 transcription factor.

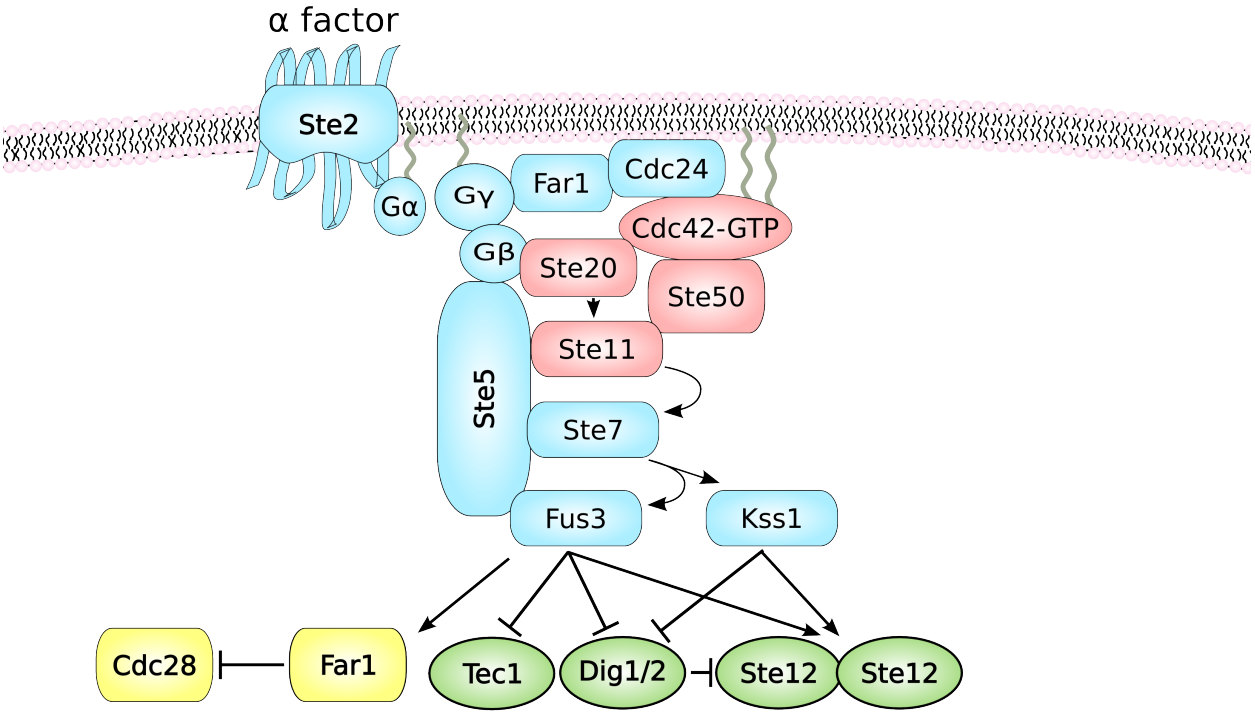
α factor
Ste2
Gα
Gγ
Gβ
Far1
Cdc24
Cdc42-GTP
Ste20
Ste50
Ste11
Ste5
Ste7
Fus3
Kss1
Cdc28
Far1
Tec1
Dig1/2
Ste12
Ste12

Prior to stimulation GPCRs are associated with three G-protein subunits referred to as the Gα, Gβ and Gγ subunits, which in yeast are encoded by *GPA1*, *STE4* and *STE18*, respectively. Upon ligand binding, the GPCR acts as a guanine nucleotide exchange factor (GEF) and stimulates the release of GDP from Gα followed by its binding GTP. Gα-GTP releases the Gβ-Gγ complex, which are invariably bound to each other. Upon their release Gβ and Gγ bind several proteins to initiate the signaling cascade (Wang and Dohlman, 2004). Gβγ binds Far1, which in this context acts as an adapter to deliver the activator of Cdc42, the GEF Cdc24, to the plasma membrane (Butty et al., 1998). Gβγ also brings the PAK Ste20 to the membrane, so that it can be activated by Cdc42-GTP, and the scaffold protein for the mating pathway Ste5. The Ste50-Ste11 heterodimer binds both Cdc42 and Ste5, an interaction that permits Ste11 phosphorylation and activation by Ste20. Ste5 membrane localization is due not only to its association with Gβγ, but it also has a PtdIns(4,5)P_2-binding pleckstrin-homology (PH) domain and membrane associating N-terminal amphipathic helix (Garrenton et al., 2006). The MAPKK Ste7 and one of the two MAPKs, Fus3, also bind to the Ste5 scaffold and are sequentially activated. A second MAPK, Kss1, is activated by this pathway, however, it does not bind Ste5 and is only weakly and transiently activated during pheromone treatment (Chen and Thorner, 2007). The entire list of substrates phosphorylated by Fus3 and Kss1 that are relevant for shmoo formation and mating is not known. However, both MAPKs phosphorylate the Dig1 and Dig2 repressors of the transcription factor Ste12, as well as Ste12 itself (Roberts and Fink, 1994; Cook et al., 1996; Tedford et al., 1997). Fus3 alone phosphorylates the CDK inhibitor Far1, which causes cell cycle arrest in G1 phase (Peter et al., 1993; Chen et al., 2010).

It is important for cells to mate only during G1 phase of the cell cycle. If, for instance, a halpoid in G1 were to mate with another haploid in G2 phase the resulting zygote would be a triploid which, although viable, cannot produce viable spores after meiosis. In order to prevent this disastrous situation, Ste5 is only present and competent to act as a scaffold during the G1 phase of the cell cycle. During other stages of the cell cycle Ste5 resides in the nucleus where it is degraded (Garrenton et al., 2009). Moreover, Cdc28 phosphorylation of the N-terminal amphipathic helix of Ste5 that usually associates with the plasma membrane renders it negatively charged and unable to associate with phospholipids (Garrenton et al., 2009; Strickfaden et al., 2007).

The filamentous growth pathway in yeast

A third MAPK pathway in yeast responds to specific nutrient deprivation (Figure 1-3). When a haploid cell is limited for glucose or a diploid cell is without a suitable nitrogen source it will change its morphology, physiology and budding pattern. Haploid cells display invasive growth and diploids exhibit psuedohyphal growth, respectively. Because yeast cells are non-motile, they cannot move to find fresh nutrients. Hence, the filamentous growth (FG) MAPK response is thought to represent an alternative mechanism that permits the cells to forage for new nutrient sources. Although haploid and diploids respond to different stimuli and yield distinct outcomes, these responses are mediated by the same MAPK pathway and result in a filamentous growth pattern (Cook et al., 1997). The FG pathway is less well understood than the HOG or mating MAPK pathways, however, it is clear that both Sho1 and Msb2 are involved (Cullen et al., 2004). Moreover, the pathway is activated at least in part through the removal of the highly glycosylated extracellular domain of Msb2. One way this cleavage is accomplished is by Yps1, a yapsin protease. Yapsins are glycosylphosphatidylinositol anchored aspartic proteases that cleave proteins C-terminal to basic residues. Yps1 production is induced during nutrient starvation, thus leading to Msb2 cleavage and FG pathway activation (Vadaie et al., 2008).

Figure 1-3. The filamentous/invasive growth MAPK pathway in *S. cerevisiae*

Components of the filamentous pathway are either blue or red. Proteins colored red are shared between the HOG, mating and filamentous growth pathways. Transcription factors are in green. The filamentous growth pathway is activated in response to nutrient starvation, however, the exact mechanism that controls the activation of this pathway is not known. It is known that the pathway is initiated in part by Yps1-dependent cleavage of the heavily-glycosylated extracellular domain of Msb2. Ste12 and Tec1 form a heterodimeric transcription factor that binds to a different set of promoters than does Ste12-Ste12 homodimer in the mating pathway. Activation of this pathway results in pseudohyphal or invasive growth as a foraging strategy to acquire additional nutrients.

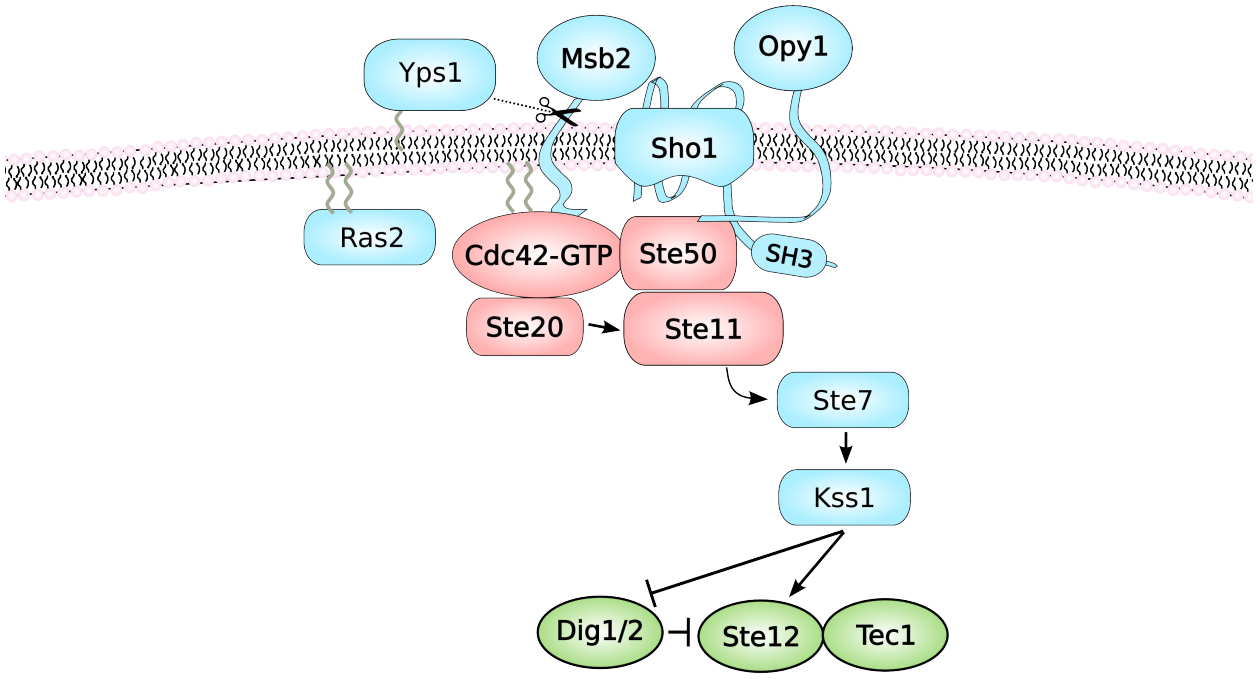
Yps1
Msb2
Opy1
Sho1
Ras2
Cdc42-GTP
Ste50
SH3
Ste20
Ste11
Ste7
Kss1
Dig1/2
Ste12
Tec1

In this pathway, Msb2 binds Cdc42 and Sho1, while Sho1 binds the Ste50-Ste11 dimer brought to the membrane through interaction with Opy2 (Yamamoto et al., 2010). Another GTPase, Ras2 is required for Cdc42 to function in this pathway for reasons that are not well understood (Mösch et al., 1996). Cdc42 then activates Ste20, which phosphorylates the MAPKKK Ste11, which in turn activates the MAPKK Ste7. Kss1 is the sole MAPK in this pathway, and its target repressors (Dig1 and Dig2) of the heterodimeric transcription factor Ste12 and Tec1, and activates Ste12 itself (Madhani and Fink, 1997; Bardwell et al., 1998).

Crosstalk between MAPK pathways

These three MAPK pathways have a special relationship with each other in that they all share common signaling proteins. A core module of Cdc42, Ste20, Ste50 and Ste11 are involved in all three, and when compared pairwise there is even more redundancy. For example, the mating and FG pathways both utilize Ste7 as the sole MAPKK. Despite the potential for cross-activation of one pathway by the other (crosstalk), stimulation of any one of the pathways results only in the appropriate response. The means by which this fidelity is imposed is known in some cases. For example, during mating pathway activation, Fus3 initiates the degradation of the Tec1 transcription factor (Chou et al., 2004). The Tec1-Ste12 heterodimer binds to different promoters than Ste12 binds on its own; therefore, despite Kss1 activation by the mating pathway, only mating pathway genes are expressed. Conversely, Ste7 does not phosphorylate Fus3 during filamentous growth pathway activation because Fus3 is only a good substrate for Ste7 when it is bound to Ste5 (Good et al., 2009).

The mechanisms that determine signaling specificity in the HOG pathway, however, are not known. It has been shown that yeast strains that lack either *HOG1* or *PBS2* will inappropriately activate both the mating and filamentous growth MAPK pathways during times of hyperosmotic stress (O'Rourke and Herskowitz, 1998). Because acutely inhibiting the kinase activity of Hog1 analog-sensitive (AS) allele during HOG pathway stimulation leads to activation of the mating pathway, it is believed that an unidentified Hog1 substrate(s) prevents crosstalk during hyperosmotic stress (Westfall and Thorner, 2006).

Overview of this thesis

The HOG pathway is a very well studied model for MAPK signaling. Despite extensive knowledge of the pathway, some very basic questions remain. The work presented in this thesis describes my interrogation of two functions that Hog1 is known to participate in, but for which the molecular details were obscure. The first was to determine exactly how Hog1 confers hyperosmotic stress resistance, particularly by identifying the substrate(s) that carry out this function. This insight is fundamental to the HOG pathway, yet only partially understood. The second goal of this thesis was to determine the mechanism by which crosstalk is prevented, which is related to more general signaling phenomena, because the question of how specificity is imposed is common to many signal transduction pathways. All three MAPK pathways described above are conserved from yeast to humans to varying extents. Despite hundreds of millions of years of evolution, Hog1 shares 52% sequence identity with its human ortholog p38α. Moreover, p38α expressed in a yeast strain lacking *HOG1* rescues the hyperosmotic stress sensitivity of those cells (Han et al., 1994). Similarly, Fus3 and Kss1 share 50% sequence identity with their mammalian cousins, ERK1 and ERK2, respectively. Yeast and human Cdc42 share 80% sequence identity. Understanding how yeast accomplishes signaling specificity among pathways sharing signaling components may shed light on how human MAPK pathways deal with their redundancy and interconnectedness.

Chapter 3 is related to the question of how Hog1 contributes to hyperosmotic stress resistance. When I began this work, Patrick Westfall, a postdoctoratal researcher in the Thorner laboratory, realized that the accepted paradigm for hyperosmotic stress resistance in yeast was fraught with assumptions. Specifically, all or most of the attention on hyperosmotic stress resistance up until that point was focused on the transcriptional output of HOG pathway.

Patrick demonstrated that nuclear entry of Hog1 during hyperosmotic shock was not necessary for stress resistance. Because the majority of the transcription factors activated (or repressors inactivated) by Hog1 reside in the nucleus, this result raised the question as to whether HOG pathway-dependent transcription was actually important for adaptation. Using global microarray analysis, I found that when Hog1 was prevented from entering the nucleus the vast majority of HOG dependent transcription was not elicited, yet the cells survived, confirming our suspicion that HOG pathway transcription was dispensable for stress resistance. If transcription was not necessary for producing factors that confer stress resistance, what was? Prior work and our own studies demonstrated that glycerol production through glycerol-3-phosphate dehydrogenase Gpd1 was necessary, however, this enzyme lacks any potential Hog1 consensus phosphorylation sites (-SP- or -TP-).

Therefore, I began a search for Hog1 substrates that when phosphorylated might lead to an increase in intracellular glycerol concentration. Much of my work focused on the three glyceraldehyde-3-phosphate dehydrogenases (GAPDH), encoded by *TDH1*, *TDH2* and *TDH3*, which, if inhibited by Hog1, might shunt more triose-phosphate toward glycerol production. Interestingly, Tdh3 has been reported to be a substrate of Hog1, however, this observation was not pursued further (Kim and Shah, 2007). Although I found that reducing GAPDH function did increase hyperosmotic stress resistance, I was unable to confirm that Tdh3 (or Tdh2 and Tdh1) were substrates of Hog1 *in vitro*. Nor did eliminating the potential Hog1 phosphorylation sites in these enzymes lead to a decrease in hyperosmotic stress resistance. Because Gpd1 oxidizes NADH to NAD+ stoichiometrically for each molecule of glycerol produced, I looked into potential Hog1 substrates that might increase the cytoplasmic NADH/NAD+ ratio. In particular, I reasoned that Hog1 dependent inhibition of the mitochondrial voltage-dependent-anion channel (VDAC) Por1, which is responsible for passage of NADH through the outer membrane of the mitochondrion, might elevate cytosolic NADH. While this search was to no avail, I did succeed in ruling out several potential substrates, narrowing down the extensive list of possibilities.

The second goal of my dissertation research was to identify the substrates that might contribute to preventing crosstalk between the HOG and mating (and FG) pathways, and to uncover the mechanism of this crosstalk inhibition. Chapter 4 describes my work to determine the general mode of crosstalk prevention. My results distinguished between two possible mechanisms: pathway insulation or cross-pathway inhibition. If the HOG pathway is insulated from the mating pathway, then any Ste11 activated in the Sho1 branch would be unable to activate the mating pathway. Whereas, in cross-pathway inhibition, Hog1 action prevents the activation of the mating pathway by directly inhibiting a component of the mating pathway, thereby blocking any output. To address these possibilities, I introduced into a *MAT***a** strain fluorescent reporters that allowed assessment of both the HOG and mating pathway. I found that under a variety of stimulant concentrations and temporal regimes, co-stimulation lead to activation of both pathways, indicating that there is no cross-pathway inhibition, thereby supporting the conclusion that crosstalk prevention is accomplished by an insulatory mechanism. This situation contrasts to the ability of activated Fus3 to initiate the degradation of the Tec1 transcription factor required for FG, thereby blocking any transcriptional output of the FG pathway.

Chapter 5 describes a genetic selection I carried out with the assistance of an undergraduate honors student, Louise Goupil, that was aimed at applying an unbiased approach toward identifying genes required for HOG pathway signaling fidelity. The selection was designed to permit the growth of mutants able to activate the mating pathway during hyperosmotic stress and to do so in a manner that depended on an intact Sho1 branch of the HOG pathway. Using this approach we identified multiple different truncated alleles of the Cdc42-GAP *RGA1*. Rga1 negatively regulates Cdc42, a component of both the HOG and mating pathways. These *rga1* alleles lead to constitutive mating pathway activation that is further increased, albeit only modestly, upon hyperosmotic challenge. These mutants also exhibited increased basal Kss1 activation, which increased substantially during hyperosmotic stress. I was able to show that Rga1 is a substrate of Hog1 *in vitro*, and that its electrophorectic mobility changes during hyperosmotic stress in a Hog1 and phosphatase-sensitive manner, an indication of *in vivo* phosphorylation. *RGA1* deletions and truncated alleles also lead to hyperstimulation of the HOG response during hyperosmotic stress, as judged by the level of Hog1 activation. These data suggest a model where during hyperosmotic stress, Hog1 directs Rga1 to down regulate the Cdc42 activated by the Sho1 branch of the HOG pathway, and that it is the precise control of the intensity and duration of Cdc42 activation that prevents inappropriate activation of the mating pathway. At the end of this thesis, Chapter 6 discusses these results and conclusions in a broader context of signaling and stress response.

Chapter 2
Materials and Methods

Yeast strains and growth conditions

Saccharomyces cerevisiae strains used and constructed in this study are listed in Table 2-1. Genetic manipulations were accomplished using standard genetic and molecular biology methods (Hicks et al., 1987; Sambrook and Russell, 2001). Moreover, essentially all haploid strains were derived from diploid mutants by sporulation and tetrad dissection to ensure proper segregation of markers and viability. Diploids strain were mutated directly or constructed by crossing the genetic alteration into the desired background. Unless otherwise noted, deletion alleles were constructed by polymerase chain reaction (PCR) amplification of the given genetic marker using primers that contained 45 base pairs (bp) of homology to the sequences flanking the coding region upstream and downstream. Prototrophic markers including *C.g.HIS3*, *C.g.LEU2* and *C.g.TRP1* were amplified from pCgH, pCgL and pCgW, respectively (Kitada et al., 1995). These markers contain the *Candida glabrata* orthologs of the respective *S. cerevisiae* genes to minimize recombination at sites other then the desired deletion locus. The geneticin, ClonNAT and hygromycin drug resistance markers were amplified from pRS306K, pRS306N and pRS306H respectively (Taxis and Knop, 2006). Point mutants were integrated either by directly replacing the wild-type allele or by integrating a plasmid containing a mutant allele into the gene's promoter in a strain where the coding sequence had been deleted.

Table 2.1 Yeast Strains used in this study

Strain	Relevant Genotype	Source or reference
BY4741	*MAT***a** *his3Δ1 leu2Δ0 met15Δ0 ura3Δ0*	Brachmann et al., 1998
BY4742	*MAT*α *his3Δ1 leu2Δ0 lys2Δ0 ura3Δ0*	Brachmann et al., 1998
BY4743	*MAT***a**/*MAT*α (BY4741 x BY4742)	Brachmann et al., 1998
YPH499	*MAT***a** *ura3-52 lys2-801 ade2-101 trp1-Δ63 his3-Δ200 leu2-Δ1*	Sikorski and Hieter, 1989
YPH500	*MAT*α *ura3-52 lys2-801 ade2-101 trp1-Δ63 his3-Δ200 leu2-Δ1*	Sikorski and Hieter, 1989
EG123	*MAT***a** *ura3 trp1 his4 can1*	O'Rourke and Herskowitz, 1998
∑1278b	*MAT***a** *ura3-52 trp1Δ63 his3Δ200*	Gimeno et al., 1992
YJP67	YPH499 *tdh3-S302A*::*URA3*	This study
YJP68	YPH499 *tdh2-S302A*::*TRP1*	This study
YJP73	YPH499 $STL1_{prom}$::HA-tdtomato::*leu2*::*ADE2* $FUS1_{prom}$::HA-eGFP::*leu2*::*ADE2*	This study
YJP115	BY4743 *TDH3*-Ypet::kanMX4/*TDH3*-Cypet::kanMX4	This study
YJP123	YPH499 $STL1_{prom}$::HA-tdtomato::*leu2*::*ADE2* $FUS1_{prom}$::HA-eGFP::*leu2*::*ADE2 HOG1-AS*::hphNT1	This study
YJP126	BY4743 *TDH3*-Ypet::kanMX4/*TDH3*	This study
YJP129	BY4743 *TDH3*-Cypet::kanMX4/*TDH3*	This study
YJP131	YPH499 $STL1_{prom}$::HA-tdtomato::*leu2*::*ADE2* $FUS1_{prom}$::HA-eGFP::*leu2*::*ADE2 hog1*::hphNT1	This study
YJP141	BY4743 *TPI1*-Ypet::kanMX4/*TPI1HOG1-AS*::hphNT1	This study
YJP142	BY4743 *TPI1*-Cypet::kanMX4/*TPI1*	This study
YJP143	BY4743 *TPI1*-Ypet::kanMX4/*TPI1*-Cypet::kanMX4	This study
YJP148	BY4743 *TDH3*-Ypet::kanMX4/*TDH3*-Cypet::kanMX4 *hog1*::hphNT1/*hog1*::hphNT1	This study
YJP151	YPH499 *tdh1*::*C.g.HIS3 tdh2*::*C.g.TRP1*	This study
YJP155	YPH499 *tdh1*::*C.g.HIS3 tdh3*::*C.g.LEU2*	This study
YJP156	YPH499 *tdh2*::*C.g.TRP1 tdh3*::*C.g.LEU2*	This study
YJP157	YPH499 *tdh1*::*C.g.HIS3 tdh2*::*C.g.TRP1 hog1*::kanMX4	This study
YJP158	YPH499 *tdh1*::*C.g.HIS3 tdh3*::*C.g.LEU2 hog1*::kanMX4	This study

YJP159	YPH499 *tdh2*::*C.g.TRP1 tdh3*::*C.g.LEU2 hog1*::kanMX4	This study
YJP163	YPH499 *tdh1*::*C.g.HIS3 tdh2*::*C.g.TRP1 hog1*::kanMX4 *far1-T306A*::hphNT1	This study
YJP164	YPH499 *tdh1*::*C.g.HIS3 tdh3*::*C.g.LEU2 hog1*::kanMX4 *far1-T306A*::hphNT1	This study
YJP165	YPH499 *tdh2*::*C.g.TRP1 tdh3*::*C.g.LEU2 hog1*::kanMX4 *far1-T306A*::hphNT1	This study
YJP166	YPH499 *hog1*::kanMX4	This study
YJP184	YPH499 *tdh1-T139A-S302A*::*LEU2 tdh2-S302A*::*TRP1 HOG1-GFP-CCaaX*^{Ras2}::hphNT1	This study
YJP185	YPH499 *tdh1-T139A-S302A*::*LEU2 tdh3-S302A*::*URA3 HOG1-GFP-CCaaX*^{Ras2}::hphNT1	This study
YJP186	YPH499 *tdh2-S302A::TRP1 tdh3-S302A*::*URA3 HOG1-GFP-CCaaX*^{Ras2}::hphNT1	This study
YJP187	YPH499 *tdh1-T139A-S302A*::*LEU2 tdh2-S302A*::*TRP1 tdh3-S302A*::*URA3 HOG1-GFP-CCaaX*^{Ras2}::hphNT1	This study
YJP212	YPH499 *STL1*$_{prom}$::HA-tdtomato::*leu2*::*ADE2 FUS1*$_{prom}$::HA-eGFP::*leu2*::*ADE2 bar1*::kanMX4	This study
YJP213	YPH499 *STL1*$_{prom}$::HA-tdtomato::*leu2*::*ADE2 FUS1*$_{prom}$::HA-eGFP::*leu2*::*ADE2 bar1*::kanMX4 *HOG1-AS:*:hphNT1	This study
YJP226	YPH499 *STL1*$_{prom}$::HA-tdtomato::*leu2*::*ADE2 FUS1*$_{prom}$::HA-eGFP::*leu2*::*ADE2 HOG1-AS:*:hphNT1 *ssk1*::*C.g.TRP1*	This study
YJP253	BY4743 *TDH3*-Ypet::kanMX4/*TDH3* [YCplac111-*TDH3*-Ypet]	This study
YJP254	BY4743 *TDH3*-Cypet::kanMX4/*TDH3* [YCplac33-*TDH3*-Cypet]	This study
YJP255	BY4743 *TDH3*-Ypet::kanMX4/ *TDH3-Cypet::kanMX4* [YCplac111-*TDH3*-Ypet] [YCplac33-*TDH3*-Cypet]	This study
YJP256	BY4743 *TDH3*-Ypet::kanMX4/ *TDH3-Cypet::kanMX4 hog1:*:hphNT1/*hog1:*:hphNT1 [YCplac111-*TDH3*-Ypet] [YCplac33-*TDH3*-Cypet]	This study
YJP274	BY4743 *tdh3*::*C.g.HIS3*/*tdh3*::*C.g.HIS3* [YCplac33] [YCplac111]	This study
YJP275	BY4743 *tdh3*::*C.g.HIS3*/*tdh3*::*C.g.HIS3* [YCCplac33] [YCplac111-*TDH3*-Ypet]	This study
YJP276	BY4743 *tdh3*::*C.g.HIS3*/*tdh3*::*C.g.HIS3* [YCplac33] [YCplac111-*TDH3-S302N*-Ypet]	This study
YJP277	BY4743 *tdh3*::*C.g.HIS3*/*tdh3*::*C.g.HIS3* [YCplac33-*TDH3*-Cypet] [YCplac111]	This study

YJP278	BY4743 *tdh3*::*C.g.HIS3*/*tdh3*::*C.g.HIS3* [YCplac33-*TDH3*-Cypet] [YCplac111-*TDH3*-Ypet]	This study
YJP280	BY4743 *tdh3*::*C.g.HIS3*/*tdh3*::*C.g.HIS3* [YCplac33-*TDH3*-*S302N*-Cypet] [YCplac111]	This study
YJP282	BY4743 *tdh3*::*C.g.HIS3*/*tdh3*::*C.g.HIS3* [YCplac33-*TDH3*-*S302N*-Cypet] [YCplac111-*TDH3*-*S302N*-Ypet]	This study
YJP295	BY4743 *TDH3*-Ypet::kanMX4/*TDH3*-Cypet::kanMX4 *gpd1*::*C.g.LEU2*/ *gpd1*::*C.g.LEU2*	This study
YJP301	YPH499 $STL1_{prom}$::HA-tdtomato::*leu2*::*ADE2* $FUS1_{prom}$::HA-eGFP::*leu2*::*ADE2* *hog1*::hphNT1 *kss1*::*C.g.HIS3*	This study
YJP308	YPH499 $STL1_{prom}$::HA-tdtomato::*leu2*::*ADE2* $FUS1_{prom}$::HA-eGFP::*leu2*::*ADE2* *HOG1-AS*::hphNT1 *bar1*::kanMX4 *kss1*::*C.g.HIS3 fus3*::*C.g.TRP1*	This study
YJP313	YPH499 $STL1_{prom}$::HA-tdtomato::*leu2*::*ADE2* $FUS1_{prom}$::HA-eGFP::*leu2*::*ADE2* *HOG1-AS*::hphNT1 *bar1*::kanMX4 *kss1*::*C.g.HIS3*	This study
YJP334	YPH499 $STL1_{prom}$::HA-tdtomato::*leu2*::*ADE2* $FUS1_{prom}$::HA-eGFP::*leu2*::*ADE2 bar1*::kanMX4 *KSS1-AS*::*LEU2 FUS3-AS*::*LEU2*	This study
YJP336	YPH499 $STL1_{prom}$::HA-tdtomato::*leu2*::*ADE2* $FUS1_{prom}$::HA-eGFP::*leu2*::*ADE2* *HOG1-AS*::hphNT1 *bar1*::kanMX4 *fus3*::*C.g.TRP1*	This study
YJP385	YPH499 $STL1_{prom}$::HA-tdtomato::*leu2*::*ADE2* $FUS1_{prom}$::HA-eGFP::*leu2*::*ADE2* *bar1*::kanMX4 *fus1*::*C.g.LEU2*	This study
YJP387	YPH499 $STL1_{prom}$::HA-tdtomato::*leu2*::*ADE2* $FUS1_{prom}$::HA-eGFP::*leu2*::*ADE2 HOG1-AS*::hphNT1 *bar1*::kanMX4 *kss1*::*C.g.HIS3 fus3*::*C.g.TRP1 fus1*::*C.g.LEU2*	This study
YJP390	YPH499 $STL1_{prom}$::HA-tdtomato::*leu2*::*ADE2* $FUS1_{prom}$::HA-eGFP::*leu2*::*ADE2* *HOG1-AS*::hphNT1 *bar1*::kanMX4 *kss1*::*C.g.HIS3 fus3*::*C.g.TRP1 fus1*::*C.g.LEU2 ssk1*::*C.g.URA3*	This study
YJP394	YPH499 $STL1_{prom}$::HA-tdtomato::*leu2*::*ADE2* $FUS1_{prom}$::HA-eGFP::*leu2*::*ADE2* *HOG1-AS*::hphNT1 *HOG1-AS*::*PBS2*::*LEU2 far1-T306A*::hphNT1 $FUS1_{prom}$::*HIS3*::*ura3*::*LYS2 sho1*::hphNT1 *kss1*::*C.g.LEU2* [pRS316-SHO1]	This study
YJP406	YPH499 $STL1_{prom}$::HA-tdtomato::*leu2*::*ADE2* $FUS1_{prom}$::HA-eGFP::*leu2*::*ADE2 bar1*::kanMX4 *ssk1*::*C.g.TRP1*	This study
YJP407	YPH499 $STL1_{prom}$::HA-tdtomato::*leu2*::*ADE2* $FUS1_{prom}$::HA-eGFP::*leu2*::*ADE2 bar1*::kanMX4 *ssk1*::hphNT1	This study

YJP413	BY4741 *bar1*::kanMX4 HOG1-td-tomato::HIS3 ste5::C.g.LEU2 [pRS316-STE5-3XGFP]	This study
YJP455	YPH499 *STL1$_{prom}$*::HA-tdtomato::*leu2*::*ADE2 FUS1$_{prom}$*::HA-eGFP::*leu2*::*ADE2 bar1*::kanMX4 *HOG1-AS:*:hphNT1 *pbs2*::*C.g.HIS3* [YCplac33 *PBS2-6A*]	This study
YJP490	YPH499 *STL1$_{prom}$*::HA-tdtomato::*leu2*::*ADE2 FUS1$_{prom}$*::HA-eGFP::*leu2*::*ADE2 bar1*::kanMX4 *HOG1-AS:*:hphNT1 *ste50*::*C.g.TRP1*::*STE50-5A*::*URA3*	This study
YJP495	YPH499 *STL1$_{prom}$*::HA-tdtomato::*leu2*::*ADE2 FUS1$_{prom}$*::HA-eGFP::*leu2*::*ADE2 bar1*::kanMX4 *HOG1-AS:*:hphNT1 *ste50*::*C.g.TRP1*::*STE50-5A*::*URA3 pbs2*::*C.g.HIS3* [YCplac33 *PBS2-6A*]	This study
YJP552	YPH499 *STL1$_{prom}$*::HA-tdtomato::*leu2*::*ADE2 FUS1$_{prom}$*::HA-eGFP::*leu2*::*ADE2 bar1*::kanMX4 *rga1*::*C.g.HIS3*	This study
YJP571	YPH499 *STL1$_{prom}$*::HA-tdtomato::*leu2*::*ADE2 FUS1$_{prom}$*::HA-eGFP::*leu2*::*ADE2 hog1*::hphNT1 *ste5*::*C.g.LEU2*	This study
YJP573	YPH499 *STL1$_{prom}$*::HA-tdtomato::*leu2*::*ADE2 FUS1$_{prom}$*::HA-eGFP::*leu2*::*ADE2 hog1*::hphNT1 *ste5*::*C.g.LEU2 kss1*::*C.g.HIS3*	This study
YJP585	YPH499 *STL1$_{prom}$*::HA-tdtomato::*leu2*::*ADE2 FUS1$_{prom}$*::HA-eGFP::*leu2*::*ADE2 bar1*::kanMX4 *HOG1-AS*::hphNT1 *rga2*::*C.g.LEU2*	This study
YJP586	YPH499 *STL1$_{prom}$*::HA-tdtomato::*leu2*::*ADE2 FUS1$_{prom}$*::HA-eGFP::*leu2*::*ADE2 bar1*::kanMX4 *HOG1-AS*::hphNT1 *rga1*::*C.g.HIS3 rga2*::*C.g.LEU2*	This study
YJP589	YPH499 *HOG1-AS*::hphNT1 *rga1*::*C.g.HIS3*	This study
YJP591	YPH499 *STL1$_{prom}$*::HA-tdtomato::*leu2*::*ADE2 FUS1$_{prom}$*::HA-eGFP::*leu2*::*ADE2 bar1*::kanMX4 *rga1*::*C.g.HIS3 ssk1*::*C.g.TRP1*	This study
YJP595	YPH499 *HOG1-AS*::hphNT1 *rga1*::*C.g.HIS3* [YCplac22-HA-*RGA1*]	This study
YJP610	YPH499 *STL1$_{prom}$*::HA-tdtomato::*leu2*::*ADE2 FUS1$_{prom}$*::HA-eGFP::*leu2*::*ADE2 bar1*::kanMX4 *HOG1-AS*::hphNT1 *rga1-505*::*URA3*::*C.g.HIS3*	This study
YJP611	YPH499 *STL1$_{prom}$*::HA-tdtomato::*leu2*::*ADE2 FUS1$_{prom}$*::HA-eGFP::*leu2*::*ADE2 HOG1-AS*::hphNT1 *rga1-505*::*URA3*::*C.g.HIS3 ssk1*::*C.g.TRP1*	This study
YJP662	YPH499 *hog1*::hphNT1 *rga1*::*C.g.HIS3* [YCplac22-HA-*RGA1*]	This study
YJP679	BY4741 *can1*::*STE2$_{prom}$*::*S.p.HIS5 lyp1*::*STE3$_{prom}$*::*LEU2* HA-	This study

	RGA1::*URA3*	
YJP707	BY4741 *can1*::*STE2*$_{prom}$::*S.p.HIS5 lyp1*::*STE3*$_{prom}$::*LEU2* HA-*RGA1*::*URA3 cdc28-1*::kanMX4	This study
YJP721	*HOG1-AS-GFP-CCaaX*^{Ras2}*::hphNT1 por1*::*C.g.TRP1*	This study
YPW14	EG123 *hog1*::*C.g.URA3 FUS1*$_{prom}$::*lacZ*::*LEU2*	Westfall et al., 2008
YPW17	EG123 *HOG1-AS FUS1*$_{prom}$::*lacZ*::*LEU2*	Westfall et al., 2008
YPW362	EG123 *HOG1-AS-GFP-CCaaX*^{Ras2} *FUS1*$_{prom}$::*lacZ*::*LEU2*	Westfall et al., 2008
YSR31	∑1278b *bar1*Δ*c fus1::FUS1prom*::GFP::kanMX4 stl1::*STL1prom*::mRFP	McClean et al., 2007

**HOG1-AS* is T100A, *KSS1-AS* is E93A and *FUS3-AS* is Q93A.

Unless stated otherwise, yeast cultures were grown at 30ºC in a shaking water bath set at 225 rpm. Cultures were grown in either a standard rich (YPD) or defined synthetic medium that contained 2% glucose or other sugars where explicitly described (Hicks et al., 1987). Where appropriate, plasmids were maintained in strains by growth in a medium lacking the appropriate nutrients or containing the appropriate drug. If an experiment required the selection for a drug resistance marker in synthetic medium, monosodium glutamate (0.1%) was used in place of the standard ammonium sulfate (0.5%) as a nitrogen source to facilitate the solubilization of the drug.

Plasmids and recombinant DNA methods

Plasmids used in this thesis (Table 2-2) were constructed and propagated in *Escherichia coli* using standard recombinant DNA methods or constructed in *S. cerevisiae* by homologous recombination (Hicks et al., 1987; Sambrook and Russell, 2001). The accuracy of all plasmids constructed in this study was verified by DNA sequencing and compared to the reference sequence that has been deposited in the Saccharomyces Genome Database (SGD) (Cherry et al., 1997). Point mutations within plasmids, insertions of small sequences or deletions of sequences were generated by site directed mutagenesis. The exact sequence of any plasmid constructed in the course of this work is available in the electronic Thorner Lab plasmid database.

Table 2.2 Plasmids used in this study

Name	Description	Source or reference
BG1805-HOG1	2μ *URA3 GALprom-HOG1*-6XHIS-HA-3C-ZZ	Open Biosystems Inc.
BG1805-HOG1-KD	2μ *URA3 GALprom-HOG1-D144A*-6XHIS-HA-3C-ZZ	This study
BG1805-HOG1-AS	2μ *URA3 GALprom-HOG1-T100A*-6XHIS-HA-3C-ZZ	This study
BG1805-JP	2μ *URA3 GALprom* MCS	This study
BG1805-TDH1	2μ *URA3 GALprom-TDH1*-6XHIS-HA-3C-ZZ	Open Biosystems Inc.
BG1805-TDH2	2μ *URA3 GALprom-TDH2*-6XHIS-HA-3C-ZZ	Open Biosystems Inc.
BG1805-JP-TDH3	2μ *URA3 GALprom-TDH3*-6XHIS-HA-3C-ZZ	This study
pCgH	*C.g. HIS3*	Kitada et al., 1995
pCgL	*C.g. LEU2*	Kitada et al., 1995
pCgW	*C.g. TRP1*	Kitada et al., 1995
pET21a	T7prom-6XHIS	Invitrogen Inc.
pETGST3C	T7prom-GST-3C-6XHIS	This study
pETGST3C-RGA1	T7prom-GST-3C-*RGA1*-6XHIS	This study
pETGST3C-RGA1-LIM	T7prom-GST-3C-*RGA1*(aa 1-339)-6XHIS	This study
pETGST3C-RGA1-Middle	T7prom-GST-3C-*RGA1*(aa 340-670)-6XHIS	This study
pETGST3C-RGA1-GAP	T7prom-GST-3C-*RGA1*(aa 671-1007)-6XHIS	This study
pETGST3C-RGA1-T470A	T7prom-GST-3C-*RGA1*(aa 340-670)-T470A	This study
pETGST3C-RGA1-T540A	T7prom-GST-3C-*RGA1*(aa 340-670)-T541A	This study
pETGST3C-RGA1-3A	T7prom-GST-3C-*RGA1*(aa 340-670)-T470A T541A T571A	This study
pETGST3C-RGA1-5A	T7prom-GST-3C-*RGA1*(aa 340-670)-T470A T541A T571A S539A T532A	This study
pETGST3C-RGA1-7A	T7prom-GST-3C-*RGA1*(aa 340-670)-T470A T541A T571A S539A T532A S519A S521A	This study

pFP68	T7prom-GST-P*BS2*-EE	Bilsland-Marchesan et al., 2000
pPP1969	*STE5prom-STE5*-3X-GFP	Winters et al., 2005
pRS306H	hphNT1	(Taxis and Knop, 2006)
pRS306K	kanMX4	Taxis and Knop, 2006
pRS306N	natNT2	Taxis and Knop, 2006
pRS316	*CEN URA3*	Sikorski and Hieter, 1989
pRS316-*POR1*	*POR1prom-POR1*	This study
pRS316-*POR1-T91A*	*POR1prom-POR1-T91A*	This study
pRS316-*POR1-T103A*	*POR1prom-POR1-T103A*	This study
pRS316-*POR1-T132A*	*POR1prom-POR1-T132A*	This study
pRS316-*POR1-2A*	*POR1prom-POR1-T25A T91A*	Yiplac128-*STL1prom*::HA-tdtomato
pRS316-*POR1-3A*	*POR1prom-POR1-T25A T91A T103A*	This study
pRS316-*POR1-4A*	*POR1prom-POR1-T25A T91A T103A S2A*	This study
pRS316-*POR1-5A*	*POR1prom-POR1-T25A T91A T103A S2A T132A*	This study
pRS316-SHO1	*SHO1prom-SHO1*	This study
YCplac111	*CEN LEU2*	Gietz and Akio, 1988
YCplac111-*TDH3*-Ypet	*TDH3prom-TDH3*-Ypet	This study
YCplac111-*TDH3-S302N*-Ypet	*TDH3prom-TDH3-S302N*-Ypet	This study
YCplac22	*CEN TRP1*	Gietz and Akio, 1988
YCplac22-	*RGA1prom-RGA1*	This study

RGA1		
YCplac22-*rga1-505*	*RGA1prom-rga1-505*	This study
YCplac22-HA-*RGA1*	*RGA1prom*-HA-*RGA1*	This study
YCplac22-HA-*RGA1-T470A*	*RGA1prom*-HA-*RGA1-T470A*	This study
YCplac22-HA-*RGA1-T541A*	*RGA1prom*-HA-*RGA1-T541A*	This study
YCplac22-HA-*RGA1-T571A*	*RGA1prom*-HA-*RGA1-T571A*	This study
YCplac22-HA-*RGA1-2A*	*RGA1prom*-HA-*RGA1-T541A T571A*	This study
YCplac22-HA-*RGA1-3A*	*RGA1prom*-HA-*RGA1-T470A T541A T571A*	This study
YCplac22-HA-*RGA1-5A*	*RGA1prom*-HA-*RGA1-T470A T541A T571A S529A S532A*	This study
YCplac22-HA-*RGA1-7A*	*RGA1prom*-HA-*RGA1-T470A T541A T571A S529A S532A S519A S521A*	This study
YCplac33	*CEN URA3*	Gietz and Akio, 1988
YCplac33-*PBS2-6A*	*PBS2prom-PBS2-S83A T164A S212A S248A T297A S415A*	This study
YCplac33-*TDH3*-Cypet	*TDH3prom-TDH3*-Cypet	This study
YCplac33-*TDH3-S302N*-Cypet	*TDH3prom-TDH3-S302N*-Cypet	This study
YIplac128	*LEU2*	Gietz and Akio, 1988
YIplac128-$FUS1_{prom}$::HA-eGFP	$FUS1_{prom}$::HA-eGFP	This study
Yiplac128-*STL1prom*::HA-tdtomato	*STL1prom*::HA-tdtomato	This study

Plasmid BG1805-JP was constructed by site directed mutagenesis of BG1805-*HOG1*. The *HOG1* sequence was removed and replaced with a multiple cloning sequencin containing the clevage sites for the following restriction enzymes: *Eco*RI, *Xho*I, *Bam*HI, *Hind*III, *Spe*I, *Sph*I and *Cla*I. BG1805-JP-*TDH3* was then made by cloning the *TDH3* coding sequence into the *Eco*RI and *Cla*I sites of BG1805-JP.

Plasmid pETGST3C was constructed by fusing the coding sequence for glutathione-S-transferase (GST) with a sequence coding for a protease 3C cleavage site. The GST sequence was amplified from pGEX-4T1 using a forward primer containing a *Vsp*I restriction enzyme site a reverse primer that contained nucleotides coding for the protease 3C clevage sequence and a *Nde*I restriction enzyme site. This PCR amplicon was then cloned into the *Nde*I site of pet21a in an orientation so that the GST-3C sequence would be under the transcriptional control of the T7 promoter. The overhanging ends of a *Vsp*I site are compatable with those of a *Nde*I site, so that the resulting plasmid contains only one *Nde*I site immediately following the 3C sequence. The coding sequence of *RGA1* was cloned into the *Nhe*I-*Hind*III sites of pETGST3C. RGA1 fragment and point mutant expressing plasmids were generated by site-directed mutagensis.

Plasmid pRS316-*POR1* contains the *POR1* coding sequence and 554 bp of the *POR1* promoter cloned into the *Xho*I site of pRS316. pRS316-*SHO1* has the *SHO1* coding sequence, 572 bp of the *SHO1* promoter and 581 bp of the *SHO1* terminator cloned into the *Not*I-*Bam*HI sites of pRS316.

TDH3-Ypet and *TDH3*-Cypet were cloned into the *Eco*RI-*Pst*I sites of YCplac33 and YCplac111, respectively. The plasmids also contain 500 bp of the *TDH3* promoter and the *ADH1* terminator after the fluorescent protein sequence. *RGA1* was cloned into YCplac22 (*Sac*I-*Hind*III sites) along with 502 bp of its promoter and 299 bp of its terminator.

The $FUS1_{prom}$-eGFP reporter consisted of 993 bp 5' of the *FUS1* start codon fused to eGFP that was hemagglutinin (HA)–tagged at its N terminus, cloned into the *Bam*HI and *Eco*RI sites of the *LEU2*-marked integration vector, YIplac128. The resulting plasmid was then linearized with *Bsa*AI and used to transform YPH499. The $STL1_{prom}$-td-tomato reporter contained 972 bp 5' of the *STL1* start codon fused to td-tomato that was also HA-tagged at its N terminus, cloned into the *Bam*HI and *Eco*RI sites of YIplac128. The resulting plasmid was linearized with *Nru*I and used to transform YPH500.

Microarray analysis of yeast cultures during hyperosmotic stress

Cultures (5 ml) of the indicated yeast strains examined were grown overnight at 25°C in YPD and used to inoculate (initial A_{600nm} = 0.3) fresh YPD medium (100 ml), and the resulting cultures were grown for 4 h at 25°C. Samples (50 ml) were withdrawn and the cells collected by centrifugation (6,000 rpm, 5 min in an SS-34 rotor of a Sorvall 5B centrifuge) and immediately frozen in liquid N_2 (0 time point). The remainder of the culture was collected by centrifugation in the same way and then resuspended in fresh pre-warmed YPD containing 1 M sorbitol. After incubation for 1 h at 25°C, the cells were collected again and immediately frozen in liquid N_2 (60-min time point). Three independent trials of this procedure (Replicates 1, 2, and 3) were conducted. Total RNA was extracted from the frozen cell pellets by using the RiboPure-Yeast method (Ambion), following the manufacturer's recommendations. Complementary amino-allyl-UTP-containing RNA (aRNA) was synthesized by using as the template 1 μg of total RNA from each sample and the Amino Allyl MessageAmp II aRNA amplification kit (Ambion) adjusted to an amino-allyl-UTP:UTP ratio of 1:1, according to the manufacturer's instructions. Cy3 and Cy5 dyes (Amersham Biosciences or Enzo Life Sciences) were coupled to the aRNA by using standard protocols (Eisen and Brown, 1999). Microarrays on which each *S. cerevisiae*

ORF is represented by a unique 70-base oligonucleotide were the generous gift of the microarray facility of the Center for Advanced Technology at the University of California, San Francisco. Samples (2.5 µg) of the aRNA to be tested (Cy3-labeled), along with a sample (2.5 µg) of the common reference pool of aRNA (Cy5-labeled) comprising a mixture of equal amounts of all of the samples in any given replicate, were hybridized to triplicate microarrays (for Replicate 1) by using standard procedures for yeast microarray post-processing, hybridization, washing, and scanning (www.microarrays.org/) or by using (for Replicates 2 and 3) microarrays carrying duplicate spots and the MAUI hybridization chamber and protocol, according to the manufacturer's recommendations. Fluorescence on the arrays was analyzed by using a GenePix 4000B scanner (Molecular Devices, Sunnyvale, CA). The resulting data were corrected with LOWESS and standard deviation normalization algorithms by using the TiGR MIDAS version 2.20 program (Saeed et al., 2003). When both independent measurements within each replicate were reliable, they were averaged and relative expression levels and fold-change were analyzed by using TiGR MeV version 3.1 program (Saeed et al., 2003). The raw and normalized data were deposited at the Gene Expression Omnibus (GEO) data base hosted by NCBI (www.ncbi.nlm.nih.gov/geo) (Edgar et al., 2002) under the accession number GSE8703.

Purification of ZZ-3C-HA-6XHIS tagged proteins from yeast

Expression plasmids (BG1805-*HOG1*, BG1805-*HOG1-KD*, BG1805-*HOG1-AS*, BG1805-*TDH1*, BG1805-*TDH2* and BG1805-*TDH3*) were introduced by DNA-mediated transformation into the protease deficient BJ2168 strain. These expression plasmids contain the coding sequence of interest C-terminally tagged with a $(HIS)_6$, Protease 3C clevage site and ZZ tag. The subsequent transformants were grown to A_{600nm} = 0.5 in 2 L of synthetic complete -Ura medium containing 2% raffinose and 0.2% sucrose, then galactose was added to a final concentration of 2%, and the cultures were incubated for 20 h at 30°C to induce expression of the tagged proteins. It was determined that 20 h of induction was the optimal expression time for the proteins purified by this method. The cells were collected by centrifugation for 10 min at 5000 x g, then washed twice with lysis buffer [50 mM Tris-Cl (pH 7.5), 200 mM NaCl, 1.5 mM MgAc, 5 mM β-mercaptoethanol, 5% glycerol] (1.3 ml/g wet weight of pellet), and then frozen in liquid N_2. Frozen pellets were then smashed with a hammer and then placed in a coffer grinder (Custom Grind™, Hamilton Beach Co., Richmond, VA) along with an equal weight of dry ice. The cells were ruptured by two 2-min pulses of grinding at maximum speed ("espresso setting"). The lysed frozen cells were then thawed and resuspended in lysis buffer (0.8 ml/g original wet pellet) containing EDTA-free Complete Protease Inhibitors (Roche Applied Sciences Inc., Indianapolis, IN) at the manufacturer's recommended final concentration. The resulting crude extract was clarified first by centrifugation at 11,000 x g for 20 min in an SS-34 rotor and RC5B centrifuge (Thermo Scientific, Waltham, MA)and then at 70,000 x g for 1 h in a Type 50Ti rotor and a L8-80M ultracentrifuge (Beckman Coulter, Brea, CA). Detergent NP-40 was added to the lysate to a final concentration of 0.15%, and the tagged proteins were bound to IgG-Sepharose 6 Fast Flow beads (GE Healthcare) (400 µl of a 50:50 slurry in lysis buffer) by incubating at 4°C on a roller drum for 1 h. The bead-containing solution was transferred to a glass column and, after settling, the resulting bed was washed 3X with 5 ml of protease 3C buffer [50 mM Tris-Cl (pH 7.0), 150 mM NaCl, 1 mM EDTA, 5 mM β-mercaptoethanol, 0.01% NP- 40]. To elute the proteins, the IgG-bound ZZ tag was removed by incubation of the beads in 1 ml of protease 3C buffer containing 40 units of PreScission Protease 3C (GE Healthcare, Inc.) at 4 °C for 18 h. The resulting cleavage product was eluted from the column and mixed with 9 ml HIS A buffer [20 mM Tris-Cl (pH 8.0), 300 mM NaCl, 20 mM imidazole, 10% glycerol]. The $(His)_6$-tagged

proteins were purified by FPLC (AKTA™, GE Healthcare, Inc.) on a 1-ml HisTrap HP™ (GE Healthcare, Inc.), by eluting with a linear gradient from HIS A buffer to HIS B buffer [20 mM Tris-Cl (pH 8.0), 300 mM NaCl, 300 mM imidazole, 10% glycerol].

For purification of Tdh1, Tdh2 and Tdh3, the resulting protein containing fractions, as judged by sodium-dodecyl-sulfate polyacrylamide gel electrophoresis (SDS-PAGE) and coomassie staining, were dialyzed against storage buffer [20 mM Tris (pH 7.5), 100 mM NaCl, 1 mM DTT, 10% glycerol] and stored at -80°C for future use. Hog1-containing fractions, however, were desalted by passage through a size exclusion column (PD-10™, GE Healthcare, Inc.), and the desalted solution was adjusted to a final volume of 10 ml in IEX A buffer [20 mM Tris-Cl (pH 8.0), 1 mM DTT, 10% glycerol]. The desalted solution was applied to a 1-ml anion exchange column (Resource Q™, GE Healthcare, Inc.) on the AKTA FPLC system and eluted with a linear gradient from IEX A buffer to IEX B buffer [20 mM Tris-Cl (pH 8.0), 1 mM DTT 10% glycerol, 1 M NaCl]. The fractions containing the bulk of the purified Hog1, as judged by Coomassie blue staining of the eluted fractions resolved by SDS-PAGE, were pooled and dialyzed against storage buffer [20 mM Tris (pH 7.5), 100 mM NaCl, 1 mM dithiothreitol (DTT), 10% glycerol] and stored at -80 °C for future use.

Purification of GST tagged proteins from E. coli

T7 promoter based bacterial expression plasmids were transformed into the protease deficient *E. coli* strain BL21(DE3) that also contains a plasmid which expresses tRNA for codons that are under-represented in *E. coli*. The resulting transformants were grown to A_{600nm} = 0.6 in LB medium (200 ml for Pbs2-EE, 1 L for all other proteins) and expression of the GST-protein fusion was induced by addition of 1 mM IPTG followed by incubation for 4 h at 20 °C. After induction, the cells were collected by centrifugation at 7000 x g for 10 min in an GS-3 rotor and RC5B centrifuge (Thermo Scientific, Waltham, MA), washed with 1X PBS, and frozen in liquid N_2. The pellets were then resuspended in 10 ml GST lysis buffer [1X PBS, 1 mM DTT, 0.5% Tween-20, 10% glycerol, 0.2 mg/ml lysozyme] containing EDTA-free Complete Protease Inhibitors at the concentration recommended by the manufacturer, incubated on ice for 30 min. Cells expressing GST-Pbs2-EE were ruptured by three 15-second pulses of sonication (Microtip, Branson), whereas cells expressing other GST-fusion proteins (e.g. Rga1 and its variants) were lysed by passage through a French pressure cell 2X 20,000 PSI. The lysates were clarified by centrifugation at 12,000 x g for 10 min.

The GST-tagged Pbs2-EE was bound to a 1-ml GSTrap HP™ column (GE Healthcare, Inc.) on the AKTA FPLC system. After washing with 12 ml of GST A buffer [1X PBS, 10% glycerol, 1 mM DTT], the bound protein was eluted with a linear gradient from GST A buffer to GST B buffer [1X PBS, 10% glycerol, 1 mM DTT, 20 mM freshly-prepared reduced glutathione]. The fractions containing the bulk of the GST-Pbs2-EE, as judged by Coomassie blue staining of the eluted fractions resolved by SDS-PAGE, were dialyzed against storage buffer and stored at -80°C.

GST-3C-Rga1 proteins were bound to 400 µl glutathione sepharose 4B (GE Healthcare, Inc.) 50% slurry that had first been washed with GST lysis buffer. GST-tagged proteins were bound to the glutathione beads by end-over-end rotation at 4°C for 2 h. The beads were then collected at the bottom of a glass column and washed 3X with 5 ml protease 3C buffer. Protease 3C buffer (1 ml) containing 40 units PreScission Protease 3C was added to the beads and the cleavage reaction was allowed to proceed for 18 h at 4°C. Because the PreScission Protease 3C itself is GST-tagged, the cleavage eluate contains pure Rga1 or its derivatives, which were then dialyzed against storage buffer overnight and stored at -80°C.

In vitro protein kinase assays

Protein kinase activity was measured as the Pbs2- or Hog1-dependent incorporation of radioactivity into potential substrate proteins from [γ-^{32}P]ATP. Assay mixtures (final volume 40 µl) contained the following components at the indicated final amount or concentrations: 1X MAPK buffer [50 mM Tris-Cl (pH 7.5), 0.1 mM EGTA, 3 mM MgAc, 1 mM sodium orthovanadate], 1% β-mercaptoethanol], GST-Pbs2-EE (1 µg), Hog1, Hog1-KD, Hog1-AS (1 µg), and 1 mM [γ-^{32}P]ATP (50,000 cpm/nmole or 1 mM ATP with 0.5 µCi [γ-^{32}P]ATP) (Perkin-Elmer NEN, Waltham, MA). substrate protein (1 µg) was added, when possible; if the substrate was more dilute, as much as could be added without exceeding the final reaction volume of 40 µl was used. Reactions were initiated by the addition of the ATP, incubated at 30°C with gentle shaking for 30 min, and terminated by addition of 13 µl 4X SDS-PAGE loading buffer [200 mM Tris-Cl (pH 7.5), 4% SDS, 20% glycerol, 2% β-mercaptoethanol, 0.02 mg/ml Bromophenol blue], followed by boiling for 10 min. The products were then analyzed by resolving 40 µl of each sample by SDS-PAGE followed by autoradiography of the dried gel with a PhosphorImager (Molecular Dynamics Division, Amersham Pharmacia Biotech, Inc.).

Measurement and calculation of FRET in vivo

Cultures (5 ml) of a strain containing the FRET pair, and control strains containing either only the donor or only the acceptor or no fluorescent proteins, were grown in synthetic medium to exponential phase to A_{600nm} = 0.8 in 5 ml. A sample (100 µl) of each strain was placed in 6 individual wells of a black clear-bottom 96 well plate (Thermo Fischer, Cat# 07-200-565). At the beginning of the time course, synthetic medium (100 µl) was added to three of these wells, and synthetic medium containing 2 M sorbitol (100 µl) was added to the other three wells. Fluorescence and absorbance measurements were made with a SpectraMax M2 96 well plate reading monochrometer fluorimeter (Molecular Devices). FRET was assessed after excitation a 433 nm by reading emission at 530 nm, using a 515 nm cut-off filter. CFP emission was assessed after excitation a 433 nm by reading at 475 nm, using a 455 nm cut-off filter. YFP emission was assessed after excitation a 490 nm by reading at 530 nm, using a 515 nm cut-off filter. Measurements were taken in that order from the bottom of the plate, with the photon multiplier tube (PMT) set to high and reading each well 25 times. The optical density of the culture was determined by measuring the absorbance at 600 nm.

Each measurement was normalized to the optical density of the well determined at time point 0, and then the background fluorescence (determined by the amount of signal detected in a strain containing no fluorescent proteins) was subtracted. YFP and CFP spillover was calculated by wells containing strains where the protein of interest was tagged with only Ypet or only Cypet. Spillover equals the amount of signal present in the FRET channel divided by the amount of signal present in the CFP or YFP channel, depending on which spillover is being assessed. Spillover was calculated at each time point in triplicate, however, an average of all these values was used for subsequent calculations. The FRET ratio was determined using readings from the strain containing both Ypet and Cypet fusions using the following formula (Muller et al., 2005):

$$\text{FRET ratio} = \frac{\text{FRET channel}}{\text{YFP channel} \times \text{YFPspillover} + \text{CFP channel} \times \text{CFPspillover}}$$

Imaging of fluorescent proteins in yeast cells

Yeast cultures (5ml) were grown in the indicated medium overnight, diluted to a low

concentration of cells per ml (A_{600nm} = 0.05 to 0.1) and then grown to mid exponential phase in the indicated medium for at least 2 generations. The exponentially growing culture was then added to an equal volume of medium containing double the desired final concentration of stimulant or drug. If the cells were going to be treated with α-factor in synthetic medium, the glass culture tubes were pre-coated with using bovine serum albumin (BSA, Sigma-Aldrich Chemical Co., St. Louis, MO). This treatment was necessary to prevent non-specific and variable α-factor peptide adsorption to the walls of the glass tube. To block the glass tubes, 5 ml 1.0% BSA in PBS was added and they were placed in a shaker for 1 h, then rinsed with 5 ml of synthetic complete medium. When multiple strains and stimulant concentrations were tested on the same day, culture manipulations were staggered by 15 min intervals to allow time for imaging of each culture while maintaining identical growth conditions between samples. After stimulation, cell cultures (1.5 ml) were pelleted by brief centrifugation, resuspended in 15 µl of synthetic complete medium and spread onto a 0.75% agarose pad. However, if the experiment at hand entailed examining the localization of fluorophore-tagged proteins, cells were either absorbed to poly-L-lysine-coated coverslips, or 0.75% agarose pads containing synthetic medium and the indicated concentration of stimulant. The extent of fluorescent reporter expression, or the localization of flurophore-tagged proteins, was then examined by epifluorescence microscopy (Model BH-2, Olympus America, Center Valley, PA) at the indicated time.

Cells expressing the MAPK fluorescent transcriptional reporters($FUS1_{promoter}$-eGFP and $STL1_{promoter}$-td-tomato), described and used extensively in Chapter 4 of this thesis, were examined using a 60X 1.4 numerical aperature (NA) objective (Olympus America). For each of the four fields captured, four images were acquired. The green GFP fluorescence was assessed using a 470 nm (40 nm bandwidth) excitation filter and a 525 nm (50 nm bandwidth) emission filter (Endow GFP 47001; Chroma Technology Corp., Rockingham, VT), and the red td-tomato fluorescence was imaged using 560 nm (40 nm bandwidth) excitation filter and a 630 nm (60 nm bandwidth) emission filter (31004 Texas Red; Chroma). For automated unbiased cell identification in images, total auto-fluorescence was monitored using a 330-385 bandpass excitation filter (UG1; Olympus America). Finally a brightfield image was acquired. Images were captured using a charge-coupled device camera (Magnafire SP CCD; Olympus America) and for any given filter set the exact same exposure times were used throughout the entire study (for strains of the YPH499 background, those exposure times were: GFP, 0.124 sec; RFP, 0.993 sec; and, UV autofluorescence, 0.175 sec). Examination of protein localization using epifluoresence microscopy and the appropriate fluorescent protein fusions was accomplished in a similar manner as explained above except that the images were acquired using 100X 1.4 NA objective (Olympus America). In one instance, the imaging of Hog1-td-tomato, a 50% neutral density filter was also used. While the neutral density filter decreased the amount of signal, it also slows the rate of photobleaching, resulting in overall better signal detection using longer exposure times.

Automated cell identification and subsequent quantitation of fluorescent protein expression in single cells

The 8-bit TIFF images were processed using automated image analysis software (CellProfiler, version 1.0.5122) (Carpenter et al., 2006). Appropriate corrections for variable background and uneven illumination were applied where necessary, cell margins were identified using auto-fluorescence aligned with the fluorescence images, and then the average pixel intensity was calculated for each cell identified. Units are arbitrary, but internally consistent for each fluorophore in each independent experiment presented. Higher pixel intensity represents

more fluorescent protein; however, due to the convolution of light under the optical conditions with which these data were acquired, the intensity signals are not strictly correlated linearly with the amount of eGFP or td-tomato present in the cells (that is double the fluorophore concentration does not yield an exact doubling of the pixel intensity). The scatter plots of average pixel intensity provide a convenient graphical means to represent the fluorescent status of individual cells in the population in the fluorescence microscope images. Moreover, flow cytometry and/or immuno-blotting to detect the HA-tagged fluorophores were used to confirm results in certain situations. Images of the localization of various fluorescent-protein fusions were also corrected for uneven illumination and background using Cell Profiler, and the absolute intensities of the images were adjusted to uniform contrast and brightness in a consistent manner for each experiment.

Preparation of protein extracts and Immuno-bloting

Cell cultures were grown to mid-exponential phase (A_{600nm} = 0.8), stimulated as stated, an equal number of cells [1.0 optical density (OD) equivalent, as determined by absorbance at 600 nm] were pelleted by brief centrifugation and frozen in liquid N_2. Frozen cell pellets were then resuspended in 150 µl of ice cold 1.85 M NaOH, 7.5% β-mercaptoethanol and incubated on ice for 10 min with periodic vortex mixing. To each sample was added 150 µl of 50% trichloroacetic acid. After incubation on ice for 10 min with periodic vortex mixing, precipitated proteins were then pelleted by centrifugation at 4ºC for 2 minutes at 16,000 x g in a microcentrifuge (Model 5519, ThermoForma, Waltham, MA), washed twice with 1 ml cold acetone, dried and resuspended in 75 µl resuspension buffer [100 mM Tris base, 5% SDS] and 25 µl 4X SDS-PAGE loading buffer [200 mM Tris-Cl (pH 7.5), 4% SDS, 20% glycerol, 2% β-mercaptoethanol, 0.02 mg/ml Bromophenol blue]. The samples were then boiled for 5 min, clarified by centrifugation at maximum speed for 5 min in a centrifuge (Model 54150, Eppendorf, Hamburg, Germany) and then 90 µl of protein extract was transferred to a fresh tube. A sample (40 µl) was analyzed by SDS-PAGE. After separation, proteins were transferred to a nitrocellulose membrane, blocked as described below, incubated overnight at 4ºC with primary antibodies prepared and used as described below. Blots were then incubated with secondary antibodies: anti-mouse immunoglobulin G (IgG) or anti-rabbit IgG diluted 1:10,000 in a 1:1 mixture of Tris-buffered saline (TBS) and Odyssey™ blocking buffer (Licor Biosciences, Lincoln, NE) containing 0.1% Tween-20 and 0.02% SDS, unless stated otherwise below. Secondary antibodies with coupled to infrared dyes that absorb light at either 700 or 800 nm and the blots were imaged on a Odyssey™ Infared Scanner (Licor Biosciences).

The rabbit anti-p42/44 antibody (9101 Cell signaling Technology, Beverly, MA) was diluted 1:250 in 5% BSA, 1X TBS, 0.1% Tween-20, 0.2% NaN_3. Samples were run on a 10% SDS-PAGE gel, and after wet-transfer to nitrocellulose, the blots were blocked with 100% Odyssey™ block buffer for 90 min. Secondary antibodies were diluted 1:10,000 in 5% BSA, 1X PBS, 0.1% Tween-20, 0.02% SDS.

The rabbit anti-phospho-p38 (3D7, Cell signaling Technology) and mouse anti-p38 (L53F8, Cell signaling Technology) antibody were diluted each to 1:500 in 5% BSA, 1X TBS, 0.1% Tween-20, 0.2% NaN_3. Samples were run on a 12% SDS-PAGE gel, and after transfer to nitrocellulose, the blots were blocked with 100% Odyssey™ block buffer.

The anti-HA.11 antibody (16B12, Covance Inc., Princeton, NJ), either raised in a mouse or rabbit, was diluted 1:1000 in 1:1 Odyssey™ block buffer:1X TBS 0.1% Tween-20. Samples were run on a 10% (75:1 acrylamide:*bis*-acrylamide) SDS-PAGE gel, and after transfer to nitrocellulose, the blots were blocked with 1:1 Odyssey™ block buffer:TBS.

Immunoprecipitation and Calf intestinal phosphatase treatment of HA-Rga1

Cell cultures (40 ml) were grown, pelleted, stimulated and frozen as described above for preparation of protein extracts. Cells were resuspended in 200 µl cold immunoprecipitation (IP) lysis buffer [40 mM Tris-HCl (pH 7.2), 125 mM potassium acetate, 0.5 mM EDTA, 0.5 mM EGTA, 1 mM DTT, 0.1% Tween 20, 12.5% glycerol, protease inhibitors (Roche Complete EDTA-free protease inhibitor tablets), 1 mM Na_3VO_4]. After adding chilled acid-washed glass beads to the meniscus, the cells were disrupted by vigorous vortex mixing in an automated device (FastPrep 120, Thermo Fischer Scientific). The lysate was separated from the glass beads and clarified by centrifugation at 16,000 x g for 5 min at 4ºC in a microcentrifuge (Model 5519, ThermoForma, Waltham, MA). A portion (20 µl) of IgG-Sepharose 6 Fast Flow beads (GE Healthcare) washed in lysis buffer was added to the lysate and the mixture was incubated end-over-end rotation for 1 h at 4ºC to pre-clear the lysate. The beads were then removed by brief centrifugation at 600 x g at 4ºC for 1 min in a microcentrifuge (Model 5519, ThermoForma, Waltham, MA), and 20 µl of fresh 50% IgG bead slurry (pre-washed with IP lysis buffer) were added along with 4 µl of mouse anti-HA.11 (16B12, 2 mg/ml, Covance Inc., Princeton, NJ). Immunoprecipitation was performed at 4ºC for 1.5 h with end-over-end rotation. Beads were then collected by brief centrifugation at 600 x g for 1 minute in a microcentrifuge (Model 5519, ThermoForma, Waltham, MA), washed 2X with 1 X phosphatase buffer [100 mM NaCl, 50 mM Tris-HCl (pH 7.9), 10 mM $MgCl_2$, 1 mM DTT] (Also referred to as NEBuffer 3, New England Biolabs Inc., Ipswich, MA). Washed beads were suspended in 40 µl 1X phosphatase buffer and were split in half. Calf Intestinal Alkaline Phosphatase (CIP; 10 units) (New England Biolabs Inc.) was added to one of the aliquots of beads, and both samples were then incubated at 30ºC for 1 h. After incubation, 4X SDS-PAGE loading buffer was added to a final concentration of 1X, the mixture was boiled for 5 min. After boiling, the supernatant solution was collected by brief centrifugation and samples were run on a 10% (75:1 acrylamide:*bis*-acrylamide) SDS-PAGE gel. Immuno-blotting was done as described above using the rabbit anti-HA.11 antibody.

Chapter 3
Hog1-dependent Hyperosmotic Stress Resistance Is Mediated by an Increase in Glycerol Production Via the Glycerol-phosphate Shunt

Introduction

To survive and continue to grow in a hypertonic environment, *Saccharomyces cerevisiae* accumulates the compatible solute glycerol. Activation of the HOG pathway and its MAPK Hog1 is required for resistance to hyperosmotic stress and to elicit an increase in intracellular glycerol. It was recognized early in the history of research on the HOG pathway that transcription of *GPD1* (NADH-dependent glycerol-3-phosphate dehydrogenase) was induced during hyperosmotic shock in a Hog1-dependent manner (Albertyn et al., 1994). The majority of the increase in *GPD1* transcript levels is accomplished by Hog1 mediated phosphorylation and activation of a transcription factor, Hot1 (Rep et al., 1999). However, Hog1 action also activates a handful of other transcription factors, including Msn2/Msn4 (a heterodimer), Msn1 and Smp1 and inactivates at least one transcriptional repressor, Sko1. Moreover, Hog1 reportedly regulates a chromatin-remodeling histone deacetylease Rpd3 and interacts directly with RNA polymerease II to influence gene expression (De Nadal et al., 2004; Pascual-Ahuir et al., 2006; Pokholok et al., 2006).

Upon its activation, Hog1 rapidly and transiently translocates into the nucleus in a manner that depends on the karyopherin and importin-β homolog Nmd5. All of the known substrates of Hog1 that regulate transcription are either predominantly or entirely localized to the nucleus. Unidentified Hog1 substrate(s) that are required to prevent crosstalk from the HOG pathway to other MAPK pathways could reside in the nucleus or the cytoplasm. Because active Hog1 goes to the nucleus, it seems to make sense that the nucleus would contain the important substrates of Hog1. For example, Hog1 may prevent the output of the mating and FG pathways by entering the nucleus and preventing transcription of those sets of genes. As means to determine whether Hog1 must enter the nucleus to prevent crosstalk, a post-doctoral researcher in the Thorner lab Dr. Patrick J. Westfall constructed an allele of Hog1 that was permanently tethered to the plasma membrane. He first fused GFP to the C-terminus of Hog1, and then fusing the 9 C-terminal residues of Ras2 (abbreviated $CCaaX^{Ras2}$) to the very end of the GFP. The two cysteines $CCaaX^{Ras2}$ sequence are S-palmitoylated and S-prenylated, respectively, and the chimera is efficiently directed to the plasma membrane (Willumsen et al., 1984; Chen et al., 1985). The "a" in the $CCaaX^{Ras2}$ sequence are for aliphatic residues (not alanine) and the exact sequence used was-GSGGCCIIS. The behavior of this construct was thoroughly analyzed by Patrick, and he showed that it was stably expressed, retained Hog1 catalytic activity and was localized to the plasma membrane (Westfall et al., 2008).

Patrick found that signaling fidelity was still maintained in cells expressing *HOG1-GFP-*$CCaaX^{Ras2}$ as the sole source of Hog1. Because crosstalk did not occur, it was concluded that the substrate Hog1 acts on to prevent crosstalk is not in the nucleus. Moreover, this *HOG1-GFP-*$CCaaX^{Ras2}$ chimera could complement the hyperosmotic sensitivity seen in *hog1*Δ strains. This latter result implies that Hog1 has access to the substrates that it modifies to adapt to stress in the cytoplasm, whereas most of the known Hog1 substrates are predominantly in the nucleus. Consistent with this conclusion, Patrick had observed that a *nmd5*Δ strain did not succumb under hyperosmotic conditions. It was possible that, in the *nmd5*Δ situation, that other importins might

get a sufficient amount of Hog1 into the nucleus, and conversely, that some small portion of the Hog1-GFP-CCaaX^{Ras2} expressed was not lipid modified, and thus, able to enter the nucleus. However, Patrick found that a *nmd5*Δ *HOG1-GFP-CCaaX^{Ras2}* strain was still resistant to hyperosmotic shock. Thus, it was concluded that Hog1 need not enter the nucleus to confer hyperosmotic stress resistance or maintain signaling fidelity (Westfall et al., 2008).

Because the transcription factors that Hog1 phosphorylates are predominantly in the nucleus, the results described above raised the question as to whether HOG pathway transcription regulation occurs in the *HOG1-GFP-CCaaX^{Ras2}* cells. Patrick compared the transcriptional induction of several diagnostic HOG pathway genes, including *GPD1*, *STL1*, *ALD3* and *CTT1* using RNA hybridization analysis. He found that, as expected, all four genes were significantly induced in a wild-type strain during hyperosmotic shock, and their expression was greatly reduced or absent in *hog1*Δ cells. By comparison, the levels of these four transcripts in the *HOG1-GFP-CCaaX^{Ras2}* strain during stress closely resembled those seen in the *hog1*Δ cells, indicating that HOG pathway genes were expressed in the *HOG1-GFP-CCaaX^{Ras2}* strain at no greater a level then the background seen in the *hog1*Δ cells. These results implied that, despite the attention previously focused on the transcriptional output of the HOG pathway, this response was dispensable for the role that Hog1 action plays in stress resistance.

A contemporaneous study published by the Van Oudenaarden laboratory (MIT) supported this notion, albeit indirectly, by investigating the frequency dependence of Hog1 nuclear entry (Mettetal et al., 2008). Their study examined the nuclear translocation of Hog1-YFP in response to a series of hyperosmotic pulses. That is, they repeatedly shocked the cells by rapidly changing the medium from isotonic to hypertonic solutions to determine the amount of time required for Hog1 to mount an effective response. They equated Hog1 nuclear entry with successful osmo-adaptation, a conclusion Patrick's study suggested is erroneous. From these studies, they concluded that the majority of Hog1-dependent “osmo-adaptation” occurred withing the first 15 min after the shock. If gene expression was a required component of HOG pathway hyperosmotic stress adaptation, they reasoned it would need to be completed within 15 min for any protective effects to be realized. The authors then repeated the experiment described above in the presence of cycloheximide (a protein synthesis inhibitor) and found that Hog1 still entered the nucleus during the initial hyperosmotic stress and exited during the subsequent “adaptation.” However, during the ensuing cycles of hyperosmotic shock, nuclear translocation of Hog1 was somewhat attenuated. The basic conclusion of this study was that the initial response and adaptation to hyperosmotic shock did not require new protein synthesis but that the response to subsequent shocks was aided by HOG pathway gene expression (Mettetal et al., 2008). It seems no surprise that protein synthesis is not necessary for pre-existing Hog1 to enter the nucleus after hyperosmotic shock. Nonetheless, in a specious leap of logic, the authors interpreted these results as indicating that gene expression was not required for cells to survive in response to hyperosmotic stress.

My work on this topic was focused on determining, first, if HOG pathway gene expression is necessary for hyperosmotic stress resistance. Patrick's work implied that HOG pathway gene expression is dispensable for stress resistance, but a more comprehensive global approach was necessary. I therefore performed whole transcriptome analysis of *HOG1-GFP*, *hog1*Δ and *HOG1-GFP-CCaaX^{Ras2}* strains, which accompanied Patrick's work and was published in a peer-reviewed journal (Proceedings of the National Academy of Sciences of the USA, © 2008; [Westfall et al., 2008]). Having demonstrated that assuming that HOG pathway transcription is not required for adaptation, I then sought to identify Hog1 substrate(s) that are

responsible for conferring hyperosmotic stress resistance.

Results

Microarray analysis shows HOG pathway dependent transcription is dispensable for hyperosmotic stress resistance

Although Patrick found that four genes known to be upregulated by the HOG pathway were no longer induced in the *HOG1-GFP-CCaaX*^{Ras2} background (comparable to their levels in a *hog1*Δ strain), others have shown that during hyperosmotic shock transcript levels of nearly 500 genes depended on Hog1 (O'Rourke and Herskowitz, 2004; Westfall et al., 2008). Therefore, I sought to measure transcript levels for the entire genome during hyperosmotic shock in *HOG1*, *hog1*Δ, and *HOG1-GFP-CCaaX*^{Ras2} strains.

Total RNA was isolated from these strains grown at room temperature before and after a 60-min treatment with 1 M sorbitol. The transcripts were then amplified and converted to amino-allyl antisense RNA for labeling by NHS-ester derevatized dye followed by hybridization to oligonucleotide microarrays. Each Cy3-labeled sample was competitively hybridized to the array against a reference pool of RNAs labeled with Cy5. This analysis was done in technical duplicates and biological triplicates, meaning that RNA from three separate yeast cultures was isolated and hybridized to microarrays in at least duplicates. After normalization, significance analysis of microarrays (SAM; (Tusher et al., 2001)) was done to identify genes that showed a statistically significant difference between the *HOG1* and *hog1*Δ strains. Also, to ensure that I was looking not only at reproducible differences but also at changes of significant magnitude, I only examined those genes which exhibited a greater than three-fold induction after hyperosmotic shock in the *HOG1* strain and a less then three-fold induction in the *hog1*Δ strain.

Figure 3-1A shows the expression levels of the genes identified by the analysis described above. In this heatmap, brighter yellow color indicates higher induction level during the hyperosmotic shock, whereas blue color indicates that repression occurred. The clear trend among these HOG pathway-dependent genes is that induction occurs in the *HOG1* strain, it does not occur or is significantly reduced in the *hog1*Δ strain, and that the *HOG1-GFP-CCaaX*^{Ras2} strain displays a response that more closely resembles that seen in *hog1*Δ cells. The expression values of each of these HOG pathway genes were averaged for each of the biological replicates and strain backgrounds and displayed as a chart in Figure 3-1B. The error bars are the averaged standard error of the mean for the thirty genes.

Although the transcriptional profiles of the *HOG1-GFP-CCaaX*^{Ras2} and *hog1*Δ strains are not identical, this result was expected for several reasons. First, the RNA hybridization analysis done by Patrick showed, for genes still weakly induced, the residual induction observed consistently had different timing in the *HOG1-GFP-CCaaX*^{Ras2} and *hog1*Δ strains. For example, no *ALD3* transcript was detectable in the *hog1*Δ strain until 60 min post shock, whereas, it was detectable in the *HOG1-GFP-CCaaX*^{Ras2} strain at 45 min post shock. It is not that there was more induction in one or the other strain, but that the timing was different. Because my microarray analysis only compared two time-points (0 and 60 min), it cannot capture differences in the kinetics of induction. Thus a higher transcript level seen in the *HOG1-GFP-CCaaX*^{Ras2} cells may reflect earlier, not higher, expression. This was also the reason as to why one of the diagnostic HOG pathway genes, *CTT1*, did not fit the criteria used to define HOG-pathway dependent genes in the microarray analysis. *GPD1* was not identified as a HOG pathway gene in the microarray analysis due to both this issue and because its high level of induction was outside the dynamic range of the microarray. Second, deletion of *HOG1* creates a different situation than tethering

Figure 3-1. Microarray analysis of transcription in cells expressing plasma membrane tethered Hog1

Hog1-GFP-expressing cells (YPW17), *hog1*Δ (YPW14), and Hog1-GFP-CCaaX^{Ras2}-expressing cells (YPW362) were grown to mid-exponential phase in YPD at 25°C. At time 0, samples were taken, and the remainder of each culture was then exposed to 1 M sorbitol for 1 h, and then a second sample was taken. Total RNA was prepared from the resulting six samples, fluorescently labeled, and hybridized in triplicate to genome-wide ORF arrays (Replicate 1), as described in detail in Chapter 2 of this thesis. Two additional independent trials of this same experiment (Replicates 2 and 3), each hybridized to microarrays in which each ORF was present in duplicate, were carried out. *HOG1* dependent genes were identified by identifying ORFs that displayed a greater then 3 fold induction during hyperosmotic shock in the *HOG1*-GFP strain, and a less then three fold induction in the *hog1*Δ strain. Significance analysis of microarrays was then used to identify 30 genes which showed the most significant and reproducible difference between the *HOG1*-GFP and *hog1*Δ strains.

(A) Heat map showing the relative induction and repression of the 30 most significant and reproducible Hog1-dependent genes. Yellow indicates induction and blue indicates repression over the 60 minute time course. Grey boxes indicate no reliable information for that data point. Each of the biological replicates is shown, as well as the aggregate of these data combined.

(B) Chart displaying the average induction for these thirty genes in each strain and each biological replicate. The standard error of the mean was calculated for each gene and each biological replicate by measuring the standard deviation in each technical replicate, and then the amount of error was averaged for the set of thirty genes. The error bars displayed on the chart represent the average amount of standard error of the mean for these thirty genes.

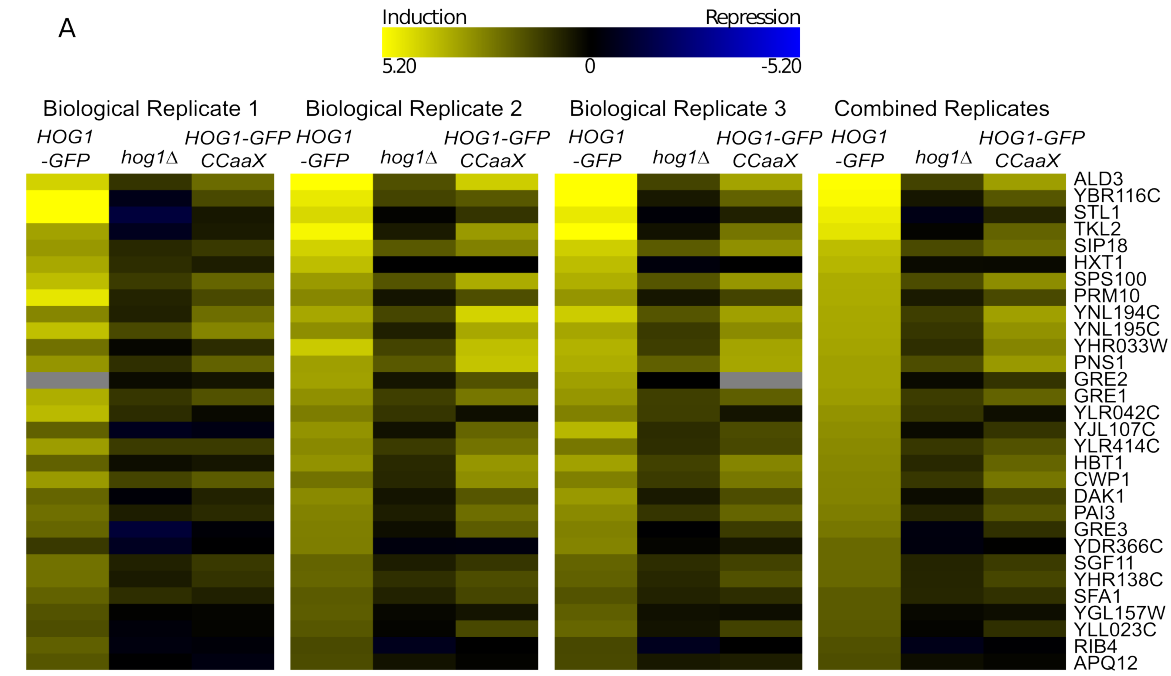
A
Induction
Repression
5.20
0
-5.20
Biological Replicate 1
Biological Replicate 2
Biological Replicate 3
Combined Replicates
HOG1 -GFP
hog1Δ
HOG1-GFP CCaaX
ALD3
YBR116C
STL1
TKL2
SIP18
HXT1
SPS100
PRM10
YNL194C
YNL195C
YHR033W
PNS1
GRE2
GRE1
YLR042C
YJL107C
YLR414C
HBT1
CWP1
DAK1
PAI3
GRE3
YDR366C
SGF11
YHR138C
SFA1
YGL157W
YLL023C
RIB4
APQ12

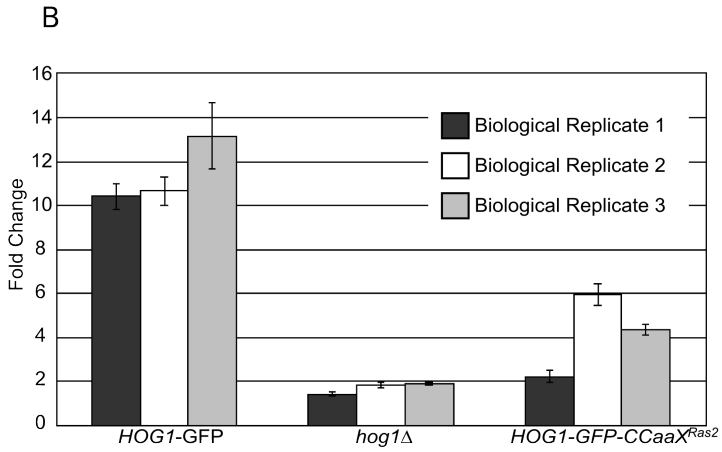
B
Fold Change
16
14
12
10
8
6
4
2
0
Biological Replicate 1
Biological Replicate 2
Biological Replicate 3
HOG1-GFP
hog1Δ
HOG1-GFP-CCaaX Ras2

it to the plasma membrane. Crosstalk occurs when *HOG1* is absent but not in the *HOG1-GFP-CCaaX*^{Ras2} strain. Therefore, the transcription profile of the *hog1*Δ strain includes activation of other Ste11-dependent MAPK pathways. The *hog1*Δ strain also succumbs to hyperosmolarity, whereas the *HOG1-GFP-CCaaX*^{Ras2} strain does not. Thus, comparing transcriptional profiles between a cell that is dying and one that is not will unavoidably introduce non-HOG-pathway-specific changes. Lastly, because the *HOG1-GFP-CCaaX*^{Ras2} strain is surviving, presumably most of the glucose present is going into the production of glycerol, potentially changing the transcriptional status of a large list of glucose-responsive genes.

Conceivably, for those transcription factors known to undergo nucleocytoplasmic shuttling, Hog1 tethered to the plasma membrane might be able to phosphorylate them when they are in the cytosol, and thus regulate their activity to effect gene expression and contribute to the conferral of hyperosmotic stress resistance. However, it was shown that deletion of any one of the known transcription factors, or the heterodimer Msn2/Msn4, in the *HOG1-GFP-CCaaX*^{Ras2} background did not render the cells hyperosmotically sensitive. Hog1 also phosphorylates Rck2, a MAPKAPK, however, deletion of *RCK2* and its paralog *RCK1* did not render the *HOG1-GFP-CCaaX*^{Ras2} strain osmosensitive. Of the genes investigated for those that would cause osmosensitivity in the *HOG1-GFP-CCaaX*^{Ras2} background, the only one that was identified was *GPD1* (Westfall et al., 2008*)*. Based on Patrick's and my work, we concluded that Hog1 nuclear translocation and subsequent transcriptional regulation were not required for hyperosmotic stress resistance but instead that Hog1 modifies cytoplasmic (or membrane associated) substrate(s) that increases Gpd1-dependent glycerol production.

Glyceraldehyde-3-phosphate dehydrogenases as possible Hog1 substrates

Gpd1 itself does not contain any consensus MAPK phosphorylation sites, specificallly serines or threonines followed by prolines (SP or TP). So, instead of direct regulation of Gpd1, Hog1 action likely increases the concentration of one or both of its substrates, glyceraldehyde-3-phosphate and reduced nicotine-adenine dinucleotide (NADH). We therefore turned our attention to other enzymes involved in glycolysis and NADH redox balance (Figure 3-2). Patrick examined the possibility that triose-phosphate isomerase (Tpi1) is phosphorylated by Hog1, and that such a modification might affect the rate of conversion of dihydroxyacetone phosphate to glyceraldehyde-3-phosphate. However, eliminating the only consensus MAPK phosphorylation site (Thr 177 to Ala) did not result in hyperosmotic stress sensitivity in the *HOG1-GFP-CCaaX*^{Ras2} strain. I, therefore, turned my attention to the three glyceraldehyde-3-phosphate dehydrogenases (GAPDHs): Tdh1, Tdh2 and Tdh3.

Although it has the lowest specific activity, Tdh3 is the major isoform and is one of the most abundant proteins in yeast. Tdh2 is also highly expressed, while Tdh1 has the lowest expression. Any one of these three enzymes can support growth and viability on glucose medium by itself, but deleting all three genes results in inviability. The native form of each enzyme is a homotetramer. While there is evidence that heterotetrameric GAPDHs can occur, it is not known specifically if yeast GAPDHs form heterotetramer complexes (Frayne et al., 2009). These enzymes catalyze the reaction: glyceraldehyde-3-phosphage to 1,3-*bis*-phosphoglycerate while reducing NAD+ to NADH (McAlister and Holland, 1985). If Hog1 were to inhibit these enzymes during hyperosmotic shock, it could lead to an accumulation of glyceraldehyde-3-phosphate, which, assuming adequate cytosolic concentrations of NADH, could then be used for the production of glycerol through Tpi1 to Gpd1 and then finally Gpp1/2 (Figure 3-2).

Figure 3-2. The glycerol-3-phosphate shuttle and NAD+/NADH redox balance

The production of glycerol is a required component of hyperosmotic stress adaptation. Although there are several biochemical processes that can result in the glycerol production, the glycerol-3-phosphate shunt appears responsible for glycerol production during hyperosmotic stress. This shunt involves the NADH dependent glycerol-3-phosphate dehydrogenases (Gpd1 and Gpd2) which reduce the glycolytic intermediate dihydroxyacetone-phosphate and to glycerol-3-phosphate. Two glycerol-3-phosphate phosphatases Gpp1/Rhr2 and Gpp2/Hor2 then remove the phosphate from glycerol-3-phosphate to produce glycerol. Presumably, the amount of glycerol produced depends on the amount of Gpd1, NADH and dihydroxyacetone-phosphate. The amount of Gpd2 present is fairly constant during hyperosmotic stress, however, *GPD2* expression is induced under anoxic conditions. Gpd1 transcription is induced during hyperosmotic shock, but this is not necessary for survival (Westfall et al., 2008). In glycolysis, dihydroxyacetone-phosphate is produced by the cleavage of fructose-1-6-bisphosphate by aldolase (Fba1), and then converted into glyceraldehyde-3-phosphate by triose phosphate isomerase (Tpi1). The glyceraldehyde-3-phosphate is then further processed by the glyceraldehyde-3-phosphate dehydrogenases (GAPDHs). The GAPDHs are the main source of the NADH generated by glycolysis, and, during fermentative growth, the NADH is re-oxidized back to NAD+ by ethanol production. Under aerobic conditions, cytoplasmic NADH is re-oxidized by the mitochondrial NADH dehydrogenase Nde1, which is located on the external side of the inner mitochondrial membrane. NADH transverses the outer mitochondrial membrane through the porin Por1.

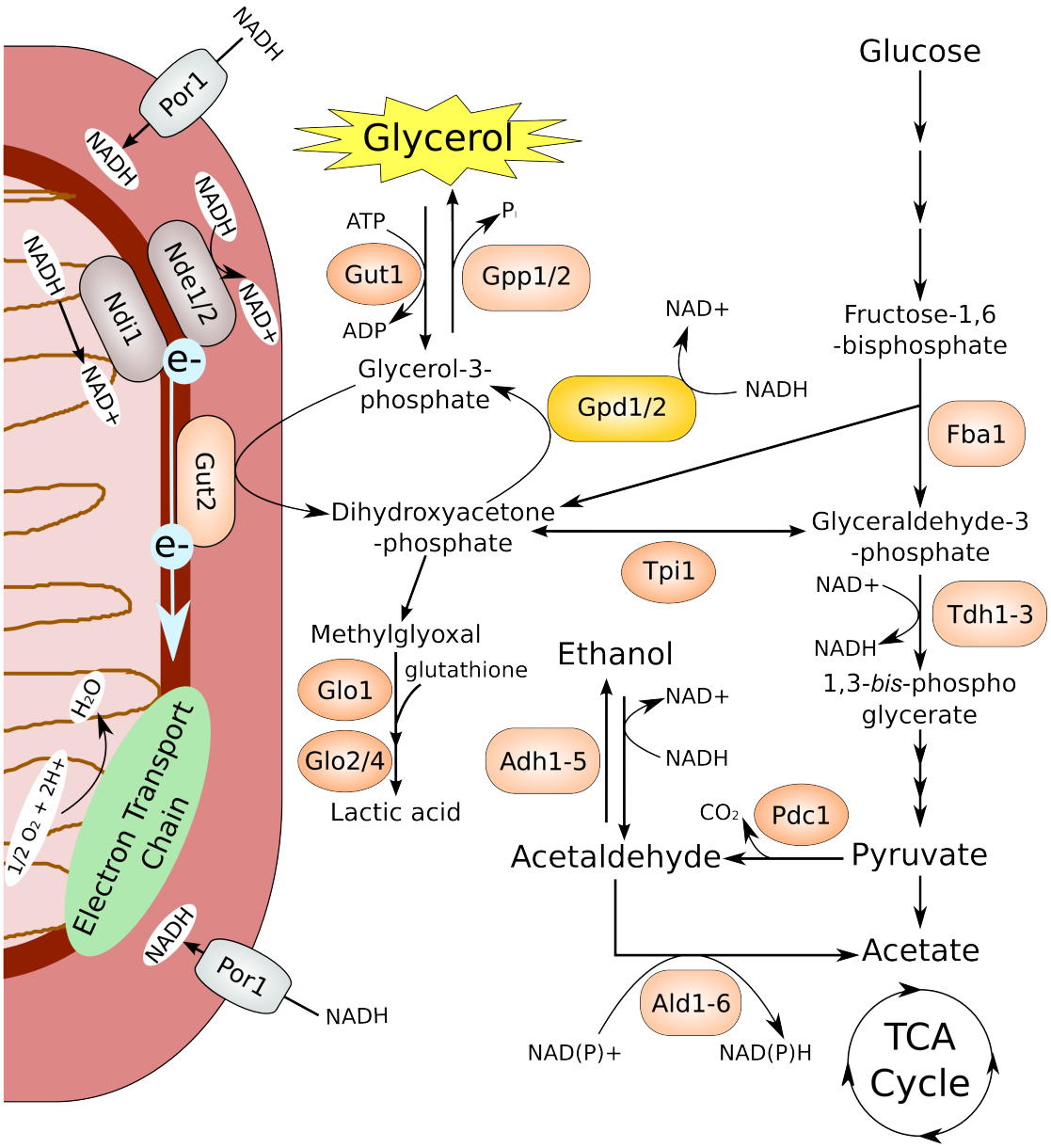
NADH
Por1
NADH
NADH
NADH
Nde1/2
NAD+
NADH
Ndi1
NAD+
e-
Gut2
e-
H2O
1/2 O2 + 2H+
Electron Transport Chain
NADH
Por1
NADH
Glycerol
ATP
Pi
Gut1
Gpp1/2
ADP
Glycerol-3-
phosphate
NAD+
NADH
Gpd1/2
Glucose
Fructose-1,6
-bisphosphate
Fba1
Dihydroxyacetone
-phosphate
Tpi1
Glyceraldehyde-3
-phosphate
NAD+
Tdh1-3
NADH
1,3-bis-phospho
glycerate
Methylglyoxal
glutathione
Glo1
Glo2/4
Lactic acid
Ethanol
NAD+
NADH
Adh1-5
CO2
Pdc1
Acetaldehyde
Pyruvate
Acetate
Ald1-6
NAD(P)+
NAD(P)H
TCA
Cycle

Moreover, Tdh3 was identified in a biochemical screen for Hog1 substrates using an analog-sensitive Hog1 mutant, Hog1(T100G) (Kim and Shah, 2007). In this screen, a 1 kg yeast cake was lysed and separated into 6 fractions using ion-exchange chromatography. Purified and active Hog1(T100G) was added to each protein extract with a radioactively-labeled ATP analog that purportedly Hog1(T100G) uses preferentially. Radiolabeled proteins were then separated using two-dimensional polyacrylamide gel electrophoresis (2D PAGE) and identified using mass spectrometry. Of 40 radiolabeled proteins identified in this way, Tdh3 was one of four that were supposedly validated. This confirmation was based on immunoprecipitating epitope-tagged Tdh3 before and after hyperosmotic shock from cells grown in the presence of $[^{32}P]PO_4^{3-}$, in the absence and presence of the Hog1(T100G) directed inhibitor 1-NM-PP1. Tdh3, as well as Shm2, Krs1 and Hsp26, appeared to become radiolabeled during hyperosmotic shock, and radiolabel incorporation diminished in the presence of 1-NM-PP1 (Kim and Shah, 2007). The functional significance of Hog1-mediated Tdh3 phosphorylation was not further investigated by the authors.

The three GAPDHs are all very similar to each other (Tdh1 v Tdh2, 88% identity; Tdh1 v Tdh3, 88% identity; Tdh2 v Tdh3, 96% identity). Each of the three has a conserved SP at position 302, and Tdh1 has an additional TP at position 139. To determine if the conserved SP was solvent exposed, I examined the three-dimensional structure of human liver GAPDH (Figure 3-3A). Although yeast Tdh3 and human liver GAPDH share 64% identity, the Ser302 (the residue at the equivalent positions is an Asn). Assuming similar tertiary structures, Ser302 in yeast GAPDH is a surface-exposed residue that lies at the interface between the subunits in the GAPDH tetramer. I found that there is conserved glutamate (E170) on the opposing subunit conserved between yeast and human GAPDHs that is within 4.3 Å of Ser302. Thus, if Ser302 were phosphorylated (Van der Waals radius of phosphate = 2.8 Å), there would be considerable electrostatic clash between the added phosphate and the opposing glutamate, leading either to disruption of the tetramer or to a change in its conformation (Figure 3-3B). If indeed phosphorylation of that Ser303 on a single subunit was sufficient to disrupt the overall conformation and function of a homotetramer, then only a small portion of the GAPDH molecules present in the cell would need to be modified to achieve drastic inhibition of the total GAPDH activity. In this situation, referred to as ultra-sensitivity, phosphorylation of merely 20% of GAPDH monomers would lead to a 70% decrease in total GAPDH activity (Goldbeter and Koshland, 1981). This mode of regulation would be particularly useful because there are more than 100,000 Tdh3 molecules per cell and Hog1 could exert control by modifying a small fraction.

For the above reasons, I sought to confirm myself that Tdh3 and possibly Tdh2 and or Tdh1 are substrates of Hog1 *in vitro*. Unfortunately, I could not express yeast GAPDHs as soluble proteins in *E.* coli. Therefore, I purified the GAPDH protein from yeast. Hog1 was also not expressed in a soluble form in *E. coli*, therefore, Hog1 and a catalytically-inactive ("kinase dead" or KD) version Hog1 (D144A) were also purified from yeast. Because Hog1 requires dual phosphorylation on its activation loop to be active, a constitutively-active version of its MAPKK Pbs2, GST-Pbs2-EE, was purified from *E. coli*. A kinase dead version of a known substrate of Hog1, the MAPKAPK Rck2 (Bilsland-Marchesan et al., 2000), was also purified from *E. coli* as a positive control. Under conditions in which Hog1 readily phosphorylated Rck2, all three of the GAPDHs failed to become radiolabeled. In case Hog1 can only phosphorylate the active version of a GAPDH, I also performed similar kinase assays in the presence of glyceraldehyde-3-phosphate, NADH and sodium arsenate. The use of arsenate instead of phosphate is necessary

Figure 3-3. Crystal structure of human liver GAPDH and the location of potential phosphophorylation sites

(A) Human liver GAPDH crystal structure (PDB #1ZNQ; Ismail and Park, 2005). GAPDHs form a homotetramer, and each subunit is represented by a different color (magenta, green, blue and yellow). NADH is displayed as space filing and is colored white. The white box near the top indicates the location of the potential Hog1 phosphorylation site and is examined more closely in (B).

(B) Close-up view of the potential phosphorylation site Ser302. This image is looking downwards from above the GAPDH tetramer represented in (A). Despite good conservation between yeast GAPDHs and the human liver GAPDH, the position occupied by Ser302 in yeast GAPDHs is an Asn in human GAPDH. The Asn was modelled as a serine in the crystal structure to assess the consequence of a Ser at that position. This position is at the interface between subunits, and, if phosphorylated, could potentially create electrostatic clash with a conserved Glu on the opposing subunit.

A

B

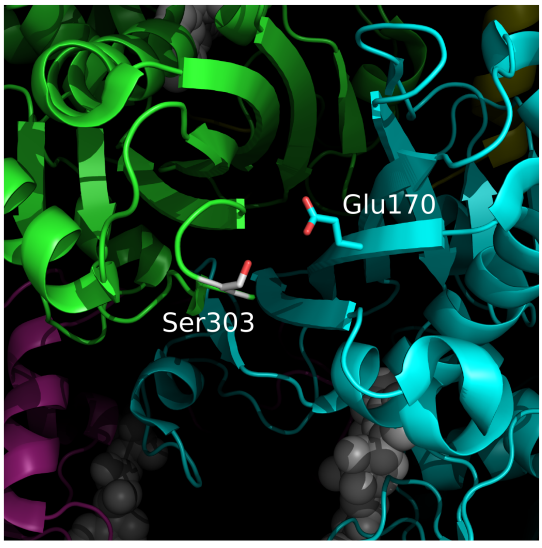

because the forward reaction (glyceraldehyde-3-phosphate to 1,3-bisphosphoglycerate) is not energetically favorable. Arsenate in this reaction generates 1-arseno-3-phosphoglycerate, which is hydrolyzed rapidly and, thus, drives the reaction in the forward direction (Krebs, 1955). *In vivo*, it is the subsequent conversion of 1,3-bisphosphoglycerate to 3-phosphoglycerate by Pgk1 that drives the GAPDH reaction in the forward direction. Based on a significant decrease in NADH concentration (as judged by absorbance at 340 nm), I observed a very large amount of GAPDH activity under these conditions. Moreover, Hog1 was still able to phosphorylate Rck2 when these additives were present. However, Tdh3 was not detectably phosphorylated by Hog1 (Figure 3-4). Therefore, under a variety of conditions tested, I could not confirm the prior report that Tdh3 was a substrate of Hog1 *in vitro*.

Is GAPDH activity reduced in vivo in a Hog1-dependent manner under hyperosmotic stress

Although, I could not demonstrate a direct interaction between Hog1 and the GAPDHs *in vitro*, there are many examples of kinases requiring so called "priming" phosphorylation sites where phosphorylation by an initiating kinase is a prerequisite for subsequent phosphorylation by a second kinase (Cohen and Frame, 2001). Also, there are cases where an adapter protein is necessary to mediate the kinase-substrate interaction, the most famous of which is the cyclin-dependent kinase (Mendenhall and Hodge, 1998). Both of these potential prerequisites were absent in my *in vitro* studies. Therefore, it remained a possibility that the GAPDHs are substrates of Hog1 and that a reduction in their catalytic activity contributes to hyperosmotic stress resistance. To test the latter possibility, I generated pairwise GAPDH deletion strains.

To construct the pairwase deletions, I knocked out all three *TDH* genes in a diploid, sporulated those cells and dissected the tetrads. As expected, the triple deletion spores were inviable. Others had reported that a *tdh2*Δ *tdh3*Δ cells was also dead (McAlister and Holland, 1985). In the strain background I used (YPH499), however, I was able to recover viable *tdh2*Δ *tdh3*Δ spores, but these cells were slow-growing. If the GAPDHs are inhibited during hyperosmotic stress, then deleting the genes might allow a *hog1*Δ strain to grow better on high osmolarity medium. While none of the double deletion mutants rescued the growth of a *hog1*Δ strain on YPD 1 M sorbitol entirely, I did notice that the *HOG1* cells containing any of the pairwise *TDH* deletions grew noticeably better on YPD containing 0.25 and 0.5 M sorbitol. Moreover, the *tdh1*Δ *tdh2*Δ *hog1*Δ and *tdh1*Δ *tdh3*Δ *hog1*Δ appear to grow somewhat more robustly then the *hog1*Δ strain on YPH + 0.25 M sorbitol (Figure 3-5). This indicates that a decrease in GAPDH does seem to increase hyperosmotic stress resistance of the wild-type strain, presumably by causing an accumulation of triose-phosphate which can then be converted to glycerol. However, since the GAPDH deletions combined with the *hog1*Δ did not grow on high osmolarity medium, it was not sufficient to rescue the lack of Hog1 activity. Moreover, just because decreasing GAPDH activity can be a means of increasing glycerol production, that does not mean that it actually occurs during hyperosmotic shock.

In a *hog1*Δ strain, not only is there no response to hyperosmotic shock, but crosstalk to both the mating and filamentous growth MAPK pathways occurs. Activation of the mating pathway results in Fus3-dependent phosphorylation and activation of the CDK inhibitor Far1, thus crosstalk also prevents cells from growing. Therefore, it was important to test for GAPDH-deletion-dependent rescue of the *hog1*Δ hyperosmotic sensitivity in a situation where the results would not be confounded by crosstalk-imposed growth inhibition. To do this, I introduced a mutant version of Far1 that cannot be phosphorylated by Fus3 (*far1-T306A*) (Gartner et al., 1998). However, even in the absence of crosstalk-induced cell-cycle arrest, none of the pairwise

Figure 3-4. *In vitro* Hog1 kinase assay

Hog1 purified from yeast was activated using a constitutively active Pbs2-EE protein isolated from bacteria. Rck2, a known Hog1 substrate, was used as a positive control to ensure that Hog1 was active under these conditions, and indeed, significant incorporation of ^{32}P into Rck2 was observed when wild type Hog1 (but not kinase dead Hog1) was present. Tdh3 was purified from yeast and incubated with the same active Hog1, however no incorporation of ^{32}P is observed. This experiment is a representative of several attempts to find conditions in which Tdh3 might become phosphorylated. In this particular experiment GAPDH substrates (glyceraldehyde-3-phosphate, NAD+, and the PO_4^{3-} mimic AsO_4^{3-}) were present and being consumed by Tdh3, demonstrating that the preparation of Tdh3 was folded and functional.

Pbs2-EE	+	+	+	+
Hog1	WT	KD	WT	KD
Rck2	+	+	–	–
Tdh3	–	–	+	+

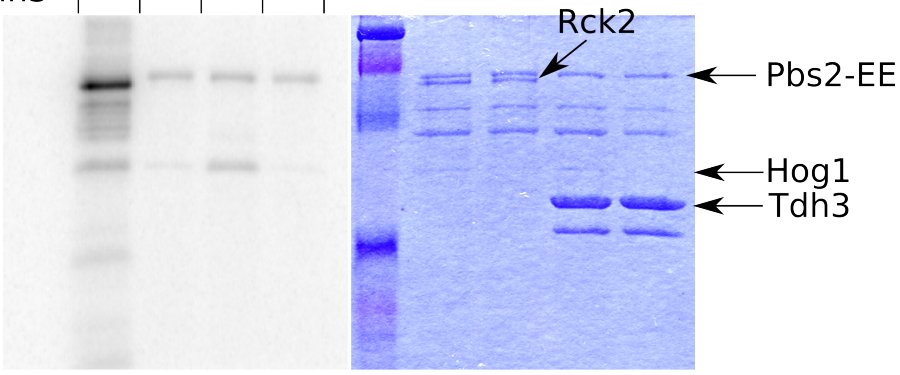

Figure 3-5. Deletion of yeast GAPDHs increases hyperosmotic stress resistance, but is not sufficient to rescue the lack of *HOG1*

(A) Strains YPH499, YJP166 (*hog1*Δ), YJP151 (*tdh1*Δ *tdh2*Δ), YJP152 (*tdh1*Δ *tdh3*Δ), YJP153 (*tdh2*Δ *tdh3*Δ), YJP157 (*hog1*Δ *tdh1*Δ *tdh2*Δ), YJP158 (*hog1*Δ *tdh1*Δ *tdh3*Δ), YJP159 (*hog1*Δ *tdh2*Δ *tdh3*Δ), YJP163 (*hog1*Δ *tdh1*Δ *tdh2*Δ *far1-T306A*), YJP164 (*hog1*Δ *tdh1*Δ *tdh3*Δ *far1-T306A*) and YJP165 (*hog1*Δ *tdh2*Δ *tdh3*Δ *far1-T306A*) were serially diluted 10-fold and spotted onto the indicated medium and incubated at 30ºC for 4 days.

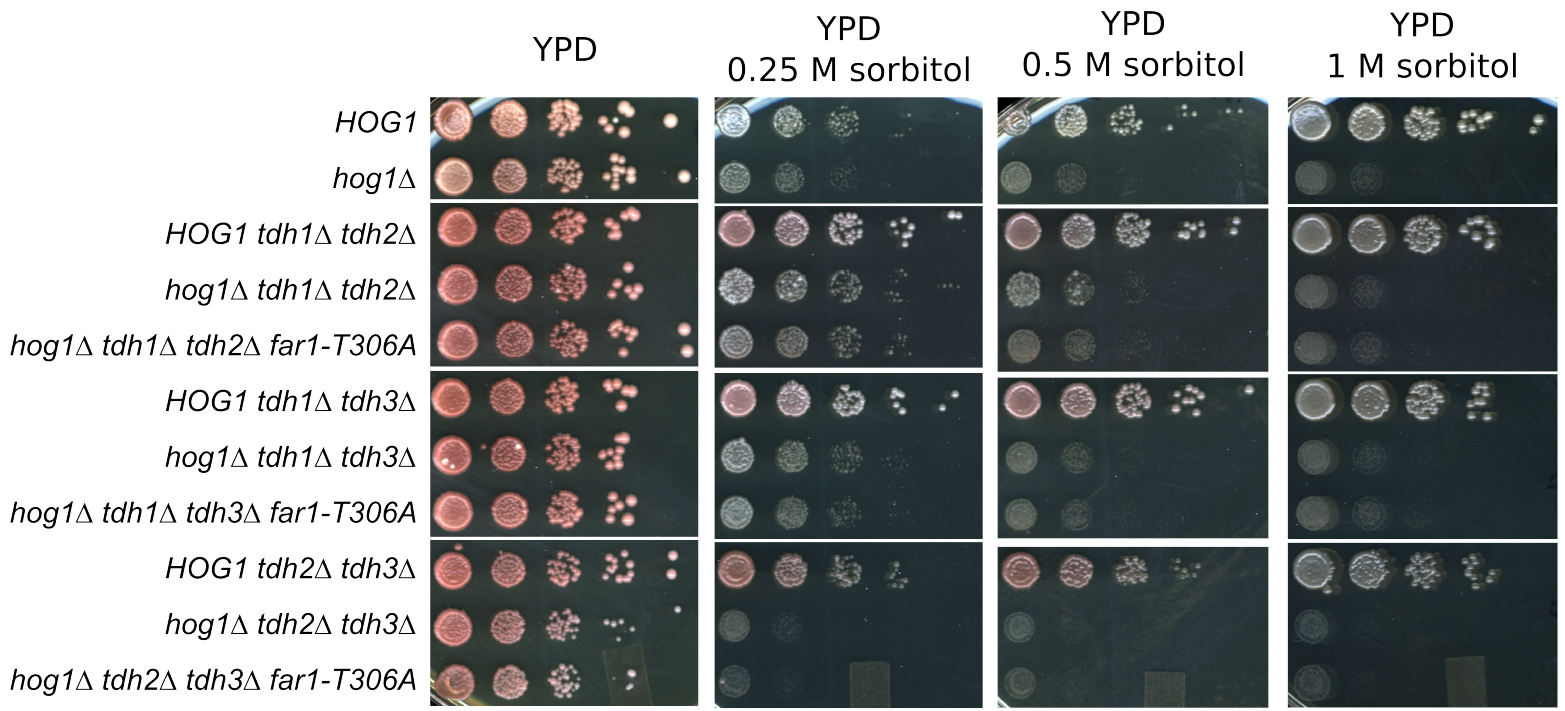
YPD
YPD
0.25 M sorbitol
YPD
0.5 M sorbitol
YPD
1 M sorbitol
HOG1
hog1Δ
HOG1 tdh1Δ tdh2Δ
hog1Δ tdh1Δ tdh2Δ
hog1Δ tdh1Δ tdh2Δ far1-T306A
HOG1 tdh1Δ tdh3Δ
hog1Δ tdh1Δ tdh3Δ
hog1Δ tdh1Δ tdh3Δ far1-T306A
HOG1 tdh2Δ tdh3Δ
hog1Δ tdh2Δ tdh3Δ
hog1Δ tdh2Δ tdh3Δ far1-T306A

deletions were sufficient to restore hyperosmotic stress resistance in Hog1-deficient cells(Figure 3-5).

If Hog1 phosphorylates the GAPDHs and inhibits their activity, then mutating the phosphorylated residues should render them uninhibitable and might cause cells to succumb to hyperosmotic stress despite the presence of functioning Hog1. However, it is important to determine whether such mutations deleteriously affect the catalytic function of the enzyme. To test for functionality, I integrated each phosphorylation site mutant into a diploid strain in which the other two GAPDH genes had been deleted. If the phosphorylation site mutant is functional, then a strain carrying it in combination with the other two deletion alleles should have the same phenotype as the double deletion mutant. It turned out, however, that mutating the phosphorylation site(s) in each GAPDH reduced its overall function. For instance, although the *TDH1 tdh2*Δ *tdh3*Δ strain grows, a *tdh1(T139A S302A) tdh2*Δ *tdh3*Δ strain was inviable. Mutating the sole MAPK consensus site in Tdh2 does not completely eliminate its function, but when combined with *tdh3*Δ (or *tdh1*Δ *tdh3*Δ), the resulting cells grew noticeably slower. The situation for Tdh3 phosphosite mutant was essentially the same as Tdh2 (Figure 3-6A). Because GAPDHs in other species have an asparagine in position 302, I also tried changing Ser303 to Asn in the yeast GAPDH and repeating the complementation analysis described above, however, these mutants behaved very similarly.

The purpose of constructing phosphorylation site mutants of the GAPDHs was to create versions of these proteins that could not be phosphoryated by Hog1 and to determine if Hog1-mediated modification is necessary for survival in response to hyperosmotic stress. Despite the fact that such mutations compromised the function of the enzymes, I nevertheless introduced them into a strain that also had the *HOG1-GFP-CCaaX*^{Ras2} allele. Figure 3-6B shows that the non-phosphorylatable GAPDHs mutants did not cause hyperosmotic stress sensitivity in the *HOG1-GFP-CCaaX*^{Ras2} background. This test was also repeated using the mutants which had the potential phosphorylation sites replaced with Asn, and even in combination with a non-phosphorylatable allele of Tpi1, all with identical results. If the phosphorylation site mutants had caused increased sensitivity to hyperosmotic conditions, this experiment would have been informative. However, it is difficult to know whether the results obtained mean that Hog1 does not phosphorylate the GAPDHs *in vivo*, or because the mutant enzymes already had reduced function, they no longer require Hog1-dependent phosphorylation and inhibition to establish the metabolic conditions that promote survival on hyperosmotic medium.

FRET analysis of GAPDHs during hyperosmotic shock

Because phosphorylation site mutants impaired the function of the GAPDHs, I sought to find an alternative way to look directly at the potential regulation of the GAPDHs by Hog1 *in vivo*. As mentioned above, the potential MAPK phosphorylation site conserved among the three GAPDHs (Ser302) is at the interface between subunits of the homotetramer and in a environment where phosphorylation could cause electrostatic clashes resulting in either dissociation of the tetramer or a significant change in its conformation. Fluorescence resonance energy transfer (FRET) is a veritable molecular ruler, that in this situation could be used to measure changes in GAPDH conformation. Basically, when the emission spectrum of one fluorophore (the donor) overlaps the absorbence spectrum of a second fluorophore (the acceptor), the energy emitted by exciting the donor fluorophore can be transferred to that of the acceptor, if they are sufficiently close together. It is not exactly that the light emitted by the donor fluorophore excites the acceptor, but dipole-dipole non-radiative energy is transferred. This transfer of resonant energy

Figure 3-6. Serine 302 is important for yeast GAPDH function and reduced GAPDH function does not compromise hyperosmotic stress resistance

(A) Tetrad dissections showing the inactivity of the Tdh1 phosphorylation site mutant. Strains YJP84 and YJP156 were mated and diploids cells isolated. The resulting diploid was sporulated and tetrads were dissected to assess the viability of the resulting mutants. Green circles indicate the *TDH1 tdh2*Δ *tdh3*Δ double mutant and red circles indicate where the *tdh1 T139A S302A tdh2*Δ *tdh3*Δ triple mutant spores should have grown up.

(B) Tetrad dissections showing the partial functionality of the Tdh2 phosphorylation site mutant. Strains YJP68 and YJP155 were mated and diploids cells isolated. The resulting diploid was sporulated and tetrads were dissected to assess the viability of the resulting mutants. Green circles indicate the *tdh1*Δ *TDH2 tdh3*Δ double mutant, yellow circles denote *TDH1 tdh2 S302A tdh3*Δ colonies and red circles indicate where the *tdh1*Δ *tdh2 S302A tdh3*Δ triple mutant spores barely have grown. *TDH1 tdh2 S302A tdh3*Δ colonies are pointed (yellow circles) out because they have a clear growth defect that is also observed in *tdh2*Δ *tdh3*Δ strains seen in panel (A).

(C) Tetrad dissections showing the partial functionality of the Tdh3 phosphorylation site mutant. Strains YJP67 and YJP154 were mated and diploids cells isolated. The resulting diploid was sporulated and tetrads were dissected to assess the viability of the resulting mutants. Green circles indicate the *tdh1*Δ *tdh2*Δ *TDH3* double mutant and red circles indicate where the *tdh1*Δ *tdh2*Δ *tdh3 S302A* triple mutant spores barely have grown.

(D) Despite the clear loss of functionality of the GAPDH phosphosite mutants, their ability to resist hyperosmotic stress was tested. Strains YPH499, YJP166, YJP184, YJP185, YJP186 and YJP187 were serially diluted and spotted on to the indicated medium. The plates were incubated for a period of 3 days before being imaged.

A

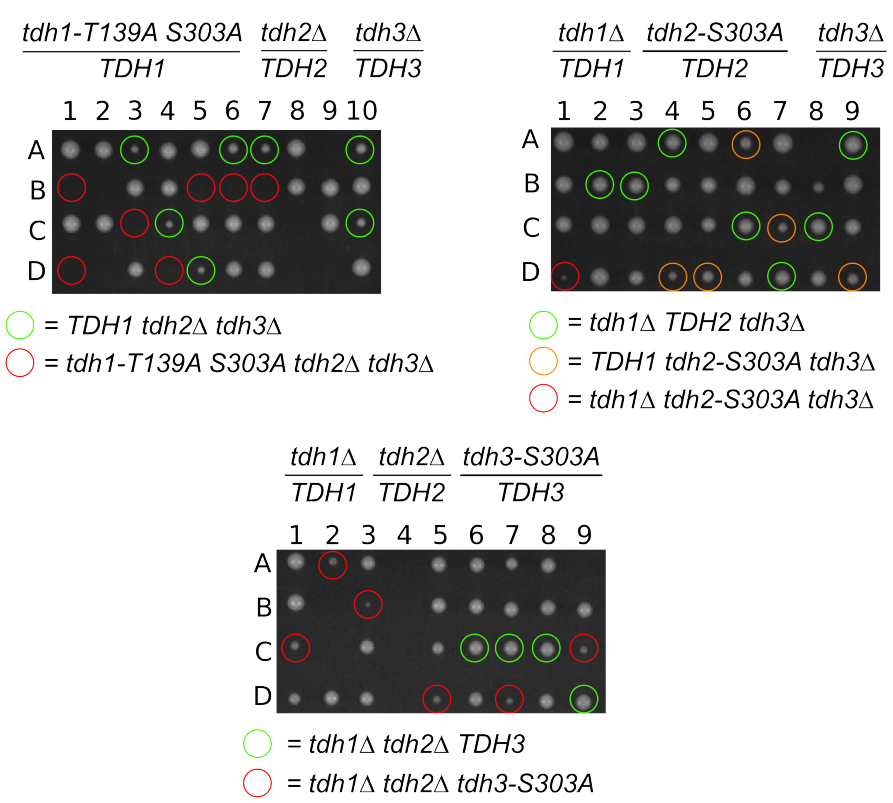
tdh1-T139A S303A / TDH1
tdh2Δ / TDH2
tdh3Δ / TDH3
1 2 3 4 5 6 7 8 9 10
A
B
C
D
= TDH1 tdh2Δ tdh3Δ
= tdh1-T139A S303A tdh2Δ tdh3Δ
tdh1Δ / TDH1
tdh2-S303A / TDH2
tdh3Δ / TDH3
1 2 3 4 5 6 7 8 9
= tdh1Δ TDH2 tdh3Δ
= TDH1 tdh2-S303A tdh3Δ
= tdh1Δ tdh2-S303A tdh3Δ
tdh1Δ / TDH1
tdh2Δ / TDH2
tdh3-S303A / TDH3
1 2 3 4 5 6 7 8 9
= tdh1Δ tdh2Δ TDH3
= tdh1Δ tdh2Δ tdh3-S303A

B

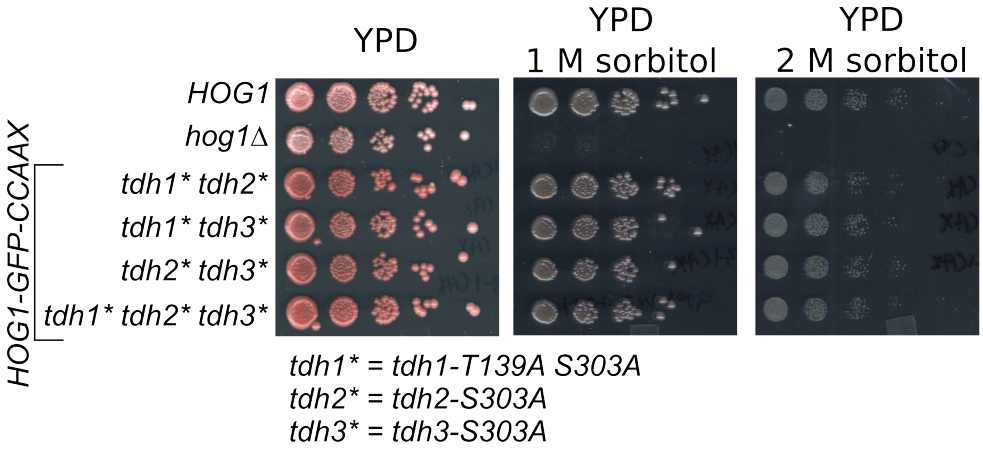
YPD
YPD
1 M sorbitol
YPD
2 M sorbitol
HOG1-GFP-CCAAX
HOG1
hog1Δ
tdh1* tdh2*
tdh1* tdh3*
tdh2* tdh3*
tdh1* tdh2* tdh3*
tdh1* = tdh1-T139A S303A
tdh2* = tdh2-S303A
tdh3* = tdh3-S303A

is dependent not only on the distance between the donor and acceptor fluorophore but on their relative orientation (Ciruela, 2008). Because the light used for excitation is not monochromatic, and neither is the emitted light, and because the cutoff filters cover a certain narrow range of wavelengths, spillover between the various channels must be accounted for. The amount of spillover that occurs per unit of fluorophore is determined with a strain that contains only one of the fluorophores and dividing the signal in the FRET channel by the amount of signal in the emission channel for that fluorophorre. The amount of FRET in the strain containing both fluorescent-protein fusions is measured by a ratio of the amount of signal present in the FRET channel divided by the amount of spillover that would be predicted based on the amount of each fluorophore present (Figure 3-7A) (Muller et al., 2005). Therefore any FRET ratio greater then 1 indicates a FRET interaction. For these experiments, I fused YFP and CFP variants (Ypet and CyPet) that have been optimized for FRET (Nguyen and Daugherty, 2005) to the C-terminus of the GAPDHs and Tpi1 in *MAT***a** and *MAT*α cells and then mated these strains to determine if a FRET interaction could be measured. Tpi1 is a homodimer and its FRET pair fusions were made to serve as a control.

A strong FRET signal could be detected between the two Tdh3 fluorescent-protein fusions. In cells stressed with 1 M sorbitol, the Tdh3 FRET increased dramatically and then returned to the baseline by approximately 45 min. The Tpi1 FRET pairs displayed weak FRET that remained constant during hyperosmotic stress. When the same Tdh3 FRET pairs were present in a diploid that was homozygous for *hog1*Δ, the same initial spike can be seen, however, the FRET ratio never descends to its baseline and instead stays at the elevated level through the length of the time course (Figure 3-7B). These results, if taken at face value, indicate that there is a change in the Tdh3 homotetramer during hyperosmotic stress and that some part of this change depends on the presence of Hog1. Because the FRET ratio increases, it does not seem likely that the tetramer dissociates during stress, but instead, that its conformation changes in a manner that either brings the FRET pairs closer together or into an orientation that is more optimal for the energy transfer.

Another possibility for the increase in the FRET ratio dynamics seen for the Tdh3 FRET pair during hyperosmotic shock is molecular crowding. As mentioned above, Tdh3 is an extraordinarily abundant protein, and during hyperosmotic shock with 1 osmole (1 M sorbitol or 0.5 M NaCl) cell volume shrinks between 30 and 40% (Schaber et al., 2010; Parmar et al., 2011). It is theoretically possible that the FRET signal observation from these FRET pairs occurs primarily due to their high concentration in the cell, and does not report their state of oligomerization or relative conformation. In this scenario, upon hyperosmotic shock, the cell's volume decreases resulting in an increase in the concentration of the FRET pairs and thus increasing the FRET. Moreover, the *hog1*Δ strain does not regain its volume during hyperosmotic stress as effectively which mimics the fact that the FRET ratio did not decrease in that strain during hyperosmotic stress.

To determine if the initial FRET ratio and changes in FRET were an artifact of the GAPDH's high concentration in the cell and molecular crowding, I transformed the Tdh3 FRET pair strain with two centromeric plasmids, one containing *TDH3*-Ypet and the other *TDH3*-Cypet, each under the control of the *TDH3* promoter. These plasmids provide a second copy of the *TDH3*-Ypet and *TDH3*-Cypet fusions, thus doubling the concentration of the Tdh3-FRET pairs in the cell. For simplicity, I will call this strain the 2X Tdh3-FRET pair strain.

As expected, the signal observed in the YFP and CFP channels in the 2X Tdh3-FRET pair strain were double that of the original Tdh3-FRET pair strain. In a wild-type background the

Figure 3-7. FRET analysis of GAPDH homotetramers during hyperosmotic shock

(A) Fluorescence resonance energy transfer can occur between two fluorescent molecules called the donor and the acceptor. In this case, the CFP is the donor and the YFP is the acceptor. Excitation of the donor results in emission of light of wavelengths within the excitation range of the acceptor fluorophore. This results in transfer of the energy from the donor to acceptor, however, this only occurs when the two fluorophores are in close proximity and is sensitive to changes in distance and orientation between the fluorophores. Measuring the FRET requires measuring the amount of FRET signal, the amount of total YFP and the amount of total CFP. Because the emission spectra overlap to some extent, there is always "spillover." Spillover is the amount of signal observed in the FRET channel per arbitrary unit of the CFP or YFP alone. Therefore the FRET ratio is the amount of signal observed in the FRET channel divided by the amount of spillover that would be expected give the total amount of CFP and YFP present in the sample.

(B) Diploid strains containing the FRET reporters (YJP115 *TDH3*-Ypet/*TDH3*-Cypet, YJP148 *TDH3*-Ypet/*TDH3*-Cypet *hog1*Δ/*hog1*Δ, YJP146 *TPI1*-Ypet/*TPI1*-Cypet) were grown to mid-exponential phase in synthetic complete medium and transferred to a black clear-bottom 96 well plate. The 96-well plate fluorimeter reads from the bottom of the plate, thus requiring a transparent bottom: however, the walls of the wells are opaque to prevent mixing of signal between the wells. An equal volume of synthetic complete medium or synthetic complete medium containing 2 M sorbitol was then added at the beginning of the time course. The background fluorescence under these conditions was determined using an unlabeled strain, BY4743. At each time point the absorbance at 600 nm was measured to normalize each well to the number of cells before subtracting the background fluorescence. The amount of spillover was determined with strains YJP126 *TDH3*-Ypet, YJP129 *TDH3*-Cypet, YJP141 *TPI1*-Ypet and YJP142 *TPI1*-Cypet. These strains were treated the exact same way as the FRET pair strains, and a spillover for each time point was calculated (however, averaging the spillover for each time point and using the average spillover for subsequent calculations resulted in more consistent results).

A

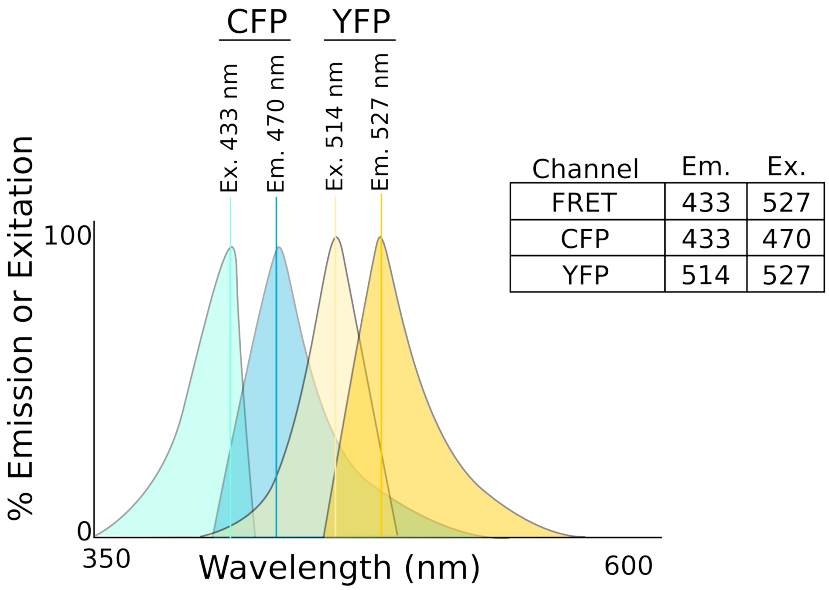

Channel	Em.	Ex.
FRET	433	527
CFP	433	470
YFP	514	527

$$\text{FRET-ratio} = \frac{\text{FRET}}{\text{CFP} \times \text{CFP}_{\text{spillover}} + \text{YFP} \times \text{YFP}_{\text{spillover}}}$$

B

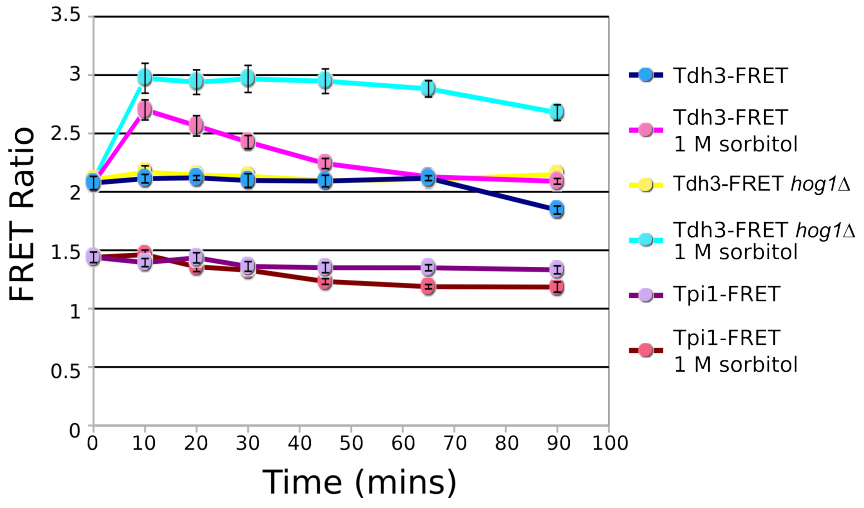

basal FRET ratio of the the 2X strain was increased from 2.35 to 2.65(Figure 3-8A). This strain also had the same initial spike and then gradual return to the baseline seen in the original FRET pair strain. This FRET-pair-concentration-dependent increase in the FRET ratio appears to imply that molecular crowding may effect the FRET signal observed. However, I would argue that based on these results molecular crowding it is not a sufficient explanation for the changes in FRET observed during hyperosmotic shock. I base this on the observation that the basal FRET ratio of the 2X Tdh3-FRET (2.65) pair is lower then that seen in the original (1X) Tdh3-FRET pair 10-20 min after hyperosmotic shock (2.75). If the spike in the Tdh3 FRET ratio seen during hyperosmotic shock was due to a decrease in cell volume and molecular crowding, then to achieve this amount of FRET, the volume change would have to be more than a 50% decrease. Hyperosmotic stress with 1 M sorbitol decreases the volume by 30-40% (Schaber et al., 2010; Parmar et al., 2011). A 30-40% volume decrease would increase the concentration of the Tdh3-FRET pairs by 42-66%, whereas for molecular crowding to be responsible for the observed FRET changes a >100% increase in concentration would be required. Therefore, while it is still possible that some part of the Tdh3 FRET ratio is influenced by molecular crowding, it does not seem explain the data entirely. Interestingly, the 2X Tdh3-FRET pair *hog1*Δ strain did not have an increased FRET ratio at all, even through the CFP and YFP channels had double the signal compared to the original Tdh3-FRET pair strain. It, therefore, seems that the increase in the FRET ratio that occurs along with higher Tdh3 concentrations depends on the presence of Hog1, further arguing against the possibility of molecular crowding.

The Tdh3 FRET ratio changes observed during hyperosmotic shock and their partial dependence on Hog1, implies that Hog1 may regulate the GAPDHs in some manner. Whether Hog1 does this directly or indirectly is not clear. Despite the inability of Hog1 to phosphorylate Tdh3 *in vitro*, as mentioned above, it is still possible there is an adapter protein or priming phosphorylation needed for Hog1 to act on Tdh3 *in vivo*. To determine if the observed changes in the Tdh3 FRET ratio depend on MAPK phosphorylation of Tdh3, I constructed plasmids containing both FRET pairs with Ser302 mutated to Asn and transformed them into a *tdh3*Δ/*tdh3*Δ diploid strain. This mutation did not change the overall dynamics of the Tdh3-FRET (Figure 3-9A). The mutant Tdh3-FRET pairs did have a slightly decreased FRET ratio, possibly due to the mutation making the homotetramer less stable. One other possible explanation is that the GAPDHs are able to form heterotetramers and Hog1 phosphorylates all three. However, when Tdh1-Tdh3 and Tdh2-Tdh3 FRET pairs were made, very little FRET was observed and there was no change in the FRET ratio during hyperosmotic shock.

I then considered the possibility that the change in Tdh3 FRET was a result of shunting glycolytic intermediates to glycerol production and repeated the Tdh3 FRET experiment in a diploid that was homozygous for *gpd1*Δ. Interestingly, the change in Tdh3-FRET in this strain was almost identical to that of the *hog1*Δ (Figure 3-9B). The Tdh3 FRET ratio increased and then remained elevated throughout the time course. This implies that the gradual return to baseline observed in the FRET ratio is an indirect result of glycerol production. One interesting thing to note, however, is that while the *hog1*Δ succumbs to hyperosmotic shock, the *gpd1*Δ strain does not; yet, at least within this time scale, the changes in the Tdh3 FRET ratio are indistinguishable.

Because the result from the *gpd1*Δ strain indicates that the Tdh3 FRET ratio is changing due to glycerol production, I then tested whether or not the changes seen were due to flux through Tdh3 itself. In order to determine this, I repeated the FRET experiments with a catalytically inactive Tdh3 mutant (Cys150 to Ser). However, in this mutant the baseline, initial

Figure 3-8. Changes in the Tdh3 FRET ratio during hyperosmotic shock are not entirely due to molecular crowding

(A) Strains YJP115 (*TDH3*-Ypet/*TDH3*-Cypet) and YJP255 (*TDH3*-Ypet/*TDH3*-Cypet YCplac33-*TDH3*-Cypet YCplac111-*TDH3*-Ypet) were grown to mid-exponential phase in synthetic complete medium. An equal volume of synthetic complete medium or synthetic complete medium containing 2 M sorbitol was then added at the beginning of the time course. Spillover was calculated with the strains YJP253 (*TDH3*-Ypet YCplac111 *TDH3*-Ypet) and YJP254 (*TDH3*-Cypet YCplac33-*TDH3*-Cypet). While increasing the concentration of the Tdh3-FRET pairs did increase the FRET ratio, it is not a large enough increase to explain the changes observed during hyperosmotic shock.

(B) YJP148 (*TDH3*-Ypet/*TDH3*-Cypet *hog1*Δ*/hog1*Δ) and YJP256 (*TDH3*-Ypet/*TDH3*-Cypet YCplac33-*TDH3*-Cypet YCplac111-*TDH3*-Ypet *hog1*Δ*/hog1*Δ) were grown to mid-exponential phase in synthetic complete medium and transferred to a black clear-bottom 96 well plate. An equal volume of synthetic complete medium or synthetic complete medium containing 2 M sorbitol was then added at the beginning of the time course. Spillover was calculated with the strains YJP253 (*TDH3*-Ypet YCplac111 *TDH3*-Ypet) and YJP254 (*TDH3*-Cypet YCplac33-*TDH3*-Cypet). The increase observed in the FRET ratio due to the increase in Tdh3-FRET pair concentration is entirely dependent on the presence of *HOG1*, an observation that is interesting in itself and rules our molecular crowding as the source of the FRET signal. It is important to note that the amount of fluorescent signal observed in the strain containing two copies of the Tdh3-FRET pairs was approximately double that seen in the original strains used, as expected.

A

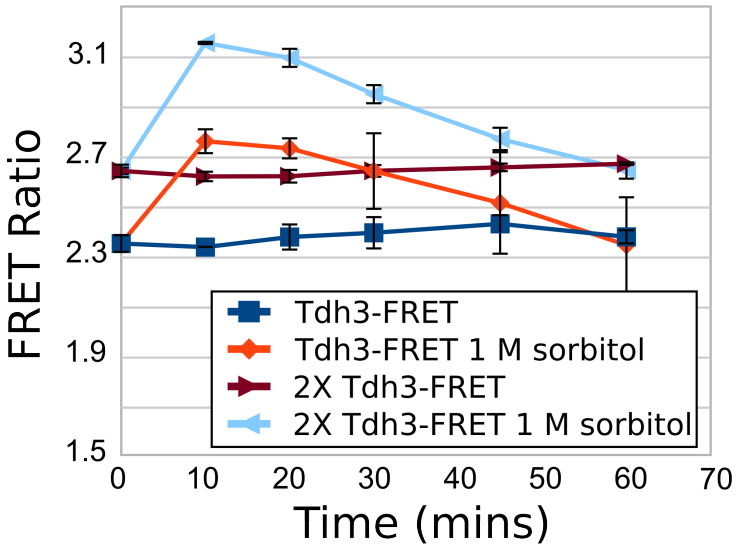

HOG1+

B

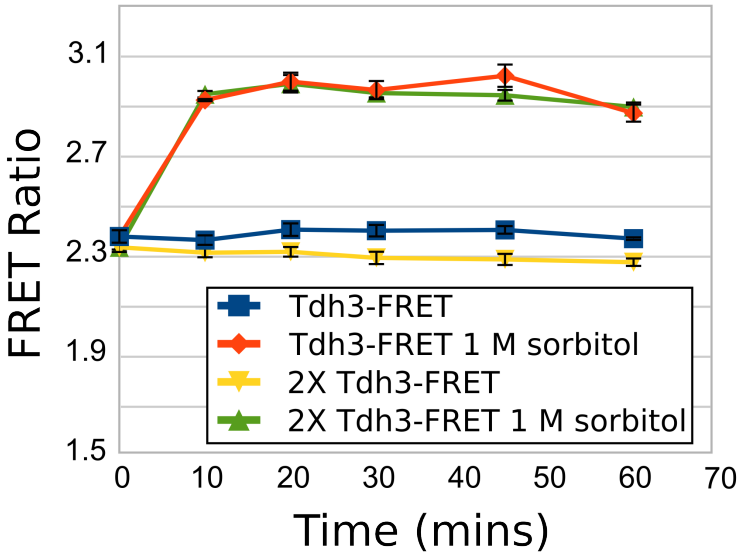

hog1Δ

Figure 3-9. Changes in the Tdh3 FRET ratio during hyperosmotic shock are not due direct phosphorylation by Hog1 but are correlated with glycerol production.

(A) Strains YJP278 (*tdh3*Δ*/tdh3*ΔYCplac33-*TDH3*-Cypet YCplac111-*TDH3*-Ypet) and YJP282 (*tdh3*Δ*/tdh3*ΔYCplac33-*TDH3-S302N*-Cypet YCplac111-*TDH3-S302N*-Ypet) were grown to mid-exponential phase in synthetic complete medium and transferred to a black clear-bottom 96 well plate. An equal volume of synthetic complete medium or synthetic complete medium containing 2 M sorbitol was then added at the beginning of the time course. The spillover was calculated with strains containing only the donor or acceptor Tdh3 fusion with or without the Ser302 mutated to Asn (YJP274, YJP275, YJP276, YJP277, YJP278). This mutant is known to not be entirely functional; however, the changes in the FRET ratio are still similar to the wild type Tdh3 FRET pair, indicating that the potential phosphorylation at Ser302 is not important for the changes observed in the FRET during hyperosmotic shock.

(B) Strains YJP115 (*TDH3*-Ypet/*TDH3*-Cypet), YJP148 (*TDH3*-Ypet/*TDH3*-Cypet *hog1*Δ*/hog1*Δ*)* and YJP295(*TDH3*-Ypet/*TDH3*-Cypet *gpd1*Δ*/gpd1*Δ*)* were grown to mid-exponential phase in synthetic complete medium and transferred to a black clear-bottom 96 well plate. An equal volume of synthetic complete medium or synthetic complete medium containing 2 M sorbitol was then added at the beginning of the time course. The amount of spillover was determined with strains YJP126 (*TDH3*-Ypet), YJP129 (*TDH3*-Cypet). Because the changes in Tdh3-FRET in the *gpd1*Δ and *hog1*Δ strains are essentially identical, it is most likely that these changes are a real-time read out of glycerol production during hyperosmotic shock.

A

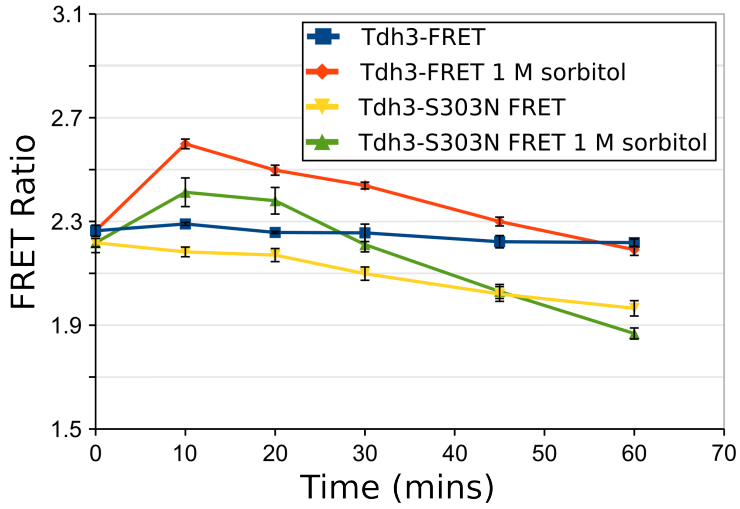
Tdh3-FRET
Tdh3-FRET 1 M sorbitol
Tdh3-S303N FRET
Tdh3-S303N FRET 1 M sorbitol
FRET Ratio
Time (mins)
3.1
2.7
2.3
1.9
1.5
0
10
20
30
40
50
60
70

B

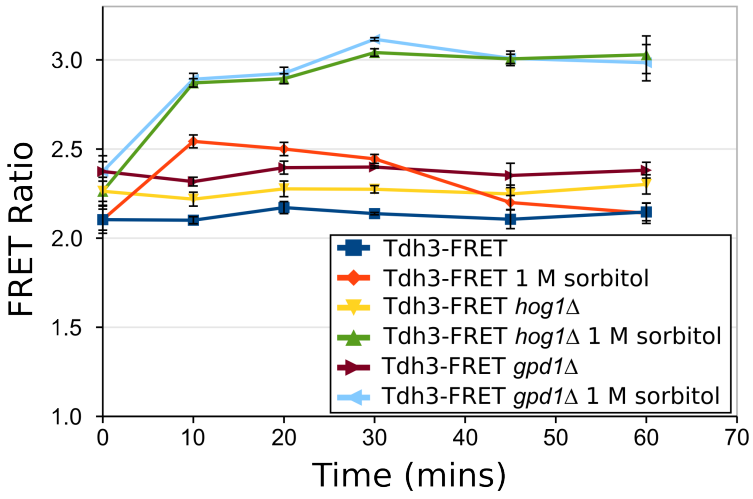
Tdh3-FRET
Tdh3-FRET 1 M sorbitol
Tdh3-FRET hog1Δ
Tdh3-FRET hog1Δ 1 M sorbitol
Tdh3-FRET gpd1Δ
Tdh3-FRET gpd1Δ 1 M sorbitol
FRET Ratio
Time (mins)
3.0
2.5
2.0
1.5
1.0
0
10
20
30
40
50
60
70

spike and gradual return to baseline FRET ratios were all the same as the wild-type Tdh3. Therefore, this is not a measure of flux through Tdh3, since in this mutant the flux would be zero at all times.

The NADH redox balance and glycerol production

Even if Hog1 does phosphorylate and inhibit the GAPDHs, that would only increase the amount of DHAP available to Gpd1. This raises the issue of where the NADH comes from to reduce DHAP to glycerol-3-phosphate. The GAPDHs are one of the primary producers of NADH in glycolysis; although there are other sources of NADH production particularly in amino acid catabolism. So inhibiting the GAPDHs would increase the amount of triose-phosphate but potentially decrease the amount of NADH. Therefore, I decided to look into possible means by which Hog1 could influence the NADH/NAD+ ratio. There are several processes that oxidize NADH. However, the big players in that game are mitochondrial respiration and ethanol production. Under the assumption that glycolysis came to a halt below the GAPDHs, thus depriving the alcohol dehydrogenases of acetaldehyde, I looked into the possibility of Hog1 affecting mitochondrial respiration.

NADH is oxidized to NAD+ on the outside surface of the inner mitochondrial membrane by Nde1 and Nde2 and on the inside of the inner mitochondrial membrane by Ndi1 (Figure 3-2). NADH cannot permeate the outer membrane without the assistance of mitochondrial porin Por1 and possibly its paralog Por2. The two porins are very similar in primary structure, however, deletion of Por1 alone significantly reduces the ability of NADH to pass through the outer membrane of mitochondria isolated from the relevant strains (Rigoulet et al., 2004). It appears that Por1 is either the sole porin responsible or it accounts for the vast majority of mitochondrial NADH permeability. There are five potential MAPK phosphorylation sites on this 19 stranded beta-barrel structured protein that also contains a single helix within the channel of the porin (Figure 3-10) (Bayrhuber et al., 2008). It is thought that the helix normally sits on top of the membrane adjacent to the porin, and the fact that it is found within the pore is an artifact of the *in vitro* conditions. Of the five potential MAPK sites, three would be accessible from the cytoplasm (S2, T25, T103 and S132). However, the three-dimensional structure (solved by both X-ray crystallography and nuclear magnetic resonance) of the human ortholog of *POR1* (hVDAC1) was not available when I first made Por1 phosphorylation site mutants, and instead there were other partially correct biochemical and bioinformatic models of the porin's topology (Casadio et al., 2002). Based on the predicted models, I mutated Ser2, Thr25, Thr91 and Thr103, all to Ala.

When the wild-type *POR1* was replaced with these mutant versions of *por1* in the *HOG1-GFP-CCaaX*^{Ras2} background, they did not cause sensitivity to hyperosmotic stress. They were functional since they complemented the temperature-sensitivity of a *por1*Δ strain grown on medium containing glycerol as a carbon source. After the tertiary structure of the human ortholog hVDAC1 was published, I compared the sequence of Por1 to this protein and predicted that Thr132 would also be exposed on the cytoplasmic side. Therefore, I mutated this potential phosphorylation site as well. However, even when all five of these sites had been altered to alanine in the *HOG1-GFP-CCaaX*^{Ras2} background, the cells were still resistant to hyperosmotic shock.

Figure 3-10. Potential Hog1 consensus phosphorylation sites within the Por1 protein are not required for hyperosmotic stress resistance.

(A) Tertiary structure of the human ortholog of *POR1* (hVDAC1; PDB# 2JK4) solved by a combination of x-ray crystallography and NMR. Both the side and top view are shown. Residues highlighted in red represent the expected positions of consensus MAPK phosphorylation sites in the yeast Por1 protein, however, only one of the five sites is conserved in hVDAC1, Thr103.

(B) Strain YJP721 (*HOG1-AS-GFP-CCaaX*^{Ras2} *por1*Δ) was transformed with a pRS316 empty vector, pRS316 containing a wild-type copy of *POR1* or pRS316 containging the indicated point mutant of *POR1*. The resulting strains were serially diluted on the indicated medium and incubated at 30ºC for 3 days. None of the POR1 mutants causes hyperosmotic stress sensitivity in the *HOG1-AS-GFP-CCaaX*^{Ras2} background.

A

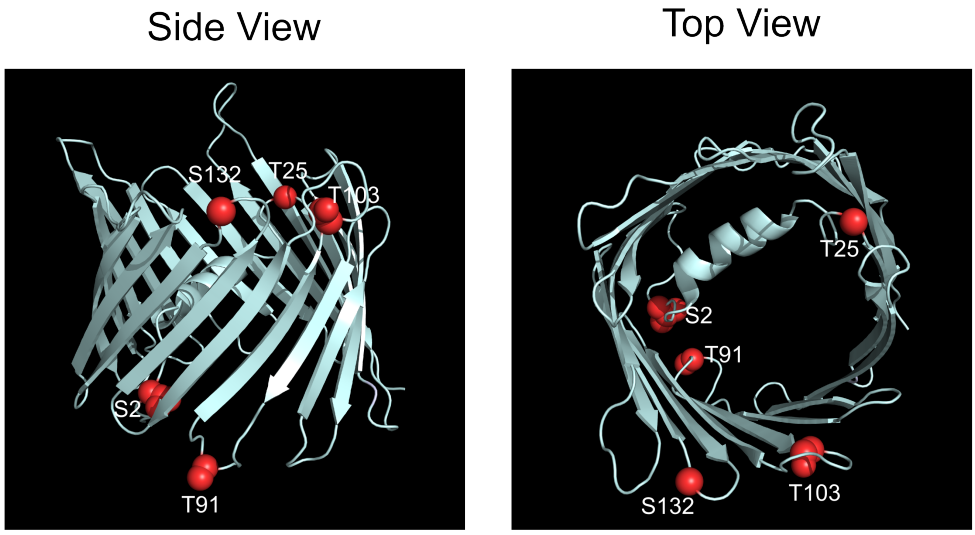

B

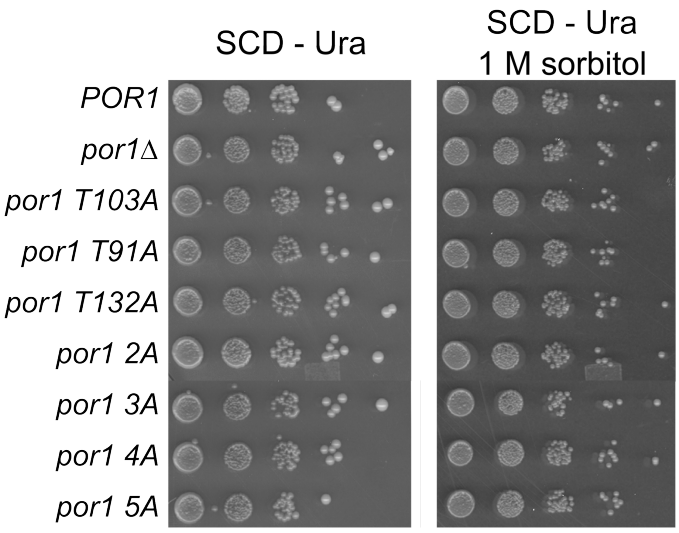

2A: T91A T25A
3A: T91A T25A T103A
4A: T91A T25A T103A S2A
5A: T91A T25A T103A S2A S132A

Discussion

While my work, Patrick Westfall's work, and work by several other groups has indicated that Hog1 directly regulates metabolism to increase glycerol production, the substrate or substrates that Hog1 modifies for this function are still not known. The list of possible Hog1 substrates is quite long, and going through that list and checking them one by one is an arduous process. Moreover, experiments are usually not as easy and straightforward as they would seem. I spent quite a large amount of time and effort trying to determine whether or not the GAPDHs are substrates of Hog1 and whether their regulation by Hog1 is responsible for glycerol production. It is still not entirely clear as to whether that is the case. However, at this point, the available evidence indicates that Hog1 does not directly regulate these enzymes.

While there are some examples of *in vitro* kinase assays resulting in false negatives, the more common problem is false positives. One example of a potential false negative is that Fus3 will not be phosphorylated by Ste7 *in vitro* unless the scaffold Ste5 is present (Good et al., 2009). It would be a bit *ad hoc* to postulate the necessity of an adapter protein or priming phosphorylation site as a prerequisite for the potential Hog1-Tdh3 interaction. The most likely explanation is that Hog1 does not phosphorylate Tdh3 and that the study (Kim and Shah, 2007) claiming that it did was in error. Tdh3 was initially identified in that study by 2D-PAGE followed by protein staining, excision of the stained protein dot and identification of the peptide by mass spectrometry. This sort of analysis often leads to misidentification due to overlapping spots. With Tdh3 being such an abundant protein it is very easy to entertain the possibility it was a contaminating peptide and not the actual phosphorylated peptide. The study confirmed the phosphorylation by immunoprecipitating Tdh3 from $[^{32}P]PO_4^{3-}$-labeled cells before and after hyperosmotic shock, with and without active Hog1. A band can be seen in the immunoprecipitate that becomes radioactive during stress only when Hog1 is active, however, that species could be another substrate of Hog1 that co-IPs with Tdh3.

Because the GAPDHs were very difficult to express in *E. coli*, I purified them via overexpression in yeast. There is a possibility that Ser302 was already phosphorylated in the GAPDH protein I purified, thus the protein used in the kinase assay could not be modified any further. This is unlikely, though, since it would require essentially all of the Tdh3 to have been phosphorylated to prevent any signal from appearing in the autoradiogram.

Pairwise double GAPDH deletion mutants reproducibly lead to an increase in hyperosmotic stress resistance. This initial result was very encouraging and is a strong argument that a decrease in GAPDH activity contributes to hyperosmotic stress resistance. However, Ser302 to Ala (or Asn) compromised GAPDH function, perhaps mimicking, instead of preventing, the reduction in function that occurs during hyperosmotic stress. Because of this, I turned to the Tdh3 FRET analysis, which allowed me to look at *in vivo* changes in Tdh3 that depend on Hog1 without having to mutate this GAPDH.

The Tdh3 FRET experiments indicate that something about this GAPDH changes during hyperosmotic shock. The amount of FRET initially increases and then returns to its original value. Strangely, it is the return to the baseline that depends on Hog1. This is not something that happens to just any FRET pair, since it was not observed with the Tpi1-FRET experiment. Experiments performed to date argue against the possibility that the entirety of the changes observed in the Tdh3 FRET ratio is due to molecular crowding. Because deletion of *GPD1* had the same effect as the deletion of *HOG1*, it seems that Hog1 is not directly effecting Tdh3, but instead the change in FRET is an indirect effect of Hog1- and Gpd1-dependent glycerol production. Finally, this is not simply measuring flux through the GAPDHs, since the

catalytically-inactive Tdh3 mutants produced the same FRET ratio changes during hyperosmotic shock. However, without understanding the molecular nature of the changes in the FRET ratio it is very difficult to come to any concrete conclusions from these experiments.

Because the GAPDH phosphorylation site mutants were only partially functional, it was as if they were produced "pre-inhibited" by Hog1 and thus could not be used to reliably test the importance of post-translational modification of these residues. The Tdh3 FRET experiment, on the other hand, gave me the opportunity to look at the GAPDHs in real time during hyperosmotic stress. Assuming the changes in Tdh3 FRET are a meaningful readout of regulation of metabolism by Hog1, the phosphorylation site mutants rule out any direct regulation of Tdh3 by Hog1. It was clear that both the initial spike and return to baseline of the FRET ratio were still present in the Tdh3 phosphosite mutants. Despite not knowing the molecular nature of the Hog1-dependent change in the Tdh3 FRET ratio, knowing that it is still present when Hog1 cannot phosphorylate Tdh3 rules out direct phosphorylation. Perhaps once it is known what part of metabolism Hog1 alters to increase glycerol production, I will be able to make sense of the changes in Tdh3 FRET. For now it has served its purpose by showing me that the GAPDHs are very unlikely to be Hog1 substrates *in vivo*.

It is entirely possible that more important thing Hog1 changes to increase glycerol production is the NADH/NAD+ ratio. I looked into the possibility that Hog1 inhibits NADH oxidation by blocking passage of NADH through the mitochondrial outer membrane. The Por1 phosphorylation site mutants tested so far indicate that it is not an essential function of Hog1 to close this channel.

After ruling out Tpi1, the GAPDHs and Por1, the next most likely candidates would be the alcohol dehydrogenases. Really, if Hog1 inhibited these enzymes it could kill two birds with one stone. It would cause a back up of glycolytic products, and it would prevent NADH from being oxidized in the production of ethanol. Working with the alcohol dehydrogenases can be intimidating because there are six of them, although, Adh1 seems to be the major isoform. Each Adh has at least one potential MAPK phosphorylation site making them potential Hog1 substrates.

The other possibility is that there are multiple redundancies in Hog1 substrates that each contribute to hyperosmotic stress resistance. For instance, increased flux through Tpi1 could cause an increase in the concentration of methylglyoxal, a toxic metabolite. Methylglyoxal is formed at a small rate from an intermediate of the triose-phosphate isomerase reaction, and is removed by the glyoxylase enzymes Glo1, 2 and 4 (Inoue et al., 1998). Hog1 is known to upregulate *GLO1* transcription, thus, at earlier time points, one relevant function of Hog1 may be in directly influencing methylglyoxal metabolism (Figure 3-2). It might be the case that several substrates must be mutated before *HOG1* cells would fail to grow in high osmolarity.

While ultimately I was unable to identify the Hog1 substrate(s) that confer hyperosmotic stress resistance, I still am satisfied with the progress made. First of all, together with Patrick Westfall, I have shown that Hog1 transcription is not required for hyperosmotic stress resistance, disproving long-standing and unquestioned dogma. I have also made progress towards understanding how Hog1 confers stress resistance by ruling out several obvious candidates. The candidate-based approach to finding a theorized substrate of a kinase is always a gamble. Moreover, the enticing result that deleting the GAPDHs increases hyperosmotic stress resistance led me to double down on that gamble several times. Undoubtedly, there are a few more candidates worth checking, however, a well-planned and unbiased genetic or biochemical screen, although always a gamble as well, will probably be more likely to succeed in finding

these Hog1 substrates.

Chapter 4
Insulation, Not Cross-inhibition, Maintains Signaling Specificity between the HOG and Mating Pheromone Response Pathway

Introduction

All eukaryotic cells express multiple MAPKs. Each MAPK is activated in response to distinct stimuli and elicits characteristic outputs. Despite the discrete nature of these signaling modules, components of one MAPK pathway can be shared with other MAPK pathways present in the same cell. This raises the issue of how inadvertant activation of the inappropriate pathway – "crosstalk" – is avoided. There are MAPK pathways in yeast that represent prime examples of signaling modules that share pleotropic signaling proteins. Cdc42 (small GTPase), Ste20 (PAK), Ste11 (MAPKKK) and Ste50 (adapter protein) are involved in the HOG, mating and filamentous growth pathways. Cdc42 is utilized in several cellular processes as well. When these proteins are engaged in the context of the HOG pathway, the result is phosphorylation and activation of only the MAPKKK Pbs2. In the mating pathway, by contrast, the same signaling proteins are active, but lead to only activation of the MAPKKK Ste7. If, however, HOG1 is deleted or its kinase activity is inhibited during hyperosmotic shock, there is inappropriate activation of both the mating and filamentous growth MAPK pathways (O'Rourke and Herskowitz, 1998; Westfall and Thorner, 2006). These data indicate that Hog1 plays an active role in suppressing this crosstalk.

There are two general modes by which crosstalk could be prevented: insulation or inhibition. Insulation is a mechanism whereby Hog1 would prevent the activated Cdc42-Ste20-Ste50-Ste11 complex from ever productively stimulating the other two MAPK pathways. That is, Hog1 action insulates the HOG pathway so no signal ever leaks out. By contrast, in an inhibition mechanism the active Cdc42-Ste20-Ste50-Ste11 does lead to activation of other the MAPK pathways, but Hog1 action squelches the consequences of activation, thereby preventing any output.

Determining by which of these two mechanisms Hog1 imposes its blockade of crosstalk is important not only to understand signaling dynamics but also in terms of identifying the substrate(s) Hog1 phosphorylates to prevent crosstalk. If cross-pathway inhibition is used, then the list of possible substrates is narrowed to those that are either required for mating and FG pathway function or those that could negatively regulate these pathways. Whereas if Hog1 action prevents spillover of the initial signal then this may be mediated by a substrate that is either a component of the HOG pathway or something that regulates one of the components of the HOG pathway.

A relatively simple experiment can be done to distinguish between these two possibilities. If Hog1 inhibits the mating pathway to prevent crosstalk, then activation of the HOG pathway should prevent activation of the mating pathway and possibly vice-versa. Whereas if the HOG pathway is insulated, cells should be capable of activating both pathways at once. To carry out such an experiment one needs to examine the output of each pathway simultaneously in single cells.

Another group reported exactly this type of experiment using strains containing two transcriptional reporters (McClean et al., 2007). The HOG pathway reporter utilized a gene, *STL1,* that is strongly induced during hyperosmotic stress in a *HOG1* dependent manner. The

authors replaced the coding sequence of *STL1* with mRFP so that upon HOG pathway activation the cells turned red. The mating pathway reporter was constructed in a similar way, except the coding sequence of *FUS1* was replaced with eGFP. *FUS1* is a gene that is strongly and specifically induced during mating pathway activation. Using this strain, they found that when treated with both mating pheromone and high osmolarity simultaneously, individual cells turned on either the HOG or the mating pathway reporter, but never both. Higher concentrations of pheromone or sorbitol during co-stimulation lead to more mating or HOG pathway activation, respectively. Moreover, pre-activation of one pathway decreased the proportion of cells that would respond to the subsequent stimulation of the other pathway. Therefore, based on these results, they concluded that crosstalk was prevented by Hog1 inhibition of the mating pathway and went so far as to claim that there is some "decision tree" cells use to determine which pathway is activated first.

I found these results to be very interesting and decided that to carry out further work on identifying potential candidates for the Hog1 substrates that prevent crosstalk it would be useful to construct similar reporters. I surmised that mutations in certain genes that might be involved in crosstalk prevention could alter the outcome of the co-stimulation experiment, either by allowing one pathway to constitutively dominate over the other, or by allowing both pathways to become active simultaneously in single cells.

Results

Construction of HOG and mating pathway reporters

I was not satisfied with the features of the fluorescent reporters constructed by (McClean et al., 2007). Particularly, I felt it was a poor choice to replace the coding sequence of *STL1* and *FUS1* with the coding-sequence for the fluorescent proteins. These genes are induced by MAPK pathways for a reason, and deleting them might alter the physiology of the cells. The reporters were also constructed in an unusual strain background (Σ1278b) which is usually only used for investigation of the filamentous growth pathway due to its hyperinvasiveness. Finally, the mRFP variant is very dim and slow-folding compared to other more recently developed RFP varients. Therefore, I used the brighter and faster folding td-tomato (Shaner et al., 2008).

I fused the promoter of *STL1* to HA-tagged td-tomato and the promoter of *FUS1* to HA-tagged eGFP. The fluorescent proteins were HA epitope-tagged so that their expression could be readily measured at the population level by quantitative immuno-blotting. These promoter-fluorophore fusions were then cloned into an integrative *LEU2*-marked plasmid. By linearizing these plasmids with a restriction site within the *FUS1* or *STL1* promoter and carrying out DNA-mediated transformation of yeast strains YPH499 and YPH500, I was able to insert these reporters at the *FUS1* or *STL1* loci without disrupting the resident *FUS1* or *STL1* genes. Basically, the plasmid integrates within the promoter of the gene but also recreates the promoter just upstream of the coding sequence, essentially a tandem duplication (Figures 4-1A and 4-1B).

YPH499 (*MAT***a**) is isogenic to YPH500 (*MAT*α) and are both *ade2* mutants. Cells that are *ade2* accumulate a red pigment that interferes with fluorescence microscopy, so I replaced the *LEU2* gene that marked each reporter with *ADE2*. These strains were then mated, the diploid was sporulated and tetrads dissected to obtain a strain that contained both reporters. I then deleted the *BAR1* gene in this strain. *BAR*1 encodes a protease secreted by *MAT***a** cells that degrades the α-factor used to stimulate the mating pathway (Ciejek and Thorner, 1979; Sprague and Herskowitz, 1981). Deleting this gene prevents variability in pheromone concentration during a time course of stimulation and also reduces the concentration of α-factor required for sustained mating pathway activation.

As expected, stimulation with α-factor resulted in an increase in $FUS1_{promoter}$-eGFP expression (Figure 4-1A), whereas treatment with sorbitol resulted in $STL1_{promoter}$-td-tomato expression (Figure 4-1B). To computationally identify individual cells, images of auto-fluorescence were collected using a UV excitation filter as an unbiased means of cell identification. Brightfield microscopy does not have enough contrast to reproducibly identify cells in images, and using either the GFP or RFP images might bias the identification process towards one or the other fluorophore. A program called Cell profiler was used to identify the cells and quantitate the pixel intensities for both GFP and RFP channels (Figure 4-1C) (Carpenter et al., 2006). The cell identification algorithm was optimized as much as possible to identify as many cells as possible without declaring spurious image artifacts as cells. However, clumped cells and those cells which were out of focus were often not identified. This did not introduce any bias into the results but instead simply decreased the total number of cells measured. Finally, during construction and testing of the mating pathway reporter, I noted that pheromone added to synthetic medium in glass culture tubes exhibited widely variable results, indicative of loss due to non-specific binding to the tube walls. I circumvented this problem by pre-coating the tubes with 1% bovine serum albumin and rinsing them with synthetic medium prior to their use. I did not observe this issue with rich-medium (YPD) presumably because there is plently of

Figure 4-1. Single-cell fluorescent reporters for the HOG and mating MAPK pathways

(A) The single-cell fluorescent reporter for the mating pathway consists of the *FUS1* promoter fused to HA-tagged GFP inserted within the promoter of the native *FUS1* locus. Integration of the plasmid within the *FUS1* promoter reconstitutes that promoter so that the *FUS1* coding sequence is still transcribed. This reporter is transcribed in response to pheromone, which activates the Fus3 and Kss1 MAPK. Fus3 and Kss1 phosphorylate and inactive two repressors (Dig1 and Dig2) of the the Ste12 transcription factor, which is able to recruit RNA polymerase II to the *FUS1* promoter. Upon pheromone treatment, the cells fluoresce green and form the characteristic shmoo morphology.

(B) The single-cell fluorescent reporter for the HOG pathway consists of the *STL1* promoter fused to HA-tagged td-tomato inserted within the promoter of the native *STL1* locus. Integration of the plasmid within the *STL1* promoter reconstitutes that promoter so that the *STL1* coding sequence is still transcribed. This reporter is transcribed in response to hyperosmotic shock, which activates the Hog1 MAPK. Hog1 phosphorylates and activates the Hot1 transcription factor which is responsible for recruiting RNA polymerase II to the *STL1* promoter. Upon hyperosmotic shock the cells fluoresce red.

(C) Cell identification using Cell Profiler cell image analysis software. Auto-fluorescence was used to identify the cells in an unbiased manner. Identified cells are shown in various colors simply to make them distinct from one another. When merged with the brightfield image it is clear that by using this method the majority of cells are identified in an accurate manner. The accuracy of this technique depends almost entirely on how well dispersed the cells are, and how well the image is focused. The various parameters used to determine the cell identification algorithm we set so that I would err on the side of caution. I set the parameters such that the likelihood of scoring artifacts (bubbles, debris, clumps of cells, etc) would be minimized. Because hundreds of cells were measured in each experiment and the cell identification process did not depend on the fluorescent reporters, missing a few cells was inconsequential to the statistical significance of the final result.

A

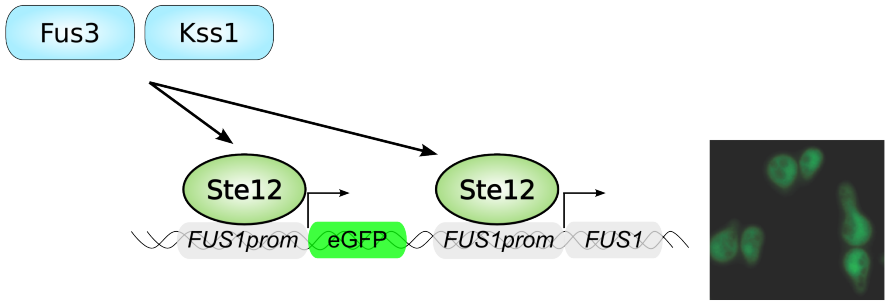
Fus3
Kss1
Ste12
Ste12
FUS1prom
eGFP
FUS1prom
FUS1

B

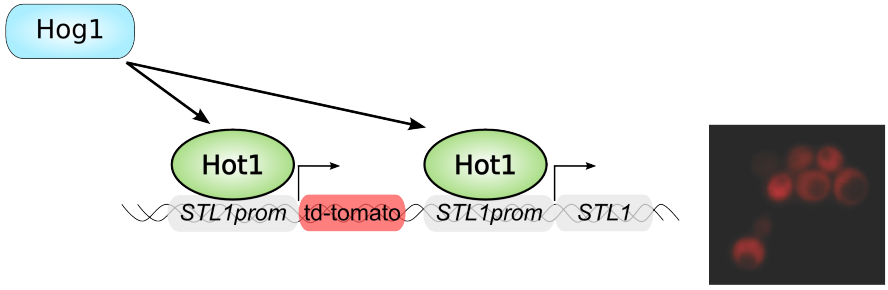
Hog1
Hot1
Hot1
STL1prom
td-tomato
STL1prom
STL1

C

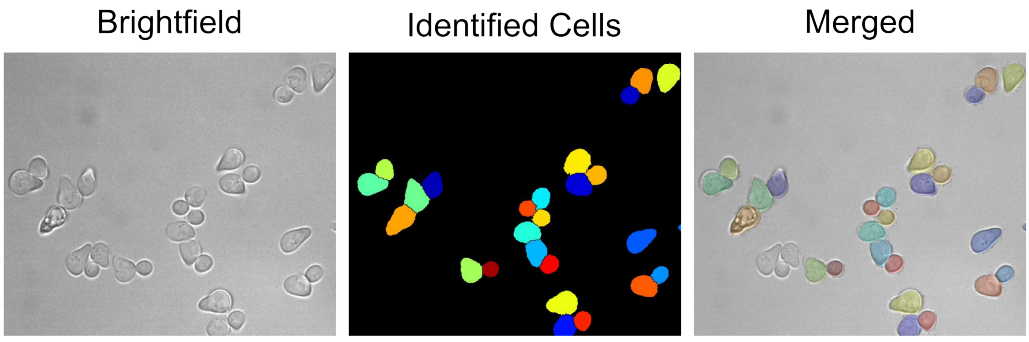
Brightfield
Identified Cells
Merged

peptide present from they yeast extract and bacto-peptone to block the binding surfaces.

Co-stimulation leads to co-activation of the HOG and mating MAPK pathways

Upon co-stimulation with 0.5 M sorbitol and 5 nM α-factor for a period of 2 h, both pathways were activated in the vast majority of cells, as judged by the levels of the $FUS1_{promoter}$-eGFP and $STL1_{promoter}$-td-tomato fluorescent reporters (Figure 4-2). Not only were both reporters induced, but the extent to which each reporter was turned on was almost identical during co-stimulation as when treated with each individual stimulant at the same concentration (Figure 4-2). I then tested the possibility that the mutual exclusivity previously reported might be only occur certain stimulant concentrations, or only within a certain time interval after stimulation. In the previous study (McClean et al., 2007), cells were stimulated with either α-factor or sorbitol for 1 h. I treated cells with 0, 5, 15 and 30 nM α-factor as well as 0, 0.25, 0.5 and 1 M sorbitol in all possible combinations for both 1 and 2 h. In all cases, the cells turned on both reporters when both stimulants were present (Figure 4-3 and 4-4). The amount of the fluorescent protein that had been produced after 1 h was significantly less then at 2 h, but enough signal was present to definitively conclude that both reporters were activated. It is important to note that these concentrations of stimulants proved to be within the dynamic range of each pathway. This means that adding more or less stimulant increased or decreased pathway output, respectively, ensuring that none of the results was compromised by saturation of the signaling potential of either pathway.

While these data demonstrated that both the HOG and mating pathway become activated at some point during the 1- and 2-h co-stimulation experiments, it was still possible that at very early time points there might be transient inhibition of one pathway by the other. For example, the HOG pathway might hold the mating pathway in check for 20 min, but then the mating pathway escapes inhibition and turns on. To investigate this possibility, I constructed strains that would allow me to monitor HOG and mating pathway activation on the min timescale. After its activation, Hog1 translocates into the nucleus within 5 min (Ferrigno et al., 1998). Similarly, after mating pathway activation, the MAPK scaffold protein Ste5 accumulates at the plasma membrane within 10 min (Garrenton et al., 2009). The strain I constructed expressed both *STE5*-3XGFP and *HOG1*-td-tomato, which allowed me to observe the translocation of both proteins simultaneously in individual cells.

Treatment of the translocation reporter strain with 1 M sorbitol resulted in Hog1-td-tomato nuclear translocation and did not change the localization of Ste5-3XGFP, whereas pheromone treatment caused Ste5-3XGFP to form puncta at the plasma membrane, but Hog1-td-tomato remained cytoplasmic (Figure 4-5). When these cells were treated with both sorbitol and α-factor for a period of 15 min, Hog-td-tomato became predominantly nuclear and Ste5-3XGFP accumulated at the plasma membrane simultaneously in individual cells (Figure 4-5). This experiment provided independent confirmation of the results obtained using the transcriptional fluorescent reporters. More importantly, it provided an earlier time point to rule out the possibility that there was mutual cross-inhibition at some point unobservable with the transcriptional reporters.

Because of the convolution of light, the measurement of the transcriptional fluorescent reporters is not exactly quantitative. While a higher pixel intensity means that there was more fluorescent protein present, double the pixel intensity does not mean there was exactly double the amount of reporter produced. Therefore, to confirm that both transcriptional reporters were being activated in individuals cells using a more quantitative method, I repeated the stimulations

Figure 4-2. Dual stimulation results in dual activation of the transcriptional fluorescent reporters

(A) Strain YJP212 containing both a mating and HOG pathway reporter was grown to mid-exponential phase in synthetic complete medium and then added to an equal volume of fresh medium containing double the concentration of the stated stimulant(s). After 2 h, the expression of the reporters was assessed in single cells by epifluorescence microscopy. The merged eGFP and td-tomato images are shown. As expected, addition of sorbitol resulting only in induction of the HOG pathway reporter ($STL1_{promoter}$-td-tomato), whereas pheromone addition only activated the mating pathway reporter ($FUS1_{promoter}$-eGFP). Addition of both sorbitol and pheromone activated both reporters in individual cells, indicating that there was no mutual cross-inhibition between the HOG and mating pathway.

(B) Data in (A) presented as a scatter plot, where each dot represents the average pixel intensity of eGFP and td-tomato for a single cell under the conditions tested (n ~ 400 per sample). Once plotted in this fashion, it is clear that not only do both reporters get induced upon co-stimulation, but the cell-to-cell variation and the range of response observed is almost identical to that for each respective stimulus alone.

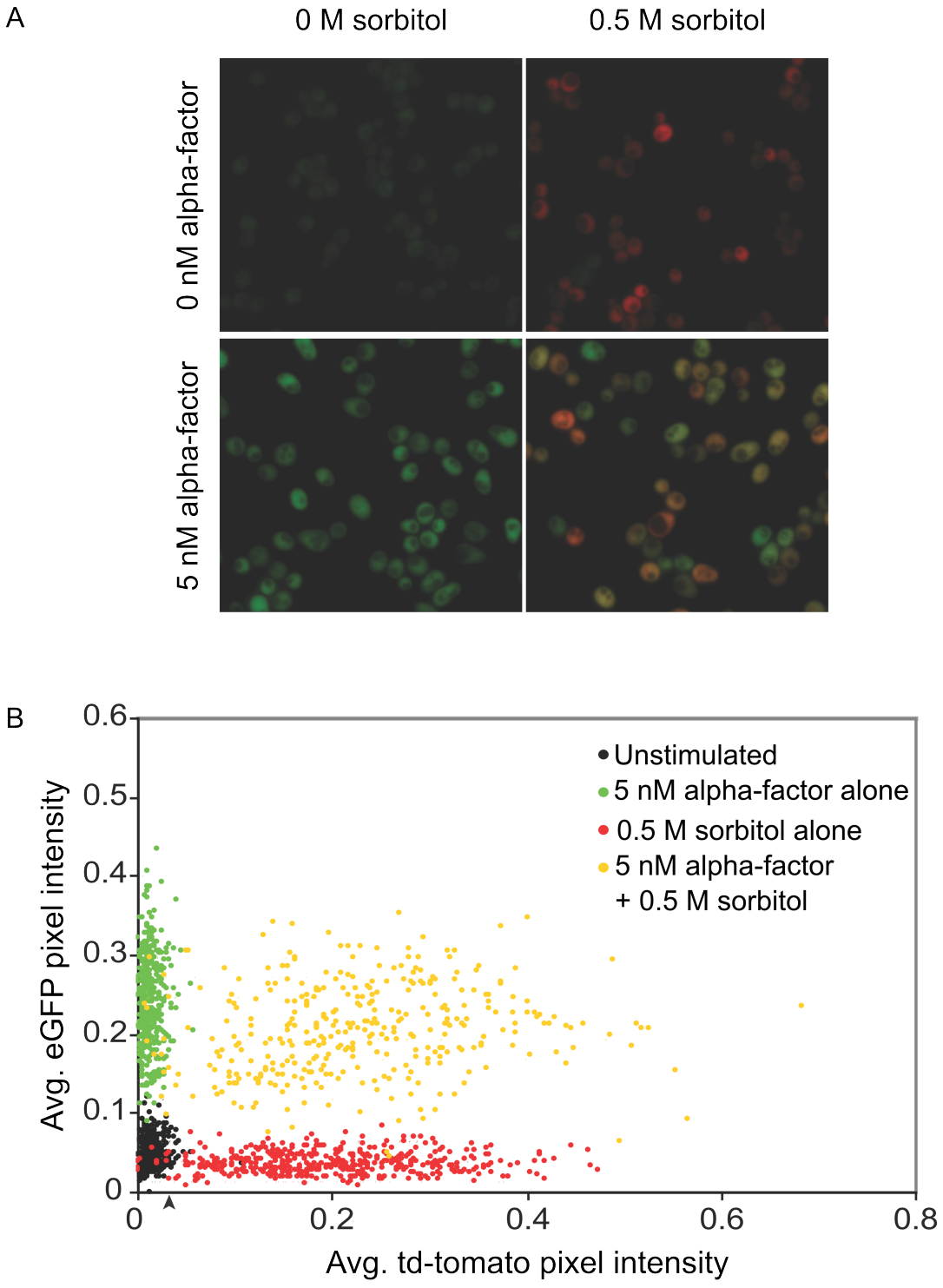
A
0 M sorbitol
0.5 M sorbitol
0 nM alpha-factor
5 nM alpha-factor
B
Avg. eGFP pixel intensity
Avg. td-tomato pixel intensity
0
0.1
0.2
0.3
0.4
0.5
0.6
0.2
0.4
0.6
0.8
Unstimulated
5 nM alpha-factor alone
0.5 M sorbitol alone
5 nM alpha-factor
+ 0.5 M sorbitol

Figure 4-3. Co-stimulation for 1 h results in co-activation of the HOG and mating pathway in single cells

(A) Strain YJP212 containing both the mating and HOG pathway reporters was grown to mid-exponential phase in synthetic complete medium and then added to an equal volume of fresh medium containing double the concentration of the stated stimulant(s). After 1 h, the expression of the reporters was assessed in single cells by epifluorescence microscopy. The merged eGFP and td-tomato images are shown. While stimulation for 1 h produced lower signals than that at 2, the micrographs show cells that have turned both green and red compared to the unstimulated sample. Thus, no mutual cross-inhibition can be observed within the first hour post-stimulation, nor does any specific combination of pheromone and sorbitol concentration result in mutual cross-inhibition.

(B) Data in (A), presented as a scatter plot, where each dot represents the average pixel intensity of eGFP and td-tomato for a single cell under the conditions tested (n ~ 400 per sample). The red dot represents the mean pixel intensities of eGFP and td-tomato for the entire population. The red bars indicate the standard deviation of eGFP and td-tomato pixel intensity observed in that population.

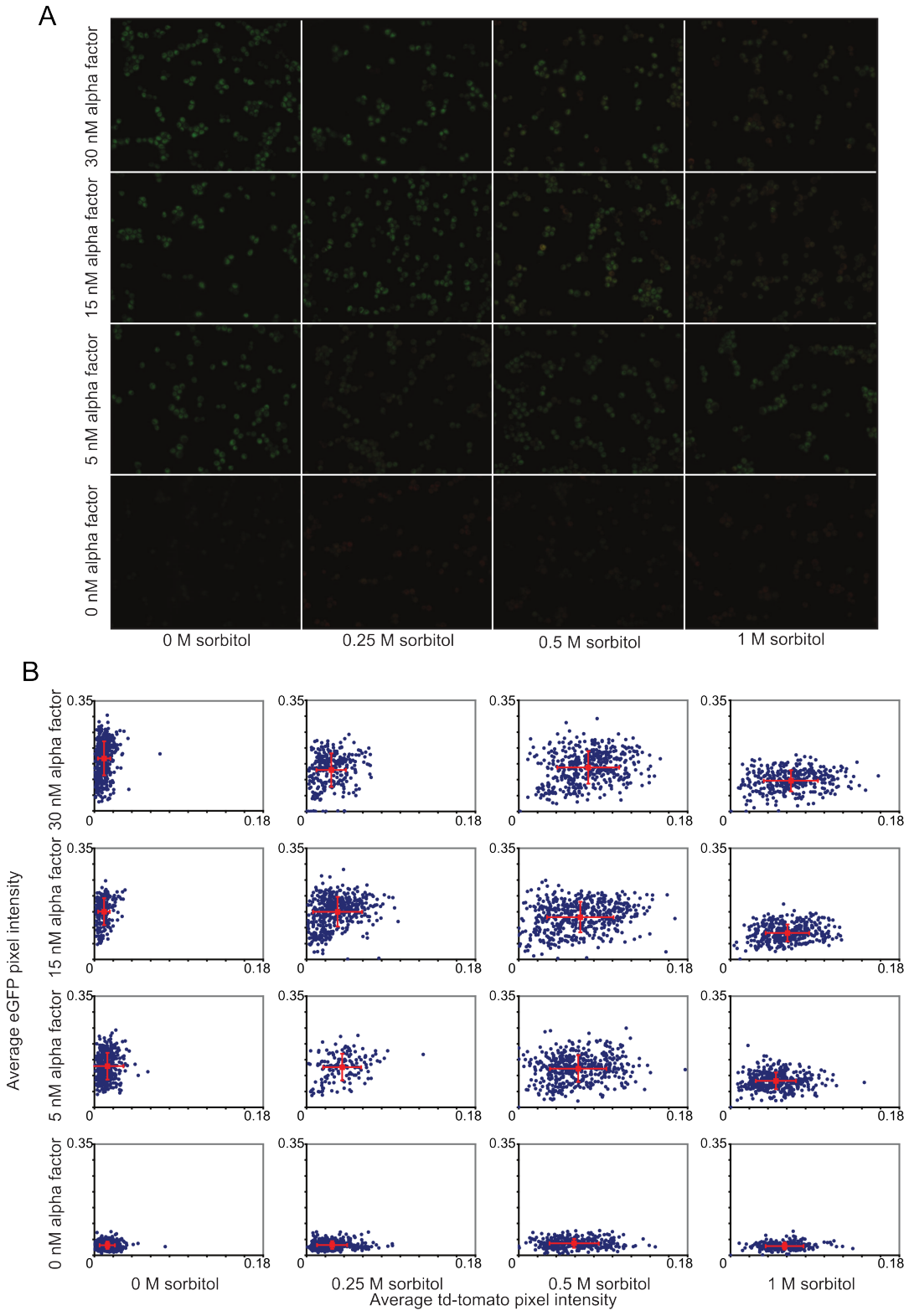
A
30 nM alpha factor
15 nM alpha factor
5 nM alpha factor
0 nM alpha factor
0 M sorbitol
0.25 M sorbitol
0.5 M sorbitol
1 M sorbitol
B
Average eGFP pixel intensity
0.35
0
0.18
Average td-tomato pixel intensity

Figure 4-4. Co-stimulation for 2 h results in co-activation of the HOG and mating pathway in single cells

(A) Strain YJP212 containing both the mating and HOG pathway reporters was grown to mid-exponential phase in synthetic complete medium and then added to an equal volume of fresh medium containing double the concentration of the stated stimulant(s). After 2 h, the expression of the reporters was assessed in single cells by epifluorescence microscopy. The merged eGFP and td-tomato images are shown. These data show that the concentrations of stimulants chosen are within the dynamic range of each MAPK pathway, since that addition of more stimulant results in more reporter production. However, at all concentrations tested co-stimulation resulted in co-activation of the HOG and mating pathway reporters.

(B) Data in (A) presented as a scatter plot, where each dot represents the average pixel intensity of eGFP and td-tomato for a single cell under the conditions tested (n ~ 400 per sample). The red dot represents the mean pixel intensities of eGFP and td-tomato for the entire population. The red bars indicate the standard deviation of eGFP and td-tomato pixel intensity observed in that population.

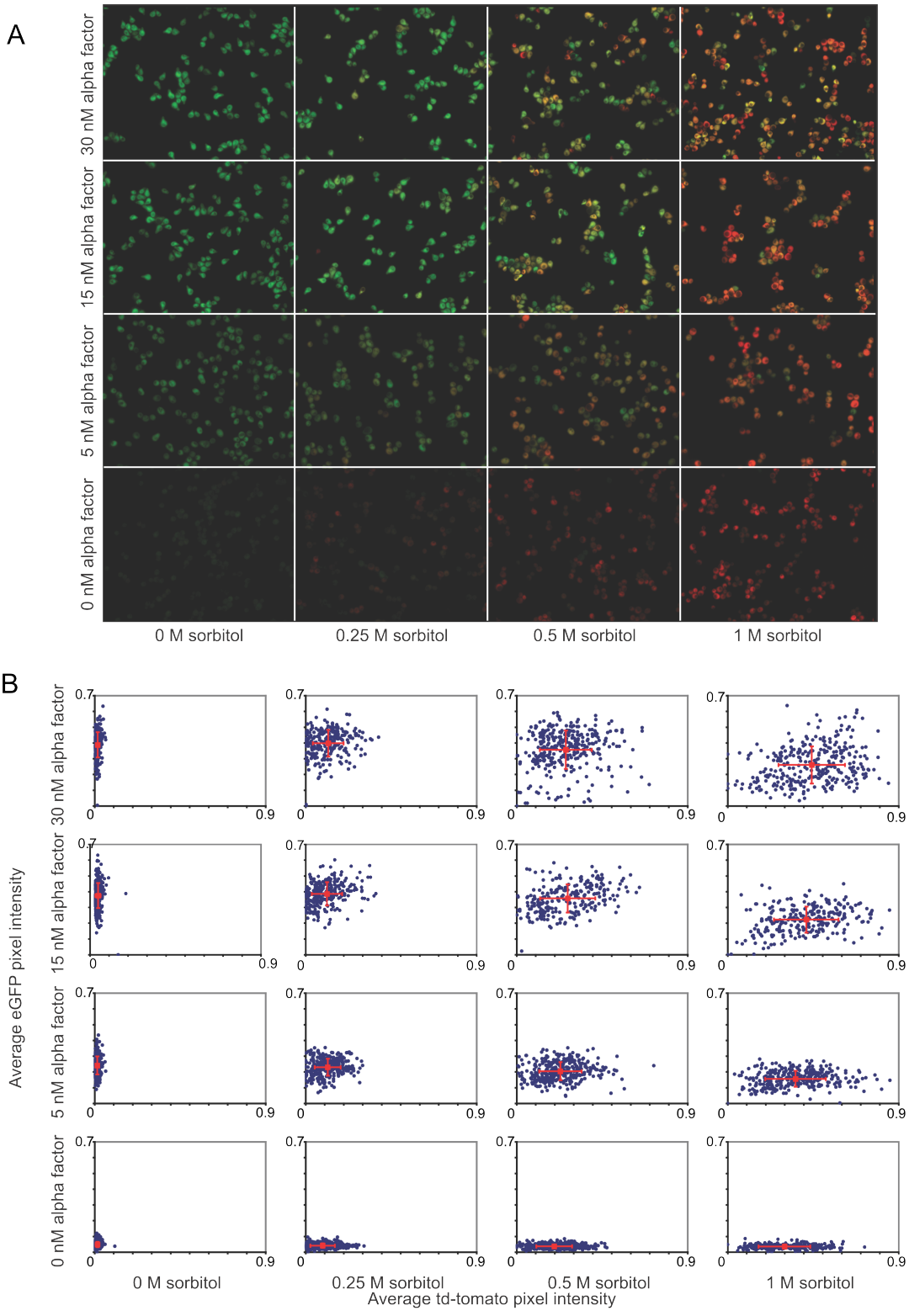
A
30 nM alpha factor
15 nM alpha factor
5 nM alpha factor
0 nM alpha factor
0 M sorbitol
0.25 M sorbitol
0.5 M sorbitol
1 M sorbitol
B
Average eGFP pixel intensity
0.7
0
0.9
Average td-tomato pixel intensity

Figure 4-5. Localization-specific reporters indicate insulation between MAPK pathways on the minute timescale

(A) Strain YJP413 (*HOG1*-td-tomato *STE5*-3XGFP) was grown in synthetic medium to mid-exponential phase, pelleted and resuspended in synthetic medium with the indicated amount of stimulant. This cell-suspension was then placed on poly-L-lysine coated slides for observation under an epifluorescence microscope. Images were acquired 15 min after addition of the stimulant(s). The Hog1-td-tomato, Ste5-3XGFP and merged images are shown for each stimulant combination. Without stimulation both Ste5-3XGFP and Hog1-td-tomato are diffuse in the cytoplasm. Addition of α-factor results in accumulation of Ste5-3XGFP at the plasma membrane, whereas sorbitol addition causes Hog1-td-tomato to translocate into the nucleus. Co-stimulation of these cells resulted in a clear accumulation of Ste5-3XGFP as puncta at the plasma membrane and Hog1-td-tomato in the nucleus in single cells (see yellow arrows). This result indicated that both pathways had been activated in individual cells even at very early time points (15 min).

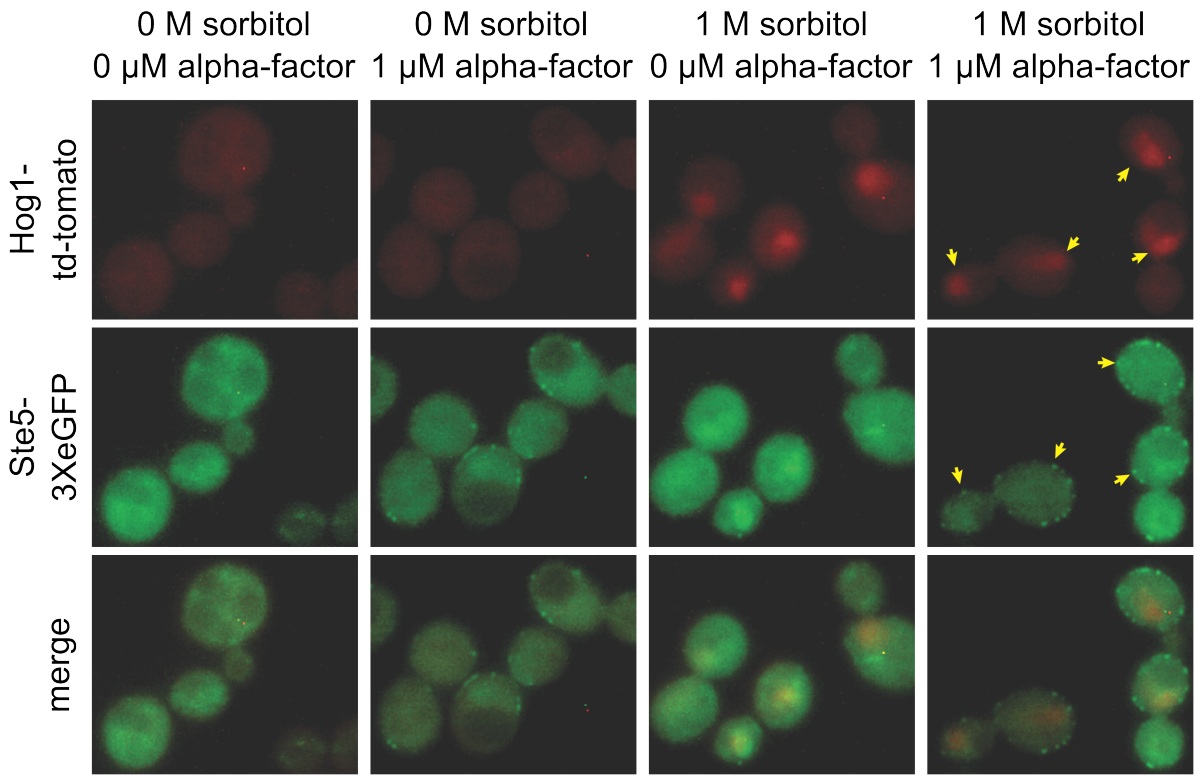
0 M sorbitol
0 µM alpha-factor
0 M sorbitol
1 µM alpha-factor
1 M sorbitol
0 µM alpha-factor
1 M sorbitol
1 µM alpha-factor
Hog1-
td-tomato
Ste5-
3XeGFP
merge

and analyzed the resulting cells using flow cytometry. As with the fluorescent micrographs, it was clear that individual cells were responding to both stimuli (Figure 4-6). This analysis further confirmed that the increase in fluorescence in both the GFP and RFP channels was not in any way an artifact of light convolution or of the microscopy analysis.

Each of these MAPK pathways has some redundancy. It was possible therefore, that the mating pathway inhibits one branch of the HOG pathway but not the other, or that the HOG pathway inhibits one of the two MAPKs in the mating pathway but not the other. To test these possibilities, I repeated the 2 h co-stimulation experiment in various mutant strains.

A *ssk1*Δ strain, which cripples the Sln1 branch of the HOG pathway, was used to determine if the mating pathway specifically inhibited the Sho1 branch of the HOG pathway. However, co-stimulation of this strain with a range of sorbitol and α-factor concentrations for 2 h resulted in both mating and HOG pathway activation (Figure 4-7). I confirmed an observation reported by others (O'Rourke and Herskowitz, 2004) that cells containing only the Sho1 branch in the HOG pathway do not respond to low concentrations of sorbitol (0.25 M), unlike wild-type cells. Performing this experiment using single-cell analysis allowed me to conclude that the reduction was due to lower HOG pathway activation in individual cells (rather than to a decrease in the proportion of cells that responded). I carried out an essentially identical experiment in a *sho1*Δ strain, in which only the Sln1 branch is present. As before, individual cells responded to both stimuli; however, the amount of mating pathway reporter induction after pheromone treatment was somewhat attenuated in the *sho1*Δ strain (Figure 4-8). Based on these observations, I concluded that the mating pathway does not inhibit either of the branches of the HOG pathway during co-stimulation.

If HOG pathway activation inhibits Fus3, then deleting *KSS1* should prevent co-activation of these pathways during co-stimulation. Conversely, if the HOG pathway inhibits Kss1, then a *fus3*Δ strain should not activate the mating pathway reporter when the HOG pathway is activated. However, in both of these instances co-stimulation with sorbitol and α-factor activated both reporters in individual cells (Figure 4-9 and 4-10). Therefore, the HOG pathway does not inhibit any individual MAPK in the mating pathway. The *FUS3* deletion decreased the amount of $FUS1_{promoter}$-eGFP transcribed to a greater extent then the did the *KSS1* deletion. This effect is due to the fact that Fus3 is the primary MAPK for the mating pathway, whereas Kss1 is only weakly and transiently activated during pheromone treatment (Sabbagh et al., 2001).

The experiments described above demonstrate that both the HOG pathway and the mating pathway can be activated simultaneously in single cells. These findings strongly argue against the idea that signaling specificity is imposed by cross-inhibition. However, it was still possible that each pathway might inhibit the other if one was activated prior to the other. In other words, cross-inhibition might require a certain amount of time to be enforced. To test this possibility, I subjected my dual fluorescent reporter strain to a series of pre-activation experiments. Cells were treated with 0.5 M sorbitol for periods of 5, 10, 20 or 45 min prior to stimulation with 15 nM α-factor. Images of the cells were acquired 2 h after addition of α-factor to determine if pre-activation of the HOG pathway prevented cells from subsequently responding to pheromone. Compared to the individual 15 nM α-factor treatment or the cells subjected to both α-factor and 0.5 M sorbitol (Figure 4-11A), there was no decrease in the $FUS1_{promoter}$-eGFP expression in cells that had already been subjected to hyperosmotic shock (Figure 4-11B). Similarly, cells were pre-stimulated with 15 nM α-factor for periods of 5, 10, 20 and 45 min, then subjected to hyperosmotic shock with 0.5 M sorbitol and examined 2 h later. Pre-activation of the mating

Figure 4-6. Flow cytometry confirms co-activation of MAPK pathways during co-stimulation

Strain YJP212 was grown to mid-exponential phase, stimulated with either 30 nM α-factor, 1 M sorbitol, or both, as indicated, for 2 h and the fluorescence in the red and green channels was measured simultaneously using a fluorescence-activated cell sorter (Becton Dickinson Influx™) and analyzed with appropriate software (FloJo™). GFP was excited with a 488 nm laser and its emission was detected with a 530/540 nm bandpass filter; td-Tomato was excited with a 561 nm laser and its emission was detected with a 593/540 nm bandpass filter. The results confirm that the observed dual activation of the MAPK pathway reporters was not due to any artifact of using fluorescence microscopy to detect reporter expression.

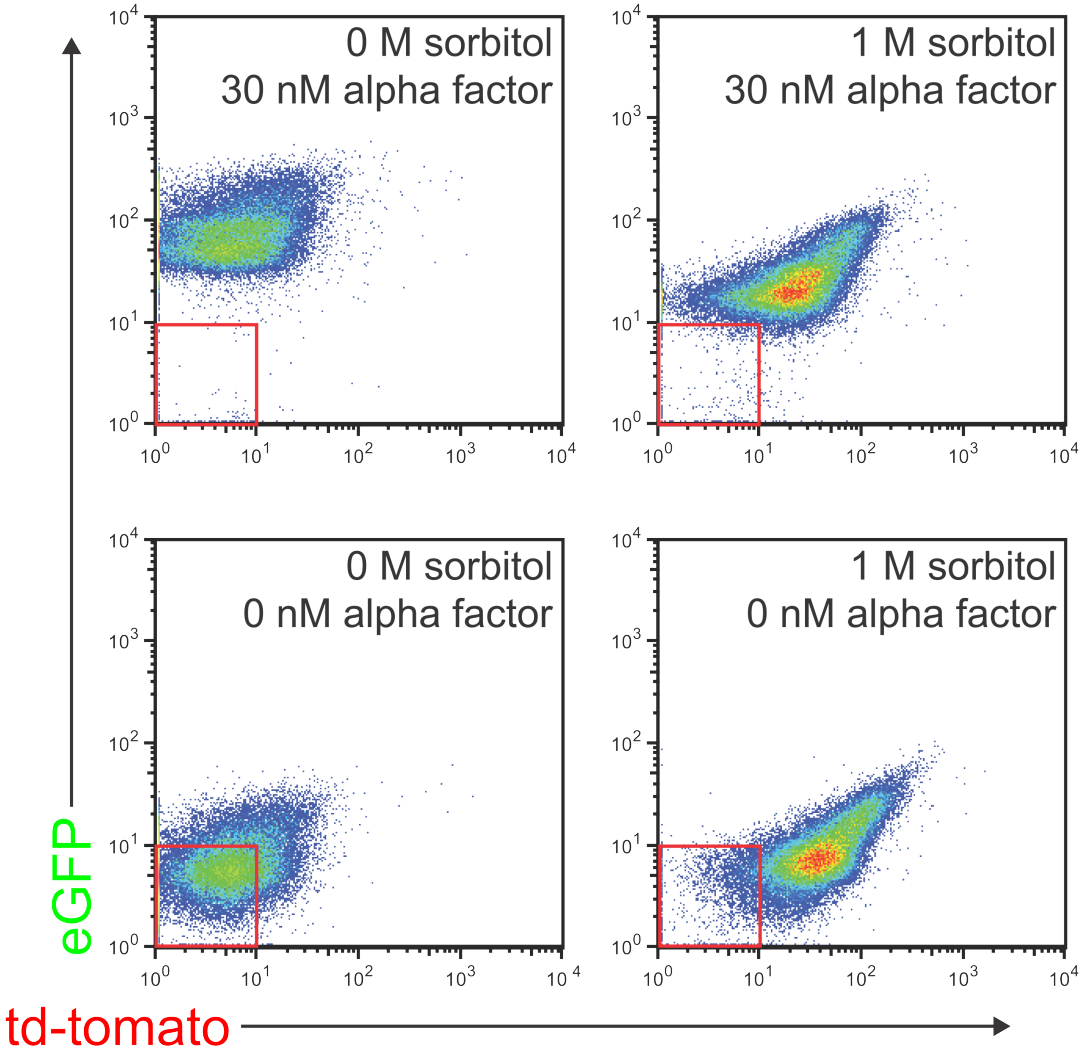
0 M sorbitol
30 nM alpha factor
1 M sorbitol
30 nM alpha factor
0 M sorbitol
0 nM alpha factor
1 M sorbitol
0 nM alpha factor
eGFP
td-tomato

Figure 4-7. The mating pathway does not inhibit the Sho1 branch of the HOG pathway during co-stimulation

(A) Strain YJP406 (*ssk1*Δ) containing both the mating and HOG pathway reporters was grown to mid-exponential phase in synthetic complete medium and then added to an equal volume of fresh medium containing double the concentration of stated stimulant(s). After 2 h, expression of the reporters was assessed in single cells by epifluorescence microscopy. The merged eGFP and td-tomato images are shown. The expression of both reporters indicates that the mating pathway does not inhibit the Sho1 branch of the HOG pathway.

(B) Data in (A) presented as a scatter plot, where each dot represents the average pixel intensity of eGFP and td-tomato for a single cell under the conditions tested (n ~ 400 per sample). The red dot represents the mean pixel intensities of eGFP and td-tomato for the entire population. The red bars indicate the standard deviation of eGFP and td-tomato pixel intensity observed in that population.

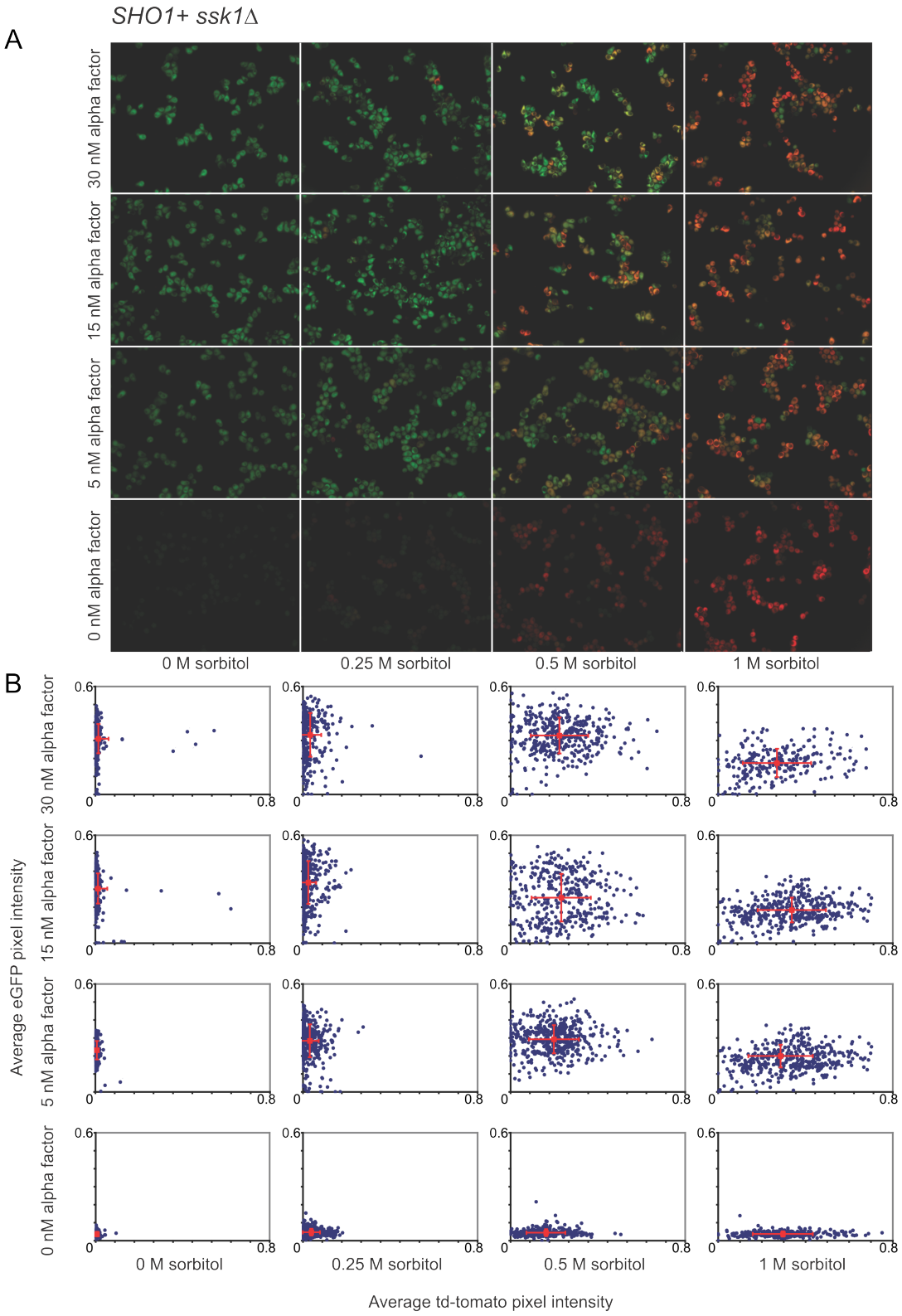
A
SHO1+ ssk1Δ
30 nM alpha factor
15 nM alpha factor
5 nM alpha factor
0 nM alpha factor
0 M sorbitol
0.25 M sorbitol
0.5 M sorbitol
1 M sorbitol
B
Average eGFP pixel intensity
Average td-tomato pixel intensity
0.6
0
0.8

Figure 4-8. The mating pathway does not inhibit the Sln1 branch of the HOG pathway during co-stimulation

(A) Strain YJP407 (*sho1*Δ) containing both the mating and HOG pathway reporters was grown to mid-exponential phase in synthetic complete medium and then added to an equal volume of fresh medium containing double the concentration of stated stimulant(s). After 2 h, expression of the reporters was assessed in single cells by epifluorescence microscopy. The merged eGFP and td-tomato images are shown. The expression of both reporters indicates that the mating pathway does not inhibit the Sln1 branch of the HOG pathway.

(B) Data in (A) presented as a scatter plot, where each dot represents the average pixel intensity of eGFP and td-tomato for a single cell under the conditions tested (n ~ 400 per sample). The red dot represents the mean pixel intensities of eGFP and td-tomato for the entire population. The red bars indicate the standard deviation of eGFP and td-tomato pixel intensity observed in that population.

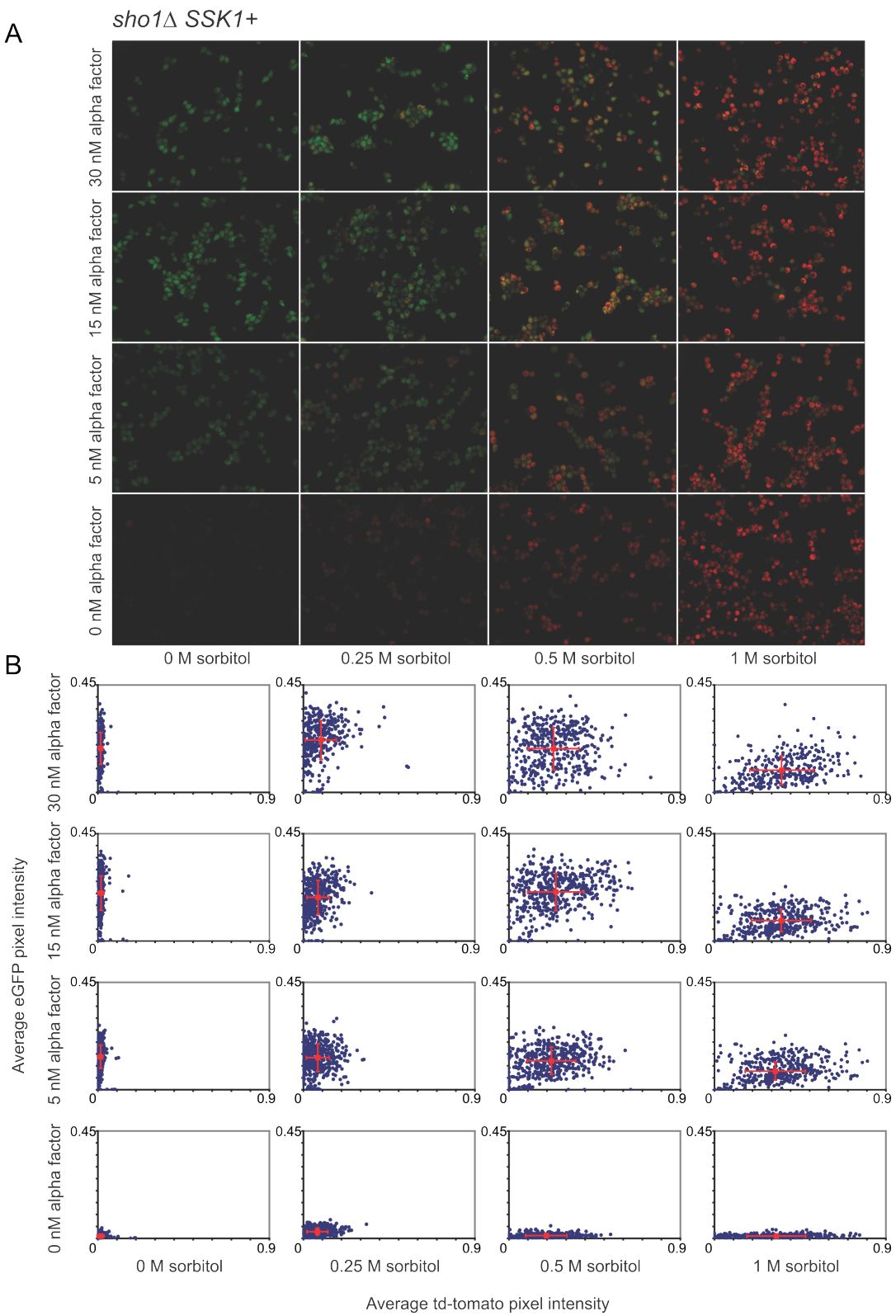
A
sho1Δ SSK1+
30 nM alpha factor
15 nM alpha factor
5 nM alpha factor
0 nM alpha factor
0 M sorbitol
0.25 M sorbitol
0.5 M sorbitol
1 M sorbitol
B
Average eGFP pixel intensity
Average td-tomato pixel intensity
0.45
0
0.9

Figure 4-9. The HOG pathway does not inhibit the Fus3 MAPK of the mating pathway during co-stimulation

(A) Strain YJP313 (*kss1*Δ) containing both the mating and HOG pathway reporters was grown to mid-exponential phase in synthetic complete medium and then added to an equal volume of fresh medium containing double the concentration of stated stimulant(s). After 2 h, expression of the reporters was assessed in single cells by epifluorescence microscopy. The merged eGFP and td-tomato images are shown. The expression of both reporters indicates that the HOG pathway does not inhibit the Fus3 MAPK of the mating pathway.

(B) Data in (A) presented as a scatter plot, where each dot represents the average pixel intensity of eGFP and td-tomato for a single cell under the conditions tested (n ~ 400 per sample). The red dot represents the mean pixel intensities of eGFP and td-tomato for the entire population. The red bars indicate the standard deviation of eGFP and td-tomato pixel intensity observed in that population.

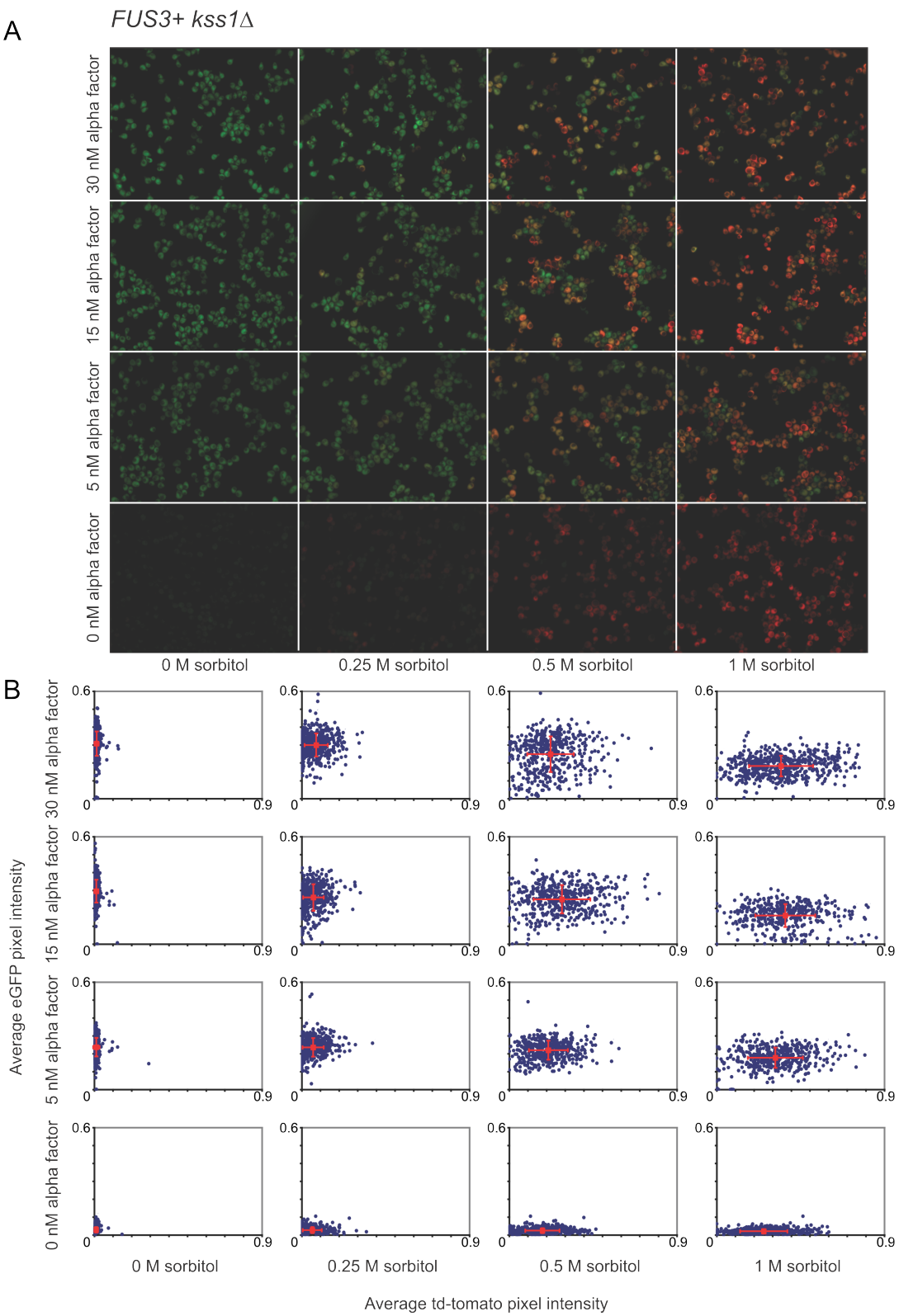
A
FUS3+ kss1Δ
30 nM alpha factor
15 nM alpha factor
5 nM alpha factor
0 nM alpha factor
0 M sorbitol
0.25 M sorbitol
0.5 M sorbitol
1 M sorbitol
B
Average eGFP pixel intensity
Average td-tomato pixel intensity
0.6
0
0.9

Figure 4-10. The HOG pathway does not inhibit the Kss1 MAPK of the mating pathway during co-stimulation

(A) Strain YJP336 (*fus3*Δ) containing both the mating and HOG pathway reporters was grown to mid-exponential phase in synthetic complete medium and then added to an equal volume of fresh medium containing double the concentration of stated stimulant(s). After 2 h, expression of the reporters was assessed in single cells by epifluorescence microscopy. The merged eGFP and td-tomato images are shown. The expression of both reporters indicates that the HOG pathway does not inhibit the Kss1 MAPK of the mating pathway.

(B) Data in (A) presented as a scatter plot, where each dot represents the average pixel intensity of eGFP and td-tomato for a single cell under the conditions tested (n ~ 400 per sample). The red dot represents the mean pixel intensities of eGFP and td-tomato for the entire population. The red bars indicate the standard deviation of eGFP and td-tomato pixel intensity observed in that population.

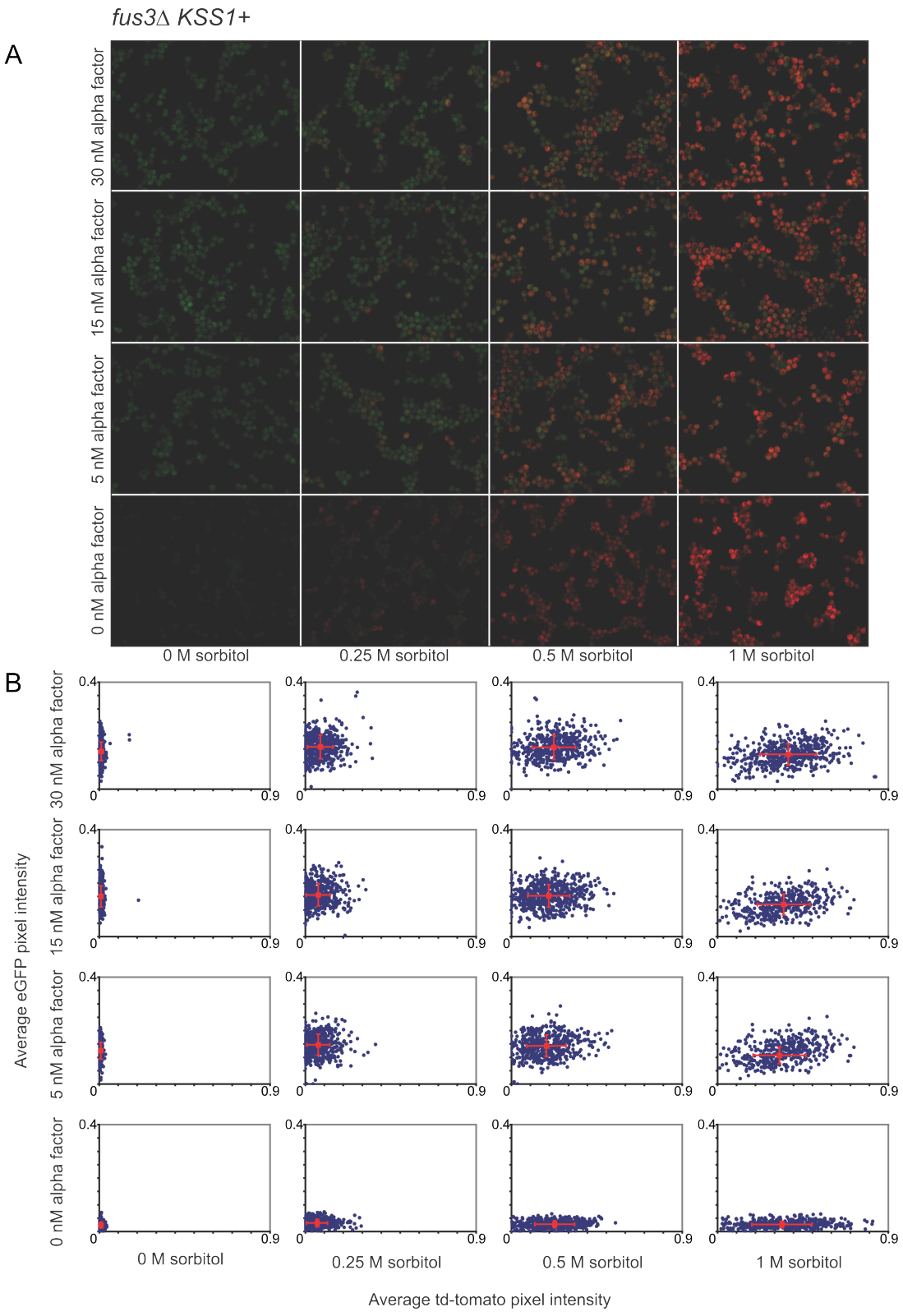
A
fus3Δ KSS1+
30 nM alpha factor
15 nM alpha factor
5 nM alpha factor
0 nM alpha factor
0 M sorbitol
0.25 M sorbitol
0.5 M sorbitol
1 M sorbitol
B
Average eGFP pixel intensity
Average td-tomato pixel intensity
0.4
0
0.9

Figure 4-11. Pre-activation of one MAPK pathway does not alter the response of subsequent stimulation of the other MAPK

(A) Strain YJP212 containing both MAPK reporters was grown to mid-exponential phase in synthetic complete medium and then added to an equal volume of fresh medium containing double the concentration of stated stimulant(s). After 2 h, expression of the reporters was assessed by fluorescence microscopy. The merged eGFP and td-tomato images are shown above corresponding scatter plots where each dot represents the average pixel intensity of eGFP and td-tomato for a single cell (n ~ 400 per sample). The red dot represents the mean pixel intensities of eGFP and td-tomato for the entire population. The red bars indicate standard deviation observed in that population. These data are meant to be used for comparison with the results shown in (B) and (C).

(B) As in (A), except that cells were first stimulated with 15 nM α-factor, and then 0.5 M sorbitol was added at the indicated time after α-factor addition. Images were acquired 2 h after the addition of sorbitol. The induction of both reporters indicate that pre-activation of the mating pathway does not prevent the subsequent activation of the HOG MAPK pathway.

(C) As in (A), except that cells were first stimulated with 0.5 M sorbitol, and then 15 nM α-factor was added at the indicated time after sorbitol addition. Images were acquired 2 h after the addition of α-factor. The induction of both reporters indicate that pre-activation of the HOG pathway does not prevent the subsequent activation of the mating MAPK pathway.

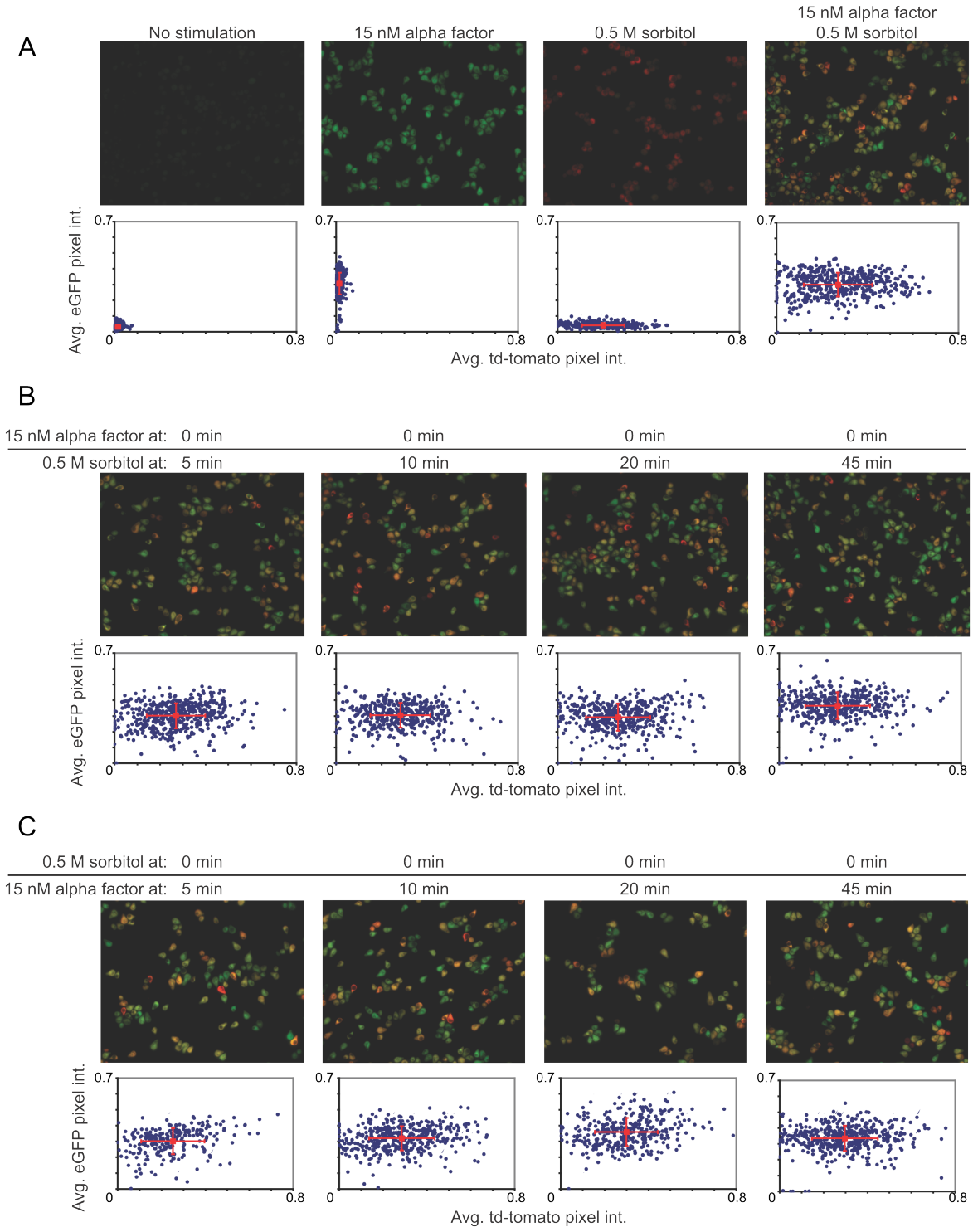
A
No stimulation
15 nM alpha factor
0.5 M sorbitol
15 nM alpha factor
0.5 M sorbitol
Avg. eGFP pixel int.
0.7
0
0.8
Avg. td-tomato pixel int.
B
15 nM alpha factor at: 0 min 0 min 0 min 0 min
0.5 M sorbitol at: 5 min 10 min 20 min 45 min
Avg. eGFP pixel int.
Avg. td-tomato pixel int.
C
0.5 M sorbitol at: 0 min 0 min 0 min 0 min
15 nM alpha factor at: 5 min 10 min 20 min 45 min
Avg. eGFP pixel int.
Avg. td-tomato pixel int.

pathway did not prevent the HOG pathway from subsequently responding to the stress (Figure 4-11C). Therefore, even if given ample time to establish inhibitory conditions, there was no detectable cross-inhibition of one MAPK pathway by the other. Taken together, all of my data strongly argue against any cross-inhibition mechanism. Furthermore, these data suggest that signaling specificity must be imposed by another mechanism, which I dubbed "insulation."

Discrepancies between my data and previously published results

Essentially all of the data presented above is at odds with a peer-reviewed and published study on this same subject (McClean et al., 2007). Whereas McClean et. al. claimed that signaling specificity between these two pathways is enforced by mutual cross-inhibition, my results indicate that no such cross-inhibition occurs. I sought to determine the reason for this discrepancy with the assumption that perhaps identifying the source of the difference might shed additional light on how these pathways work.

One of the most obvious disparities that could influence the results is the use of a different strain background. The previous study used Σ1278b, whereas I integrated my reporters into the YPH499 background (a derivative of S288c). There are 3.2 single nucleotide polymorphisms per kilobase between S288c and Σ1278b (Dowell et al., 2010). Given that the haploid genome of *S. cerevisiae* is 12,000 kilobases, YPH499 and Σ1278b differ by approximately 40,000 polymorphisms. I introduced my reporters into the Σ1278b background and repeated the co-stimulation experiment. I found that both reporters were induced upon co-stimulation. McClean et al. (2007) made their mating pathway reporter by replacing the *FUS1* coding sequence, hence their cells lacked Fus1. Fus1 is known to interact with Sho1 and potentially inhibit its activity (Nelson et al., 2004). To determine if the absence of Fus1 might alter the outcome of my experiments, I deleted this gene in my strain background. However, I still observed co-expression of the fluorescent reporters. I then acquired the strain (YSR31) constructed by McClean et al. (2007) and attempted to reproduce the results reported therein. When I stimulated YSR31 with both α-factor and sorbitol, individual cells turned on both the mating and HOG pathway reporters, although the HOG pathway reporter in this strain was quite dim (Figure 4-12). This result immediately ruled out any genetic difference between the strains as the causative factor for our contrasting results.

Thus, it seemed likely that the difference arose from how the cells were prepared, stimulated and scored. The previous study attached the cells to a poly-L-lysine-coated coverslip and then perfused stimulant(s) under that coverslip. Moreover, because Σ1278b is a rather clumpy strain, the previous study dispersed these clumps by mild sonication of the cells prior to analysis. In my experiments, cells were simply stimulated in liquid culture and then placed on an agarose pad for visualization by microscopy. I, therefore, used my reporter strain but treated it and examined it exactly as described by the McClean et al. (2007). In the process, I found that mild sonication actually killed a significant fraction of the cells and that such dead cells had an intense auto-fluorescence signal that was primarily apparent in the RFP channel but lacked the spectral qualities of RFP (Figure 4-13). The combination of sonication and hyperosmotic shock increased the proportion of cells that were killed and that exhibited this spurious signal. In fact, the image shown in Figure 4-13 looks almost identical to the data presented in the previously published report; however, in the brightfield images, the red fluorescent cells are clearly sick, dead or dying. Therefore, It became clear that the mutual cross-inhibition reported in the previous study was due to an unfortunate artifact. McClean et al. scored the dead cells as having activated the HOG reporter, and overlooked the real HOG pathway mRFP reporter, because it

Figure 4-12. Differences between my results and previously published observations are not due to any differences in genetic background or reporter construction

YSR31, the strain from a previously published report (McClean et al., 2007) claiming mutual cross-inhibition between these MAPK pathways, was grown to mid-exponential phase in YPD and then added to an equal volume of fresh medium containing double the concentration of stated stimulant(s). The individual eGFP and mRFP images are shown as well as the merged fluorescent micrographs. Although the reporters are different than the ones I constructed, the eGFP (green) reporter is for the mating pathway and the mRFP (Red) reporter is for the HOG pathway. Although the HOG pathway reporter is dim, its expression is still clearly detectable. Most significantly, co-stimulation results in co-activation of both reporters, as with my dual fluorescent reporter strain.

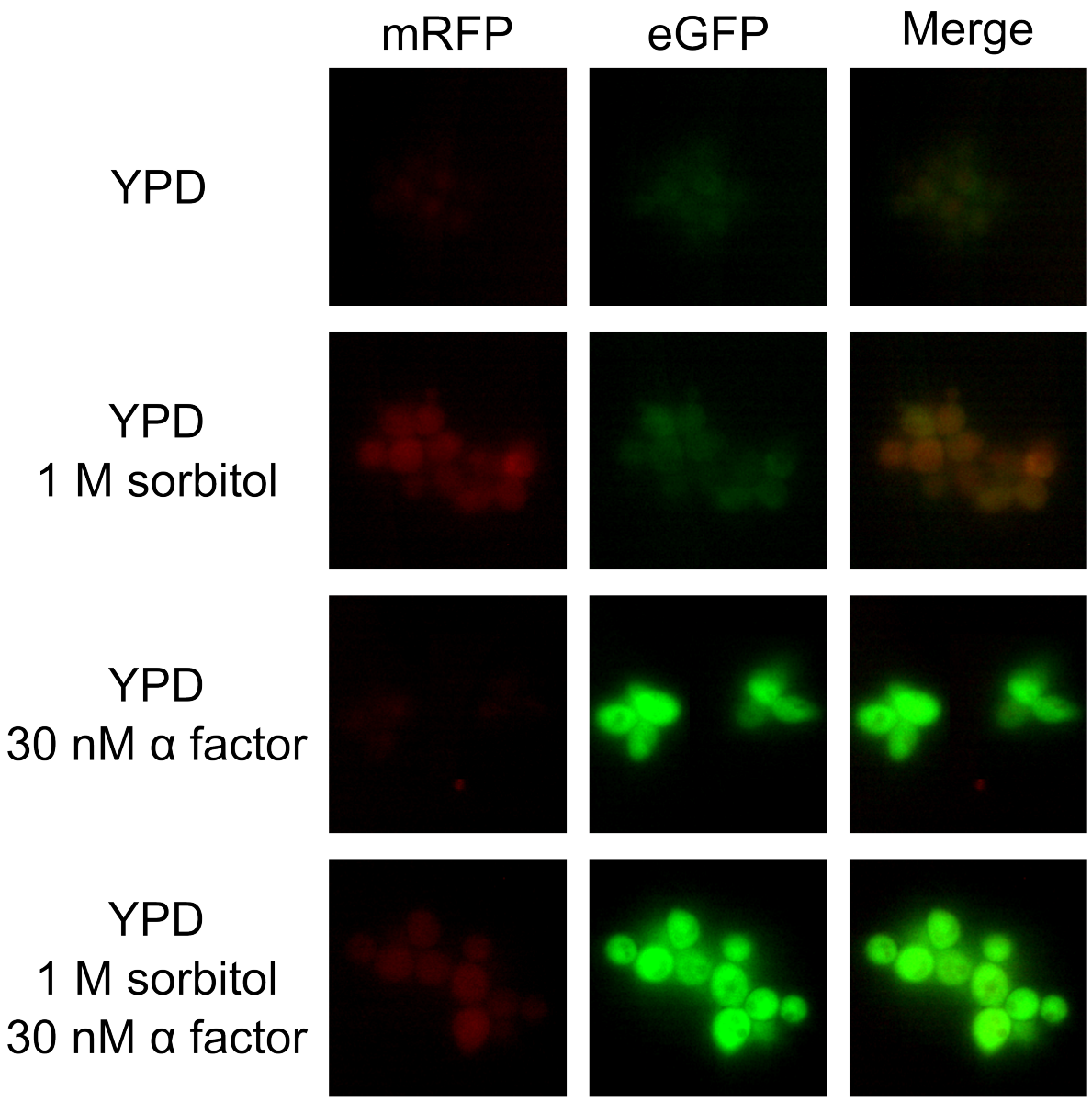
mRFP
eGFP
Merge
YPD
YPD
1 M sorbitol
YPD
30 nM α factor
YPD
1 M sorbitol
30 nM α factor

Figure 4-13. The combination of sonication and hyperosmotic shock results in cell death accompanied by an increase in auto-fluorescence

Strain YJP73 containing both MAPK reporters was grown to mid-exponential phase in synthetic complete medium, cells were then pelleted and resuspended in 100 µl synthetic complete medium and sonicated for 5 sec at an intermediate level (level 3). The cells were then attached to a poly-L-lysine cover slip and placed on a glass slide covered with synthetic complete medium containing 1 M sorbitol and 1 µM α-factor. The cells were incubated on the clover slip in stimulants for 2 h, and then the amount of the fluorescent reporter expression was assessed by epifluorescence microscopy. A brightfield image is shown, and the arrows indicate cells whose permeability barrier has clearly been compromised by this treatment. To the right is the merged td-tomato and eGFP micrograph. The red cells correspond to the dead cells. This red fluorescence is not due to the HOG pathway reporter, as judged by its different spectral properties compared to td-tomato.

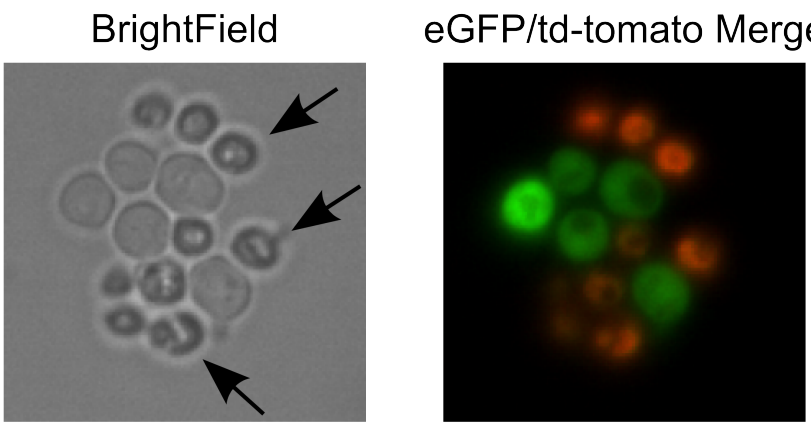
BrightField
eGFP/td-tomato Merge

was so dim. It is unfortunate that the spurious red fluorescence caused by a combination of sonication and hyperosmotic shock was interpreted as a HOG pathway response. Thus, during their co-stimulation some cells had died and turned red, whereas other cells survived and responded to the α-factor. While it is impossible for me to know whether or not the cells imaged by McClean et al. (2007) were dead, it seems the most likely explanation for the mistaken conclusions about the apparent mutually exclusive pathway induction and cross-inhibition.

Crosstalk occurs from the HOG pathway to Fus3 in a Ste5 dependent manner

Others studying the mechanisms of signaling specificity between the mating and HOG pathway have come to the conclusion that there is no crosstalk between these two pathways. They have concluded that mating pathway activation does not occur during hyperosmotic shock in a *hog1*Δ strain but rather that only the Kss1 MAPK of the filamentous growth pathway becomes activated (Shock et al., 2009). Crosstalk has mostly been quantitated by measuring *FUS1* transcriptional output, and either Kss1 or Fus3 is capable of inducing this gene (see for example Figures 4-9 and 4-10). The arguments used to support this notion are based on two observations. The first is that *STE5*, while essential for mating pathway activation, is not required for crosstalk to occur, as judged by *FUS1* transcription. This is an unreasonable argument, however, because it is entirely possible that Fus3 is activated in a Ste5-dependent manner at the same time that Kss1 is activated in a Ste5-independent manner, both of which could contribute to *FUS1* transcription. The second argument is that if one uses phospho-specific antibodies to examine the phosphorylation state of Kss1 and Fus3, much more phospho-Kss1 can be detected than phospho-Fus3. Thus, implying that Kss1 is activated to a greater extent during crosstalk than is Fus3. This antibody (also used in chapter 5 of this thesis) was raised against the phosphorylated activation loop of mammalian Erk2, which is the human homolog of Kss1, but recognizes the activated forms of Fus3 and its human homolog Erk1 as well. Based on analyzing the sequence homology between the activation loops of Erk2, Kss1 and Fus3, it seems very likely that this antibody binds to activated Kss1 much more avidly than activated Fus3. Using this antibody to compare the relative levels of Fus3 and Kss1 MAPK activation is inappropriate without proper calibration, which has not been done.

```
                                        * *
Erk1 DFGLARIA-------DPEHDHTGFLTEYVATRWYRAPE
Erk2 DFGLARVA-------DPDHDHTGFLTEYVATRWYRAPE
Kss1 DFGLARCLASSS---DSRETLVGFMTEYVATRWYRAPE
Fus3 DFGLARIIDESAADNSEPTGQQSGMTEYVATRWYRAPE
```

Above is an alignment of the activation loops of these human and yeast MAPKs. The Thr and Tyr marked with the asterisks are the residues which are phosphorylated during MAPK activation. The residues amino-proximal to the phospho-Thr and phospho-Tyr in Kss1 are very similar to the sequences found in Erk1 and Erk2, whereas, there has been significant divergence in this region of the activation loop within Fus3. Specifically, Fus3 lacks the conserved bulky-hydrophobic Phe and contains a Gln two positions towards the N-terminus instead of the iso-steric Thr or Val found in the other MAPKs.

I, therefore, sought to determine whether crosstalk from the HOG pathway activates the *FUS1* reporter through the *STE5* dependent mating pathway. I compared $FUS1_{promoter}$-eGFP expression in wild-type, *hog1*Δ, *hog1*Δ *kss1*Δ, *hog1*Δ *ste5*Δ and *hog1*Δ *ste5*Δ *kss1*Δ strains in response to hyperosmotic challenge. As expected, no crosstalk occurred in the wild-type strain, whereas significant crosstalk could be detected in the *hog1*Δ strain (Figure 4-14). Deleting *KSS1*

Figure 4-14. Cross-activation of the mating pathway during hyperosmotic stress in strains lacking *HOG1*

Strains YJP212 (wild type), YJP131 (*hog1*Δ), YJP301 (*kss1*Δ *hog1*Δ), YJP571 (*ste5*Δ *hog1*Δ) and YJP573 (*kss1*Δ *ste5*Δ *hog1*Δ) were grown to mid-exponential phase in synthetic complete medium and then added to an equal volume of fresh medium containing 2 M sorbitol. After 2 h, the expression of the reporters in single cells was assessed by epifluorescence microscopy. The chart displays the average eGFP signal for the entire population after hyperosmotic shock as an indication of the amount of mating pathway activation that occurred due to crosstalk (n ~ 400). Bars indicate the standard deviation for the population. As expected, deletion of *HOG1* resulted in $FUS1_{promoter}$-eGFP expression during hyperosmotic shock. Deletion of either *STE5* or *KSS1* alone only partially reduced the amount of $FUS1_{promoter}$-eGFP expression, indicating that this signal can be propagated through either the *STE5*-dependent mating pathway or the *KSS1*-dependent filamentous growth pathway. Deletion of both *STE5* and *KSS1* significantly reduced the amount of $FUS1_{promoter}$-eGFP induction.

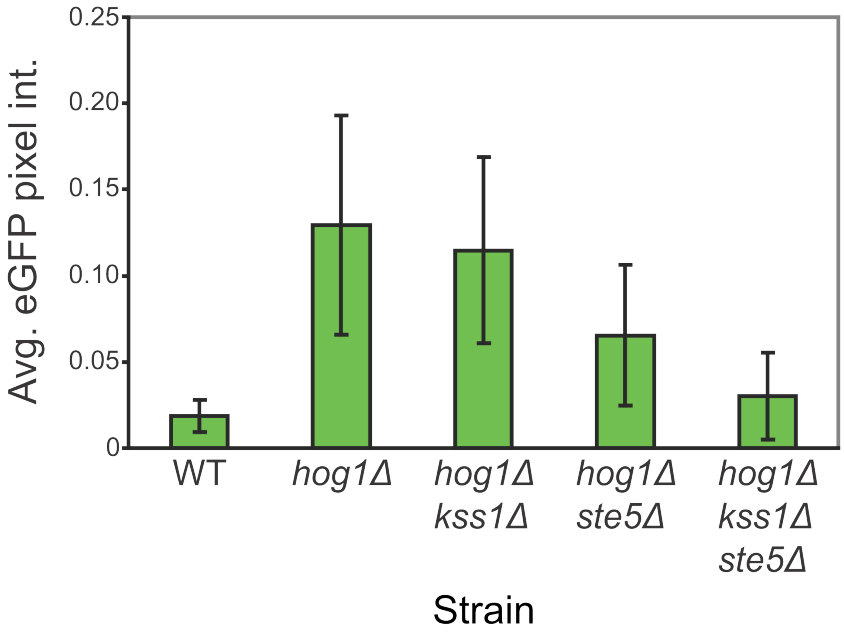
Avg. eGFP pixel int.
0.25
0.20
0.15
0.10
0.05
0
WT
hog1Δ
hog1Δ kss1Δ
hog1Δ ste5Δ
hog1Δ kss1Δ ste5Δ
Strain

had no noticeable effect, whereas the *hog1*Δ *ste5*Δ strain had somewhat reduced $FUS1_{promoter}$-eGFP expression. Most tellingly, when both *STE5* and *KSS1* were deleted in the *hog1*Δ background, the amount of crosstalk was drastically reduced (Figure 4-14). My results demonstrate that $FUS1_{promoter}$-eGFP transcription can occur through either Ste5-independent Kss1 activation or Ste5-dependent Fus3 activation. Moreover, since eliminating *STE5* alone reduced the $FUS1_{promoter}$-eGFP signal during crosstalk, a significant portion of the signal measured in the *hog1*Δ strain is Ste5-dependent, and thus Fus3-mediated. Finally, since crosstalk was not entirely eliminated by deletion of both *STE5* and *KSS1*, Fus3 can be activated by Ste7 in the absence of Ste5, albeit very inefficiently.

Toxicity associated with hyperosmotic shock and pheromone treatment

I found that when cells were subjected to high concentrations of sorbitol and α-factor there was a marked loss of viability as judged by the appearance of dark non-refractile cells in the brightfield images (Figure 4-15). My observations were reminiscent of a previous study in which it was observed that *ssk1*Δ cells would not grow on a plate in the presence of both sorbitol and pheromone (Nelson et al., 2004). The strain used in that study was also a *far1* mutant (so that the α-factor treatment did not result in G1 arrest). In that prior study, Fus1 was identified as a protein that interacts with the SH3 domain of Sho1. Fus1 is a single-pass transmembrane protein whose extracellular domain is heavily O-glycosylated and whose cytoplasmic tail contains an SH3 domain. *FUS1* is also the gene whose promoter is used as a transcriptional mating pathway reporter in this and many other studies. The authors speculated that because *FUS1* is induced during mating pathway activation, co-stimulation with both sorbitol and pheromone resulted in Fus1 binding to the SH3 domain of Sho1 and blocking HOG pathway signaling through the Sho1 branch. Indeed, if cells lacked *FUS1*, they were then able to grow on a medium containing both sorbitol and α-factor (Nelson et al., 2004).

To determine if I was observing the same phenomenon, I deleted *FUS1* in my dual fluorescent reporter strain and subjected the cells to co-stimulation. High concentrations of sorbitol and α-factor resulted in roughly one-third of the population of *FUS1* cells to appear sick, dead or dying, but only 2% of the *fus1*Δ cells were non-refractile (Figure 4-15). There is a very important distinction between the study described above and my observation about co-stimulation-induced toxicity. The previous experiments were done in a strain that lacked a functional Sln1 branch of the HOG pathway, thus proposing a model where Fus1 blocks the Sho1 branch and abrogates Hog1 activation is reasonable (Nelson et al., 2004). My experiments, however, were performed in a strain containing both the Sho1 branch and the Sln1 branch, so that even if Fus1 were to block the Sho1-Pbs2 interaction, presumably Pbs2 could still be activated by the Ssk2/22 MAPKKKs. Moreover, there was still significant toxicity when *sho1*Δ cells were co-stimulated with high concentrations of sorbitol and α-factor, and this toxicity was not further increased in a *ssk1*Δ strain. So, although I confirmed that there is Fus1-dependent toxicity during co-stimulation with high concentrations of sorbitol and α-factor, it cannot arise solely from Fus1 binding to Sho1 and blocking Pbs2-dependent activation of Hog1.

Using the dual fluorescent reporters and MAPK analog-sensitive alleles to investigate pathway specificity at the single-cell level

Combining single-cell transcriptional reporters with analog sensitive (AS) alleles of MAPKs, which are inhibitable by the drug 1-NM-PP1 (Bishop et al., 2000), further allowed for a unique interrogation of the parameters controlling signal specificity. Inhibiting the kinase

Figure 4-15. *FUS1* dependent toxicity associated with pheromone treatment in high osmolarity

Strains YJP212 (*FUS1*) and YJP385 (*fus1*Δ) were grown to mid-exponential phase in synthetic complete medium and then added to an equal volume of fresh medium containing 2 M sorbitol and 60 nM α-factor (1 M sorbitol, 30 nM α-factor final concentration). After 2 h, the expression of the reporters in single cells was assessed by epifluorescence microscopy. Bright field images are shown on the left to display the dark non-refractile cells present only in the *FUS1* strain. Deletion of *FUS1* did not alter the ability of the cells to activate both $FUS1_{promoter}$-eGFP and $STL1_{promoter}$-td-tomato during co-stimulation.

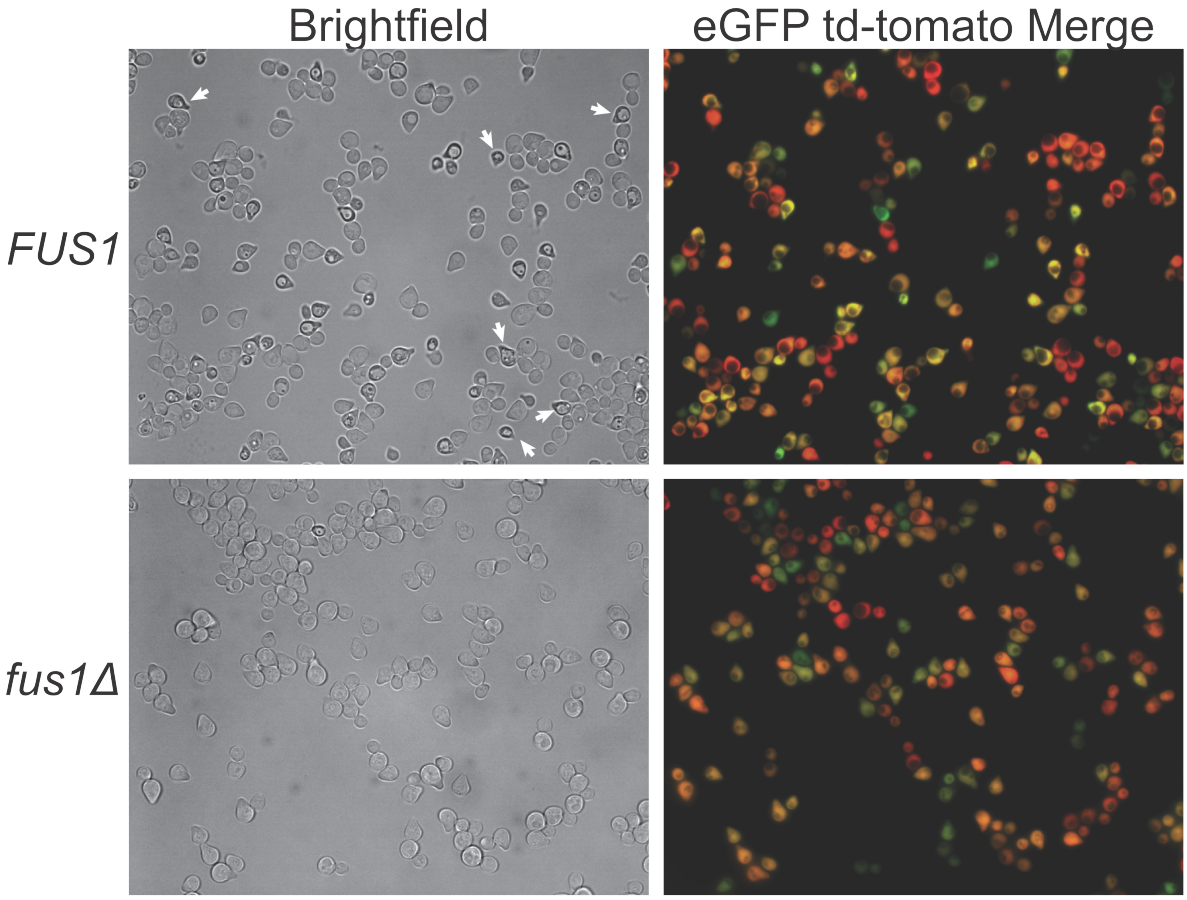
Brightfield
eGFP td-tomato Merge
FUS1
fus1Δ

activity of Hog1 results in crosstalk to the mating pathway and, on a population-based level, the amount of crosstalk is inversely correlated with the amount of Hog1 activity. However, at intermediate levels of Hog1 activity where the amount of crosstalk is also intermediate, it is not known if the amount of mating pathway activation in each cell is decreased or if the proportion of cells exhibiting crosstalk is decreased. As expected, in cells carrying a *HOG1-AS* derivative of my dual fluorescent reporter strain that was treated with 1 M sorbitol and an amount of 1-NM-PP1 (15 μM) sufficient to completely inhibit Hog1-AS $STL1_{promoter}$-tdtomato transcription was no longer induced, but the mating pathway reporter $FUS1_{promoter}$-eGFP transcription was activated. Lower concentrations of inhibitor decreased the extent of mating pathway activation, while increasing the amount the HOG pathway reporter in the same individual cells. At a certain concentration of inhibitor (0.15 uM) and sorbitol (1.0 M), a large number of cells had activated both the HOG and the mating pathway (Figure 4-16). In these cells there is enough Hog1 activity to induce $STL1_{promoter}$-td-tomato transcription but not enough to entirely suppress crosstalk, indicating a higher threshold of Hog1 activity is needed for the later function. Moreover, these data further support the notion that these pathways are normally insulated from each other since crosstalk and HOG pathway signaling can occur simultaneously in individual cells when Hog1 activity is compromised, but not entirely eliminated. If the pathways did cross-inhibit one another, it would be expected that either HOG pathway signaling or crosstalk would occur, but not both.

By inhibiting Hog1-AS at various time points after hyperosmotic stimulation I was able to determine the amount of time Hog1 needs to be active to prevent crosstalk to the mating pathway. This experiment indicated that the Hog1 pathway needs to be on for at least 10 min to initiate *STL1* transcription, and it needs to be on for twice as long (~20 min) to efficiently insulate itself from the mating pathway (Figure 4-17). The catalytic activity of Hog1 is continuously required to prevent crosstalk even after cells have adapted to elevated osmolarity (Westfall and Thorner, 2006). Therefore, addition of 1-NM-PP1 after the acute phase of stress response is complete will still result in a detectable crosstalk.

The function of Hog1 in preventing crosstalk to the mating pathway during stress is well documented. Whether Fus3 or Kss1 are required to prevent Ste11 from activating the HOG pathway during pheromone treatment was not well established. Pheromone treatment has been shown to activate the HOG pathway when certain "diverter" scaffolds (Park et al., 2003) and Hog1 has been shown to be phosphorylated during activation of the filamentous growth MAPK pathway in a stain lacking *KSS1* (Yang et al., 2009). To determine if Fus3 or Kss1 actively maintain signaling specificity during mating pathway activation, I constructed a strain containing *FUS3-AS* and *KSS1-AS* alleles and treated it with 15 μM 1-NM-PP1 and 30 nM α-factor. As expected, these cells no longer induced the $FUS1_{promoter}$-eGFP reporter; however, they also failed to activate the HOG pathway as judged by $STL1_{promoter}$-tdtomato transcription (Figure 4-18A). Using a strain containing *fus3Δ* and *kss1Δ* alleles or higher concentrations of α-factor (1 uM) did not activate the HOG pathway under these conditions either (Figure 4-18B). I also tested a strain where *FUS1*, *SSK1* or both had been deleted, in case either the Sln1 branch or Fus1 was in fact suppressing the Sho1 branch of the HOG pathway but still observed no HOG pathway reporter expression (Figure 4-18B). The lack of crosstalk to the HOG pathway may be due to the MAPK scaffold Ste5, which possibly prevents the Ste11 activated by the mating pathway from leaving that signaling protein complex.

Gradually decreasing the amount of 1-NM-PP1 added to *FUS3-AS KSS1-AS* cells during pheromone stimulation indicated that different thresholds of Fus3 activity are necessary to elicit

Figure 4-16. Titration of 1-NM-PP1 during hyperosmotic stress in a *HOG1-AS* strain

Strain YJP123 (*HOG1-AS*) was grown to mid-exponential phase in synthetic complete medium and then added to an equal volume of fresh medium containing 2 M sorbitol and twice the indicated concentration of the Hog1-AS inhibitor 1-NM-PP1. After 2 h, expression of the reporters in single cells was assessed by fluorescence microscopy.

(A) Merged eGFP and td-tomato fluorescence micrographs of cells post-stimulation (top) and scatter plots (bottom) showing the distribution of reporter expression in individual cells within the population. The red dot in the scatter plot represents the mean pixel intensities of eGFP and td-tomato for the entire population. The red bars indicate the standard deviation of eGFP and td-tomato pixel intensity observed in that population.

(B) The population average of eGFP (green squares) and td-tomato (red triangles) pixel intensities for the samples shown in (A). Bars indicate the standard deviation in the population. The bottom axis (1-NM-PP1 concentration) is on a Log scale, except for the 0 μM 1-NM-PP1 point, which was added for comparison.

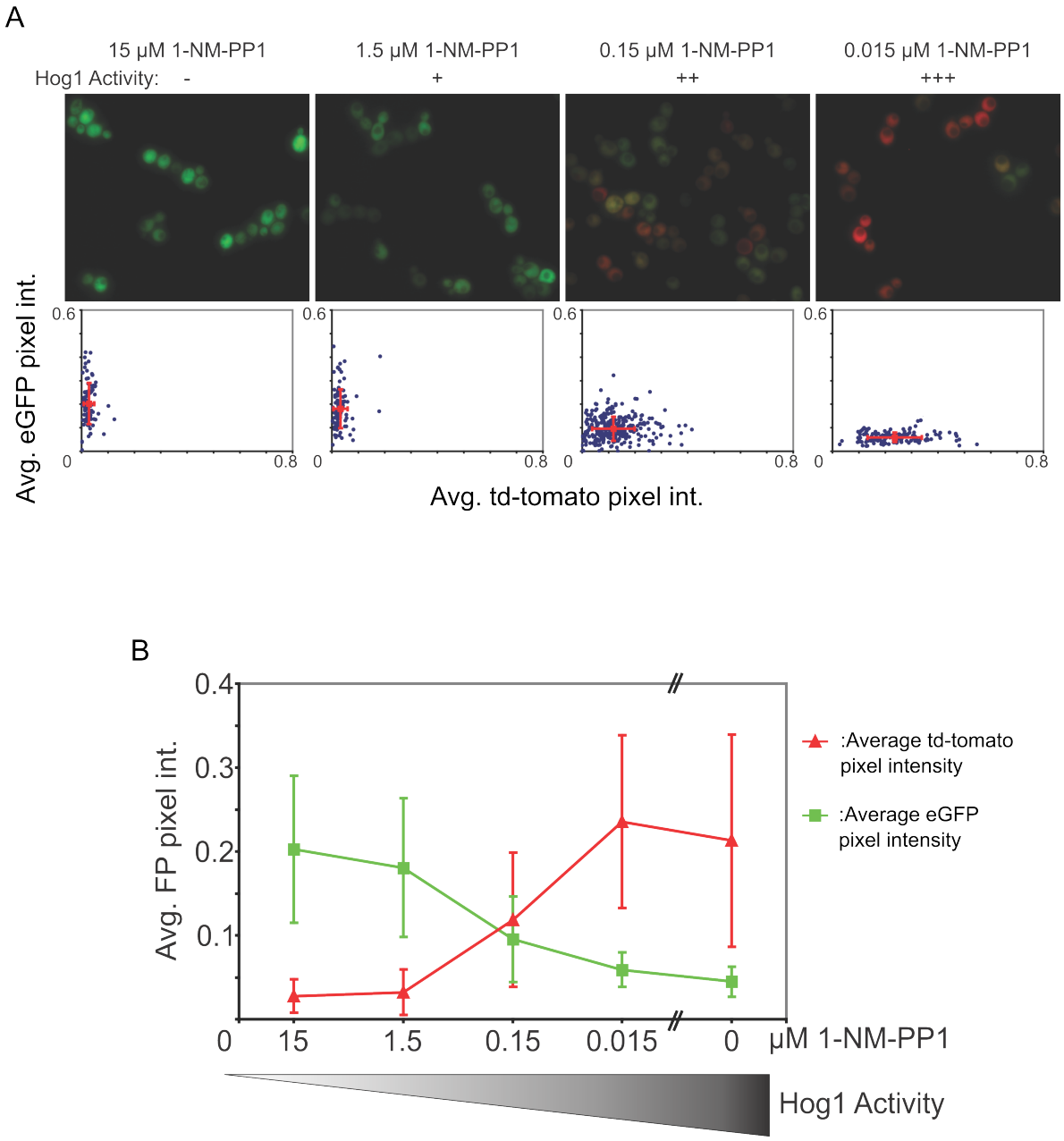
A
15 μM 1-NM-PP1
1.5 μM 1-NM-PP1
0.15 μM 1-NM-PP1
0.015 μM 1-NM-PP1
Hog1 Activity: - + ++ +++
Avg. eGFP pixel int.
0.6
0
0.8
Avg. td-tomato pixel int.
B
0.4
0.3
0.2
0.1
Avg. FP pixel int.
0 15 1.5 0.15 0.015 0 μM 1-NM-PP1
:Average td-tomato pixel intensity
:Average eGFP pixel intensity
Hog1 Activity

Figure 4-17. Sustained Hog1 activity is required to prevent crosstalk to the mating pathway

Strain YJP123 (*HOG1-AS*) was grown to mid-exponential phase in synthetic complete medium and then added to an equal volume of fresh medium containing 2 M sorbitol. At the indicated time 15 μM 1-NM-PP1 was added to the culture, and, after 2 h in the presence of inhibitor, the expression of the reporters in single cells was assessed by fluorescence microscopy.

(A) Merged eGFP and td-tomato fluorescence micrographs of cells post-stimulation (top) and scatter plots (bottom) showing the distribution of reporter expression in individual cells amongst the population. The red dot in the scatter plot represents the mean pixel intensities of eGFP and td-tomato for the entire population. The red bars indicate the standard deviation of eGFP and td-tomato pixel intensity observed in that population.

(B) The population average of eGFP (green squares) and td-tomato (red triangles) pixel intensities for the samples shown in (A). Bars indicate the standard deviation in the population.

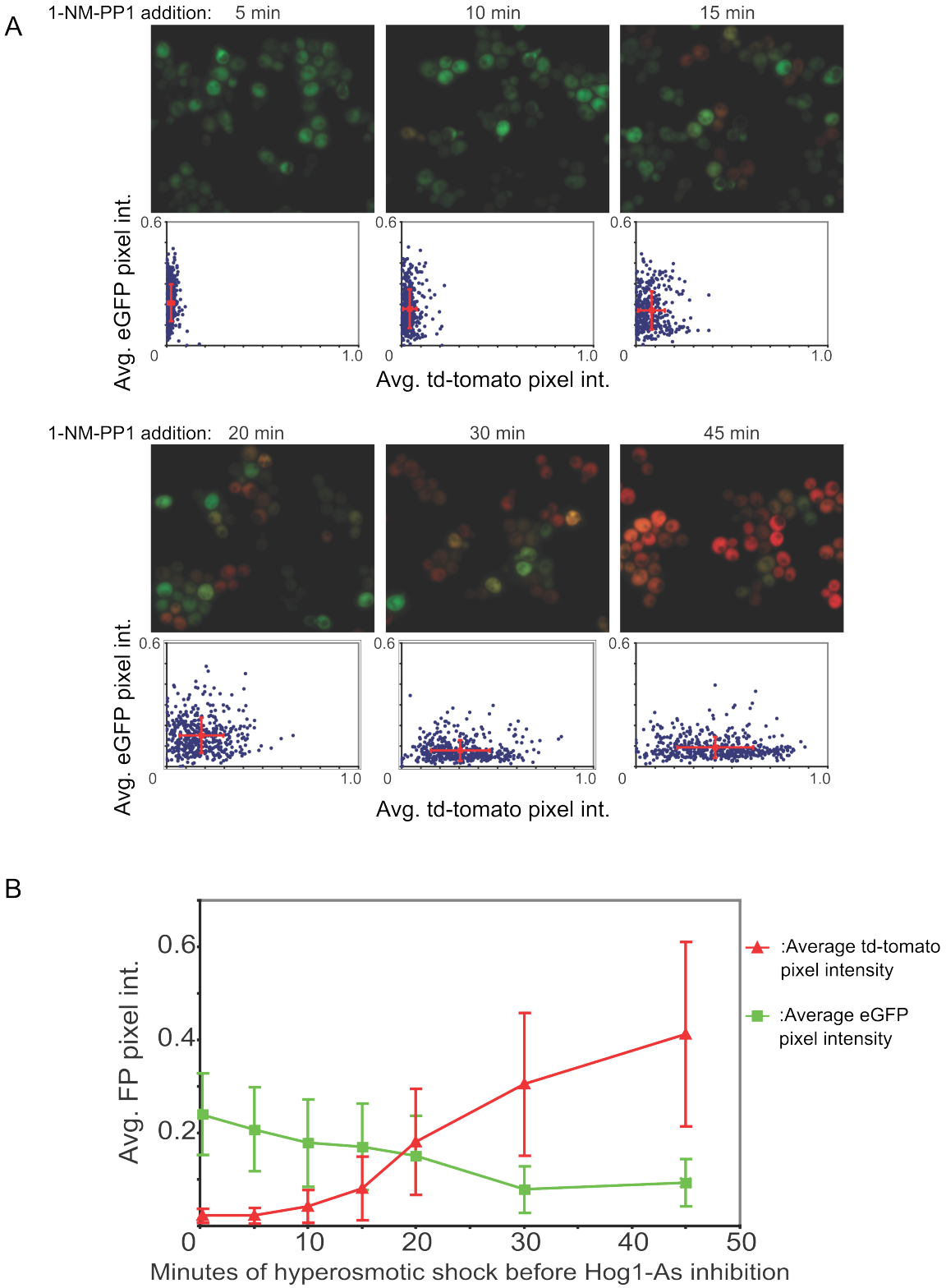
A
1-NM-PP1 addition: 5 min
10 min
15 min
Avg. eGFP pixel int.
0.6
0
1.0
Avg. td-tomato pixel int.
1-NM-PP1 addition: 20 min
30 min
45 min
Avg. eGFP pixel int.
Avg. td-tomato pixel int.
B
Avg. FP pixel int.
0.6
0.4
0.2
0
10
20
30
40
50
Minutes of hyperosmotic shock before Hog1-As inhibition
:Average td-tomato pixel intensity
:Average eGFP pixel intensity

Figure 4-18. Cross activation from the mating pathway to the HOG pathway does not occur in mating pathway mutants treated with pheromone

(A) Strain YJP334 (*FUS3-AS KSS1-AS*) was grown to mid-exponential phase in synthetic complete medium and then treated with 30 nM α-factor and the indicated concentration of 1-NM-PP1 for 2 h before being examined by fluorescence microscopy. The bright field, eGFP and td-tomoto images are overlaid (top). Below the images are scatter plots where each dot represents the average pixel intensity of eGFP and td-tomato for a single cell under the conditions tested (n ~ 400 per sample). The red dot represents the mean pixel intensities of eGFP and td-tomato for the entire population. The red bars indicate the standard deviation of eGFP and td-tomato pixel intensity observed in that population. At the bottom is a table showing the abundance of cells with a particular morphology in each sample. Inspection of the images reveal that essentially all cells that formed a shmoo had robust activation of the $FUS1_{promoter}$-eGFP reporter.

(B) Strains YJP308 (*fus3*Δ *kss1*Δ), YJP387 (*fus3*Δ *kss1*Δ *fus1*Δ) and YJP390 (*fus3*Δ *kss1*Δ *fus1*Δ *ssk1*Δ) were grown to mid-exponential phase and then treated with 1 μM α-factor for 2 h before being examined by fluorescence microscopy. The brightfield, eGFP and td-tomato images are overlaid (top). Below the images are scatter plots where each dot represents the average pixel intensity of eGFP and td-tomato for a single cell (n ~ 400 per sample). The red dot represents the mean pixel intensities of eGFP and td-tomato for the entire population. The red bars indicate the standard deviation of eGFP and td-tomato pixel intensity observed in that population. In none of the mutants tested did stimulation of the mating pathway result in HOG pathway activation.

A

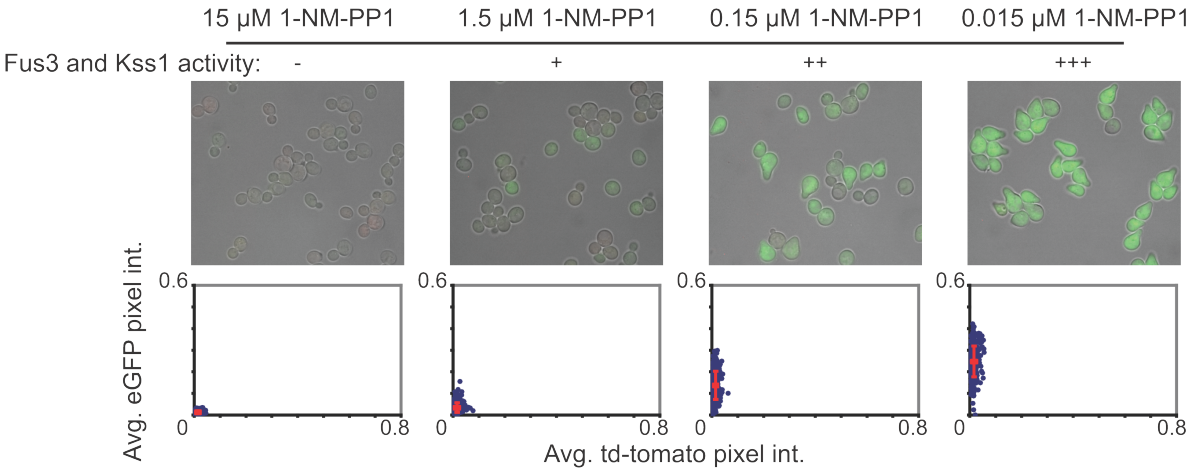

Unbudded	7%	25%	73%	100%
Shmoo	0%	0%	56%	97%
Bright Green Shmoo	0%	0%	49%	96%

B

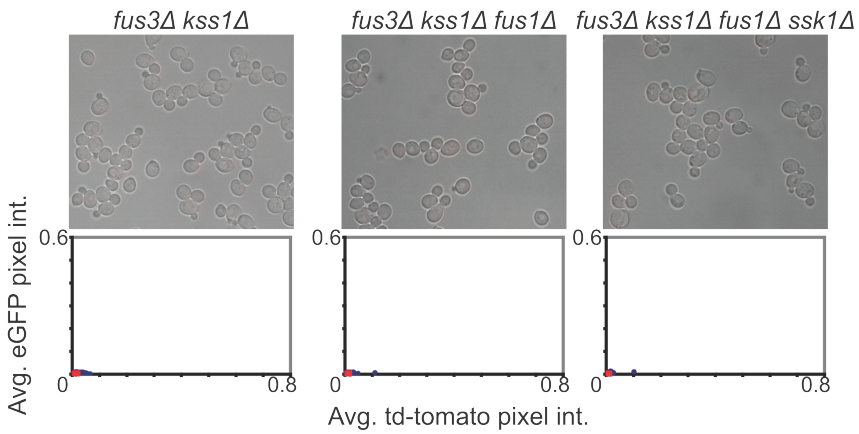

different responses (Figure 4-18A). Active Fus3 phosphorylates Far1, which inhibits the cyclin-dependent kinase Cdc28 and arrests the cells in G1, the only stage of the cell cycle in which mating pathway activation can occur. Combining *FUS1* transcriptional analysis with microscopy allows one to interrogate the G1 arrest, shmoo formation and transcriptional outputs of the mating pathway all at the same time in individual cells. If the amount of Fus3 activity required to induce transcription is greater than the amount needed to arrest in G1 and form a shmoo, then it would be expected that, at an intermediate amount of Fus3 inhibition, shmoos would be present that had not turned on the $FUS1_{promoter}$-eGFP reporter. This was not observed, however. Instead, essentially every single cell that had enough Fus3 activity to form a shmoo also displayed robust $FUS1_{promoter}$-eGFP transcription. My results confirmed prior studies, which found that of the several mating pathway outputs examined, shmoo formation required the highest concentration of pheromone (Moore, 1983). However, my work was the first to show this directly at the level of MAPK activity.

Discussion

By constructing and analyzing HOG and mating pathway fluorescent transcriptional reporters, I corrected a previously published report that mistakenly misled us and others and uncovered the true relationship between these MAPK pathways. By eliminating the model of cross-inhibition as the means by which crosstalk is prevented, I was able to narrow the focus of the field to more productive avenues of research aimed at understanding the mechanism of insulation. The previous report garnered much attention due to the purported implications for cells to achieve "decision making" when confronted with two different stimuli. They claimed that, when faced with the choice of whether to respond to hyperosmotic stress or mate, the relative strength and timing of each stimulus is taken into account before the cell goes down one path or the other. However, I found instead that the cells respond to both stimuli at the same time. The latter situation makes more sense, because mating without responding to stress would compromise cell viability and if responding to the stress blocked mating, it would negate the positive effects mating has on the fitness of the organism. Insulation is not the only mechanism for crosstalk prevention. It has already been shown that activation of the mating pathway prevents subsequent activation of the filamentous growth pathway at the transcriptional level (Chou et al., 2004; Bao et al., 2004). The mating and filamentous growth pathways appear to be in a developmental hierarchy. In this situation, an either-or response does make sense since activation of either pathway results in distinct morphological changes (shmoo formation versus filamentation), which presumably are mutually exclusive.

While the idea of decision-making in yeast piqued the interest of certain researchers at the time of its publication, I think it is equally or even more fascinating that the shared components between these pathways are capable of multitasking two completely separate functions without any loss or degradation of signal. It is not multitasking in the sense that a single molecule of Ste11 is functioning in both the mating and HOG pathways at once, but more likely that there are separate pools of Ste11 that are executing these different functions. Moreover, this same situation is a fantastic example of the plasticity of MAPK signaling cascades. The appearance of entirely new signaling proteins is not required for the creation of a novel pathway, but pre-existing kinases can be requisitioned into new and distinct pathways while maintaining signaling fidelity.

Some other noteworthy points arose from my experiments on single cells. First, as can be seen in Figure 4-4, at high concentrations of sorbitol and α-factor, the amount of $FUS1_{promoter}$-eGFP reporter observed is somewhat less than that seen in the sample containing the same concentration of α-factor alone. One way to interpret these results is that HOG pathway activation does exert some inhibition on the mating pathway output. However, to be detected the fluorescent reporters genes used in this experiment must be transcribed and translated. High osmolarity is known to inhibit translation in a non-specific global manner (Melamed et al., 2008; Uesono and Toh-e, 2002; Sunnerhagen, 2007). While Hog1 does control the translation efficiency of a specific set of genes, the global reduction in translation efficiency is not Hog1-dependent. Thus, the simplest explanation for the modest decrease in mating pathway reporter expression seen under co-stimulation conditions is that it is due to the non-specific depression of translation by high osmolarity. Moreover, when cells were subjected to high osmolarity prior to pheromone addition the same degree of decrease was observed, indicating that prior activation of Hog1 does not cause a more severe effect. Unfortunately, if one tried to test the *HOG1* dependence of phenomenon by deleting *HOG1*, crosstalk to the mating pathway would occur and

confound the results. The only experiment I can think of that could address whether the translation repressing effects of hyperosmotic stress are mediated by Hog1 or not, is to artificially activate the HOG pathway. This can be accomplished via induction of a constitutively-active *PBS2* or use of temperature-sensitive *SLN1* allele and could determine if Hog1 activation decreases the response of the $FUS1_{promoter}$-eGFP reporter even in the absence of hyperosmotic conditions, but that has not been done.

I also observed a modest decrease in pheromone response in a *sho1*Δ strain. I believe that the slight decrease in mating pathway reporter production in the *sho1*Δ strain is due to an unfortunate mistake on my part and caused by the primers I used to knock out *SHO1*. These primers were specifically designed to prevent recombination between the *sho1*Δ locus and a *SHO1*-containing plasmid for experiments described in Chapter 5 of this thesis, and thus also removed the terminator of *SHO1*. However, by removing more then the exact *SHO1* coding sequence, they also inadvertently removed sequence coding for the very end of the C-terminus of Rpl23b, a ribosomal protein. A decrease in translation efficiency caused by this mishap is the most likely explanation for the attenuation in $FUS1_{promoter}$-eGFP reporter production.

My results also appeared to be in conflict with other published studies showing that Kss1 becomes phosphorylated and presumably active during hyperosmotic shock in *HOG1*+ cells (Wang et al., 2009; Shock et al., 2009). This activation of Kss1 is weak, transient, occurs only during the first 15 min of hyperosmotic shock, and depends on the presence of *SHO1*. Because Kss1 is activated during hyperosmotic shock, however, it would seem that crosstalk occurs in a wild-type strain, and that Hog1 must inhibit the output of this crosstalk. There are several reasons why these data do not support the notion of mutual cross-inhibition as the mechanism that prevents crosstalk. First, while the activation of Kss1 during stress depends on Sho1, this protein functions in both the HOG pathway and the filamentous growth pathway. It is unclear if this Kss1 activation is due to crosstalk or if the filamentous growth pathway itself is transiently activated during hyperosmotic stress. Second, if a *hog1*Δ strain is subjected to hyperosmotic stress, there is sustained and strong activation of both Kss1 and Fus3 (Flatauer et al., 2005; Wang et al., 2009). Therefore, the amount of Kss1 and Fus3 activation observed in a wild-type strain during hyperosmotic shock does not recapitulate the amount seen in a *hog1*Δ strain. Finally, if indeed this Kss1 transient activation observed in wild-type cells during hyperosmotic stress is due to crosstalk from the HOG pathway, it simply further supports my observation (shown in Figure 4-17) that Hog1 requires 10-20 min before it can enforce pathway insulation.

The results described in this chapter were published this work in a peer-reviewed journal (Science Signaling, © 2010) (Patterson et al., 2010). In conclusion, my findings provided a new model for maintenance of signaling fidelity between the HOG and mating pathways, and correct the erroneous conclusions of McClean et al. (2007).

Chapter 5
The Cdc42-GAP Rga1 is Required for HOG MAPK Pathway Insulation

Introduction

Redundancies in signaling components between various MAPK pathways create a situation with the potential for inadvertent crosstalk. For example (reviewed in (Krishna and Narang, 2008), the MAPKKs (MKK4 and MKK7) of the human JNK MAPK pathway can also activate the p38 MAPK pathway (Cuadrado and Nebreda, 2010), which is analogous to the yeast HOG pathway (Han et al., 1994). Thus, it is of general interest and importance to determine the mechanisms by which specificity is maintained. My findings (Patterson et al., 2010), presented in detail in Chapter 4 of this thesis, demonstrated that cross-inhibition from the HOG pathway cannot explain how crosstalk to the mating pathway is prevented. Clearly, determining how Hog1 action prevents crosstalk to the mating (and FG) pathway may shed light on how other MAPK pathways can elicit distinct outputs despite the use of shared components.

Theoretically, there are several general mechanisms by which Hog1 function could block cross-stimulation of the mating and FG pathways. These could involve spatial separation (such as by subcellular compartmentation or by restricted localization via scaffolding or other protein-protein or protein-membrane interactions) and/or temporal separation (such as by kinetic barriers or by negative feedback loops) (reviewed in (Schwartz and Madhani, 2004)). In the case of the Sho1 branch of the HOG pathway, the pool of Ste50- and Opy2-associated Ste11 (Wu et al., 2006; Ekiel et al., 2009; Yamamoto et al., 2010) that is interacting with Sho1-, Msb2- and Hkr1-bound Pbs2 may be segregated away from the pool of Ste50- and Cdc42-associated Ste11 (Truckses et al., 2006) that is associated with Ste7 in the FG pathway (Pitoniak et al., 2009) and from the Ste50-associated Ste11 that is bound to the Ste5 scaffold protein of the mating pathway (Elion, 2001; Good et al., 2009) (Figs. 1-1, 1-2 and 1.3).

It is clear that all three pathways are initiated by transmembrane proteins at the plasma membrane. At least one shared component, Cdc42, is a peripheral plasma membrane protein. Therefore, further compartmentalization of Ste11- and Cdc42- containing complexes require non-exchangeable membrane domains for each pathway. There are examples of this type of membrane compartmentalization occurring in MAPK signaling. Neurons treated with Nerve Growth Factor (NGF) have distinct responses depending on whether this ligand is presented to the distal axon terminus or to the cell body (Watson et al., 2001). Similarly, recruitment of the Ste5 scaffold and sustained Fus3 activation depend on their PtdIns4,5P_2-mediated recruitment to the shmoo tip (Garrenton et al., 2010).

Temporal separation of MAPK pathways could include scenarios in which there were only certain stages of the cell cycle during which either pathway could respond. That is, the mating pathway can only function in the G1 stage of the cell cycle (Garrenton et al., 2009). If the HOG pathway were competent to respond only during G2, then sharing of signaling proteins would not be an issue. However, the HOG pathway does respond in G1 cells, as data presented in Chapter 4 of this thesis demonstrated. Both pathways can be active simultaneously in individual cells (Patterson et al., 2010), ruling out differential competence during non-overlapping cell-cycle stages as a mechanism for imposing specificity.

As mentioned, scaffolding and/or protein-protein interactions could be sufficient to prevent crosstalk by sequestering activated Ste11 into complexes that contain only the appropriate substrate, Ste7 or Pbs2. Appropriate protein-protein interactions can serve just as

well as a devoted scaffold. For example, in addition to its role as the Hog1-specific MAPKK, Pbs2 also binds to upstream components of the HOG pathway, specifically Sho1 and Ste11 (Posas and Saito, 1997). The Ste5 protein serves as an essential scaffold for the mating pathway, and likely explains why crosstalk does not occur from the mating pathway to the HOG pathway when Fus3 and Kss1 are inhibited (Patterson et al., 2010). Since the catalytic activity of Hog1 is needed continuously to prevent crosstalk (Westfall et al., 2008), then if protein-protein complexes are involved in preventing Ste11 activated in the Sho1 branch from "escaping," then the assembly of such complexes must require Hog1-dependent modifications.

Finally, kinetic insulation is a mechanism whereby modifying the extent or duration of HOG pathway activation prevents crosstalk to the mating pathway. In wild-type cells, only a small amount of active Ste11 may be needed, and only for a limited amount of time, to trigger the HOG pathway. Keeping activation of Ste11 to a minimum and ensuring that is only activated when in association to the other components of the HOG pathway, would prevent any appreciable spillover to the other MAPK pathways. Likewise, Hog1 could inhibit the mating and FG pathways during hyperosmotic stress by some means. However, the activation of Ste11 within the mating or FG pathway would overcome Hog1-dependent inhibition during co-stimulation. That is, Hog1-dependent inhibition of the mating and FG pathways sets up a kinetic barrier that is strong enough to block crosstalk from the HOG pathway, but not strong enough (or not able) to prevent legitimate mating or FG pathway activation. In either case, absence of Hog1 would lead to sustained hyperactivation of Ste11 in response to hyperosmotic shock, and this active Ste11 can eventually find its way into the other two MAPK pathways. If one thinks of the HOG pathway as a pipe with the signal flowing through it, deleting *HOG1* clogs the pipe and, for as yet unknown reasons, crosstalk arises from the resulting overflow. It is even theoretically possible that crosstalk is prevented by the adaptation to high osmolarity. Once *HOG1*+ cells have adjusted their internal osmolarity the HOG pathway is no longer stimulated, whereas *hog1*Δ cells can never adapt, leading to chronic sustained signaling through the upper end of the HOG pathway. However, deletion of the glycerol producing enzymes Gpd1 and Gpd2 does not result in crosstalk, implying that adaptation alone is not sufficient to explain how it is prevented (O'Rourke and Herskowitz, 1998).

If crosstalk prevention is achieved by a kinetic insulation mechanism, the most reasonable hypothesis would be to propose a Hog1-dependent negative feedback loop. Early on in the study of HOG pathway crosstalk it was proposed that Hog1 phosphorylates Sho1, turning off the upstream activators before crosstalk could occur. Indeed Hog1 was found to phosphorylate Sho1. However, mutating that phosphorylation site does not result in activation of the mating pathway during hyperosmotic stress (Hao et al., 2007). Likewise, it was proposed that Hog1 phosphorylates Ste50, which somehow prevents crosstalk (Hao et al., 2008). However, we (Patterson et al., 2010) and others (Shock et al., 2009) have found, that while Hog1 does phosphorylate Ste50, this modification is not sufficient to block crosstalk.

Experimentally, a cross-inhibition mechanism, potentially, is a more tractable problem to solve. For signaling specificity to be imposed by Hog1-dependent cross-inhibition, Hog1 would likely phosphorylate and inhibit one of the proteins unique to the mating MAPK pathway, which is a fairly short list. However, when one considers proteins or other factors that could be involved in enforcing insulation by subcellular compartmentalization, scaffolding or kinetic insulation, the number of possible substrates grows to a quite large number. Instead of taking the arduous candidate based approach, I designed and carried out a genetic selection for mutants that result in crosstalk from the HOG to the mating MAPK pathway. This endeavor, described in this

chapter and carried out with an undergraduate honors student in the Chemical Biology major, Ms. Louise Goupil, resulted in identification of many truncated alleles of the Cdc42 GAP Rga1. Our subsequently obtained evidence indicates that Rga1 action contributes to suppression of crosstalk between the HOG and mating pathways.

Results

Hog1-dependent phosphorylation of Ste50 is dispensable for crosstalk prevention

It had been reported that Hog1 phosphorylates the adapter protein, Ste50, that binds to the MAPKKK, Ste11, and that mutation of the phosphorylation sites within Ste50 to alanine resulted in mating pathway activation during hyperosmotic stress (Hao et al., 2008). In this model, Hog1-dependent modification of Ste50 during hyperosmotic stress altered the substrate specificity of its binding partner, Ste11, so that only Pbs2 would be activated. The authors of this study reported a slight increase in mating pathway reporter activation during hyperosmotic stress. I confirmed that Ste50 is phosphorylated by Hog1 *in vitro*. However, when a strain in which the only copy of *STE50* present lacked the consensus MAPK sites thought to be modified by Hog1, was subjected to hyperosmotic stress, no activation of the mating pathway reporter could be measured.

During these kinase assays, I observed that Pbs2 had significant radiolabel incorporation when wild-type Hog1 was present, but none at all when incubated in the presence of catalytically inactive Hog1 (Figure 5-1A). This implies that while Hog1 is a substrate of Pbs2, Pbs2 may also be a substrate of Hog1. This type of MAPK to MAPKK feedback phosphorylation is known to occur in the mating MAPK pathway as well, where Fus3 is known to phosphorylate its activator, Ste7 (Errede et al., 1993). It was possible that after Hog1 becomes active, it phosphorylates Pbs2, increasing its affinity for activated Ste11 and preventing crosstalk through stabilizing that protein-protein interaction. I introduced into a yeast strain a version5 of *PBS2* lacking all 6 consensus MAPK phosphorylation sites. However, when this strain, or a strain containing both *PBS2* and *STE50* phosphorylation site mutants, was subjected to hyperosmotic stress, no activation of the mating pathway was observed. While Hog1-dependent modification of Ste50 and Pbs2 is not necessary for crosstalk prevention, it is possible that they are part of several redundant mechanisms for inhibiting crosstalk.

A genetic selection to identify potential substrates of Hog1 that prevent crosstalk to the mating pathway

To identify the substrate or substrates of Hog1 that enforce insulation of the HOG pathway, I designed a genetic selection that relied on construction of a rather complex reporter strain, which I will refer to as the Xtalk strain for simplicity. The goal of constructing this strain was to be able to identify mutants in which the mating pathway was activated during hyperosmotic stress in a manner that depended on the Sho1 branch of the HOG pathway.

First, to select for mutants that activated the mating pathway, a $FUS1_{promoter}$-*HIS3* reporter was integrated at the *HIS3* locus. Similar to the $FUS1_{promoter}$-eGFP reporter described in Chapter 4 of this thesis, this reporter is activated in a mating pathway dependent manner. However, because the strain does not contain any other functional *HIS3* gene, only when the $FUS1_{promoter}$-*HIS3* reporter is transcribed are cells capable of growing on plates lacking histidine (Stevenson et al., 1992). Secondly, the *FAR1* locus was replaced with the *far1-T306A* allele, which produces a version of Far1 that can no longer be phosphorylated by Fus3. If the wild-type version of *FAR1* was present then mating pathway activation would result in the Far1 dependent inhibition of the CDK Cdc28 and cells would arrest their growth in G1, the *far1-T306A* allele avoids this problem and permits growth. Third, the *HOG1* locus was replaced with an analog-sensitive Hog1(T100A) allele, in order to do a proof-of-principle experiment, which is described below.

Figure 5-1. Hog1-dependent feedback phosphorylation of Pbs2 and Ste50 does not contribute to crosstalk prevention

(A) Wild-type (WT) or catalytically inactive "kinase dead" (KD; D144A) Hog1 protein, purified from yeast, was combined with constitutively active Pbs2 protein, purfied by bacterial expression, and incubated with [γ-^{32}P]ATP. The amount of radiolabel incorporated into these two proteins was then assessed by SDS-PAGE and auto-radiography. When wild-type Hog1 is activated by Pbs2, it, in turn, phosphorylates Pbs2, whereas the Hog1 kinase dead does not.

(B) Strains YJP490 (*STE50-5A*), YJP455 (*PBS2-6A*) and YJP495 (*PBS2-6A STE50-5A*) were grown to mid-exponential phase in synthetic complete medium and then treated with or without 1 M sorbitol for 2 h before being examined by fluorescence microscopy. The bright field, eGFP and td-tomato images are overlaid (top). Below the images are scatter plots where each dot represents the average pixel intensity of eGFP and td-tomato for a single cell under the conditions tested (n ~ 400 per sample). The red dot represents the mean pixel intensities of eGFP and td-tomato for the entire population. The red bars indicate the standard deviation of eGFP and td-tomato pixel intensity observed in that population. The removal of the consensus MAPK phosphorylation sites within these proteins did not result in cross-activation of the mating pathway during hyperosmotic stress in a *HOG1* cell.

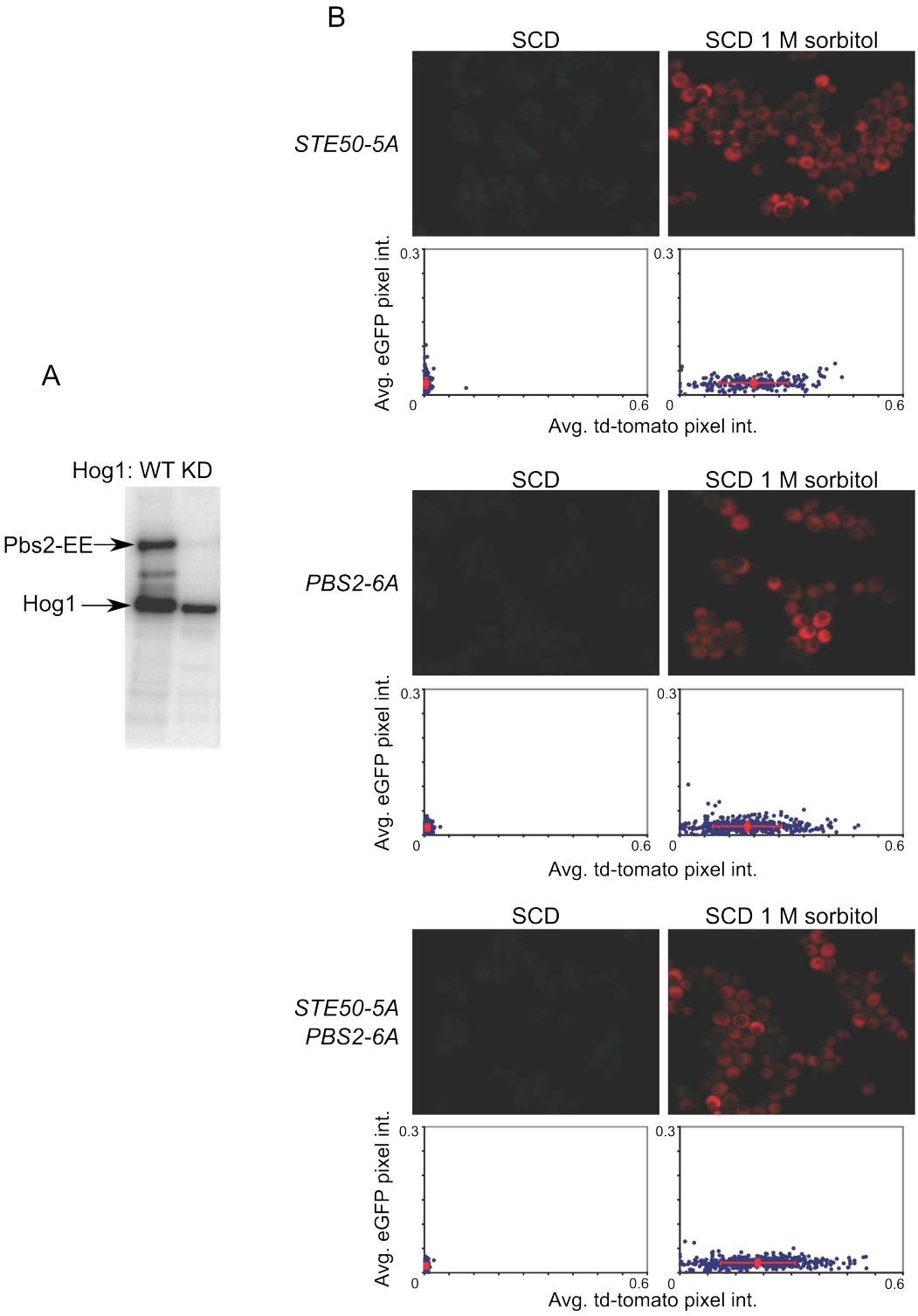
A
Hog1: WT KD
Pbs2-EE
Hog1
B
SCD
SCD 1 M sorbitol
STE50-5A
PBS2-6A
STE50-5A
PBS2-6A
Avg. eGFP pixel int.
Avg. td-tomato pixel int.
0.3
0
0.6

Fourth, because it is already known that loss of function mutations of *HOG1* or *PBS2* will result in crosstalk to the mating pathway upon hyperosmotic stress, and to avoid isolating mutations in either of these genes, an extra copy of *HOG1-AS* and of *PBS2* were integrated at the *LEU2* locus in tandem. Fifth, to focus specifically on crosstalk to the mating pathway and to not confound my results by potential activation of the FG pathway activation, *KSS1* was deleted. Sixth, *SHO1* was deleted and the *SHO1* gene was reintroduced on a *URA3*-marked centromeric (*CEN*) plasmid. This approach was taken so that I could first identify mutants that activated the mating pathway on high osmolarity medium, then remove the functioning copy of *SHO1* to determine if the $FUS1_{promoter}$-*HIS3* transcription depended on the Sho1 branch of the HOG pathway. This secondary criterion is a critically important aspect of this genetic selection. There are many mutations that might lead to mating pathway activation and $FUS1_{promoter}$-*HIS3* transcription; however, testing the Sho1-dependence demands that the signal that caused mating pathway activation originated in the HOG pathway. Finally, the Xtalk strain contained both the HOG pathway reporter, $STL1_{promoter}$-td-tomato, and the mating pathway reporter, $FUS1_{promoter}$-eGFP (described in chapter 4), so the mutants obtained could be further confirmed prior to the subsequent work required to identify the causative mutant alleles.

Before embarking on a time consuming genetic selection, I wanted to make sure that the strain constructed was useful for successfully identifying the types of mutants I sought. Because the Xtalk strain contained the *HOG1-AS* allele and the $FUS1_{promoter}$-*HIS3* reporter, if Hog1-AS is inhibited in high osmolarity medium, crosstalk should allow the cells to become HIS+. Inhibiting the Hog1-AS allele in a high osmolarity medium, however, also causes the cells to succumb to the hyperosmotic stress. As described in chapter 4, at an intermediate concentration of the Hog1-AS inhibitor 1-NM-PP1, Hog1 activity is sufficiently high to induce HOG-pathway gene expression, but not sufficient to squelch crosstalk to the mating pathway. Therefore, I plated a lawn of the Xtalk strain onto -Ura, -His plates containing 1 M sorbitol 9 mM 3-aminotriazole (3-AT) and then placed a sterile filter disc on the lawn. I then spotted 5 µl of 10 mM 1-NM-PP1 onto the disc. Diffusion creates a radial concentration gradient of the drug around the disc. 3-AT is a competitive inhibitor of His3 (imidazoleglycerol-phosphate dehydratase), and including 3-AT in the medium raises the threshold for the amount of His3 required for robust growth on -His medium. The plates lacked uracil to select for the *SHO1* plasmid and contained sorbitol to activate the HOG pathway. If our prediction that the Xtalk strain will only proliferate when crosstalk to the mating pathway is occurring is correct, then a halo of growth should appear at a certain distance around the disc. Figure 5-2A shows that this is indeed the case, and that this halo of growth only appeared when the *SHO1* containing plasmid was present and not the empty *URA3* vector, confirming the functionality of the Xtalk strain.

Figure 5-2B outlines the general strategy involved in isolating mutants that activate the mating pathway due to crosstalk. Because of the ease in plating millions of yeast cells, I elected to isolate spontaneous mutants. This approach avoids the need to deal with any dangerous mutagen and decreases the likelihood of cells acquiring multiple mutations. If, for example, one were to sequence the entire genome of a candidate mutant as a means to find the causative allele (something not far fetched now days), then the presence of even a few dozen polymorphisms could make identification of the important alteration an arduous process.

Mutants were selected on -Ura/-His plates containing 1 M sorbitol and 9 mM 3-AT. This His+ colonies were then isolated. The resulting colonies were plated on 5-fluororotic acid(5-FOA) medium to select for derivatives that had lost the *URA3*-marked *SHO1* containing plasmid. 5-FOA is converted to a toxic uracil analog by Ura3 (orotidine-5'-phosphate decarboxylase).

Figure 5-2. Genetic selection to identify the substrate of Hog1 that prevents crosstalk

(A) A lawn of strain YJP394 (*FUS1*$_{promoter}$*-HIS3 far1-T306A HOG1-AS sho1*Δ *kss1*Δ pRS316-*SHO1*), referred to as the Xtalk strain and an otherwise strain YJP393 lacking the *SHO1*-containing *URA3*-marked pRS316 plasmid, were plated on -Ura/-His plates containing 1 M sorbitol and 9 mM 3-AT. A sterile filter disc was placed on the lawn and 5 µl of 10 mM 1-NM-PP1 was added to the disc. After incubation for 4 days at 30ºC, the plates were photographed. Growth around the sterile filter disc indicates that at a certain concentration of Hog1-AS inhibitor, crosstalk to the mating pathway induces the *FUS1*$_{promoter}$*-HIS3* reporter enough to support growth. The dependence on *SHO1* indicates that growth depends on the HOG pathway.

(B) Outline of the strategy used to isolate mutants from the Xtalk strain that activate the mating pathway during hyperosmotic stress in a manner that depends on an intact Sho1 branch of the HOG pathway.

A

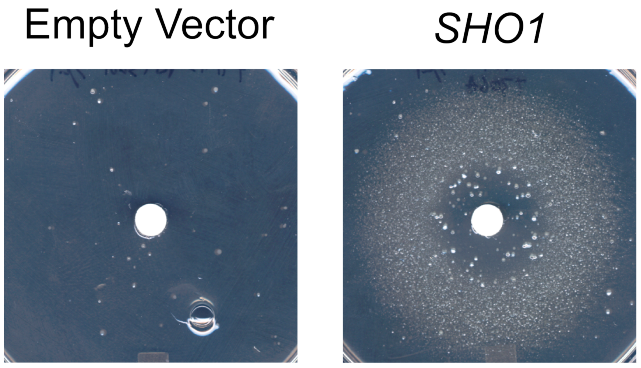

B

Xtalk Strain: *MAT***a** *FUS1prom*-HA-eGFP *STL1prom*-HA-td-tomato *FUS1prom-HIS3::his3*Δ *far1-T306A HOG1-AS HOG1-AS::PBS2::LEU2 kss1*Δ *sho1*Δ *ura3*Δ pRS316-*URA3-SHO1*

↓

Select for mutants on -Ura/-His plates containing 9 mM 3-AT and 1 M sorbitol

↓

Examine phenotype of candidate mutants on 5-FOA plates
(i.e. in the absence of *SHO1*-containing plasmid)

↓

Confirm mutants require SHO1 for mating pathway activation by
growth on -His plates containing 9 mM 3-AT and 1 M sorbitol

↓

Transform mutants with a genomic DNA plasmid library, enrich for complemented transformtants using FACS, identify complemented transformants by lack of growth on -Ura/-His plates containing 9 mM 3-AT and 1 M sorbitol

Therefore, on 5-FOA medium, only the cells that have spontaneously lost the *SHO1 URA3* plasmid will survive. These Ura- derivatives were then plated on -His plates containing 1 M sorbitol and 9 mM 3-AT and those that could not grow under these conditions were potential crosstalk mutants that were characterized further. Since these cells were His-, they presumably could no longer induce the $FUS1_{promoter}$-*HIS3* reporter when *SHO1* was absent; hence I attributed the phenotype as due to crosstalk from the HOG pathway. Figure 5-3A shows three representatives of the 18 mutants isolated from this selection. The parental Xtalk strain grows fine on -Ura medium and -Ura medium containing 1 M sorbitol; however, it does not express enough of His3 to grow on the -Ura/-His plates containing 1 M sorbitol and 9 mM 3-AT . The mutants, on the other hand, grow readily on all three media, but only if the *SHO1*-containing plasmid is present.

Because the Xtalk strain used in this selection contained both a HOG ($STL1_{promoter}$-td-tomato) and a mating ($FUS1_{promoter}$-eGFP) pathway reporter, I further characterized the activation of these responses after 2 h of hyperosmotic stress. As described in Chapter 4 of this thesis, the fluorescent proteins expressed by these reporters are also tagged with the HA epitope. Due to the large number of potential mutants to test, I analyzed expression of both reporters before and after hyperosmotic shock by immuno-blotting (as opposed to microscopy). Because HA-td-tomato is a tandem dimer of the tomato variant RFP, it runs at a significantly slower mobility than the HA-eGFP. Most of the mutants had constitutive activation of the mating pathway reporter even without any hyperosmotic shock and did not have any obvious increase the expression of the $FUS1_{promoter}$-eGFP reporter after hyperosmotic shock. In contrast, three mutants – #25, #26 and #31 – showed higher basal expression of the mating pathway reporter protein, further induction of the mating pathway reporter upon hyperosmotic treatment. Both of these properties were dependent on the presence of the *SHO1*-containing plasmid (Figure 5-3B).

None of the mutants isolated from the screen seem to phenocopy the behavior of a *hog1*Δ strain. In a *hog1*Δ strain, the mating pathway reporter is not expressed until the strain has been hyperosmotically stressed, and, after stress, there is a very large amount of HA-eGFP produced. My best mutants showed constitutive mating pathway activation that increased modestly during hyperosmotic shock. At this point, I had to make a decision on whether to spend more time generating mutants until I found one that phenocopied the crosstalk seen in a *hog1*Δ strain, or to go forward with the strongest candidates identified thus far. It would have been very informative if I could have separated the mutants into complementation groups to assess the degree of saturation of my selection. However, the crosstalk occurring in these mutants no longer happens in diploid cells. I decided to attempt identification of the causative alleles for 2 candidate mutants: #25 and #31.

Identification of the causative alleles was achieved by enrichment of plasmid-complemented transformants using fluorescence activated cell sorting (FACS). During the initial selection process, any mutants that grew on -Ura/-His plates containing 1 M sorbitol and 9 mM 3-AT were our candidates. Complementing such mutants required transforming them with a library of plasmids containing random fragments of yeast genomic DNA (gDNA) and then identifying the transformants that were no longer able to grow on -Ura/-His plates containing 1 M sorbitol and 9 mM 3-AT. Finding cells that grow is significantly easier and more reliable then attempting to find the cells that are not growing. However, we could take advantage of the fluorescent reporters in our Xtalk strain. Therefore, to increase our chances of success, I pooled the gDNA library transformants, grew them up in liquid culture, subjected them to hyperosmotic shock and then sorted the cells using FACS. I collected those that failed to induce the

Figure 5-3. Characterization of mutants isolated by this genetic selection

(A) The Xtalk strain (YJP394), along with three mutants isolated and named by the order in which they were identified, were serially diluted on the media indicated. After incubation at 30ºC for four days, the plates were photograph. Only when the mutants contained the plasmid-borne copy of *SHO1* were able to induce the $FUS1_{prom}$-*HIS3* reporter and grow on the -Ura/-His plates containing 9 mM 3-AT and 1 M sorbitol.

(B) Immuno-blot of the parental Xtalk strain and representative mutant #31 to examine the expression of both the mating ($FUS1_{promoter}$-HA-eGFP) and HOG ($STL1_{promoter}$-HA-td-tomato) pathway reporters. The cells were grown to mid-exponential phase in synthetic complete medium and then added to an equal volume of fresh medium or fresh medium containing 2 M sorbitol. After 2h, an equal number of cells were pelleted, protein was isolated by trichloroacetic acid precipitation, solubilized and analyzed by SDS-PAGE. Proteins were then transferred to a nitrocellulose filter and incubated with antibodies raised against the HA epitope and, as a loading control, Pgk1 (phosphoglycerate kinase, Baum et a., 1978). While both the eGFP and td-tomato are HA tagged, the eGFP is one half the molecular weight of td-tomato, allowing the fusion to be readily resolved from one another. Mutant #31 shows *SHO1*-dependent high basal $FUS1_{promoter}$-HA-eGFP expression that is further increased during hyperosmotic shock.

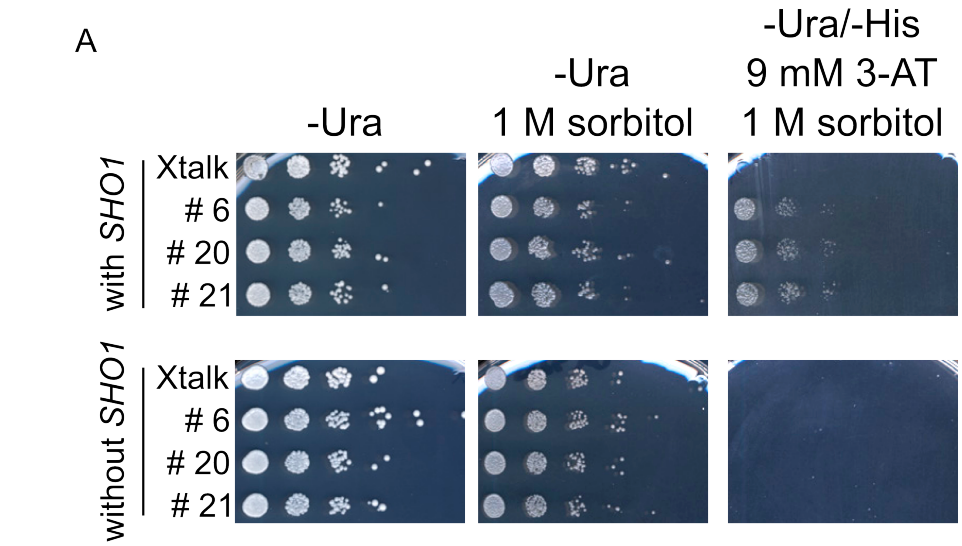
A
-Ura
-Ura
1 M sorbitol
-Ura/-His
9 mM 3-AT
1 M sorbitol
with SHO1
Xtalk
6
20
21
without SHO1
Xtalk
6
20
21

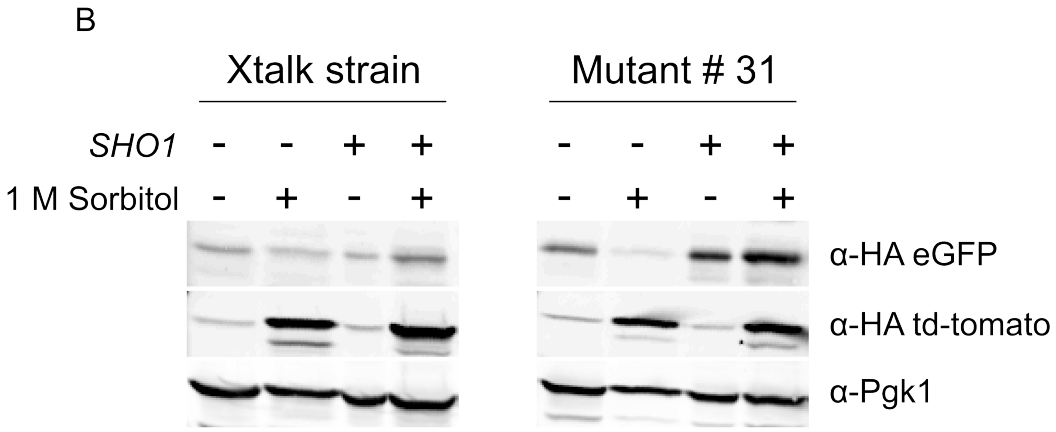
B
Xtalk strain
Mutant # 31
SHO1 - - + + - - + +
1 M Sorbitol - + - + - + - +
α-HA eGFP
α-HA td-tomato
α-Pgk1

FUS1$_{promoter}$-eGFP reporter. A threshold of eGFP expression was used so that 27% of the parental Xtalk strain cells were below that threshold, where as only 2.5% of the mutant cells were (Figure 5-4). If the mutant allele had been complemented in any given transformant, it would be 10 times more likely to be below that threshold than a non-complemented transformant. Based on the construction of the gDNA plasmid library, approximately 1 in 6,000 transformants would be complemented (Jauert et al., 2005). By going through the process of the the FACS enrichment three times, we could expect 1 in 6 to represent a complemented mutant.

The gDNA library plasmids from the transformants that no longer grew on -Ura/-His medium containing 1 M sorbitol and 9 mM 3-AT were isolated from the yeast and submitted for DNA sequence analysis. Several plasmids isolated from mutant #25 transformants contained fragments of the yeast genome that encoded *RGA1*, a Cdc42 GTPase activating protein (GAP). I isolated different gDNA plasmids that contained overlapping regions of the *RGA1* locus, but were not identical. I also isolated a handful of plasmids containing *URA3*. This outcome was an unforseen issue with my method, in that a gDNA library plasmid containing *URA3* would allow for the loss of the *SHO1 URA3* plasmid and the mating pathway reporter would no longer be induced. However, it was relatively straight forward to discard the plasmid isolates containing *URA3*. In hindsight, I would have used an integrated a functional copy of SHO1 prior to the FACS analysis. FACS enrichment for mutant #31 was unsuccessful. My best guess is that this mutant frequently generated a subpopulation of petite cells, which did not express the *FUS1*$_{promoter}$-eGFP reporter and overwhelmed my ability to identify authentic complemented transformants.

Truncated alleles of RGA1 result in SHO1 dependent activation of the mating pathway

Because several plasmids containing the *RGA1* promoter and coding sequence were isolated from the complemented transformants of mutant #25, I sequenced the *RGA1* locus in the Xtalk strain, and in mutants #25 and #31. Mutant #25 contained a 1 bp deletion which resulted in a frame shift in the middle of the *RGA1* ORF and mutant #31 contained a nonsense mutation at position 505 in *RGA1* ORF. So, the causative alleles in both mutants appeared to be the same. We then sequenced the *RGA1* locus in the remaining 16 mutants and 10 out of the 16 also carried *rga1* mutations. Because three mutants had the same genetic lesion, and thus appeared to be siblings, 8 unique alleles were isolated from the 10 *rga1* mutants (Table 5-1). Tellingly, all of the mutant alleles result in a truncated versions of Rga1. Because I identified the same gene so many times, I am confident that our screen was reasonably saturated, however, the identity of the remaining 6 mutants is not known. Figure 5-5 shows the general structure of Rga1, as well as the position of the truncations. Rga1 is 1007 residues in length, contains a pair of N-terminal LIM domains and a C-terminal GAP domain (Smith et al., 2002). LIM domains were named after the three proteins in which they were initially described: Lin11, Isl-1 and Mec-3. Each LIM domain contains a pair of zinc fingers which are thought to mediate protein-protein interactions (Kadrmas and Beckerle, 2004). Unfortunately, there is no binding specificity known for the LIM domains that might help predict what sort of protein-protein interactions the LIM domains in Rga1 might be used for. Immediately following the LIM domains is a noticeably basic region. There are a total of 15 potential MAPK phosphorylation sites in Rga1.

There are two other demonstrated Cdc42 GAPs in yeast, Rga2 and Bem3 (Figure 5-5) (Smith et al., 2002). Rga2 is a clear paralog of Rga1 and contains the N-terminal LIM domains as well as the predicted coiled-coil sequence. While these elements are well conserved between the two, the connecting sequences are only moderately conserved. Bem3 does not have any

Figure 5-4. FACS enrichment of complemented transformants

Mutant #25 was transformed with a yeast gDNA library of plasmids. These transformants were pooled and grown to mid-exponential phase. A small part of the culture was maintained in isotonic synthetic medium, whereas the majority of the culture was added to an equal volume of the same synthetic medium containing 2 M sorbitol and subjected to hyperosmotic shock for 2 h. The parental Xtalk strain was treated the same, as a control. Fluorescence in the red and green channels was measured simultaneously with a fluorescence-activated cell sorter (FACS, Becton Dickinson Influx™). GFP was excited with a 488 nm laser and its emission was detected with a 530/540 nm bandpass filter; td-Tomato was excited with a 561 nm laser and its emission was detected with a 593/540 nm bandpass filter.

The scatter plots show the distribution of the Xtalk and mutant #25 strain with and without hyperosmotic shock. While the median td-tomato signal increased during hyperosmotic shock in both strains, only the mutant shows an increase in eGFP expression (numbers are in a log scale). The purple box at the bottom of each scatter plot indicates the range of eGFP and td-tomato expression used to sort mutant #25 transformants that had not turned on the $FUS1_{promoter}$-eGFP reporter. For the mutant #25 that was treated with 1 M sorbitol, anything within that purple box was kept, and that consisted of 2.5% of the population. 27% of the parental strain was within that box, indicating a 10-fold enrichment for complemented transformants. This FACS enrichment was repeated sequentially 3 times, presumably providing a 1000-fold enrichment.

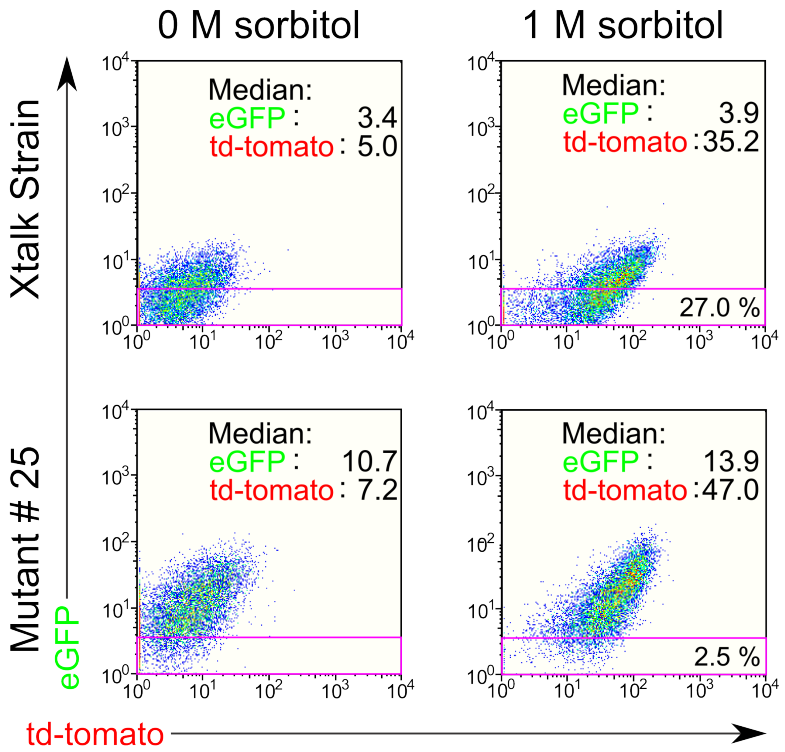
0 M sorbitol
1 M sorbitol
Xtalk Strain
Mutant # 25
eGFP
td-tomato
Median:
eGFP : 3.4
td-tomato : 5.0
Median:
eGFP : 3.9
td-tomato : 35.2
27.0 %
Median:
eGFP : 10.7
td-tomato : 7.2
Median:
eGFP : 13.9
td-tomato : 47.0
2.5 %

Table 5-1. The location and nature of *RGA1* mutants isolated

Mutant Number	Genetic alteration*	Consequence	Last correctly coded residue in mutant ORF
10	G 2018 → T	Nonsense	672
20	A 1763 deleted	Frameshift	587
21	2381 T inserted	Frameshift	795
25	A 1763vdeleted	Frameshift	587
26	C 1723 → T	Nonsense	574
28	G 1882 → T	Nonsense	627
30	A 1763 deleted	Frameshift	587
31	G 1516 → T	Nonsense	505
161	G 2877 → A	Nonsense	958
258	C 2146 → T	Nonsense	715

* Number represents the position relative to the beginning of the ORF (i.e. “A” in the start codon ATG would be #1)

Figure 5-5. Domains and general structure of the confirmed Cdc42-GAPs

Three well characterized Cdc42-specific GAPs are encoded in the *S. cerevisiae* genome, Rga1, Rga2 and Bem3. Both of the Cdc42-GAPs contain a pair of N-terminal LIM domains, a central predicted coiled-coil motif (CC) and the C-terminal GAP domain. Bem3 contains a PH domain in the center of its primary structure and a C-terminal GAP domain. PH domains interact with membrane phosphoinositides. The positions of the Rga1 truncations isolated in our genetic selection are shown with red bars. Some of these truncations are frame shift mutants, therefore, after the frame shift the normal Rga1 sequence is no longer present and replaced with incorrect amino acids until the coding sequence hits a stop codon created by the frame shift. In these cases, the red bar indicates the position of the frameshift mutant, not the stop codon created by the shift.

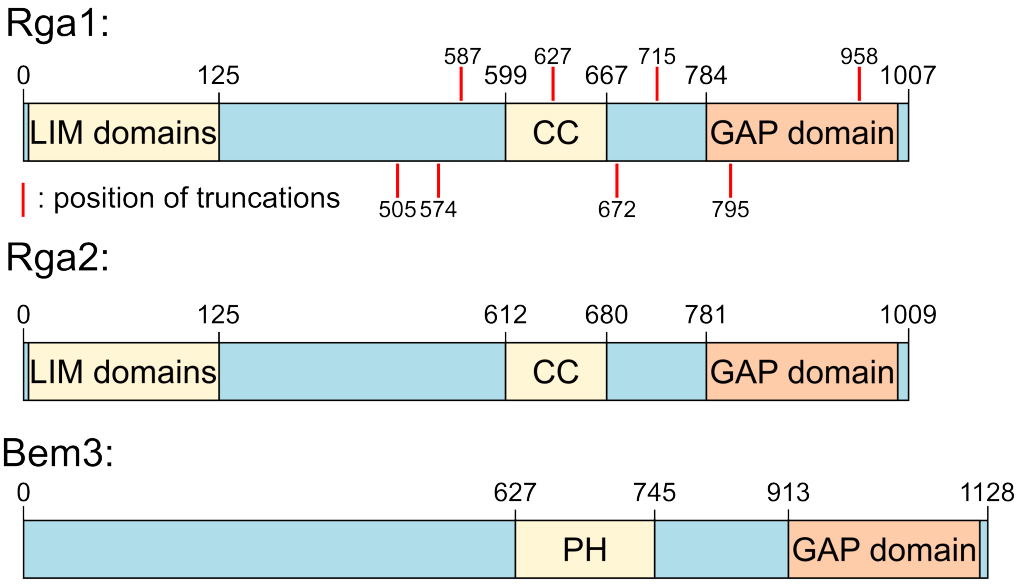
Rga1:
0
125
587
599
627
667
715
784
958
1007
LIM domains
CC
GAP domain
: position of truncations
505
574
672
795
Rga2:
0
125
612
680
781
1009
LIM domains
CC
GAP domain
Bem3:
0
627
745
913
1128
PH
GAP domain

LIM domains or predicted coiled-coil sequence. Instead Bem3 has a pleckstrin homology (PH) domain that binds to membrane phosphatidylinositides. There are at least six other proteins encoded in the yeast genome that contain Rho-GAP domains similar in primary structure to that in Rga1; however, most of them have either been shown to not have GAP activity for Cdc42 or have been demonstrated to be involved in other processes (Smith et al., 2002).

RGA1-containing plasmids complemented the mutant phenotype and I identified 8 different *rga1* mutants in my selection. Thus, I that felt it was extremely likely that these Rga1 truncations cause the crosstalk observed. Nonetheless, the definitive way to determine that such was the case was to clone the mutant sequence, replace the wild-type *RGA1* allele with the mutant version and test for the crosstalk phenotype. If, in fact, the Rga1 truncation is the causative allele, it alone should be sufficient to recapitulate the phenotype. To do this, *RGA1* was deleted in the dual fluorescent reporter strain described in Chapter 4. An empty vector, as well as *CEN* plasmids containing *RGA1* or *rga1-505* (Figure 5-5) under the control of its own promoter were transformed into this *rga1*Δ derivative. The truncated allele from mutant #31 was designated *rga1-505* because it contains a nonsense mutation, causing the ORF to code for only aa 1-505. Figure 5-6 shows the extent of the HOG and mating pathway reporter expression before and after hyperosmotic shock. The phenotype of the *rga1*Δ strain, which contained an empty vector, was barely discernible from the strain that contained the wild-type version of *RGA1* in terms of the expression of the HOG and mating pathway reporters. There was a very small, but measurable, increase in mating pathway reporter expression both before and after hyperosmotic shock in the *rga1*Δ strain. By contrast, the strain that contained the *rga1-505* plasmid recapitulated the phenotype of the original mutants; that is, this strain reproducibly displayed higher basal expression of the mating pathway reporter that increased somewhat during hyperosmotic stress.

The observation that the *rga1-505* allele results in more potent activation of the mating pathway than complete loss of *RGA1* is very interesting. First this situation highlights why traditional genetic methods can have some advantages over the shortcuts offered by more "modern" genetic techniques. One option I considered while planning my selection was to use the yeast knockout collection to identify potential mutants. This tactic ensures that every non-essential gene is tested and circumvents the work required to identify the causative allele. However, clearly that screen would have failed to identify *RGA1* because the deletion allele has very little or no impact on mating pathway activation. Second, my results suggest that the truncated allele is expressed and interferes and acts in a semi-dominant manner in crosstalk prevention, most likely by binding to some protein and blocking any other protein from compensating for the loss of *RGA1*. The most likely candidate for that compensating protein would be Rga2, which has very similar architecture to Rga1, something that is discussed and tested further below.

RGA1 was first identified in a study published in 1995 via a genetic screen for mutants that allowed activation of the mating pathway in a strain that lacked Ste4, the Gβ subunit (Stevenson et al., 1995). The mutant isolated from this screen contained loss of function alleles, both of which were necessary to achieve robust mating pathway activation: *rga1* and *pbs2*. Neither mutation alone activated the mating pathway significantly; the phenotype was only observed when both mutations were present (Stevenson et al., 1995). This result already strongly suggested that when Hog1 cannot function, Rga1 action prevents crosstalk to the mating pathway. To confirm this conclusion, I treated my *rga1*Δ and *rga1-505* cells with the Hog1-AS inhibitor (1-NM-PP1) for 2 h. When Hog1-AS was inhibited, both the *rga1*Δ or *rga1-505* cells

Figure 5-6. Rga1 truncations mutants result in crosstalk to the mating pathway

(A) *RGA1* and the truncated *rga1-505* mutant were cloned into YCplac22 *CEN* plasmids under the control of their own promoters and transformed into YJP552 (*HOG1-AS rga1*Δ) along with the empty vector. Cells were grown to mid-exponential phase in synthetic complete medium and then added to an equal volume of fresh medium containing double the concentration of stated stimulants or 1-NM-PP1. After 2 h stimulation, expression of the reporters was assessed in single cells by epifluorescence microscopy. The merged eGFP and td-tomato images are shown. Deletion of *RGA1* did not result in significant basal $FUS1_{promoter}$-eGFP expression or its induction during hyperosmotic shock. It did, however, result in $FUS1_{promoter}$-eGFP expression during iso-osmotic inhibition of Hog1-AS. The *rga1-505* truncation allele reproduced the phenotype observed in the mutants during hyperosmotic shock. In the truncation mutant, there was higher basal $FUS1_{promoter}$-eGFP transcription that was modestly increased during hyperosmotic shock. The truncation mutant also showed significant $FUS1_{promoter}$-eGFP expression when the Hog1-AS was inhibited without hyperosmotic shock.

(B) The data in (A) presented as a scatter plot, where each dot represents the average pixel intensity of eGFP and td-tomato for a single cell under the conditions tested (n ~ 400 per sample). The red dot represents the mean pixel intensities of eGFP and td-tomato for the entire population. The red bars indicate the standard deviation of eGFP and td-tomato pixel intensity observed in that population.

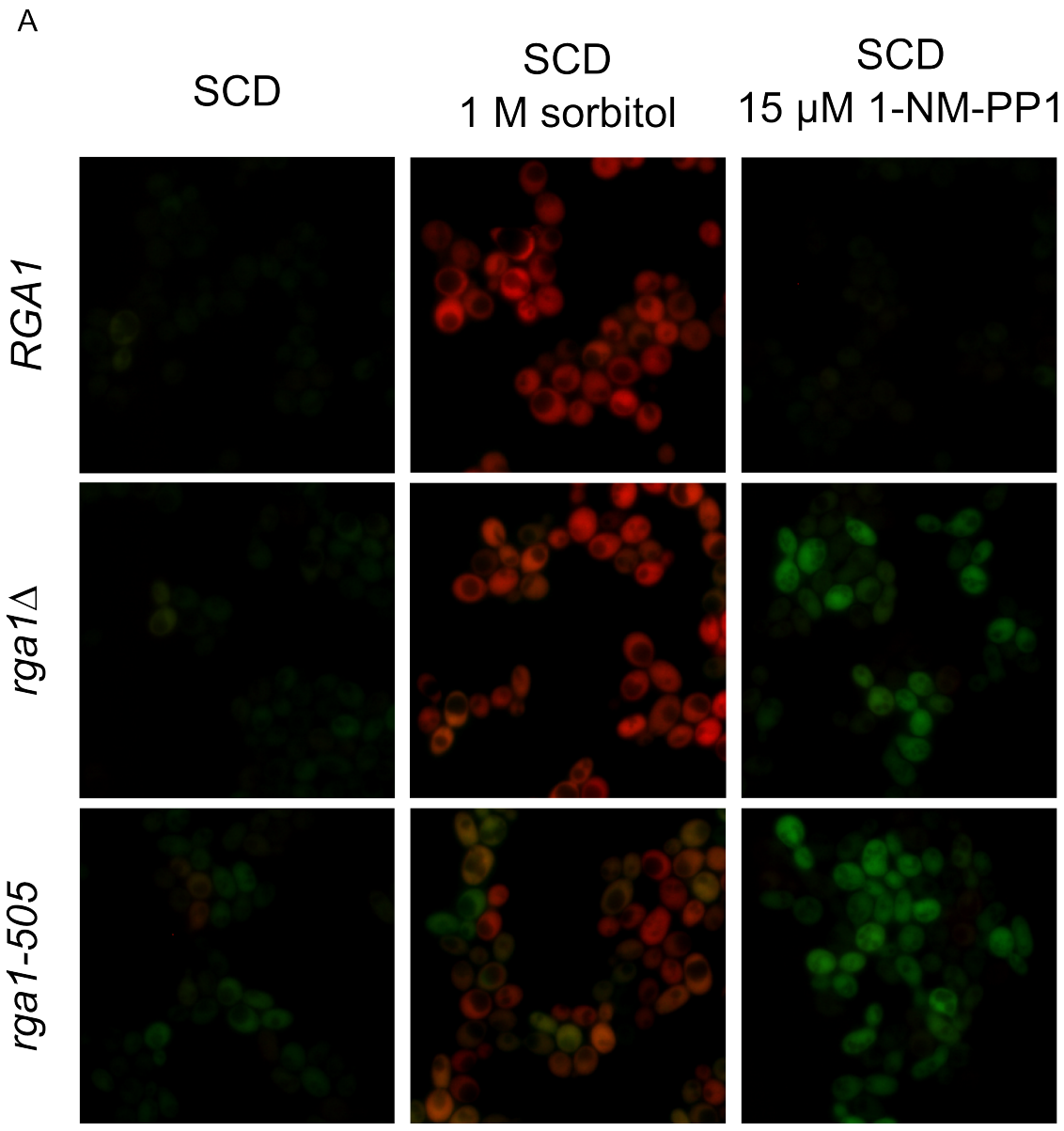
A
SCD
SCD
1 M sorbitol
SCD
15 μM 1-NM-PP1
RGA1
rga1Δ
rga1-505

B

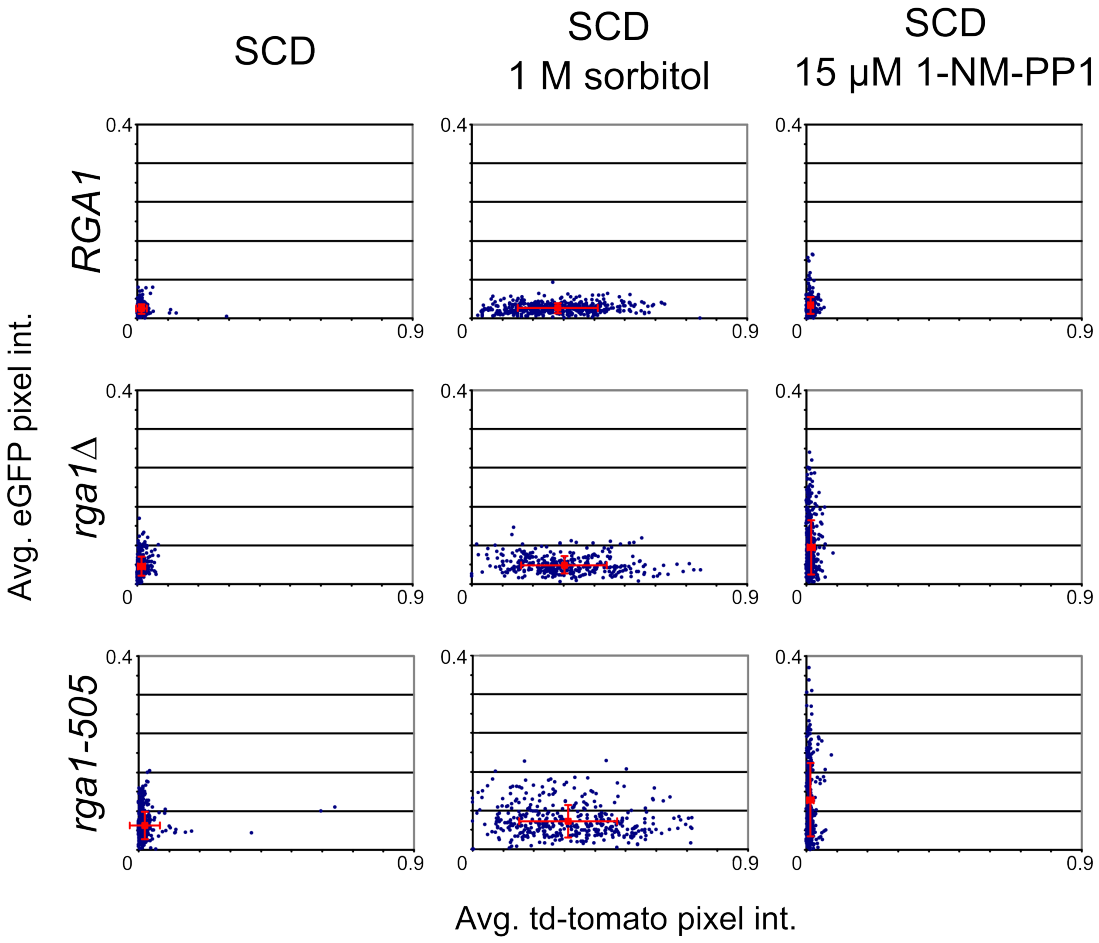
SCD
SCD
1 M sorbitol
SCD
15 μM 1-NM-PP1
RGA1
rga1Δ
rga1-505
Avg. eGFP pixel int.
Avg. td-tomato pixel int.
0.4
0
0.9

robustly activated the mating pathway reporter, whereas *RGA1* cells did not. Thus, I confirmed that loss of HOG pathway output in *rga1* mutant strains results in activation of the mating pathway even without any hyperosmotic shock. In hindsight, the work of Stevenson et al. (1995) made Rga1 a good candidate to be the Hog1 substrate that squelches crosstalk. Perhaps I only fully appreciated their work in the context of my experiments, where I know that such mating pathway activation depends on the presence of *SHO1*. Moreover, the main conclusion of that study was that Rga1 negatively regulates the mating pathway, not that it prevents crosstalk from the HOG pathway. While Rga1 may contribute to negative regulation the mating pathway in some manner, the results presented in Chapter 4 of this thesis preclude that it is sufficient to squelch mating pathway function when both the HOG and mating pathways are stimulated.

Perhaps the reason for overlooking Rga1 as a potential substrate of Hog1 that prevents crosstalk is due to the fact that simply deleting the gene results in a barely detectable increase in mating pathway activity that is not effected by hyperosmotic shock. By contrast, the genetic selection I carried out identified a more potent truncated allele, that reproducibly causes a modest increase in mating pathway reporter expression after hyperosmotic shock. I postulated that the truncated alleles, which all contain the LIM domains and an additional 400 residues C-terminal to those domains, bind to an unidentified protein and block the binding of Rga2 to that protein. This theory assumes that, in the *rga1*Δ strain, Rga2 compensates for the lack of Rga1. The first test of this theory was to delete both *RGA1* and *RGA2* and to assess mating pathway activation. Deletion of *RGA2* by itself produced no phenotype in terms of HOG or mating pathway reporter expression before or after stress. The *rga1*Δ *rga2*Δ strain, however, behaved in a fashion almost identical to the *rga1-505* mutant strain (Figure 5-7). There was higher basal mating pathway activation that showed a further modest increase during hyperosmotic stress. This result supports the notion that Rga1 and Rga2 function redundantly in preventing the mating pathway activation seen, and that the truncated alleles are blocking Rga2. The putative shared binding partner has not yet been identified. Alternatively, Rga1 and Rga2 may need to heterodimerize via their Lim domains, and the LIM-containing fragment of Rga1 may block Rga2 homodimerization.

Although the $FUS1_{promoter}$-eGFP reporter is a convenient way to assess mating pathway activation, it provides a measure of the most distal output of the mating pathway. Also, there is always a slight possibility that the *rga1* mutants might result in activation of this reporter independently of Fus3 or Kss1. To ensure that the mating pathway MAPKs were, in fact, activated during hyperosmotic stress in *rga1* mutants, I monitored their activation state using phospho-specific antibodies. The anti-p42/44 antibody was raised against the phosphorylated activation loop of Erk2, and recognizes activated Erk1 and Erk2. Kss1 is more similar to Erk2, whereas Fus3 is closer to Erk1. Erk1 and Erk2 have nearly identical activation loops. As described in chapter 4, because of the higher similarity of Kss1's activation loop to the Erk1 and 2 consensus activation loop than that seen in Fus3, I believe that this antibody recognizes active Kss1 much more avidly than active Fus3. Thus, this reagent can be used to compare the level of active MAPK before and after stimulation. It cannot be used to reliably compare the levels of active Kss1 to the level of active Fus3.

I used the anti-phospho-Erk antibody to assess the amount of Fus3 and Kss1 activation after hyperosmotic shock in *RGA1*, *rga1*Δ, and *rga1-505* strains (Figure 5-8). As reported before, I observed that *rga1* mutations increased basal Kss1 phosphorylation (Rodríguez-Pachón et al., 2002). Moreover, there is weak and transient activation of Kss1 during hyperosmotic shock, even in a wild-type background, as also reported previously (Wang et al., 2009; Shock et al., 2009). However, in the *rga1*Δ and *rga1-505* cells, Kss1 activation after hyperosmotic shock

Figure 5-7. Rga1 and Rga2 work together to prevent mating pathway activation

Strains YJP585 (*rga2*Δ) and YJP586 (*rga1*Δ *rga2*Δ) were grown to mid-exponential phase in synthetic complete medium and then added to an equal volume of fresh medium containing double the concentration of stated stimulants. After 2 h, expression of the reporters was assessed in single cells by epifluorescence microscopy. The merged eGFP and td-tomato images are shown (top). Scatter plots (bottom) of the MAPK reporter expression where each dot represents the average pixel intensity of eGFP and td-tomato for a single cell under the conditions tested (n ~ 400 per sample). The red dot represents the mean pixel intensities of eGFP and td-tomato for the entire population. The red bars indicate the standard deviation of eGFP and td-tomato pixel intensity observed in that population. Deletion of both *RGA1* and *RGA2* appears to reproduce the phenotype observed in the *rga1-505* truncation mutant.

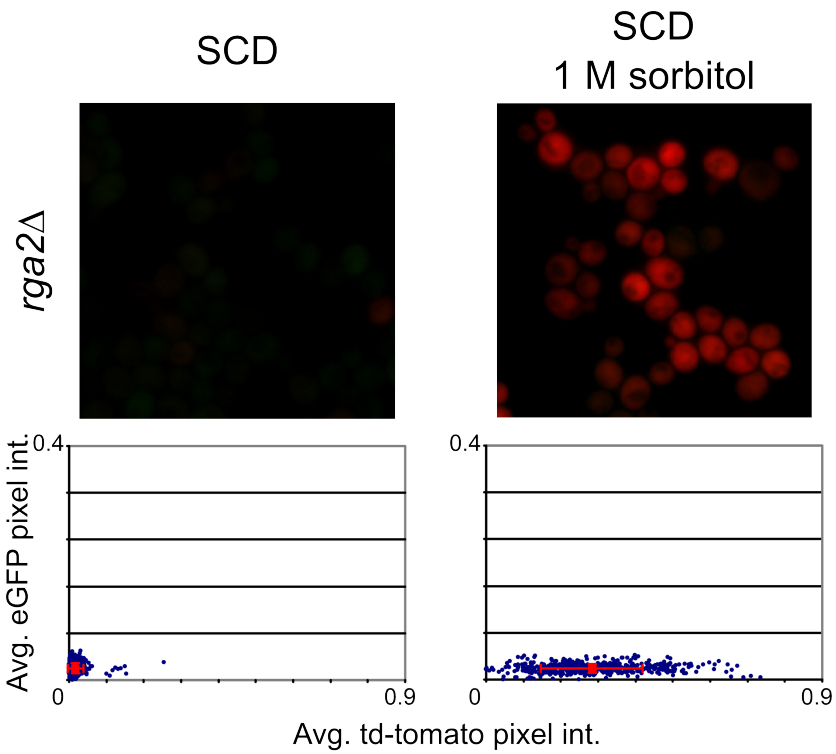
SCD
SCD
1 M sorbitol
rga2Δ
Avg. eGFP pixel int.
0.4
0
0.9
0.4
0
0.9
Avg. td-tomato pixel int.

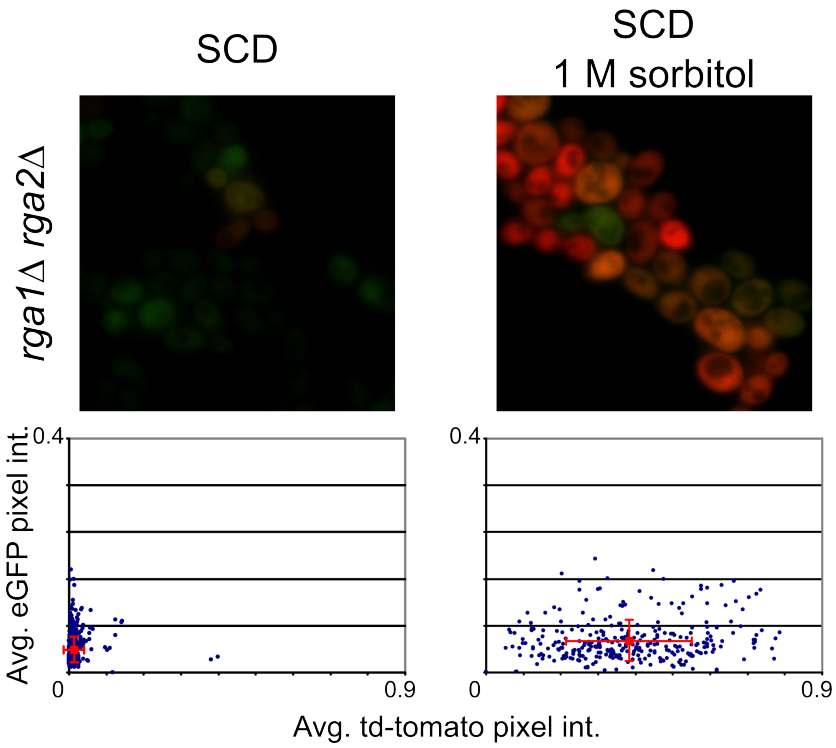
SCD
SCD
1 M sorbitol
rga1Δ rga2Δ
Avg. eGFP pixel int.
0.4
0
0.9
0.4
0
0.9
Avg. td-tomato pixel int.

Figure 5-8. Fus3 and Kss1 activation during hyperosmotic shock in *rga1* mutants

RGA1 and the truncated *rga1-505* mutant were cloned into YCplac22 *CEN* plasmids under the control of their own promoters and transformed into YJP552 (*HOG1-AS rga1*Δ) along with the empty vector. These strains were grown to mid-exponential phase in synthetic complete medium and were then treated with 1 M sorbitol or 30 nM alpha factor. After 15 mins in the presence of α-factor or the indicated time under hyperosmotic shock, an equal number of cells were pelleted, protein was isolated by trichloroacetic acid precipitation, solubilized and analyzed by SDS-PAGE. Proteins were then transferred to a nitrocellulose filter and incubated with anti-phospho-p42/44 antibody that recognize activated Kss1 and Fus3 (very specific immuno-blotting and incubation conditions are required for detection by this antibody, see Chapter 2 for details). Kss1 is strongly activated during hyperosmotic shock in the *rga1*Δ and *rga1-505* strains. Detectable active Fus3 is also found in the *rga1-505* cells.

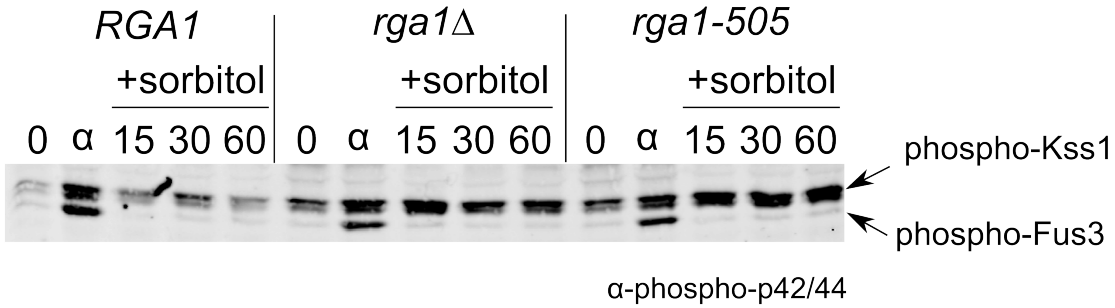
RGA1
rga1Δ
rga1-505
+sorbitol
+sorbitol
+sorbitol
0 α 15 30 60 0 α 15 30 60 0 α 15 30 60
phospho-Kss1
phospho-Fus3
α-phospho-p42/44

is stronger and more persistent compared to the *RGA1* strain. Perhaps due to the selectivity off the anti-phospho-Erk antibody, Fus3 is hard to detect. However, a small amount of active Fus3 was seen in the *rga1-505* strain and appeared to increase during hyperosmotic shock. The inability to detect robust Fus3 activation was surprising because the *rga1-505* mutant was isolated in a *kss1*Δ strain and exhibited mating pathway reporter induction. The response to α-factor appeared to be equivalent among the three strains. I repeated this experiment in *kss1*Δ derivatives of the same strains; however, this background did not increase the level of phosphorylated Fus3 levels over what was observed in the *KSS1* cells (data not shown).

Rga1 is a negative regulator of Cdc42 in the context of the HOG pathway

One possibility for the results described above is that Rga1 is a negative regulator of the mating pathway. Mutating or deleting *RGA1* possibly results in higher basal activation of the mating pathway because of increased intrinsic activity of the mating pathway itself and not due to crosstalk. Indeed, in *rga1-505* cells, there is mating pathway reporter expression prior to hyperosmotic shock, and it is only modestly increased during stress. However, this model does not explain the need for Sho1 or why inhibiting Hog1-AS increases the reporter induction dramatically. Moreover, the results from Chapter 4 explicitly show that Hog1 action cannot block pheromone stimulated mating pathway output. If Rga1 is a substrate of Hog1 that helps to prevent crosstalk, it may do so by down-regulating the pool of Cdc42 that is initially associated with HOG pathway components in the Sho1 branch. In this scenario, Rga1 action promotes Cdc42-GTP hydrolysis before crosstalk can occur. This mode of regulation would represent a kinetic insulation mechanism.

I therefore wanted to determine if Rga1 negatively regulates Cdc42 in the Sho1 branch of the HOG pathway. The Sln1 branch of the HOG pathway is responsive to smaller (0.25 M sorbitol) changes in extracellular osmolarity than the Sho1 branch, which requires a stronger hyperosmotic shock for activation (>0.5 M sorbitol). Thus, a wild-type strain will show a response to 0.2 M sorbitol, whereas a strain that only contains the Sho1 branch of the HOG pathway (a *ssk1*Δ strain) will not. This differential response provides an excellent means to determine whether Rga1 is a negative regulator of the Sho1 branch. If Rga1 action, in fact, down-regulates Cdc42 in the Sho1 branch, then Hog1 should be activated more strongly upon moderate hyperosmotic stress in *rga1* mutants. To assess phospho-Hog1 I used an antibody raised against active p38 (the human homolog of Hog1), which detects activated Hog1 well (Westfall et al., 2008). To limit response to the Sho1 branch, I constructed *ssk1*Δ derivatives of my *RGA1*, *rga1*Δ and *rga1-505* strains.

The amount of phosphorylated Hog1 observed, relative to the total Hog1 present, was measured in the *SSK1* and *ssk1*Δ backgrounds after 15 min of hyperosmotic shock with 0.0, 0.2 or 1.0 M sorbitol (Figure 5-9). As expected in an otherwise wild-type strain, deletion of *SSK1* severely reduced the amount of active Hog1 seen after hyperosmotic shock, with almost no apparent response to 0.2 M sorbitol, and a significantly reduced response to 1.0 M sorbitol. The *rga1*Δ *ssk1*Δ strain displayed higher basal Hog1 activity, a readily detectable response to 0.2 M sorbitol and a nearly wild-type response to 1.0 M sorbitol. The *rga1-505 ssk1*Δ strain showed a significant response to both 0.2 and 1.0 M sorbitol. Thus, as the model anticipated, the lack of Rga1 caused the Sho1 branch of the HOG pathway to be more responsive to mild hyperosmotic shock indicating that Rga1 contributes to signal flux through the Sho1 branch of the HOG pathway at the level of Cdc42.

The experiment described above showed that at 15 min post-hyperosmotic shock Rga1

Figure 5-9. Rga1 negatively regulates the Sho1 branch of the HOG pathway

(A) Strains YJP212 (wild type), YJP226 (*ssk1*Δ), YJP552 (*rga1*Δ), YJP591 (*rga1*Δ *ssk1*Δ), YJP610 (*rga1-505*) and YJP611 (*rga1-505 ssk1*Δ) were grown to mid-exponential phase in synthetic complete medium and then added to an equal volume of fresh medium containing twice the indicated concentration of sorbitol. After 15 min, an equal number of cells were pelleted, protein was isolated by trichloroacetic acid precipitation, solubilized and separated by SDS-PAGE in triplicate. Proteins were then transferred to a nitrocellulose filter and incubated with anti-p38 and anti-phospho-p38 antibodies that recognize the total Hog1 and phosphorylated Hog1, respectively. The three lanes for each strain and sorbitol concentration are replicates. Mutants lacking the Sln1 branch (*ssk1*Δ) do not respond well to low concentrations of sorbitol, indicating tht the Sho1 branch only responds to severe hyperosmotic shock. When *RGA1* is deleted or truncated, however, the Sho1 branch responds well to low concentrations of hyper osmolarity.

(B) Quantitation of results presented in (A). The amount of phosphorylated Hog1 per unit total Hog1 is compared between different concentrations of sorbitol. Each graph is normalized so that 100% Hog1 phosphorylation equivalent to the amount of phosphorylation observed in the *SSK1* strain at 1 M sorbitol. Error bars indicated the standard error of the mean for the biological triplicates.

A

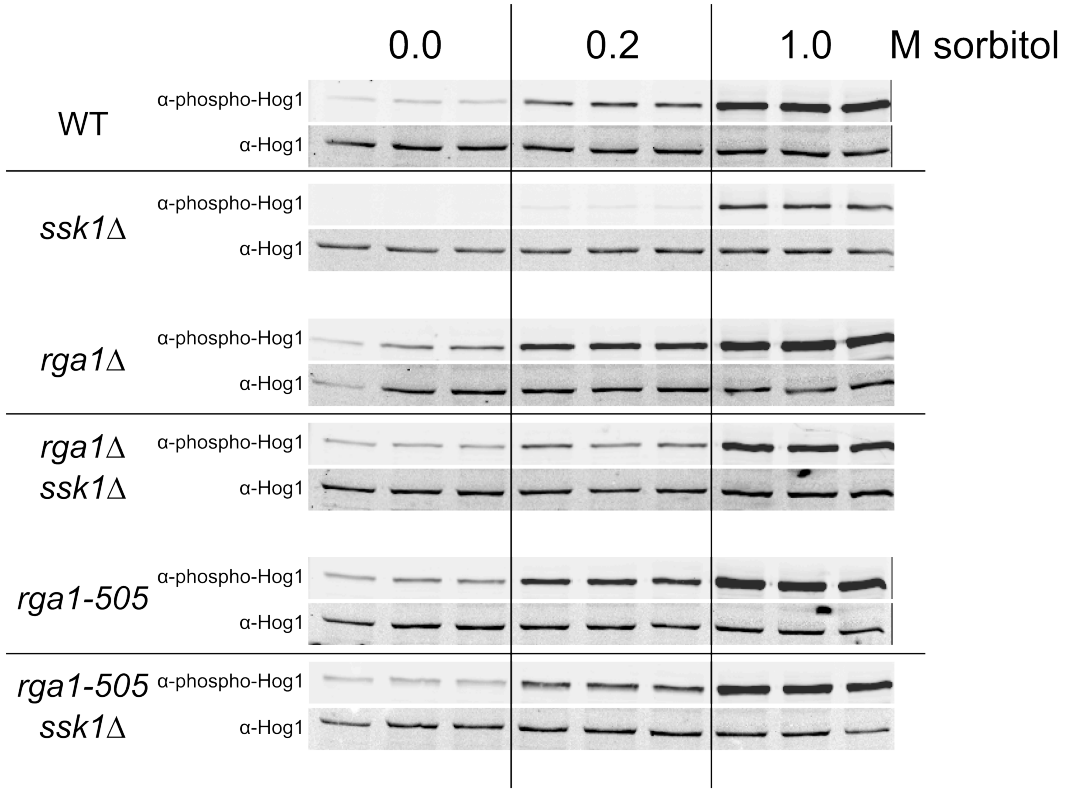
0.0
0.2
1.0
M sorbitol
WT
α-phospho-Hog1
α-Hog1
ssk1Δ
α-phospho-Hog1
α-Hog1
rga1Δ
α-phospho-Hog1
α-Hog1
rga1Δ ssk1Δ
α-phospho-Hog1
α-Hog1
rga1-505
α-phospho-Hog1
α-Hog1
rga1-505 ssk1Δ
α-phospho-Hog1
α-Hog1

B

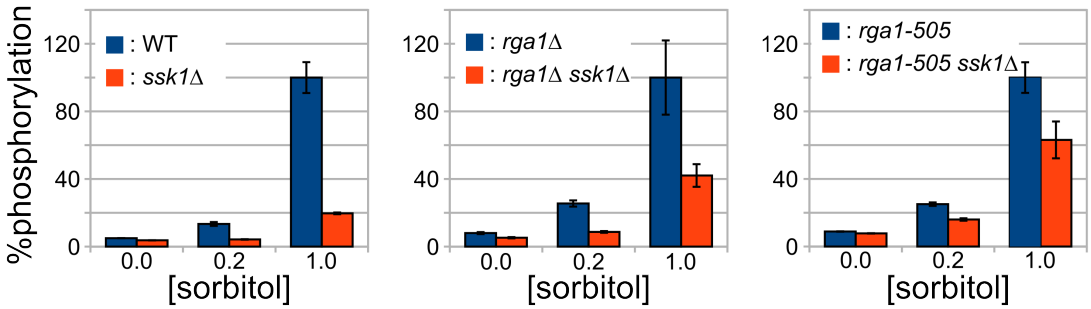
%phosphorylation
120
80
40
0
: WT
: ssk1Δ
0.0
0.2
1.0
[sorbitol]
: rga1Δ
: rga1Δ ssk1Δ
: rga1-505
: rga1-505 ssk1Δ

function limits Hog1 activation. I also wanted to determine if Rga1 regulated the dynamics of HOG pathway activation. Removal of this negative regulator may simply increase the amplitude of HOG pathway activation, but if Rga1 also regulates the duration of Cdc42 activation within the HOG response, then absence of Rga1 may also shift or change the shape of the Hog1 activation curve. Normally, Hog1 activation peaks at 5 min post-hyperosmotic shock and then decreases over the course of an hour. Although the HOG pathway is turned off after adaptation to increased osmolarity, the level of Hog1 activation post-adaptation is maintained at a higher level than prior to the hyperosmotic challenge (Westfall et al., 2008). When the dynamics of Hog1 activation in *rga1*Δ *ssk1*Δ and *rga1-505 ssk1*Δ strains were compared to that of a *ssk1*Δ strain, the activation of the HOG pathway and its return to an adapted state were not changed (Figure 5-10). Strikingly, however, the plateau of active Hog1 post-adaptation was at least two-fold higher in both the *rga1*Δ *ssk1*Δ and *rga1-505 ssk1*Δ strains. Moreover, as expected from the previous experiment (Figure 5-9), the absolute level of active Hog1 was also higher (but, in this case, the absolute amounts of active Hog1 detected were normalized to the 5 min time point to permit comparison of the shapes of the curves).

These data suggest that Rga1 action helps attenuate the Sho1 branch during activation and helps suppress basal signaling during homeostasis. Measuring activated Hog1 may not capture all of the nuances of this system. The level of phospho-Hog1 is determined by activated Pbs2 (dictated by the activity of the Sho1 branch of the HOG pathway) and by the rate of de-phosphorylation of by various phosphatases. Once activated Hog1 translocates into the nucleus where it is dephosphorylated by Ptp2 and Ptp3 (Wurgler-Murphy et al., 1997). Therefore, the more activated Hog1, the more readily it is turned off. Hog1 can also be inactivated by cytoplasmic phosphatases such as Ptc1. However, the majority of Hog1 inactivation occurs in the nucleus (Westfall et al., 2008). The result of these opposing forces is that the level of phospho-Hog1 will not be strictly correlated with the activity of the Sho1 branch. It would be very useful to directly measure activation of the upstream components in the Sho1 branch, but there currently are not adequate reagents to do so.

Rga1 is a substrate of the Hog1 MAPK in vitro

A prerequisite for Rga1 being a substrate of Hog1 that contributes to preventing crosstalk, is that Rga1 undergoes Hog1-dependent changes in its phosphorylation state after hyperosmotic shock. I purified full-length recombinant Rga1 by expressing N-terminally GST-tagged Rga1 in *E. coli*, and carrying out affinity purification on glutathione-sepharose beads. The purified protein was then incubated with either Hog1 or catalytically-inactive Hog1-KD in the presence of constitutively-active Pbs2-EE and [γ-^{32}P]ATP. Full-length Rga1 became phosphorylated only when functional Hog1 was present, as judged by auto-radiography, indicating the Rga1 is a substrate of Hog1 *in vitro*.

We next sought to identify which of the 15 potential MAPK phosphorylation sites in Rga1 were getting modified by Hog1. First to narrow down the list, we truncated Rga1 into three fragments based on the division of predicted secondary structure elements: LIM domains GST-Rga1(1-339), Coiled-coils GST-Rga1(340-670), GAP domain GST-Rga1(671-1007). These smaller fragments also proved to be much easier to express and purify from bacteria. When the kinase assay described above was repeated using these fragments, it was clear that all of the Hog1 phosphorylation sites resided within the middle fragment (Figure 5-11A). This narrowed down the list of potential sites from 15 to 8.

To identify which of the 8 potential sites were in fact being modified in vitro, we repeated

Figure 5-10. Rga1 is required to complete the attenuation of Hog1 activation after hyperosmotic stress adaptation

(A) Strains YJP226 (*ssk1*Δ), YJP591 (*rga1*Δ *ssk1*Δ) and YJP611 (*rga1-505 ssk1*Δ) were grown to mid-exponential phase in synthetic complete medium and then added to an equal volume of fresh medium containing twice the indicated concentration of sorbitol. At the indicating time after addition of the sorbitol, an equal number of cells were pelleted, protein was isolated by trichloroacetic acid precipitation, solubilized and separated by SDS-PAGE. Proteins were then transferred to a nitrocellulose filter and incubated with anti-p38 and anti-phospho-p38 antibodies to measure the total Hog1 and phosphorylated Hog1, respectively. Each time course was performed in biological triplicate, and representative immuno-blots are shown. Truncation or deletion of *RGA1* did not alter the overall dynamics of Hog1 activation during acute stress; however, the amount of active Hog1 present after stress adaptation remained significantly higher in both the *rga1*Δ and *rga1-505* strains.

(B) Quantitation of results presented in (A). The amount of phosphorylated Hog1 per unit total Hog1 throughout the time course is compared between the three strains. Data obtained from each strain is normalized so that 100% Hog1 phosphorylation equivalent to the amount of phosphorylation observed at 5 min Error bars indicated the standard error of the mean for the three independent trials.

A

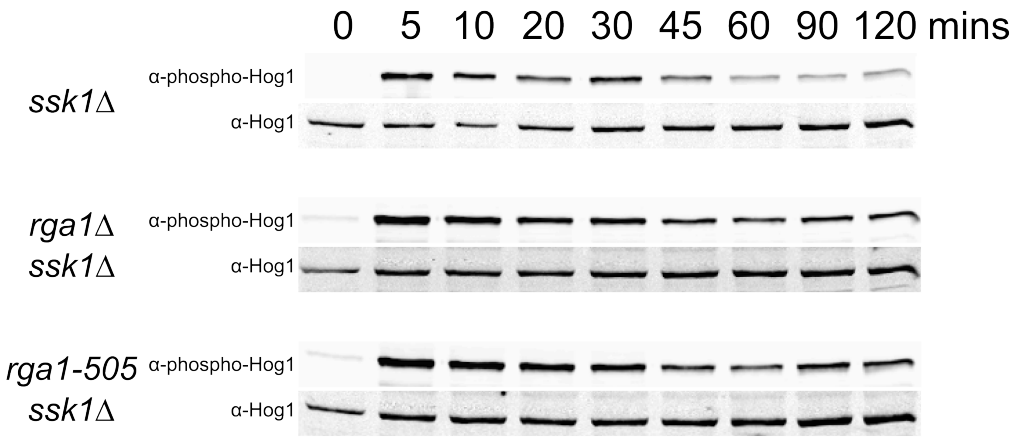
0 5 10 20 30 45 60 90 120 mins
ssk1Δ
α-phospho-Hog1
α-Hog1
rga1Δ ssk1Δ
α-phospho-Hog1
α-Hog1
rga1-505 ssk1Δ
α-phospho-Hog1
α-Hog1

B

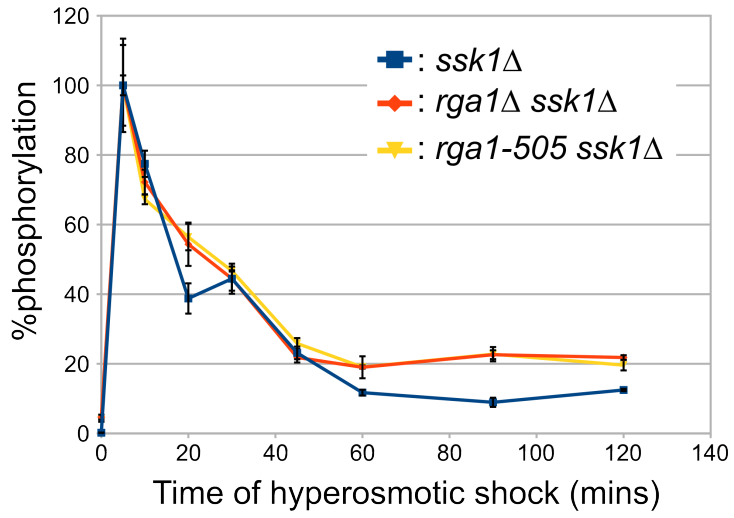
%phosphorylation
Time of hyperosmotic shock (mins)
: ssk1Δ
: rga1Δ ssk1Δ
: rga1-505 ssk1Δ
0
20
40
60
80
100
120
140

Figure 5-11. Hog1 phosphorylates Rga1 *in vitro*

(A) Hog1 purified from yeast was activated using a constitutively-active Pbs2-EE protein isolated from bacteria. Both wild-type (WT) and kinase-dead (KD) versions of were incubated with full-length Rga1 and the three Rga1 fragments indicated. Mobility of each protein is indicated (arrows).

(B) Coomassie dye staining of purified Hog1 protein following SDS-PAGE. The only visible band is Hog1.

(C) Mass spectrometry results of the Rga1 middle fragment (residues 340-670) exhaustively phosphorylated by Hog1 *in vitro* using excess non-radioactive ATP. The phosphorylated fragment was run on an SDS-PAGE gel and then subjected to in-gel digestion with trypsin. Serines and threonines that were phosphorylated are in red, all potential MAPK phosphorylation sites (S / T P) are in bold and the regions in blue were not identified in the mass spectra.

(D) Hog1 purified from yeast was activated using a constitutively-active Pbs2-EE protein isolated from bacteria. The ability of the listed Rga1 middle fragment phosphorylation site mutants to be phosphorylated by the active Hog1 was determined. Mobility of the various proteins is indicated (arrows). The loading for the Rga1 fragments was reasonably equivalent except for the 5A mutant, which has significantly less protein present.

A

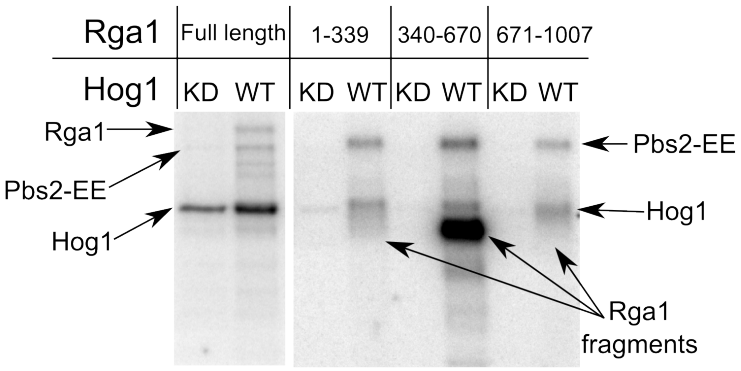
Rga1
Full length
1-339
340-670
671-1007
Hog1
KD WT KD WT KD WT KD WT
Rga1
Pbs2-EE
Hog1
Pbs2-EE
Hog1
Rga1
fragments

B

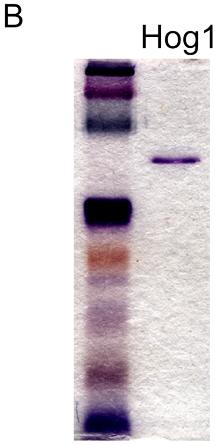
Hog1

C

340 KGSNTDIFNTGEISQMDPSLSRKVLNNIVEETNALQRPVVEVVKEDRSVPDLA 393

394 GVQQEQAEKYSYSNNSGKGRKISRSLSRRSKDLMINLKSRATGKQDSNVKLSP 446

447 ASKVTSRRSQELMRDNDSHTGLDTPNSNSTSLDILVNNQKSLNYKRFTDNGTL 499

500 RVTSGKEPALEEQKNHSFKSPSPIDHLLQSPATPSNVSMYRTPPLDSSLTFDR 552

553 RNGSSYSNQNYSIPSWQKTPKTQLENSDNFEEQKETLYENSESRNDPSLDKEI 605

606 VTAEHYLKQLKINLKELESQREELMKEITEMKSMKEALRRHIESYNSEKNKLY 658

659 LDSNELSNNPPM 670

470 532 541 571

Phosphorylated
Not covered

D

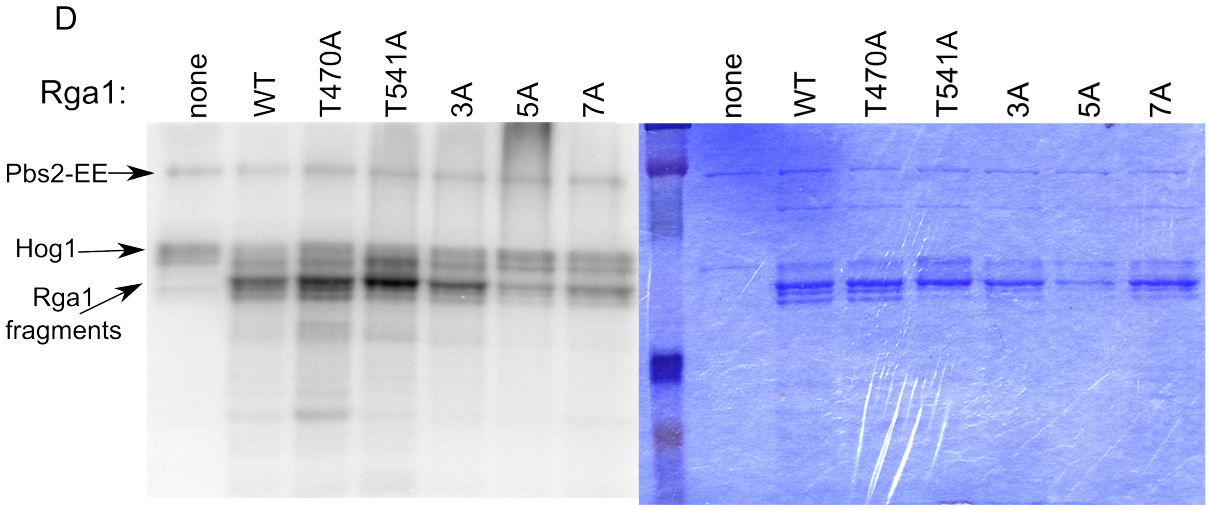

3A: T470A T541A T571A
5A: 3A + S529A T532A
7A: 5A + S519A S521A

the Hog1 phosphorylation of GST-Rga1(340-670) using only non-radioactive ATP and identified the modified sites by mass spectrometry. This procedure was repeated several times until nearly all the potential sites had been covered by the mass spectrometry analysis. By this analysis, four of the eight S/T P sites were identified as phosphorylated (Figure 5-11C). The mass spectrometry experiments had some issues, however. Specifically, 13 non-S/T P sites were identified as phosphorylated. It is extremely unlikely that GST-Rga1(340-670) was phosphorylated in *E. coli* prior to the kinase assay. Moreover, Hog1 has high specificity towards SP or TP sites (Mok et al., 2010), and should not appreciably modify other sequences. Because the Hog1 used for these kinase reactions was purified from yeast, it seems likely explanation is that there was a contaminating kinase in the Hog1 preparations used in the mass spectrometry experiments. However, the GST-Rga1(340-670) was not phosphorylated when the kinase assay reaction included the Hog1-KD, so either the contaminating kinase requires active Hog1, or it does not co-purify with the Hog1-KD. The Hog1 was purified by overexpression of Hog1 which was C-terminally tagged with 6XHIS-HA-3C-ZZ in yeast. The protein was first enriched from extracts by the interaction between its ZZ domain with IgG-coated beads, and then the ZZ domain was cleaved off using protease 3C. The resulting protein was then affinity purified again using a IMAC on a Ni^{2+} charged NTA resin column attached to an FPLC and, finally, the Hog1-containing fractions from the IMAC column were resolved on an ion exchange column. Peak fractions from the ion exchange column were then dialyzed, and the only apparent band visible by coomassie dye staining was Hog1 (Figure 5-11B). To determine which, if any, other kinases might be present in our purified Hog1, I submitted them for tandem mass spectrometry analysis. Sequences corresponding to only one other kinase were detected at a very low level, namely the MAPK Slt2/Mpk1, which only phosphorylates S/T P sites.

I then purified the Hog1-AS mutant protein and repeated the kinase assay using furanyl-furane γS-ATP (FU-γS-ATP). This ATP analog is reported to be only readily used by analog-sensitive kinase mutants (Allen et al., 2007), and, because it contains the γ-thio-phosphate, should have allowed us to distinguish Hog1-dependent modifications from spurious signals. However, subsequent mass spectrometry indicated again that non-S/T P sites were modified with thio-phosphate. Thus, contrary to published claims, the other kinase contaminating our Hog1-AS preparation must be able to use FU-γS-ATP.

I therefore decided that it would be best to determine the sites that Hog1 phosphorylates within this Rga1 fragment by mutagenesis, instead of mass spectrometry. The phosphorylation sites identified by the mass spectrometry, as well as some that were not, were mutated to alanine. These mutant Rga1 fragments were then purified and used as substrates in a Hog1 kinase assay. Figure 5-11D shows the result of that kinase assay. The 7A mutant, which only has all but one potential MAPK phosphorylation site removed, shows significantly less overall phosphorylation. Thus, the bulk of the Hog1-dependent phosphorylation is occurring primarily on these -SP- and -TP- sites.

The phosphorylation state of Rga1 changes during hyperosmotic shock in vivo

While the *in vitro* kinase assay demonstrated that Rga1 can be phosphorylated by Hog1, it is perhaps more important to determine if Rga1 is phosphorylated by Hog1 *in vivo*. One of the most common means of identifying phosphorylation *in vivo* is by electrophoretic mobility shift in SDS-PAGE detected by immuno-blotting. While a commercial Rga1 (Santa Cruz) antibody is available, it did not work at all in my hands. I therefore tagged Rga1 at its N-terminus with the hemagglutinin (HA) epitope tag. I found that addition of a HA tag onto the C-terminus of Rga1

rendered it non-functional, as judged by mating pathway reporter induction during inhibition of Hog1-AS function. When run on a 10% (75:1 acrylamide to *bis*-acrylamide) gel, transferred to a nitrocellulose membrane and probed with an anti-HA antibody, the HA-Rga1 appears to run as a smear of 2 or more bands (Figure 5-12A). During hyperosmotic shock the smear collapses. This collapse takes approximately 15 min to go to completion, and the electrophoretic mobility of HA-Rga1 gradually converts to 2 bands (resembling the initial phosphoryation state) over the course of 60 mins. In a strain containing the Hog1-AS allele, the presence of 1-NM-PP1 prevents the collapse of the smear during hyperosmotic shock (Figure 5-12B). The changes in electrophoretic mobility were due to phosphorylation, since treatment of HA-Rga1 with calf-intestinal phosphatase collapsed the smear into a single band (Figure 5-12C).

To determine which potential phosphorylation sites were responsible for the observed in mobility patterns before and after hyperosmotic stress, we repeated this experiment using phosphorylation site mutants of the HA-Rga1 protein. By this means, we found that Thr541 is necessary to observe the slower mobility HA-Rga1 species seen prior to hyperosmotic shock (Figure 5-13A). It is likely the case that the phosphorylation state of other sites within HA-Rga1 change, yet do not effect the mobility of the protein under these conditions.

These experiments show that there is a Hog1-dependent change in Rga1's phosphorylation state during hyperosmotic stress. However, it is clear that HA-Rga1 is already phosphorylated prior to hyperosmotic shock. I tested whether the initial phosphorylation state of HA-Rga1 depends on Hog1 by performing the electrophoretic mobility assay in a *hog1*Δ strain. In this background the initial distribution of HA-Rga1 is the same, and, as expected, does not collapse during hyperosmotic shock. Therefore the phosphorylation seen prior to challenge with high osmolarity is not dependent on Hog1 and must be due to the action of another kinase. Rga1 has been reported to be a substrate of the CDK Cdc28 and possibly regulated in a cell cycle-dependent manner (Holt et al., 2009). We therefore introduced HA-Rga1 into a *cdc28-1* temperature-sensitive strain and isolated protein before and after hyperosmotic shock at the permissive and restrictive temperature (Figure 5-13B). This experiment clearly demonstrated that the slower mobility HA-Rga1 isoform seen in naïve cells is due to Cdc28 dependent phosphorylation.

Hog1-mediated phosphorylation of the middle region of Rga1 is not sufficient for preventing crosstalk

Based on the results described above, I tested the hypothesis that Hog1 phosphorylation of the S/T P sites within the middle region of Rga1 is required for preventing crosstalk. A plasmid containing HA-*RGA1-7A* was transformed into a derivative of the dual-fluorescent reporter strain in which *RGA1* had been deleted (YJP552). *RGA1-7A* contains 7 phosphorylation site mutations: T470A, T541A, T571A, S529A, T532A, S519A and S521A. This mutant lacks all of the phosphorylation sites identified by mass spectrometry thus far, and no longer displays a change in electrophoretic mobility during hyperosmotic shock.

Yeast cells expressing this *rga1-7A* mutant did not have any altered expression of the HOG or mating pathway reporters (Figure 5-14). There was no increase in basal mating pathway reporter expression, nor induction of that reporter during hyperosmotic shock. Moreover, there was no induction of the mating pathway reporter when Hog1-AS was inhibited without hyperosmotic shock, as was seen with the *rga1*Δ strain. Therefore the 7A mutant complemented the *RGA1* deletion at least in this regard. Based on these results it is apparent that none of those 7 potential Hog1 phosphorylation sites are necessary the function of Rga1 in preventing

Figure 5-12. Phosphorylation state of HA-Rga1 changes *in vivo* during hyperosmotic shock in a Hog1-dependent manner

(A) Strain YJP595 (*HOG-AS HA-RGA1*) was grown to mid-exponential phase and then added to an equal volume of medium containing 2 M sorbitol. After 15 min, cells were pelleted and protein extracts prepared by trichloroacetic acid precipitation. After solubilization, SDS-PAGE on a 10% (75:1 acrylamide : *bis*-acrylamide) gel and transfered to a nitrocellulose membrane, anti-HA antibody was used to assess the mobility of HA-Rga1. As can be seen, HA-Rga1 runs as a smear, which transiently collapses during hyperosmotic shock. If the Hog1-AS is inhibited with 1-NM-PP1, the mobility of HA-Rga1's does not change during hyperosmotic shock.

(B) Strain YJP662 (*hog1*Δ *HA-RGA1*) was grown, protein extract prepared and immuno-blotting performed as in (A). As with Hog1-AS inhibition, the mobility of HA-Rga1 does not change during hyperosmotic shock. However, the smear of HA-Rga1 species is present in the *hog1*Δ strain, indicating that Hog1 is not responsible for the modification state observed in iso-osmotic conditions.

(C) Strain YJP595 (*HOG-AS HA-RGA1*) was grown as in (A), protein extracts were prepared by bead-beating and subsequent clarification. The HA-Rga1 was then immunoprecipitated with anti-HA antibody bound to protein A / protein G sepharose beads, washed, and then treated with calf intestinal phosphatase (CIP) or identical conditions without the phosphatase. Electrophoresis and immuno-blotting were performed as described in (A). Because the smear collapses into a single band after CIP treatment, the variable mobility of HA-Rga1 is due to differential phosphorylation.

A

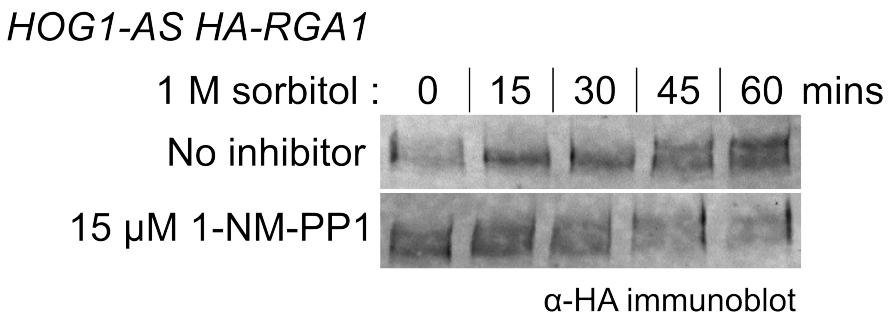
HOG1-AS HA-RGA1
1 M sorbitol : 0 | 15 | 30 | 45 | 60 mins
No inhibitor
15 μM 1-NM-PP1
α-HA immunoblot

B

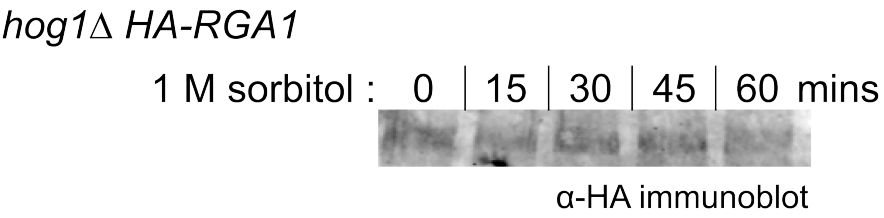
hog1Δ HA-RGA1
1 M sorbitol : 0 | 15 | 30 | 45 | 60 mins
α-HA immunoblot

C

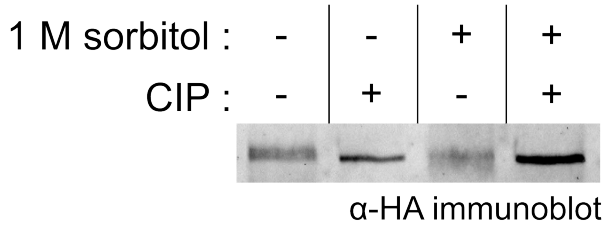
1 M sorbitol : - - + +
CIP : - + - +
α-HA immunoblot

Figure 5-13. Resting state of HA-Rga1 phosphoprotein is due to phosphorylation of Thr541 by Cdc28

(A) Strain YJP589 (*HOG-AS rga1*Δ) was transformed with YCplac22 plasmids containing *RGA1* and the indicated *RGA1* phosphorylation site mutants under the control of their own promoter. These strains were grown, protein extract prepared and immuno-blotting performed as in (Figure 5-12A), except that cells were collected at a single time point (15 min) post shock. 2A: T541A T571A, 3A: T470A T541A T571A, 5A: T470A T541A T571A S529A T532A, 7A: T470A T541A T571A S529A T532A S519A S521A. The slower mobility HA-Rga1 species observed prior to hyperosmotic shock appears to be primarily dependent on Thr541.

(B) Strains YJP679 (*HA-RGA1*) and YJP707 (*cdc28-1 HA-RGA1*) were grown to mid-exponential phase in synthetic medium at 25ºC. One portion of the YJP707 culture was kept at 25ºC, where as the other portion, and the YJP679 culture, were shifted to 37ºC. After 2 h, cells were collected for time point zero, and the remaining culture was treated with 1 M sorbitol for 15 min. The slower mobility HA-Rga1 species present before hyperosmotic shock is absent when Cdc28 is inactivated.

A

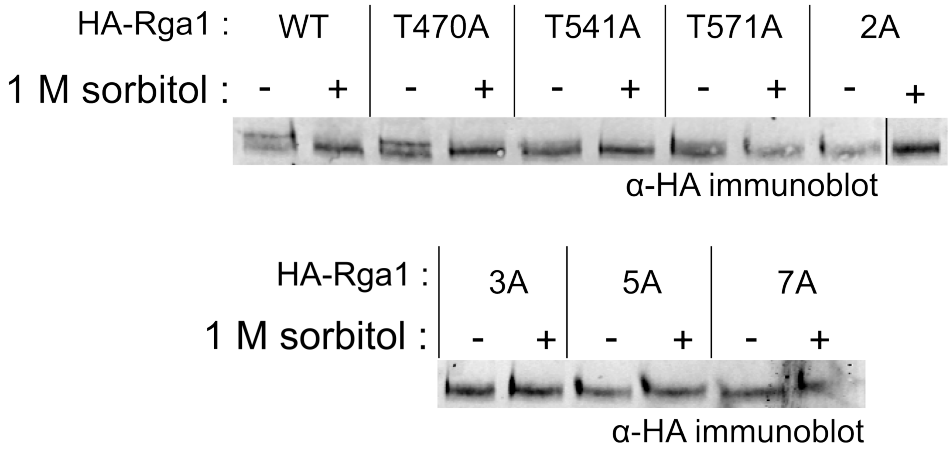
HA-Rga1 :
WT
T470A
T541A
T571A
2A
1 M sorbitol :
- + - + - + - + - +
α-HA immunoblot
HA-Rga1 :
3A
5A
7A
1 M sorbitol :
- + - + - +
α-HA immunoblot

B

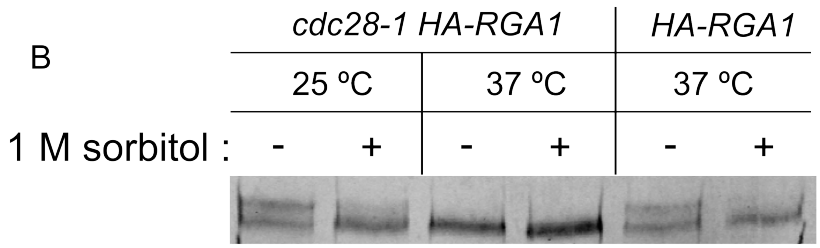
cdc28-1 HA-RGA1
HA-RGA1
25 ºC
37 ºC
37 ºC
1 M sorbitol :
- + - + - +

Figure 5-14. Hog1-mediated phosphorylation of the middle domain of Rga1 is not required for prevention of crosstalk

Strain YJP552 (*rga1*Δ) transformed with a plasmid containing *HA-RGA1-7A* was grown to mid-exponential phase in synthetic complete medium and then added to an equal volume of fresh medium containing double the concentration of stated stimulants. After 2 h, expression of the reporters was assessed in single cells by epifluorescence microscopy. The merged eGFP and td-tomato images are shown (top). Scatter plots (bottom) of the MAPK reporter expression where each dot represents the average pixel intensity of eGFP and td-tomato for a single cell under the conditions tested (n ~ 400 per sample). The red dot represents the mean pixel intensities of eGFP and td-tomato for the entire population. The red bars indicate the standard deviation of eGFP and td-tomato pixel intensity observed in that population. Removal of these 7 phosphorylation sites did not abrogate Rga1's action towards prevention of crosstalk.

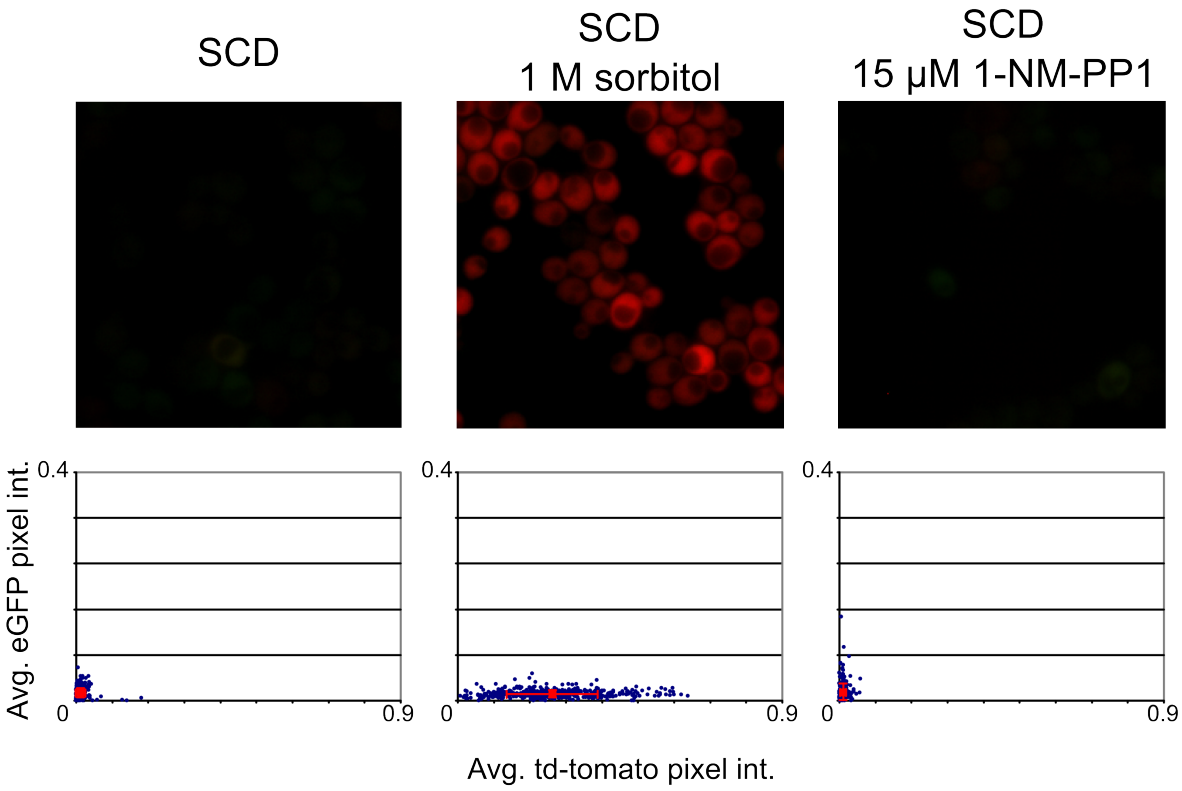
SCD
SCD
1 M sorbitol
SCD
15 μM 1-NM-PP1
Avg. eGFP pixel int.
0.4
0
0.9
0.4
0
0.9
0.4
0
0.9
Avg. td-tomato pixel int.

crosstalk. However, this result does not rule out Rga1 as the Hog1 substrate that prevents crosstalk, a point that will be discussed further below.

Discussion

The genetic selection described in this chapter identified the Cdc42-GAP Rga1 as a factor that helps prevents crosstalk between the HOG and mating pathway. My findings demonstrate that Rga1 has a role in controlling the amount of Hog1 activated by the Sho1 branch of the HOG pathway and in preventing spill over of Cdc42-GTP to other MAPK pathways. Because *rga1* mutants do not entirely recapitulate the crosstalk observed in a *hog1*Δ strain during stress, there are likely other factors involved in addition to Rga1. However, it is still possible that, collectively, the Cdc42 GAPs are what prevent crosstalk in its entirety.

When a *hog1*Δ strain is hyperosmotically stressed, crosstalk occurs to the mating pathway, but at the same time the cells fail to adapt to the hyperosmotic stress. The lack of adaptation in the *hog1*Δ strain likely leads to sustained activation of the Sho1 branch of the HOG pathway creating more active Ste11 to participate in the crosstalk. Cdc42-GTP stimulated Ste20 is necessary to produce activated Ste11. When our *rga1* mutants are hyperosmotically stressed, presumably there is crosstalk to the mating pathway, but Hog1 is functional so adaptation occurs. Thus, activation of the Sho1 branch is transient. These circumstances may explain the modest increase in mating pathway reporter expression observed in our *rga1* mutants. An experiment that might address this issue is to create a *HOG1* strain that cannot adapt to hyperosmotic stress either by preventing glycerol production (*gpd1*Δ *gpd2*Δ mutant) or by the presence of a constitutively open Fps1 glyceroporin channel that lets the glycerol leak out of the cell (Hedfalk et al., 2004).

The observation that inhibition of Hog1-AS in a *rga1*Δ strain results in significant induction of the mating pathway even in the absence of hyperosmotic shock reporter is very interesting. This result, along with the increase in basal mating pathway reporter expression, implies that Rga1 is involved in suppressing basal Sho1 branch signaling from interacting with the mating pathway. The increase in signal during Hog1-AS inhibition could mean that there is a second substrate of Hog1 that is involved in a negative feedback loop to the Sho1 branch of the HOG pathway. This increase could also be due to a loss of osmotic homeostatsis in the cell. That is, Hog1 functions to maintain the correct intracellular osmolarity, and when it can no longer do that, the Sho1 branch of the HOG pathway is likely turned on in an attempt to compensate for the lower Hog1 function. This might increase the levels of basal signal, which ends up leaking into the mating pathway.

While the middle fragment of Rga1 is a very good substrate of Hog1 *in vitro*, the dynamics of its phosphorylation state *in vivo* are still not entirely clear. The *in vitro* kinase assays coupled with mass spectrometry analysis imply that there are contaminating kinases in our Hog1 purification. Moreover, mutating 7 of the 8 S/TP sites reduced, but did not eliminate, radiolabel incorporation into the Rga1 middle fragment. Thr541 appears to be a site that is phosphorylated in Rga1 by Cdc28 prior to hyperosmotic and, for now, may even be dephosphorylated after hyperosmotic shock in a Hog1-dependent manner. To get around the various problems with the *in vitro* kinase assays, I am currently conducting a mass spectrometry analysis of Rga1 that has been immunoprecipitated before and after hyperosmotic shock in *HOG1* and *hog1*Δ strains. I believe this type of assay will have a much better chance of identifying the sites in Rga1 that Hog1 phosphorylates. In any event, phosphorylation of Rga1 by the CDK Cdc28 implies that it is cell-cycle regulated. Work is underway to determine at which stage of the cell cycle Cdc28 modifies Thr541.

Because the HA-Rga1 bandshift collapses during hyperosmotic shock it is possible that a

Hog1 dependent phosphatase acts on Rga1. This is further supported by the collapse of the band in the T541A mutant and in the *cdc28-1* strain at restrictive temperature. However, it is also possible that Hog1 phosphorylates Rga1, and that these modifications increase the mobility of HA-Rga1 creating the appearance of the band collapse. That is, because phosphorylation can increase or decrease the mobility of a protein in these conditions, multiple phosphorylations may cancel each other out. The mass spectrometry experiment described above will also address this issue. Moreover, work is underway to visualize HA-Rga1 protein that has been run on a Phos-Tag SDS-PAGE gel (Kinoshita et al., 2006). Phos-tag is a reagent that is covalently linked to the acrylamide in the gel, and chelates the phosphate groups as the gel runs. This system consistently retards phosphorylated species and will support the mass spectrometry results in terms of determining whether Rga1 becomes more or less phosphorylated during hyperosmotic shock in a Hog1-dependent manner.

Based on the data collected to date, however, it is possible that Hog1 regulates a phosphatase that then acts on Rga1. I am currently looking into the possibility that the phosphatase PP2A is responsible for this, mainly by analogy to reports describing regulation of PP2A by p38α in human tissue culture cells (Junttila et al., 2008). If it can be confirmed that Rga1 is dephosphorylated during hyperosmotic shock, the entire list of yeast phosphatases will be investigated in an unbiased manner. Hog1 activating a phosphatase to remove phosphates from Rga1 is not mutually exclusive with Rga1 being a substrate of Hog1 as well.

This point leads me to my second argument as to why the *rga1* mutants isolated and constructed so far may not reproduce entirely the crosstalk phenotype displayed by *hog1*Δ cells during hyperosmotic stress. In a *hog1*Δ strain, the HA-Rga1 banding pattern remains as a smear of two or more bands. Clearly, the situation is different when Rga1 is truncated, absent, or lacks some of its potential Hog1 sites. Therefore, we do not yet have a mutant that reproduces the effect on Rga1 phosphorylation that the lack of Hog1 would have. If, in fact, Rga1 becomes dephosphorylated during hyperosmotic stress, it would seem that the de-phosphorylated form is what participates in preventing crosstalk. One prediction of this scenario is that the Rga1-7A mutant should be able to prevent crosstalk even when Hog1-AS was inhibited. This was tested, and the prediction did not hold true (data not shown). In the end, however, fully understanding the dynamics of Rga1 phosphorylation during hyperosmotic stress may shed light on how Rga1 contributes to crosstalk prevention.

A third possible explanation as to why the *rga1* truncation mutants do not phenocopy a *hog1*Δ cell in terms of crosstalk is *RGA2*. Genetic evidence supports the notion that the truncations isolated in our screen have a more penetrant phenotype due to blocking of a binding site that is shared with Rga2. Clearly, biochemical evidence is still required for support this claim, and identifying that putative shared binding site would be very revealing. Rga2 is very similar in structure to Rga1 and has also been reported to be a substrate of both Cdc28 and Pho85 CDKs (Sopko et al., 2007; Holt et al., 2009). It is not known if Rga2 is a substrate of Hog1, however, given its similarity to Rga1 this is rather likely. The third Cdc42 GAP, Bem3, has not been tested for any role in crosstalk prevention. Due to their similarity, I have focused on Rga1 and Rga2, but it might be the case that all three Cdc42 GAPs share a semi-redundant role in crosstalk prevention.

At this point, and given the data available, it seems that Rga1 contributes to crosstalk prevention via serving in a negative feedback loop that confines the Cdc42-GFP involved in the Sho1 branch of the HOG pathway to this response. In this model, upon HOG pathway stimulation, Hog1 activates a phosphatase that dephosphorylates Rga1 on some sites, and Hog1

may phosphorylate Rga1 on other sites. The resulting altered Rga1 then stimulates Cdc42-GTP hydrolysis dampening the amount of this component before the cross activation of the mating pathway has a chance to occur.

Chapter 6
Conclusions and Perspectives

In this dissertation, I have described my studies of how the Hog1 MAPK confers hyperosmotic stress resistance and maintains signaling fidelity between the HOG and other MAPK pathways that share upstream signaling components. I set two goals for myself at the beginning of my graduate career, identify the substrate(s) of Hog1 that are required for stress adaptation and the substrate(s) that prevent crosstalk. I feel I have made significant progress towards both, and will present the major conclusions and discuss the implications of my work here.

HOG pathway dependent hyperosmotic stress resistance

First, together with Patrick Westfall (Westfall et al., 2008), I showed that Hog1-dependent transcription is dispensable for hyperosmotic stress resistance. This uprooted a commonly held belief in the HOG pathway field that the transcriptional changes evoked by Hog1 were required for adaptation. It is not to say that transcription is unimportant. The transcript levels of many genes change during hyperosmotic shock, and the vast majority of these changes occur independently of Hog1. It is specifically the Hog1 dependent transcriptional changes that are not necessary for survival after hyperosmotic shock.

I then investigated several candidate proteins that could potentially be phosphorylated by Hog1 and be the cause of the increase in intracellular glycerol concentration. Inhibition of one or more of the three GAPDHs by Hog1 was a very attractive idea for stimulating glycerol production. However, my work on this subject makes this notion unlikely. It is true that pairwise deletions of the GAPDHs increase stress resistance somewhat. Because I could not obtain phosphorylation site mutants of the GAPDHs that remained functional, it was not possible to directly test the importance of their potential phospho-regulation by Hog1 and its effect on stress adaptation. Instead, I turned to FRET as a means of investigating potential regulation of these enzymes by Hog1. The FRET experiments suggest that there is a Hog1-dependent change in the conformation of Tdh3 during stress, however, this change is not due to phosphorylation at the only MAPK consensus site (Ser302). Instead, the Hog1-dependent change seems due indirectly to glycerol production through Gpd1. The change in the FRET ratio of Tdh3-FRET pairs may very well be an important clue as to how Hog1 increases the production of glycerol, but without knowing the molecular nature of those changes it is difficult to draw any concrete conclusions. I also looked into the possibility that Hog1 increases the amount of cytosolic NADH available to Gpd1 by closing the mitochondrial NADH porin, Por1. However, none of the Por1 phosphorylation site mutants resulted in sensitivity to hyperosmotic stress.

The most likely explanation is that Hog1 must phosphorylate several different substrates which together re-route glycolysis towards glycerol production. Other potential substrates include: the alcohol dehydrogenases; enzymes involved in amino acid synthesis that reduce NAD+; enzymes involved in the reduction of methyglyoxal (a byproduct off the triosephosphate isomerase reaction) to lactate; any substrate that would shut down mitochondial NADH oxidation; or other kinases and phosphatases. If Hog1 regulates other kinases and/or phosphatases there might be an extra layer of regulation between Hog1 and its relevant substrates. Gpd1 does not have any consensus MAPK phosphorylation sites; however, if Hog1 phosphorylates another kinase, Gpd1 may be an indirect substrate of Hog1. However, the

kinases known or suspected to be substrates of Hog1, Rck1 and Rck2 (Bilsland-Marchesan et al., 2000), are not required for hyperosmotic stress resistance (Westfall et al., 2008). While not entirely successful, I still find this question fascinating. During this stress response, the metabolic engine that is driving ATP and NADH generation temporarily shifts gears towards a different goal, glycerol production. This method of adaptation is more rapid and reversible than can be achieved at the transcriptional level. Moreover, if the cell is dealing with a stressful situation, it must utilize what it has available, and not go through the process of generating new proteins.

Insulation of the HOG pathway

Construction of a strain carrying single-cell dual fluorescent reporters allowed for a more sophisticated interrogation of signaling specificity in single cells. By measuring the amount of activation of each pathway in individual cells, I was able to conclusively demonstrate that activated Hog1 is not sufficient to block signaling in the mating pathway, which is not consistent with a previously proposed cross-inhibition model (McClean et al., 2007) for how signaling specificity is imposed. By examining both pathway outputs simultaneously, I was able to conclude that activation of the HOG pathway did not inhibit either MAPK (Fus3 or Kss1) of the mating pathway, and also that activation of the mating pathway did not inhibit either branch of the HOG pathway. Moreover, pre-activation of one pathway did not attenuate the response to stimulation of the other pathway. These dual fluorescent reporters used in conjunction with the analog-sensitive MAPK alleles furthered our understanding of kinetics of crosstalk prevention and the relative kinase activity thresholds required for the MAPKs to execute their various functions.

The observation that both the HOG and mating pathway can be activated simultaneously is not merely the expected result. The activation of other MAPK pathways are mutually exclusive with each other. For instance, Fus3 activation in the mating pathway results in the ubiquitin-dependent degradation of Tec1, preventing subsequent signaling output from the FG MAPK pathway. Insulating one MAPK pathway from another with shared components is likely to be a more complicated process than simple cross-inhibition.

The Cdc42-GAP Rga1 contributes to HOG pathway insulation

The genetic selection that was performed by undergraduate researcher Louise Goupil and me, identified *RGA1* as a gene that, when mutated appropriately, causes activation of the mating pathway in a HOG pathway-dependent manner. There were two aspects of this genetic selection that were very important for its success. First, demanding that any mutant required Sho1 for its phenotype was a quick and effective way to cull mutants unrelated to crosstalk. Second, the presence of the dual fluorescent reporters allowed us to identify complemented transformants very rapidly. The truncated versions of Rga1 identified in our screen resulted in higher basal mating pathway activity, and a modest, but reproducible, increase in expression of the mating pathway after hyperosmotic shock. There was significant activation of Kss1 during stress in our *rga1* mutant strains, but Fus3 was not strongly activated. It could be that Fus3 requires a larger amount of signal to become activated during crosstalk on this timescale and that *rga1* mutations only partially recapitulate the crosstalk phenomenon.

I found that inhibiting the Hog1-AS protein in an *rga1* mutant strain resulted in activation of the mating pathway even without any hyperosmotic stress. This finding indicates that there is some basal signaling through the HOG pathway, and that this flux is further increased in *rga1*

mutants. It also implies that there are other substrates of Hog1 that could also contribute to prevention of crosstalk, possibly the other Cdc42 GAPs, Rga2 and Bem3. Hog1 may exert negative feedback on another component of the Sho1 branch. Possibly on Sho1 itself or the MAPKKK adapter Ste50 (Hao et al., 2007, 2008). However, none of the substrates, by itself, is the dominant factor in squelching crosstalk.

Analysis of Hog1 activation at various concentrations of extracellular osmolarity in the *rga1* mutants confirmed my suspicion that Rga1 does in fact act as a negative regulator of the Sho1 branch of the HOG pathway. Based on kinetic experiments, its seems that Rga1 generally attenuates Cdc42's activation during stress, and in particular is important for a return to basal pathway signaling, since Hog1 remained more active after adaptation in my *rga1* mutants. Thus, Rga1 seems to help prevent crosstalk by ensuring the GTP-bound state of the shared protein Cdc42 is turned off efficiently. However, there are three other shared signaling components: Ste50, Ste11 and Ste20. Possibly, these need to be shut off as well, and whatever processes may accomplish that control, might also be involved in preventing crosstalk. It makes sense that Cdc42 need to be down-regulated to reduce the likelihood of crosstalk because it is the most upstream shared component.

Despite my effort to determine if Rga1 is phosphorylated by Hog1 *in vivo* during hyperosmotic stress, it is still not entirely clear. Rga1 appears to be a substrate *in vitro*; however, due to complications with obtaining extremely pure Hog1, I have not been able to map the exact sites of phosphorylation unequivocally. I have found that, *in vivo* and prior to hyperosmotic shock, Rga1 is phosphorylated by Cdc28 on Thr541. During hyperosmotic shock it appears that this modification is removed in a Hog1-dependent manner. It is still possible that Hog1 directly phosphorylates Rga1, and that Hog1-dependent phosphorylation increases the mobility of HA-Rga1 (meaning the phosphate on Thr541 is not removed); however, based on the data thus far, the most parsimonious interpretation of my gel mobility patterns is that there is a Hog1 activated phosphatase. Work is currently being done to determine which of these two possibilities is the case, and to further understand the changes in Rga1 phosphorylation during hyperosmotic shock.

Collectively, I believe I have made significant contributions to our understanding of the HOG pathway and hyperosmotic stress resistance. Because the HOG pathway is so well conserved from yeast to humans, it will be interesting to see how much of the ideas and data I have presented hold true for mammalian p38. Does p38 need to enter the nucleus to help cells adapt to the various stresses that result in its activation? While there is not a clear cut homolog of Rga1 in the human genome, there are a several dedicated Cdc42 GAPs encoded in the human genome. Are any of the human Cdc42 GAP proteins required to maintain the signaling specificity observed in human tissue culture cells? Based on the conservation of both sequence and function between Hog1 and p38 (Han et al., 1994), it seems very likely that the information I have obtained about Hog1 and its upstream activators can be applied to human signaling processes.

Literature Cited

Albertyn J, Hohmann S, Thevelein JM, Prior BA (1994) GPD1, which encodes glycerol-3-phosphate dehydrogenase, is essential for growth under osmotic stress in *Saccharomyces cerevisiae*, and its expression is regulated by the high-osmolarity glycerol response pathway. Mol. Cell. Biol. *14*, 4135-4144.

Allen JJ, Li M, Brinkworth CS, Paulson JL, Wang D, Hubner A, Chou W, Davis RJ, Burlingame AL, Messing RO, Katayama CD, Hedrick SM, Shokat KM (2007) A semisynthetic epitope for kinase substrates. Nat. Meth. *4*, 511-516.

Bao MZ, Schwartz MA, Cantin GT, Yates JR, Madhani HD (2004) Pheromone-dependent destruction of the Tec1 transcription factor is required for MAP kinase signaling specificity in yeast. Cell *119*, 991-1000.

Bardwell L, Cook JG, Voora D, Baggott DM, Martinez AR, Thorner J (1998) Repression of yeast Ste12 transcription factor by direct binding of unphosphorylated Kss1 MAPK and its regulation by the Ste7 MEK. Genes. Dev. *12*, 2887-2898.

Bayrhuber M, Meins T, Habeck M, Becker S, Giller K, Villinger S, Vonrhein C, Griesinger C, Zweckstetter M, Zeth K (2008) Structure of the human voltage-dependent anion channel. Proc. Natl. Acad. Sci. USA *105*, 15370-15375.

Bilsland-Marchesan E, Arino J, Saito H, Sunnerhagen P, Posas F (2000) Rck2 kinase is a substrate for the osmotic stress-activated mitogen-activated protein kinase Hog1. Mol. Cell. Biol. *20*, 3887-3895.

Bishop AC, Ubersax JA, Petsch DT, Matheos DP, Gray NS, Blethrow J, Shimizu E, Tsien JZ, Schultz PG, Rose MD, Wood JL, Morgan DO, Shokat KM (2000) A chemical switch for inhibitor-sensitive alleles of any protein kinase. Nature *407*, 395-401.

Brachmann CB, Davies A, Cost GJ, Caputo E, Li J, Hieter P, Boeke JD (1998) Designer deletion strains derived from *Saccharomyces cerevisiae* S288C: a useful set of strains and plasmids for PCR-mediated gene disruption and other applications. Yeast *14*, 115-132.

Brewster JL, de Valoir T, Dwyer ND, Winter E, Gustin MC (1993) An osmosensing signal transduction pathway in yeast. Science *259*, 1760-1763.

Burg MB, Kador PF (1988) Sorbitol, osmoregulation, and the complications of diabetes. J. Clin. Invest. *81*, 635-640.

Butty AC, Pryciak PM, Huang LS, Herskowitz I, Peter M (1998) The role of Far1p in linking the heterotrimeric G protein to polarity establishment proteins during yeast mating. Science *282*, 1511-1516.

Carpenter AE, Jones TR, Lamprecht MR, Clarke C, Kang IH, Friman O, Guertin DA, Chang JH, Lindquist RA, Moffat J, Golland P, Sabatini DM (2006) CellProfiler: image analysis software for identifying and quantifying cell phenotypes. Genome Biol. *7*, R100.

Casadio R, Jacoboni I, Messina A, De Pinto V (2002) A 3D model of the voltage-dependent anion channel (VDAC). FEBS Lett. *520*, 1-7.

Chen RE, Patterson JC, Goupil LS, Thorner J (2010) Dynamic localization of Fus3 mitogen-activated protein kinase is necessary to evoke appropriate responses and avoid cytotoxic effects. Mol. Cell. Biol. *30*, 4293-4307.

Chen RE, Thorner J (2007) Function and regulation in MAPK signaling pathways: Lessons learned from the yeast *Saccharomyces cerevisiae*. Biochimica. Biophysica. Acta. *1773*, 1311-1340.

Chen ZQ, Ulsh LS, DuBois G, Shih TY (1985) Posttranslational processing of p21 ras proteins involves palmitylation of the C-terminal tetrapeptide containing cysteine-186. J. Virol. *56*, 607-612.

Cherry JM, Ball C, Weng S, Juvik G, Schmidt R, Adler C, Dunn B, Dwight S, Riles L, Mortimer RK, Botstein D (1997) Genetic and physical maps of *Saccharomyces cerevisiae*. Nature *387*, 67-73.

Chou S, Huang L, Liu H (2004) Fus3-regulated Tec1 degradation through SCFCdc4 determines MAPK signaling specificity during mating in yeast. Cell *119*, 981-990.

Ciejek E, Thorner J (1979) Recovery of *S. cerevisiae* **a** cells from G1 arrest by alpha factor pheromone requires endopeptidase action. Cell *18*, 623-635.

Ciruela F (2008) Fluorescence-based methods in the study of protein-protein interactions in living cells. Curr. Opin. Biotechnol. *19*, 338-343.

Clotet J, Escoté X, Adrover MA, Yaakov G, Garí E, Aldea M, de Nadal E, Posas F (2006) Phosphorylation of Hsl1 by Hog1 leads to a G2 arrest essential for cell survival at high osmolarity. EMBO J. *25*, 2338-2346.

Cohen P, Frame S (2001) The renaissance of GSK3. Nat. Rev. Mol. Cell. Biol. *2*, 769-776.

Cook JG, Bardwell L, Kron SJ, Thorner J (1996) Two novel targets of the MAP kinase Kss1 are negative regulators of invasive growth in the yeast *Saccharomyces cerevisiae*. Genes Dev. *10*, 2831-2848.

Cook JG, Bardwell L, Thorner J (1997) Inhibitory and activating functions for MAPK Kss1 in the *S. cerevisiae* filamentous-growth signalling pathway. Nature *390*, 85-88.

Coombe BG (1987) Distribution of solutes within the developing grape berry in relation to its

morphology. Am. J. Enol. Vitic. *38*, 120-127.

Cuadrado A, Nebreda A (2010) Mechanisms and functions of p38 MAPK signalling. Biochem. J. *429*, 403-417.

Cullen PJ, Sabbagh W, Graham E, Irick MM, van Olden EK, Neal C, Delrow J, Bardwell L, Sprague GF (2004) A signaling mucin at the head of the Cdc42- and MAPK-dependent filamentous growth pathway in yeast. Genes Dev. *18*, 1695-1708.

De Nadal E, Zapater M, Alepuz PM, Sumoy L, Mas G, Posas F (2004) The MAPK Hog1 recruits Rpd3 histone deacetylase to activate osmoresponsive genes. Nature *427*, 370-374.

Dowell RD, Ryan O, Jansen A, Cheung D, Agarwala S, Danford T, Bernstein DA, Rolfe PA, Heisler LE, Chin B, Nislow C, Giaever G, Phillips PC, Fink GR, Gifford DK, Boone C (2010) Genotype to phenotype: A complex problem. Science *328*, 469.

Edgar R, Domrachev M, Lash AE (2002) Gene Expression Omnibus: NCBI gene expression and hybridization array data repository. Nucleic Acids Res. *30*, 207 -210.

Eisen MB, Brown PO (1999) DNA arrays for analysis of gene expression. Meth. Enzymol. *303*, 179-205.

Ekiel I, Sulea T, Jansen G, Kowalik M, Minailiuc O, Cheng J, Harcus D, Cygler M, Whiteway M, Wu C (2009) Binding the atypical RA domain of Ste50p to the unfolded Opy2p cytoplasmic tail is essential for the High-Osmolarity Glycerol Pathway. Mol. Biol. Cell *20*, 5117-5126.

Elion EA (2001) The Ste5p scaffold. J. Cell. Sci. *114*, 3967-3978.

Errede B, Gartner A, Zhou Z, Nasmyth K, Ammerer G (1993) MAP kinase-related Fus3 from *S. cerevisiae* is activated by Ste7 in vitro. Nature *362*, 261-264.

Escote X, Zapater M, Clotet J, Posas F (2004) Hog1 mediates cell-cycle arrest in G1 phase by the dual targeting of Sic1. Nat. Cell Biol. *6*, 997-1002.

Ferrigno P, Posas F, Koepp D, Saito H, Silver PA (1998) Regulated nucleo/cytoplasmic exchange of HOG1 MAPK requires the importin beta homologs Nmd5 and Xpo1. EMBO J. *17*, 5606-5614.

Flatauer LJ, Zadeh SF, Bardwell L (2005) Mitogen-activated protein kinases with distinct requirements for Ste5 scaffolding influence signaling specificity in *Saccharomyces cerevisiae*. Mol. Cell. Biol. *25*, 1793-1803.

Frayne J, Taylor A, Cameron G, Hadfield AT (2009) structure of insoluble rat sperm glyceraldehyde-3-phosphate dehydrogenase (GAPDH) via heterotetramer formation with *Escherichia coli* GAPDH reveals target for contraceptive design. J. Biol. Chem. *284*, 22703-22712.

Garrenton LS, Braunwarth A, Irniger S, Hurt E, Künzler M, Thorner J (2009) Nucleus-specific and cell cycle-regulated degradation of mitogen-activated protein kinase scaffold protein Ste5 contributes to the control of signaling competence. Mol. Cell. Biol. *29*, 582-601.

Garrenton LS, Stefan CJ, McMurray MA, Emr SD, Thorner J (2010) Pheromone-induced anisotropy in yeast plasma membrane phosphatidylinositol-4,5-bisphosphate distribution is required for MAPK signaling. Proc. Natl. Acad. Sci. USA *107*, 11805-11810.

Garrenton LS, Young SL, Thorner J (2006) Function of the MAPK scaffold protein, Ste5, requires a cryptic PH domain. Genes Dev. *20*, 1946-1958.

Gartner A, Jovanović A, Jeoung DI, Bourlat S, Cross FR, Ammerer G (1998) Pheromone-dependent G1 cell cycle arrest requires Far1 phosphorylation, but may not involve inhibition of Cdc28-Cln2 kinase, in vivo. Mol. Cell. Biol. *18*, 3681-3691.

Gasch AP, Spellman PT, Kao CM, Carmel-Harel O, Eisen MB, Storz G, Botstein D, Brown PO (2000) genomic expression programs in the response of yeast cells to environmental changes. Mol. Biol. Cell *11*, 4241-4257.

Gervais P, Marechal PA, Molin P (1992) Effects of the kinetics of osmotic pressure variation on yeast viability. Biotechnol. Bioeng. *40*, 1435-1439.

Gietz R, Akio S (1988) New yeast-Escherichia coli shuttle vectors constructed with in vitro mutagenized yeast genes lacking six-base pair restriction sites. Gene *74*, 527-534.

Goldbeter A, Koshland DE (1981) An amplified sensitivity arising from covalent modification in biological systems. Proc. Natl. Acad. Sci. USA *78*, 6840-6844.

Good M, Tang G, Singleton J, Reményi A, Lim WA (2009) The Ste5 scaffold directs mating signaling by catalytically unlocking the Fus3 MAP kinase for activation. Cell *136*, 1085-1097.

Han J, Lee JD, Bibbs L, Ulevitch RJ (1994) A MAP kinase targeted by endotoxin and hyperosmolarity in mammalian cells. Science *265*, 808-811.

Hao N, Behar M, Parnell SC, Torres MP, Borchers CH, Elston TC, Dohlman HG (2007) A systems-biology analysis of feedback inhibition in the Sho1 osmotic-stress-response pathway. Curr. Biol. *17*, 659-667.

Hao N, Zeng Y, Elston TC, Dohlman HG (2008) Control of MAPK specificity by feedback phosphorylation of shared adapter protein Ste50. J. Biol. Chem. *283*, 33798-33802.

Hedfalk K, Bill RM, Mullins JGL, Karlgren S, Filipsson C, Bergstrom J, Tamás MJ, Rydström J, Hohmann S (2004) A regulatory domain in the C-terminal extension of the yeast glycerol channel Fps1p. J. Biol. Chem. *279*, 14954-14960.

Hicks J, Fink G, Sherman F (1987) Methods in yeast genetics: a laboratory course manual. Cold Spring Harbor Laboratory Press.

Holt LJ, Tuch BB, Villén J, Johnson AD, Gygi SP, Morgan DO (2009) Global analysis of Cdk1 substrate phosphorylation sites provides insights into evolution. Science *325*, 1682 -1686.

Inoue Y, Tsujimoto Y, Kimura A (1998) Expression of the glyoxalase I gene of *Saccharomyces cerevisiae* is regulated by high osmolarity glycerol mitogen-activated protein kinase pathway in osmotic stress response. J. Biol. Chem. *273*, 2977-2983.

Jacoby T, Flanagan H, Faykin A, Seto AG, Mattison C, Ota I (1997) Two protein-tyrosine phosphatases inactivate the osmotic stress response pathway in yeast by targeting the mitogen-activated protein kinase, Hog1. J. Biol. Chem. *272*, 17749 -17755.

Jauert PA, Jensen LE, Kirkpatrick DT (2005) A novel yeast genomic DNA library on a geneticin-resistance vector. Yeast *22*, 653-657.

Junttila MR, Li S, Westermarck J (2008) Phosphatase-mediated crosstalk between MAPK signaling pathways in the regulation of cell survival. FASEB J. *22*, 954 -965.

Kadrmas JL, Beckerle MC (2004) The LIM domain: from the cytoskeleton to the nucleus. Nat. Rev. Mol. Cell Biol. *5*, 920-931.

Kim S, Shah K (2007) Dissecting yeast Hog1 MAP kinase pathway using a chemical genetic approach. FEBS Lett. *581*, 1209-1216.

Kinoshita E, Kinoshita-Kikuta E, Takiyama K, Koike T (2006) Phosphate-binding tag, a new tool to visualize phosphorylated proteins. Mol. & Cell. Prot. *5*, 749 -757.

Kitada K, Yamaguchi E, Arisawa M (1995) Cloning of the *Candida glabrata TRP1* and *HIS3* genes, and construction of their disruptant strains by sequential integrative transformation. Gene *165*, 203-206.

Krebs E (1955) Glyceraldehyde-3-phosphate dehydrogenase from yeast : GAP + DPN + P <->1,3-Diphosphoglycerate + DPNH + H+ Meth. in Enzymol. , Vol. 3 p. 407-411.

Krishna M, Narang H (2008) The complexity of mitogen-activated protein kinases (MAPKs) made simple. Cell. Mol. Life Sci. *65*, 3525-3544.

Madhani HD, Fink GR (1997) Combinatorial control required for the specificity of yeast MAPK signaling. Science *275*, 1314-1317.

Maeda T, Takekawa M, Saito H (1995) Activation of yeast Pbs2 MAPKK by MAPKKKs or by binding of an SH3-containing osmosensor. Science *269*, 554-558.

Mapes J, Ota IM (2004) Nbp2 targets the Ptc1-type 2C Ser/Thr phosphatase to the HOG MAPK

pathway. EMBO J. *23*, 302-311.

McAlister L, Holland MJ (1985) Differential expression of the three yeast glyceraldehyde-3-phosphate dehydrogenase genes. J. Biol. Chem. *260*, 15019-15027.

McClean MN, Mody A, Broach JR, Ramanathan S (2007) Cross-talk and decision making in MAP kinase pathways. Nat. Genet. *39*, 409-414.

Melamed D, Pnueli L, Arava Y (2008) Yeast translational response to high salinity: Global analysis reveals regulation at multiple levels. RNA *14*, 1337 -1351.

Mendenhall MD, Hodge AE (1998) Regulation of Cdc28 cyclin-dependent protein kinase activity during the cell cycle of the yeast *Saccharomyces cerevisiae*. Microbiol. Mol. Biol. Rev. *62*, 1191-1243.

Mettetal JT, Muzzey D, Gómez-Uribe C, van Oudenaarden A (2008) The frequency dependence of osmo-adaptation in *Saccharomyces cerevisiae*. Science *319*, 482-484.

Mok J et al. (2010) Deciphering protein kinase specificity through large-scale analysis of yeast phosphorylation site motifs. Sci. Signal. *3*, ra12.

Moore SA (1983) Comparison of dose-response curves for alpha factor-induced cell division arrest, agglutination, and projection formation of yeast cells. Implication for the mechanism of alpha factor action. J. Biol. Chem. *258*, 13849-13856.

Mösch HU, Roberts RL, Fink GR (1996) Ras2 signals via the Cdc42/Ste20/mitogen-activated protein kinase module to induce filamentous growth in *Saccharomyces cerevisiae*. Proc. Natl. Acad. Sci. USA. *93*, 5352-5356.

Muller EG, Snydsman BE, Novik I, Hailey DW, Gestaut DR, Niemann CA, O'Toole ET, Giddings TH, Sundin BA, Davis TN (2005) The organization of the core proteins of the yeast spindle pole body. Mol. Biol. Cell *16*, 3341-3352.

Nelson B, Parsons AB, Evangelista M, Schaefer K, Kennedy K, Ritchie S, Petryshen TL, Boone C (2004) Fus1p interacts with components of the Hog1p mitogen-activated protein kinase and Cdc42p morphogenesis signaling pathways to control cell fusion during yeast mating. Genetics *166*, 67-77.

Nevoigt E, Stahl U (2006) Osmoregulation and glycerol metabolism in the yeast *Saccharomyces cerevisiae*. FEMS Microbiol. Rev. *21*, 231-241.

Nguyen AW, Daugherty PS (2005) Evolutionary optimization of fluorescent proteins for intracellular FRET. Nat. Biotech. *23*, 355-360.

O'Rourke SM, Herskowitz I (2002) A third osmosensing branch in *Saccharomyces cerevisiae* requires the Msb2 protein and functions in parallel with the Sho1 branch. Mol. Cell. Biol. *22*,

4739-4749.

O'Rourke SM, Herskowitz I (2004) Unique and redundant roles for HOG MAPK pathway components as revealed by whole-genome expression analysis. Mol. Biol. Cell *15*, 532-542.

O'Rourke SM, Herskowitz I (1998) The Hog1 MAPK prevents cross talk between the HOG and pheromone response MAPK pathways in *Saccharomyces cerevisiae*. Genes Dev. *12*, 2874-2886.

Park S, Zarrinpar A, Lim WA (2003) Rewiring MAP kinase pathways using alternative scaffold assembly mechanisms. Science *299*, 1061-1064.

Parmar JH, Bhartiya S, Venkatesh KV (2011) Characterization of the adaptive response and growth upon hyperosmotic shock in *Saccharomyces cerevisiae*. Mol. BioSyst. *7*, 1138-1148.

Pascual-Ahuir A, Struhl K, Proft M (2006) Genome-wide location analysis of the stress-activated MAP kinase Hog1 in yeast. Methods *40*, 272-278.

Patterson JC, Klimenko ES, Thorner J (2010) Single-cell analysis reveals that insulation maintains signaling specificity between two yeast MAPK pathways with common components. Sci. Signal. *3*, ra75.

Pearson G, Robinson F, Beers Gibson T, Xu B, Karandikar M, Berman K, Cobb MH (2001) Mitogen-activated protein (MAP) kinase pathways: regulation and physiological functions. Endocr. Rev. *22*, 153-183.

Peter M, Gartner A, Horecka J, Ammerer G, Herskowitz I (1993) FAR1 links the signal transduction pathway to the cell cycle machinery in yeast. Cell *73*, 747-760.

Pitoniak A, Birkaya B, Dionne HM, Vadaie N, Cullen PJ (2009) The signaling mucins Msb2 and Hkr1 differentially regulate the filamentation mitogen-activated protein kinase pathway and contribute to a multimodal response. Mol. Biol. Cell *20*, 3101-3114.

Pokholok DK, Zeitlinger J, Hannett NM, Reynolds DB, Young RA (2006) Activated signal transduction kinases frequently occupy target genes. Science *313*, 533-536.

Poolman B, Glaasker E (1998) Regulation of compatible solute accumulation in bacteria. Mol. Microbiol. *29*, 397-407.

Posas F, Saito H (1997) Osmotic activation of the HOG MAPK pathway via Ste11p MAPKKK: scaffold role of Pbs2p MAPKK. Science *276*, 1702 -1705.

Posas F, Wurgler-Murphy SM, Maeda T, Witten EA, Thai TC, Saito H (1996) Yeast HOG1 MAP kinase cascade is regulated by a multistep phosphorelay mechanism in the Sln1-Ypd1-Ssk1 "two-component" osmosensor. Cell *86*, 865-875.

Raitt DC, Posas F, Saito H (2000) Yeast Cdc42 GTPase and Ste20 PAK-like kinase regulate

Sho1-dependent activation of the Hog1 MAPK pathway. EMBO J. *19*, 4623-4631.

Rep M, Reiser V, Gartner U, Thevelein JM, Hohmann S, Ammerer G, Ruis H (1999) Osmotic stress-induced gene expression in *Saccharomyces cerevisiae* requires Msn1p and the novel nuclear factor Hot1p. Mol. Cell. Biol. *19*, 5474-5485.

Rigoulet M, Aguilaniu H, Avéret N, Bunoust O, Camougrand N, Grandier-Vazeille X, Larsson C, Pahlman I, Manon S, Gustafsson L (2004) Organization and regulation of the cytosolic NADH metabolism in the yeast *Saccharomyces cerevisiae*. Mol. Cell Biochem. *256*, 73-81.

Roberts RL, Fink GR (1994) Elements of a single MAP kinase cascade in *Saccharomyces cerevisiae* mediate two developmental programs in the same cell type: mating and invasive growth. Genes Dev. *8*, 2974-2985.

Rodríguez-Pachón JM, Martín H, North G, Rotger R, Nombela C, Molina M (2002) A novel connection between the yeast Cdc42 GTPase and the Slt2-mediated cell integrity pathway identified through the effect of secreted *Salmonella* GTPase modulators. J. Biol. Chem. *277*, 27094-27102.

Sabbagh W, Flatauer LJ, Bardwell AJ, Bardwell L (2001) Specificity of MAP kinase signaling in yeast differentiation involves transient versus sustained MAPK activation. Mol. Cell *8*, 683-691.

Saeed AI et al. (2003) TM4: a free, open-source system for microarray data management and analysis. BioTechniques *34*, 374-378.

Saito H, Tatebayashi K (2004) Regulation of the osmoregulatory HOG MAPK cascade in yeast. J. Biol. Chem. *136*, 267 -272.

Sambrook J, Russell DW (2001) Molecular Cloning: a Laboratory Manual. Cold Spring Harbor Laboratory Press.

Schaber J, Adrover MÀ, Eriksson E, Pelet S, Petelenz-Kurdziel E, Klein D, Posas F, Goksör M, Peter M, Hohmann S, Klipp E (2010) Biophysical properties of *Saccharomyces cerevisiae* and their relationship with HOG pathway activation. Eur. Biophys. J. *39*, 1547-1556.

Schwartz MA, Madhani HD (2004) Principles of MAP kinase signaling specificity in *Saccharomyces cerevisiae*. Annu. Rev. Genet. *38*, 725-748.

Shaner NC, Lin MZ, McKeown MR, Steinbach PA, Hazelwood KL, Davidson MW, Tsien RY (2008) Improving the photostability of bright monomeric orange and red fluorescent proteins. Nat. Methods *5*, 545-551.

Shock TR, Thompson J, Yates JR, Madhani HD (2009) Hog1 mitogen-activated protein kinase (MAPK) interrupts signal transduction between the Kss1 MAPK and the Tec1 transcription factor to maintain pathway specificity. Eukaryot. Cell *8*, 606-616.

Sikorski RS, Hieter P (1989) A system of shuttle vectors and yeast host strains designed for efficient manipulation of DNA in *Saccharomyces cerevisiae*. Genetics *122*, 19-27.

Smith GR, Givan SA, Cullen P, Sprague GF (2002) GTPase-activating proteins for Cdc42. Eukaryot. Cell *1*, 469-480.

Sopko R, Huang D, Smith JC, Figeys D, Andrews BJ (2007) Activation of the Cdc42p GTPase by cyclin-dependent protein kinases in budding yeast. EMBO J. *26*, 4487-4500.

Sprague GF, Herskowitz I (1981) Control of yeast cell type by the mating type locus. I. Identification and control of expression of the a-specific gene *BAR1*. J. Mol. Biol. *153*, 305-321.

Stevenson BJ, Ferguson B, De Virgilio C, Bi E, Pringle JR, Ammerer G, Sprague GF (1995) Mutation of *RGA1*, which encodes a putative GTPase-activating protein for the polarity-establishment protein Cdc42p, activates the pheromone-response pathway in the yeast *Saccharomyces cerevisiae*. Genes Dev. *9*, 2949-2963.

Stevenson BJ, Rhodes N, Errede B, Sprague GF (1992) Constitutive mutants of the protein kinase *STE11* activate the yeast pheromone response pathway in the absence of the G protein. Genes Dev. *6*, 1293-1304.

Strickfaden SC, Winters MJ, Ben-Ari G, Lamson RE, Tyers M, Pryciak PM (2007) A mechanism for cell-cycle regulation of MAP kinase signaling in a yeast differentiation pathway. Cell *128*, 519-531.

Sunnerhagen P (2007) Cytoplasmatic post-transcriptional regulation and intracellular signalling. Mol. Genet. Genomics *277*, 341-355.

Sweeney TE, Beuchat CA (1993) Limitations of methods of osmometry: measuring the osmolality of biological fluids. Amer. J. Physiol. *264*, R469 -R480.

Tatebayashi K, Tanaka K, Yang H, Yamamoto K, Matsushita Y, Tomida T, Imai M, Saito H (2007) Transmembrane mucins Hkr1 and Msb2 are putative osmosensors in the SHO1 branch of yeast HOG pathway. EMBO J. *26*, 3521-3533.

Tatebayashi K, Yamamoto K, Tanaka K, Tomida T, Maruoka T, Kasukawa E, Saito H (2006) Adaptor functions of Cdc42, Ste50, and Sho1 in the yeast osmoregulatory HOG MAPK pathway. EMBO J. *25*, 3033-3044.

Taxis C, Knop M (2006) System of centromeric, episomal, and integrative vectors based on drug resistance markers for *Saccharomyces cerevisiae*. BioTechniques *40*, 73-78.

Tedford K, Kim S, Sa D, Stevens K, Tyers M (1997) Regulation of the mating pheromone and invasive growth responses in yeast by two MAP kinase substrates. Curr. Biol. *7*, 228-238.

Thorsen M, Di Y, Tängemo C, Morillas M, Ahmadpour D, Van der Does C, Wagner A, Johansson E, Boman J, Posas F, Wysocki R, Tamás MJ (2006) The MAPK Hog1p modulates Fps1p-dependent arsenite uptake and tolerance in yeast. Mol. Biol. Cell *17*, 4400-4410.

Truckses DM, Bloomekatz JE, Thorner J (2006) The RA domain of Ste50 adaptor protein is required for delivery of Ste11 to the plasma membrane in the filamentous growth signaling pathway of the yeast *Saccharomyces cerevisiae*. Mol. Cell. Biol. *26*, 912-928.

Tusher VG, Tibshirani R, Chu G (2001) Significance analysis of microarrays applied to the ionizing radiation response. Proc. Natl. Acad. Sci. USA *98*, 5116 -5121.

Uesono Y, Toh-e A (2002) Transient inhibition of translation initiation by osmotic stress. J. Biol. Chem. *277*, 13848 -13855.

Vadaie N, Dionne H, Akajagbor DS, Nickerson SR, Krysan DJ, Cullen PJ (2008) Cleavage of the signaling mucin Msb2 by the aspartyl protease Yps1 is required for MAPK activation in yeast. J. Cell Biol. *181*, 1073 -1081.

Wang Y, Abu Irqeba A, Ayalew M, Suntay K (2009) Sumoylation of transcription factor Tec1 regulates signaling of mitogen-activated protein kinase pathways in yeast. PLoS ONE *4*, e7456.

Wang Y, Dohlman HG (2004) Pheromone signaling mechanisms in yeast: a prototypical sex machine. Science *306*, 1508 -1509.

Watson FL, Heerssen HM, Bhattacharyya A, Klesse L, Lin MZ, Segal RA (2001) Neurotrophins use the Erk5 pathway to mediate a retrograde survival response. Nat. Neurosci. *4*, 981-988.

Westfall PJ, Ballon DR, Thorner J (2004) When the stress of your environment makes you go HOG wild. Science *306*, 1511-1512.

Westfall PJ, Patterson JC, Chen RE, Thorner J (2008) Stress resistance and signal fidelity independent of nuclear MAPK function. Proc. Natl. Acad. Sci. USA *105*, 12212-12217.

Westfall PJ, Thorner J (2006) Analysis of mitogen-activated protein kinase signaling specificity in response to hyperosmotic stress: use of an analog-sensitive *HOG1* allele. Eukaryot. Cell *5*, 1215-1228.

Willumsen BM, Norris K, Papageorge AG, Hubbert NL, Lowy DR (1984) Harvey murine sarcoma virus p21 ras protein: biological and biochemical significance of the cysteine nearest the carboxy terminus. EMBO J. *3*, 2581-2585.

Winters MJ, Lamson RE, Nakanishi H, Neiman AM, Pryciak PM (2005) A membrane binding domain in the Ste5 scaffold synergizes with Gβγ binding to control localization and signaling in pheromone response. Mol. Cell *20*, 21-32.

Wu C, Jansen G, Zhang J, Thomas DY, Whiteway M (2006) Adaptor protein Ste50p links the Ste11p MEKK to the HOG pathway through plasma membrane association. Genes Dev. *20*, 734-746.

Wurgler-Murphy SM, Maeda T, Witten EA, Saito H (1997) Regulation of the *Saccharomyces cerevisiae HOG1* mitogen-activated protein kinase by the *PTP2* and *PTP3* protein tyrosine phosphatases. Mol. Cell. Biol. *17*, 1289-1297.

Yamamoto K, Tatebayashi K, Tanaka K, Saito H (2010) Dynamic control of yeast MAP kinase network by induced association and dissociation between the Ste50 scaffold and the Opy2 membrane anchor. Mol. Cell *40*, 87-98.

Yang H, Tatebayashi K, Yamamoto K, Saito H (2009) Glycosylation defects activate filamentous growth Kss1 MAPK and inhibit osmoregulatory Hog1 MAPK. EMBO J. *28*, 1380-1391.